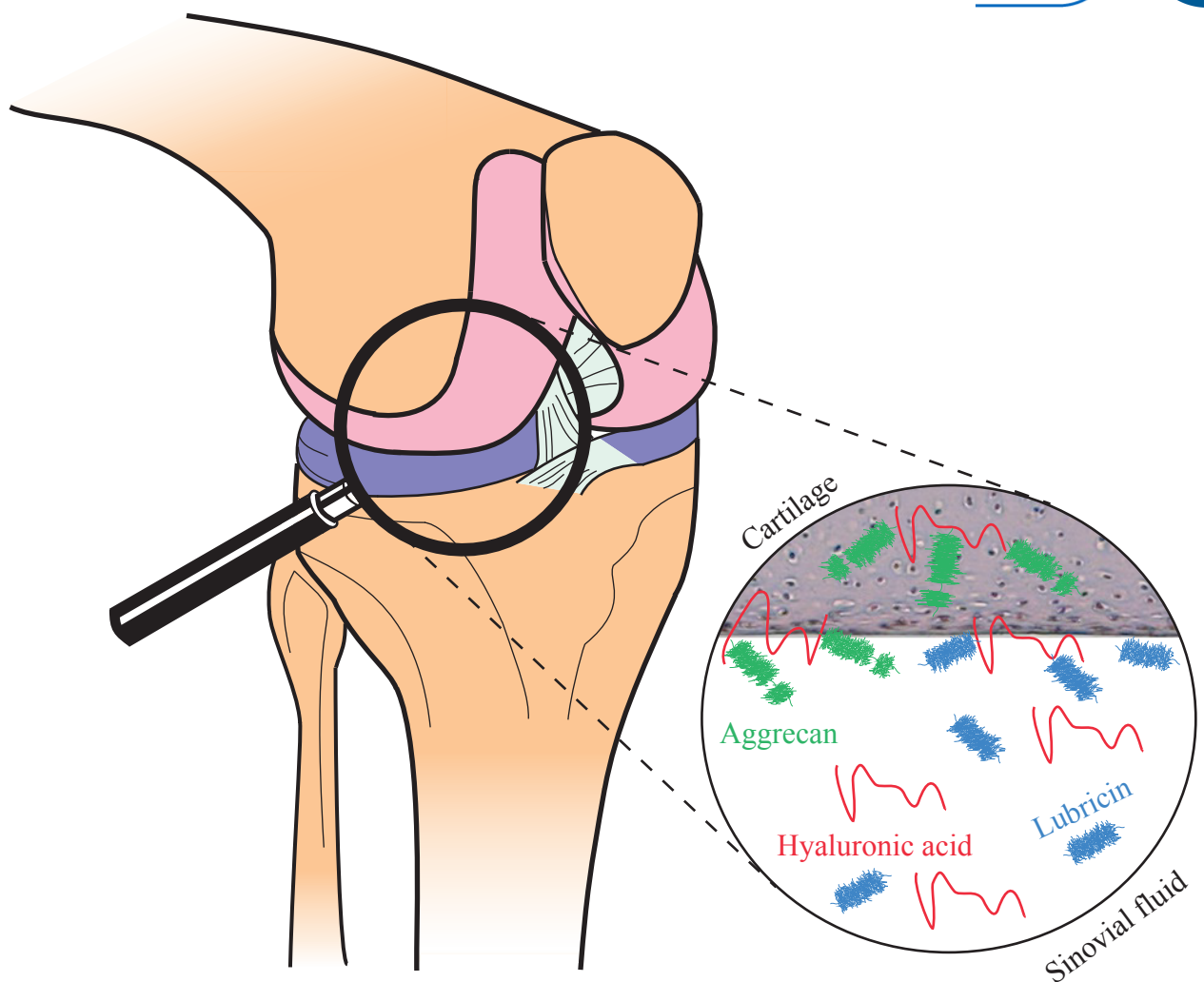


Biotribology and biomechanics of articular cartilage





Technische Universität München
Fakultät für Maschinenwesen
Professur für Biomechanik

Biotribology and biomechanics of articular cartilage

Kathrin Both

Vollständiger Abdruck der von der Fakultät für Maschinenwesen der Technischen Universität München zur Erlangung des akademischen Grades eines

Doktor-Ingenieurs (Dr.-Ing.)

genehmigten Dissertation.

Vorsitzender: Univ.-Prof. Dr.-Ing. Karsten Stahl

Prüfer der Dissertation:

1. Univ.-Prof. Dr. rer. nat. Oliver Lieleg
2. Univ.-Prof. dr. ir. Daniel Rixen
3. Univ.-Prof. Tannin A. Schmidt, Ph.D.,
University of Calgary / Canada

Die Dissertation wurde am 31.03.2016 bei der Technischen Universität München eingereicht und durch die Fakultät für Maschinenwesen am 14.09.2016 angenommen.

Abstract

Articular cartilage is a complex biomaterial which combines well-orchestrated viscoelastic and tribological properties. Although cartilage lacks the ability to regenerate itself after injury or damage, it can perform its function for the greater part of a human lifetime. It remains enigmatic how this is achieved by the tissue. The aim of this thesis is to advance the understanding of physiological lubrication strategies and, in particular, of the low-friction and wear-resistance of cartilage which are, up to now, unmatched by any artificial system. Therefore, the surface and bulk properties of cartilage were investigated as well as the fluid phase of the tissue, the lubricating fluid (synovial fluid) and their interactions. These investigations were conducted by applying loss of function and consecutive gain of function principles to identify the crucial molecular components that are responsible for the extraordinary material properties of articular cartilage.

To examine the contributions of the bulk and fluid phase to cartilage mechanical properties, and to grasp the resilience of the tissue to ongoing loading, the tissue was dehydrated and consecutively rehydrated with fluids of different ionic strength. It was found that a broad range of mechanical and structural properties of articular cartilage can be restored after rehydration, provided that a physiological salt solution is used. The influence of the ionic strength of the interstitial fluid on cartilage tribology was further evaluated using atomic force microscopy and macro-friction experiments. The ionic strength of the lubricant changed the frictional behavior differently on the observed measuring length scales and influenced the wear resistance of articular cartilage.

To analyze the contributions of synovial fluid components to the tribological function of cartilage, hyaluronic acid solutions were used. This specific component was chosen as it is already clinically used in viscosupplementation to enhance joint lubrication, whereas the exact mechanism of action behind this treatment is still unknown. It was revealed, that lubrication with Sinovial, a commercially available viscosupplement, has no significant impact on the friction coefficient but reduces wear formation. Physiologically, hyaluronic acid is not the only lubricating molecule in joints: multiple biopolymers are present in the synovial fluid to achieve optimal friction reduction and wear protection. In joint lubrication, hyaluronic acid has been shown to interact with the glycoprotein lubricin to form a surface protective layer that is accountable for the tribological properties of cartilage. Elsewhere in the human body, for instance on all wet epithelia, the tissue surface is covered with a similar layer, which is called mucus. It mainly consists of the glycoprotein mucin, which is thought to mediate friction and wear. So far, there is no experimental evidence for the wear protective properties of mucin and how it reduces friction. Therefore, in a first step, the ability of porcine gastric mucin to reduce friction on synthetic surfaces was analyzed. It was shown that mucin glycans control the hydration and lubrication ability of mucins, which is based on hydration lubrication. As a consequence, lectin conjugated polyethylene glycol repair motifs were successfully used to restore mucin hydration and the lubricity of partially deglycosylated mucins. Secondly, the ability of mucin to lubricate cartilage surfaces was tested and it was revealed that mucin reduces friction equally well as lubricin between two cartilage surfaces. Moreover, mucin was, in contrast to lubricin, able to minimize cartilage wear.

The new insights described in this thesis on how biopolymers mediate the biomechanical and biotribological properties of cartilage could guide the path towards the design of biomimetic materials, which make use of physiological lubrication strategies. Particularly the outstanding resilience of articular cartilage should be

considered in the development of cartilage substitute materials. In addition, the results gained here suggest that native mucins or novel mucin-mimetics might be useful for the treatment of osteoarthritis or as surface coatings on implant materials. The novel repair motifs for deglycosylated mucins could be a new treatment strategy for patients with defective mucus production or glycosylation as caused by the Sjögren or dry eye syndrome.

Zusammenfassung

Unsere lebenslange uneingeschränkte Bewegungsfähigkeit verdanken wir, neben Muskeln und Knochen, besonders dem Gewebe auf den Gelenkoberflächen: dem hyalinem Gelenkknorpel. Dieser zeichnet sich durch seine außerordentlichen biomechanischen und tribologischen Eigenschaften aus, verringert die Reibung im Gelenk und zeigt kaum Abrieb. In Gelenken für industrielle Anwendungen wird eine ähnliche Belastungsfähigkeit und Lebensdauer bis heute nicht erreicht, was unter anderem zur Entwicklung von vergleichbar teuren und aufwendigen Luftlagern geführt hat. Daher ist es nicht nur für die medizinische Forschung von großem Interesse die Leistungsfähigkeit von hyalinem Knorpel zu verstehen. Dies gilt insbesondere, da das Gewebe diese nicht durch eine hohe Regenerationsfähigkeit erzielt.

In der vorliegenden Dissertation wurden die Oberflächen- und Materialeigenschaften von Knorpel sowie das Zusammenspiel des Gewebes mit der Interstitial- und Gelenkflüssigkeit untersucht. Um den Einfluss einzelner Komponenten der Gelenkflüssigkeit besser zu verstehen, wurden diese zunächst entfernt und ein künstlicher Funktionsverlust herbeigeführt. In einem zweiten Schritt wurde analysiert, ob die Funktionalität durch erneute Zugabe der entfernten Komponenten oder durch synthetische Zusätze wiederhergestellt werden kann.

Um zu verstehen, wie sich das Zusammenspiel zwischen dem Gewebe und der Interstitialflüssigkeit in Abhängigkeit von der Ionenstärke auf die mechanischen Eigenschaften von hyalinem Knorpel auswirkt, wurde das Gewebe zunächst de- und anschließend rehydriert. Physiologisch tritt eine solch drastische Veränderung des Flüssigkeitsgehaltes zwar nicht auf, allerdings wird Knorpel während normaler Bewegungsabläufe anhaltend partiell de- und rehydriert. Die durchgeführten Versuche haben gezeigt, dass die meisten der strukturellen und biomechanischen Knorpel-eigenschaften durch Rehydratation mit einer physiologischen Kochsalzlösung wiederhergestellt werden können. Der Einfluss der Ionenstärke der Flüssigkeiten auf die tribologischen Eigenschaften von Knorpel wurde mittels Rasterkraftmikroskopie und in Makro-Reibversuchen untersucht. Hierbei konnte festgestellt werden, dass die Ionenstärke des Schmiermittels das Reib- und Abriebverhalten beeinflusst und die relative Änderung des Reibkoeffizienten von der Messtechnik bzw. der untersuchten Größenskala abhängt.

Der Einfluss der unterschiedlichen Komponenten in der Gelenkflüssigkeit auf die tribologischen Knorpel-eigenschaften wurde zunächst anhand von Hyaluronsäure-Lösungen getestet. Obwohl der Einfluss von Hyaluronsäure auf die Schmierung von Gelenken noch nicht vollständig erforscht ist, werden diese Lösungen bereits klinisch zur Behandlung von Gelenkerkrankungen verwendet (Viskosupplementation). Eines dieser kommerziell erhältlichen Präparate, Sinovial, wurde in dieser Arbeit analysiert. Hierbei konnte kein signifikanter Einfluss auf die Reibung festgestellt werden, allerdings reduzierte sich der auf der Knorpeloberfläche ersichtliche Abrieb. Physiologisch betrachtet besteht die Gelenkflüssigkeit aus einer Vielzahl von Molekülen, unter anderem Hyaluronsäure, die zur Reibungs- und Abriebverminderung beitragen. Es ist bekannt, dass Hyaluronsäure auf der Knorpeloberfläche mit Lubricin interagiert und so einen Schutzfilm auf dem Gewebe bildet. Vergleicht man diesen Prozess in Gelenken mit den Schmiermechanismen auf anderen Geweben, so fällt auf, dass zum Beispiel auf Epithelgeweben ein ähnlicher Schutzfilm, Mucus, gebildet wird. Dieser besteht hauptsächlich aus dem Glykoprotein Mucin, das unter anderem für seine reibungsvermindernden Eigenschaften bekannt ist. In einem ersten Schritt wurde die schmierende Wirkung von Mucin-

lösungen (gereinigtes Mucin aus Schweinemägen) auf synthetischen Oberflächen untersucht, und es konnte gezeigt werden, dass die Zuckeranteile für diesen Effekt verantwortlich sind. Beim Verlust der Zuckeranteile des Proteins konnten die Mucine nicht mehr ausreichend Wasser binden und verloren in Folge dessen ihre schmierende Wirkung, die normalerweise durch einen oberflächengebundenen Flüssigkeitsfilm gesichert ist („hydration lubrication“). Synthetische Polymere konnten erfolgreich als Reparaturstrategie genutzt werden, um sowohl die Hydrierung als auch die Schmierung wieder herzustellen. In einem zweiten Schritt wurde untersucht, ob sich der physiologische Schmiermechanismus der Mucine auf ein anderes Gewebe, Knorpel, übertragen lässt. Mucin war hierbei in gleichem Maße wie das physiologisch vorkommende Glykoprotein Lubricin geeignet, die Reibung auf Knorpeloberflächen zu vermindern. Außerdem konnte durch die Schmierung mit Mucinen der Abrieb auf der Knorpeloberfläche verringert werden.

In dieser Dissertation konnten somit neue Erkenntnisse zum Einfluss von Biopolymeren auf die biomechanischen und biotribologischen Eigenschaften von hyalinem Gelenkknorpel gewonnen werden. Die erzielten Ergebnisse können für die Entwicklung von Knorpelersatzmaterialien verwendet werden und bilden den Ausgangspunkt, um physiologische Schmierprozesse mit synthetischen Materialien nachzuahmen. Insbesondere die Widerstandsfähigkeit von Knorpel sollte bei der Entwicklung von Knorpelersatzmaterialien berücksichtigt werden. Außerdem liefern die hier gezeigten Daten erste Anhaltspunkte für weitere Studien um zu analysieren, ob Mucine zur Behandlung von Osteoarthritis oder als Oberflächenbeschichtung für Implantatmaterialien eingesetzt werden können. Abschließend könnte die hier vorgestellte Reparaturstrategie für beschädigte Mucine Abhilfe bei Erkrankungen mit dauerhaft veränderter Mucus-Produktion oder -Glykosylierung schaffen, wie zum Beispiel im Fall des Sjögren-Syndroms oder dem Syndrom des trockenen Auges.

Danksagung

Zum Erfolg meiner Promotion haben viele Personen auf unterschiedliche Weise beigetragen, bei denen ich mich an dieser Stelle herzlich bedanken möchte:

Mein besonderer Dank gilt Herrn Prof. Dr. Oliver Lieleg für die Möglichkeit meine Doktorarbeit anzufertigen und die herausragende Betreuung. Ich weiß es sehr zu schätzen, dass seine Tür für Fragen, Diskussionen und Unterstützung immer offen steht!

Des Weiteren möchte ich mich bei meinem Prüfungskomitee, Herrn Prof. dr. ir. Daniel Rixen und Herrn Prof. Dr. Karsten Stahl, bedanken. I would also like to thank Mr. Prof. Tannin Schmidt, Ph.D. for the possibility to visit his lab and conduct my research exchange at the University of Calgary. Thanks alot for the smooth and successful collaboration and being part of my supervisory committee. Bei Herrn Prof. Dr. Thorsten Hugel und Herrn Priv.-Doz. Dr. Rainer Burgkart möchte ich mich dafür bedanken, dass dieses Projekt möglich wurde und sie mir mit fachlicher Unterstützung zur Seite standen. Der International Graduate School of Science and Engineering (IGSSE) sowie deren engagierten Mitarbeitern, spreche ich meinen Dank für die Finanzierung dieses Projektes und die organisatorische Unterstützung während der vergangenen drei Jahre aus.

Für ihre Unterstützung, nicht nur im Labor, sondern u.a. auch bei den vielen Fahrten zum Schlachter, möchte ich Tina Bidmon und Sabine Günzkofer danken. Vielen Dank Iris König-Decker, Rudolf Lehrhuber und den Kolleginnen und Kollegen am IMETUM für die administrative und praktische Unterstützung meiner Versuche. Außerhalb der TUM möchte ich mich bei der Firma Anton Paar, insbesondere bei Frau Dr. Christine Wurm, Herrn Dr. Frederik Wolf und Herrn Mesut Atas, für die zuverlässige Unterstützung bedanken.

Meinen Studenten (Ulrike, Julia, Ushnish, Max, Jonas und Jan) die ich während meiner Doktorarbeit betreuen durfte, möchte ich für ihr Engagement und ihre tatkräftige Hilfe danken, allen voran Julia Nachtsheim für ihre Unterstützung und die schöne Zeit im Labor und in den (Kaffee-)Pausen! Ein großes Dankeschön geht außerdem an Peter, Joanna, Sandra, Lorenz, Leo und Lara für ihre Hilfe und die vielen gemeinsamen Diskussionen.

Vielen Dank Benni, Stefan, Tin und Fabi - den Doktoranden meiner Arbeitsgruppe - für die schöne Zeit, die Unterstützung und für das gemeinsame Lachen, Ablenken, Kickern, "weil wir's können", fachliche Hilfe und Diskussionen, Korrektur lesen, die Pausen in der Sonne, "hoch die Hände", die seelische Unterstützung, die Zeit im Quiet Room, ...

Mein ganz persönlicher Dank gilt meinen Freunden, besonders Jelena, Philipp und Moritz, sowie meiner Mutter, meiner Schwester und meiner Familie für ihre vielseitige Unterstützung, auf die ich mich wirklich jederzeit verlassen kann! Damian, dir möchte ich ganz besonders danken, für deine Unterstützung, Motivation, Geduld und Rückhalt und dafür, dass du immer an meiner Seite bist!

Garching, im März 2016

Kathrin Both, geb. Boettcher

Contents

| | |
|--|------------|
| Abstract | I |
| Zusammenfassung | III |
| Danksagung | V |
| 1. Introduction | 1 |
| 1.1. Biotribology | 1 |
| 1.1.1. Friction | 1 |
| 1.1.2. Lubrication | 2 |
| 1.1.3. Wear | 4 |
| 1.2. Biomechanics | 5 |
| 1.3. Articular cartilage | 6 |
| 1.3.1. Structure of articular cartilage | 6 |
| 1.3.2. Biomechanics of articular cartilage | 8 |
| 1.3.3. Tribology of articular cartilage | 8 |
| 1.3.4. Osteoarthritis | 11 |
| 1.4. Macromolecular boundary lubricants | 12 |
| 1.4.1. Hyaluronic acid | 12 |
| 1.4.2. Lubricin | 13 |
| 1.4.3. Mucin | 13 |
| 1.5. Aims and objectives | 15 |
| 2. Materials & Methods | 17 |
| 2.1. Articular cartilage | 17 |
| 2.2. Lubricants | 18 |
| 2.2.1. Lubricin | 18 |
| 2.2.2. Hyaluronic acid | 18 |
| 2.2.3. Sinovial | 18 |
| 2.2.4. Porcine gastric mucin | 19 |
| 2.3. Mechanical characterization | 19 |
| 2.3.1. Indentation measurements | 19 |
| 2.3.2. Oscillatory shear measurements | 21 |
| 2.3.3. Viscosity measurements | 22 |
| 2.4. Tribology experiments | 22 |
| 2.4.1. Cartilage/cartilage friction setup | 23 |
| 2.4.2. Glass/cartilage friction setup | 24 |
| 2.4.3. Wear generation | 24 |
| 2.4.4. Steel/PDMS friction setup | 24 |
| 2.5. Structural characterization | 25 |
| 2.5.1. Histology | 25 |

| | | |
|-----------|---|------------|
| 2.5.2. | 1,9-Dimethylmethylene blue assay | 26 |
| 2.5.3. | Scanning electron microscopy | 26 |
| 2.5.4. | Adsorption measurements | 27 |
| 2.5.5. | Profilometer measurements | 27 |
| 3. | Summaries of publications | 31 |
| 3.1. | Adapting a commercial shear rheometer for applications in cartilage research | 31 |
| 3.2. | The structure and mechanical properties of articular cartilage are highly resilient towards transient dehydration | 33 |
| 3.3. | Comparison of friction and wear of articular cartilage on different length scales | 35 |
| 3.4. | Modulating mucin hydration and lubrication by deglycosylation and polyethylene glycol binding | 37 |
| 3.5. | Porcine gastric mucins reduce friction and wear in cartilage boundary lubrication | 39 |
| 4. | Discussion & Outlook | 41 |
| | Appendix | 53 |
| A. | Publications | 55 |
| B. | Supplemental information | 105 |
| C. | Licenses for publications | 121 |
| D. | Full list of publications | 137 |
| | Bibliography | 139 |

1. Introduction

1.1. Biotribology

Tribology (from the Greek words $\tau\rho\acute{\iota}\beta\omega$ (tribó) meaning "to rub" and $\lambda\acute{o}\gamma\omicron\varsigma$ (lógos) meaning "the study of") is the science of interacting surfaces in relative motion and includes the studies of friction, wear and lubrication. It is important to note that, although counterintuitive, friction and wear are not necessarily correlated¹. The interdisciplinary field of tribology spans disciplines from physics and chemistry to mechanical engineering and material science and is of economic importance as many product failures are caused by tribological problems. Historically, tribology evolved in the classical age. Egyptian wall paintings (Figure 1.2c) show that lubrication with water was invented as an early tribological strategy to facilitate the movement of large objects across rough sand surfaces during the construction process of the pyramids. Nowadays, it is most commonly applied in bearing design; however, in recent years, the field of tribology spread from macroscopic questions to nanoscopic studies² and became more important for other disciplines, for instance, electronics and biomedical engineering.

The emerging field of biotribology investigates friction, wear and lubrication of biological systems³ and the term was first introduced by Dowson & Wright in 1973⁴. Tribological principles of, e.g., eyes, joints (Figure 1.1) or the human mouthfeel are tackled to develop products, i.e., joint prostheses, contact lenses with greater comfort or groceries with an optimized taste/perception.

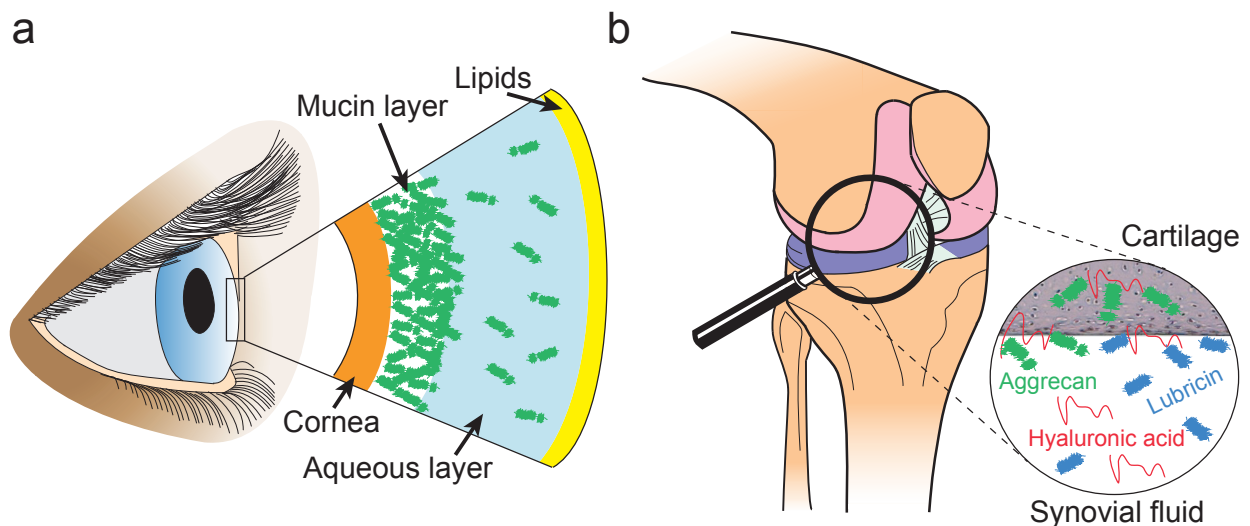


Figure 1.1.: Biotribology: In the eye (a) and joints (b) friction and wear are mediated by the interaction of biomacromolecules in the lubricating fluid with the tissue surface. The glycoproteins mucin and lubricin as well as other biopolymers are known for their influence on the tribological properties of tissue surfaces.

1.1.1. Friction

Friction is the force opposing the relative motion of two contacting surfaces. When these surfaces slide past each other, the friction between the two surfaces converts kinetic energy into thermal energy. Friction

can be, for example, caused by plowing, adhesion forces and asperity removal. It can be subdivided into dry friction (between two solid surfaces), fluid friction (between two viscous fluids) and lubricated friction (between two surfaces separated by a lubricating fluid). In dry and lubricated friction, different friction types, for instance, static, kinetic and rolling friction can be distinguished. Static friction occurs between non-moving surfaces which are in contact through a normal force F_n , and the friction force equals the force F_{\max} (Equation 1.1) that needs to be overcome before relative motion can occur. Kinetic friction (sliding friction/dynamic friction, F_f , Equation 1.2) exists between moving surfaces, and the friction force equals the product of the coefficient of kinetic friction and the normal force. These two regimes do not always arise separately, an alternation between the regimes is called stick-slip friction. The friction coefficient itself is a dimensionless scalar value describing the ratio of the friction force and the normal force and depends on the opposing materials.^{5,6} It is important to note that the friction coefficient is a system parameter and not a material property, i.e., that this value depends on the utilized experimental setup¹.

$$F_{\max} = \mu_s F_n \quad (1.1)$$

$$F_f = \mu_k F_n \quad (1.2)$$

As dry friction, also called coulomb friction⁷, does not or rarely occur physiologically, biotribology focuses on fluid friction, better known as viscosity, and lubricated friction.

1.1.2. Lubrication

In lubricated friction, different regimes can be distinguished⁸⁻¹⁰. The Stribeck curve (Figure 1.2) illustrates these different lubrication regimes by displaying the friction coefficient as a function of the so called Sommerfeld number (also called Stribeck number, lubrication parameter or Hersey number)^{7,8,11}. This dimensionless parameter is the product of the fluid viscosity η , the sliding speed v and the contact area A divided by the normal force F_n (Equation 1.3).

$$\text{Sommerfeld number} = \frac{\eta v A}{F_n} \quad (1.3)$$

Fluid film lubrication describes the lubrication at high sliding speeds. Here, the load is fully supported through lubricant-mediated viscous forces between the surfaces. The fluid film thickness h is larger than the surface roughness S_q and contact between the opposing surfaces is avoided. In this regime, the friction coefficient is a function of the lubricant properties, especially the viscosity. With increasing sliding velocities, the increasing shear forces inside the fluid entail a linear incline of the friction coefficient. Hydrostatic lubrication and hydrodynamic lubrication are subtypes of fluid film lubrication. If the lubricant is stabilized between the surfaces through external pressure, the regime is called hydrostatic lubrication. Hydrodynamic lubrication occurs when the material and/or system design are responsible for maintaining the fluid in between the surfaces. Here, the lubricant film breaks down and the surfaces might wear as soon as the relative motion between the surfaces subsides. The theory of elastohydrodynamic lubrication includes the ability of surfaces to deform elastically as well as the ability of the lubricant viscosity to change under pressure.

The transition from elastohydrodynamic or hydrodynamic to boundary lubrication is described by the mixed lubrication regime. During this phase, the fluid film thickness decreases with decreasing velocity and contact

between the surface asperities can occur.

Boundary lubrication occurs at low sliding speeds when the opposing surfaces come into close contact and force is transmitted via solid-solid contact points. This process usually leads to heat, surface wear and a higher friction coefficient and is mediated by the surface chemistry as well as components in the molecular thin film layer (1 – 10 nm) between the surfaces¹⁰. These components are called boundary lubricants and their lubricity is thought to be mainly linked to their ability to adsorb to the surfaces and requires them not to be squeezed out of the contact. Organic boundary lubricants for metal surfaces are fatty acids and esters as they are able to adhere to the metal with their polar end. In biological systems, hydrated polymer brushes act as organic lubricants. All these molecules share a common molecular design as they all exhibit a high chain length. The effectiveness of boundary lubricants depends, in addition to their ability to adsorb, on their molecular weight, degree of branching and molecular configuration in the adsorbed state¹⁰. Inorganic boundary lubricants involve compounds of chlorine, phosphorus, sulfur and iodine, and provide good lubrication at elevated temperatures and pressures.

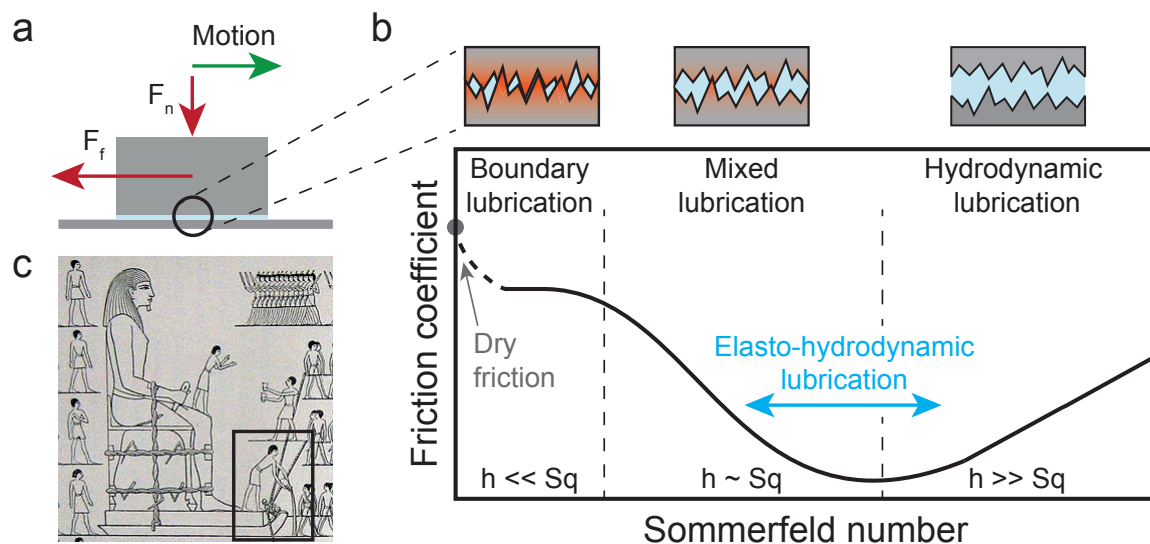


Figure 1.2.: Origin and description of lubrication. The friction coefficient μ is the ratio of the friction force F_f and the normal force F_n (a). The Stribeck curve describes the different lubrication regimes and their dependence on surface roughness. Therefore, the friction coefficient is plotted against the Sommerfeld number (b). The Egyptian wall painting "The tomb of Djehutihotep" depicts a person pouring water over the sand in front of a sledge (c, adapted¹²).

Boundary lubrication is the least understood lubrication regime and only few fairly controversial models and theories exist on how boundary lubricants achieve energy dissipation and thereby friction reduction¹⁰. Physical and chemical adsorption of the lubricants plays a major role in this process as subsequent shearing off the adsorbed molecules from the surface leads to energy dissipation (sacrificial layer mechanism)¹³. Moreover, tightly adsorbed molecules are able to build a protective surface layer (e.g., a sulfide layer on steel) or dissipate energy through the exchange of trapped water molecules with free water molecules in the fluid¹⁴. The latter process is called hydration lubrication and is based on two phenomena (Figure 1.3): First, water molecules are trapped between two surfaces due to charges presented by the adsorbed surface molecules (confined water) and second, the water molecules show repulsion due to their large dipole (hydration repulsion)¹⁵.

Hydration lubrication is one of many possible dissipation mechanisms to reduce friction. As soon as the examined system, lubricant or opposing materials, exhibit additional dissipation mechanism, the friction coefficient might show different trends in the lubrication regimes as described above and depicted by the classical Stribeck curve. Non-Newtonian fluids, which exhibit a dependency between the viscosity and the shear rate, are an example for additional energy dissipation through the lubricant. Here, a simple scaling of the Stribeck curve for the changing viscosity is not possible. The Stribeck curve is therefore also entitled as the Newtonian master curve, as it enables only the direct comparison of Newtonian lubricants and measurements conducted at different contact pressures on rather simple material surfaces.

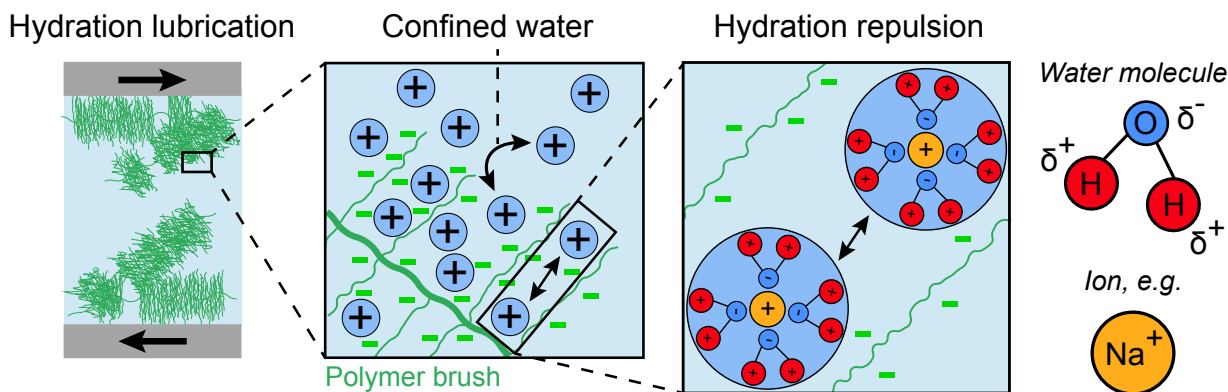


Figure 1.3.: Hydration lubrication is based on two mechanisms: confined water and hydration repulsion. Water molecules have a strong dipole and cluster around ions, e.g., Na⁺, out of the fluid phase. These hydrated ions are trapped in the highly negatively charged, surface-bound polymer brushes and can be exchanged quickly, for instance, under shear, with free hydrated ions in the fluid phase. Therefore, a fluid film is continuously maintained near the surfaces, even under relative motion (confined water). The trapped hydrated ions themselves show repulsion and thus enable the surface layer to sustain large normal loads (hydration repulsion).

1.1.3. Wear

Wear is defined as the damage to the surface of a sliding interface, which generally involves the progressive loss of material¹⁶. Similar to the coefficient of friction, wear is not a material property, but a system response. Depending on, e.g., the load, sliding speed and material type, different mechanism of wear can be distinguished. Major types of wear include abrasion, adhesion, erosion, fatigue, fretting and corrosion (Figure 1.4).

Abrasive wear is defined as the loss of material and occurs when a hard, rough material slides across a softer material. Adhesion is the most common reason of wear and arises from the contact between surface asperities under shear. It is defined as the material transfer between two surfaces and occurs due to the displacement of material compounds from one surface to another. Erosion is generated by impacting particles/molecules which slowly damage the material surface through repeated deformations and gradual material removal. Fatigue occurs when the surface of a material is weakened by cyclic loading and micro-cracks growing on the surface. Fretting is a consequence of repeated cyclical rubbing between two surfaces and material is being removed from both countering surfaces. Corrosion occurs due to chemical reaction of a material with its surrounding and is therefore the only wear type not dependent on the relative mate-

rial motion. A common example for corrosive wear is the oxidation of metals. Wear generation is reported preferably as a volume loss or, if not possible, a weight loss. Moreover, the number and shape of the wear debris as well as the roughness of the worn surfaces are common parameters to quantify wear.^{3,17,18}

A variety of different test setups exist to perform friction, lubrication and wear experiments. They include pin-on-disc and pin-on-plate setups as well as more complex and application-specific motion simulators. For pre-clinical development and clinical approval, standard tests are necessary to ensure the comparability of different test procedures and to establish a quality standard. As an example, the wear testing of total hip joint prostheses is defined in ISO 14242:2012, which specifies the loading and displacement parameter, methods of measurements and the test environment¹⁹. Wear analysis for hip joint prostheses has proven to be especially important as wear generation and thereby caused aseptic loosening of the implants is the most common reason for revision surgeries²⁰.

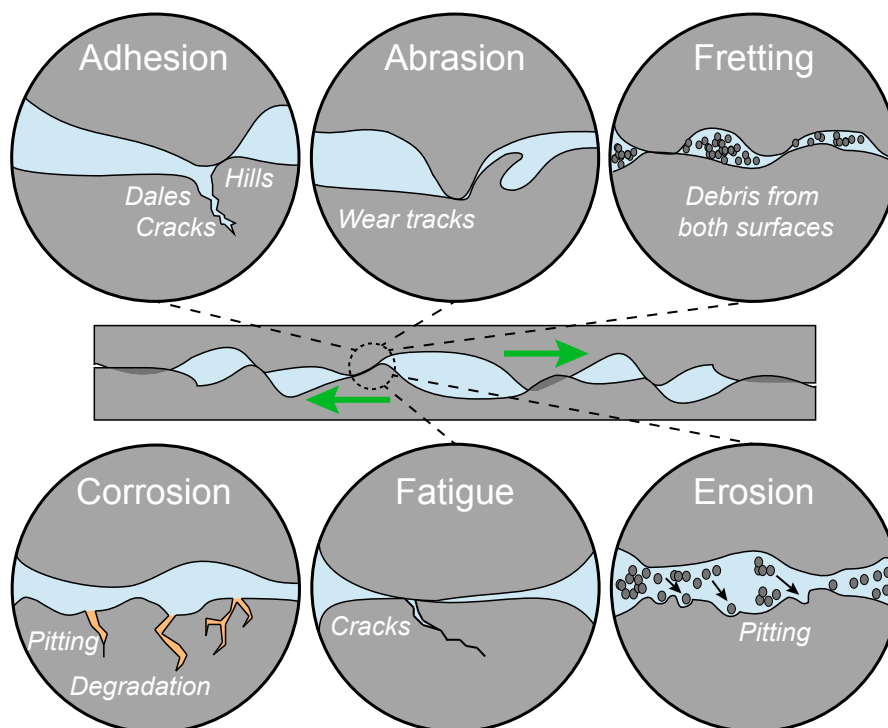


Figure 1.4: Commonly described wear mechanism include adhesion, abrasion, fretting, erosion, fatigue and corrosion. These phenomena occur over time and, except from corrosion, under relative motion. Often a plethora of wear types is responsible for surface damage and material failure.

1.2. Biomechanics

Biomechanics combines fields of research which study the mechanical principles (movement and structure) of biological systems such as humans, animals, plants, organs, and cells. On a macroscopic scale, in sports biomechanics, different locomotion principles are investigated to, e.g., enhance athletic performances, prevent injuries or mimic the natural movement. On a more microscopic scale, the relation between the microstructure and the mechanical properties of biomaterials is investigated.

The vast majority of biomaterials exhibit time dependent material properties with both elastic and viscous

characteristics and are therefore called viscoelastic. When a viscoelastic material is subjected to a constant stress, the material responds with creep, a slow progressive deformation, and it relaxes internal stresses when subjected to a constant strain. The viscoelastic response is caused by macromolecular motion, e.g., in polymers through bending/stretching rearrangements of the polymer chains and through ensuing dissipative pressure with surrounding fluids. Viscoelasticity is a key feature of biomaterials, as one tissue often fulfills very different functions and is, for instance, able to isolate vibrations, damp and adsorb shocks depending on the impact amplitude and frequency. It is therefore not only important to analyze the time-dependence but also the frequency-dependence of the viscoelastic properties. The viscoelastic properties of a material can be determined by using dynamic mechanical analysis methods as described in Section 2.3.2. Here, a small oscillatory stress is applied and the resulting strain is measured (Figure 1.5). For purely elastic materials, the stress and strain are in phase, whereas in purely viscous materials the strain γ follows the stress τ with a 90° phase lag (δ , Equation 2.7). As viscoelastic materials combine both aspects, they exhibit a phase lag of $0^\circ < \delta < 90^\circ$.^{21,22}

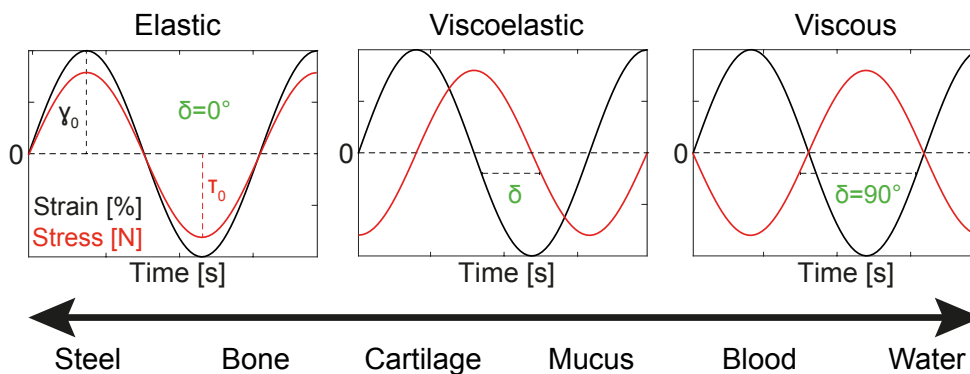


Figure 1.5.: Viscoelastic materials exhibit both viscous and elastic material characteristics. When they are subjected to strain with an amplitude of γ_0 , the stress response with an amplitude of τ_0 exhibits a phase lag of $0^\circ < \delta < 90^\circ$. For purely elastic materials stress and strain are in phase, whereas in purely viscous materials the phase lag is 90° .

1.3. Articular cartilage

1.3.1. Structure of articular cartilage

Articular cartilage is a viscoelastic, porous, avascular, aneural tissue lining the bone surfaces in joints. Its thickness varies between 0.1 and 7 mm²³ and it is composed of a fluid (70–80 % wet wt.) and a solid phase. The solid phase of articular cartilage contains only a single cell type (chondrocytes, < 5 % vol.) embedded in an extracellular matrix (ECM). Due to the avascular nature of cartilage, the chondrocytes obtain nutrients through diffusion. The ECM comprises a type II collagen fiber network (50–75 % dry wt.) and proteoglycans (15–30 % dry wt.), and is hierarchically structured (Figure 1.6a). Further constituents of the ECM are non-collagenous proteins and glycoproteins, constituting 15–20 % of the dry weight of cartilage. Their exact function however is not yet fully understood. They are involved in binding between chondrocytes and macromolecules of the ECM and have an organizing and stabilizing function within the ECM.²⁴

The cartilage surface is covered by a thin, acellular and non-fibrous layer, the lamina splendens. This layer is

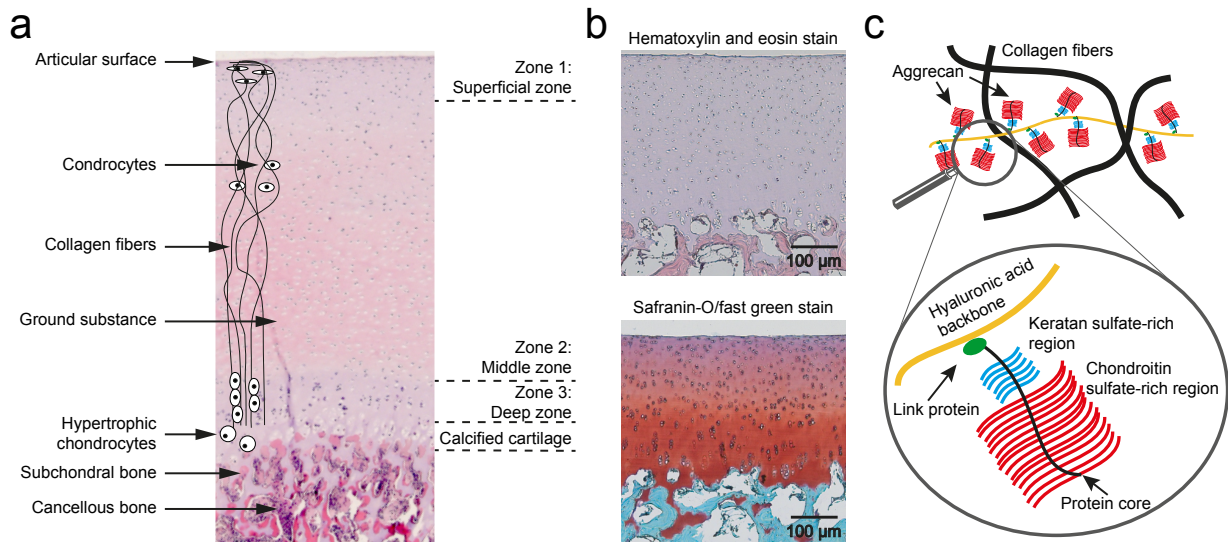


Figure 1.6.: Articular cartilage structure: Cartilage is hierarchically structured into different zones (a), which vary in terms of, e.g., collagen fiber orientation, proteoglycan content and chondrocyte shape. H&E stainings (b, upper image) are used to evaluate the overall cartilage structure and differences in glycosaminoglycan content (red) can be examined in the Safranin-O/fast green stain (b, lower image). A systematic drawing shows the solid structure of cartilage (c): Here, a hyaluronic acid (HA) chain entangled in the collagen fiber network is visualized and, in a detailed sketch, aggrecan is depicted which is bound to the HA chain via a link molecule.

thought to have a thickness in the nano- or micrometer range and consists of proteins and molecules from the synovial fluid. Underneath, in the superficial zone, the small but densely packed collagen fibers are aligned in parallel to the surface. The proteoglycan content as well as the permeability of the tissue are comparably low and the cells appear flat. In the middle zone, the fiber orientation is random, the proteoglycan content is maximal and the cells appear spherical and are arranged in columns. In the deep zone, the collagen fibers have a large diameter, form bundles orientated perpendicularly to the cartilage surface and are anchored to the underlying subchondral bone. The proteoglycan content as well as the cell density are low and the cells appear slightly elongated and orientated in the direction of the collagen fibers. The so-called tidemark in the deep zone separates the non-calcified from the calcified area of cartilage, which forms the anchorage point of cartilage in the subchondral bone. Calcification is carried out by chondrocytes as they become hypertrophic (enlarged).^{24–26}

Proteoglycans are large, highly glycosylated macromolecules formed by a protein core with attached glycosaminoglycans. Glycosaminoglycans are repeating, unbranched polysaccharide chains composed of repeating, but differently composed, disaccharide units. The most common proteoglycan in cartilage is aggrecan. It exhibits a bottlebrush structure and consists of a protein core (~ 230 kDa) with chondroitin sulfate A and C and keratan sulfate glycosaminoglycan chains (Figure 1.6c). Other glycosaminoglycans present in the cartilage matrix are dermatan sulfate and hyaluronic acid (HA)²⁴. Large proteoglycan aggregates are formed by the non-covalent linkage of aggrecan molecules to HA chains via a link protein. The sulfated glycosaminoglycans carry negative charges and establish a high negative fixed charge density in the cartilage tissue²⁴. This negative net charge attracts mobile counterions (e.g., Na^+ , Ca^{2+}) from the fluid phase to achieve electroneutral conditions inside the tissue. The resulting imbalance of mobile ions inside and outside the tissue leads to an osmotic pressure (Donnan pressure); this process is called interstitial fluid pressuriza-

tion and can be described by the triphasic theory²⁷. It combines the biphasic theory, accounting for the fluid and solid phase, with the physico-chemical theory for ionic and polyionic (proteoglycan) solutions²⁸. Due to the osmotic gradient, water is drawn into the tissue and the pressurized fluid inside the cartilage ECM is able to support up to 95 % of the applied load. This mechanism protects the EMC and contributes to the resilience of articular cartilage^{29,30}. Under constant loading or due to pathological changes in the proteoglycan concentration, the fluid exudes from the joint, and the load support is transferred to the ECM²⁴. To prevent this process and enable long-lasting daily joint loading, the point of loading migrates during movement over the cartilage surface and the loaded area can regain its fluid content after each loading cycle.

1.3.2. Biomechanics of articular cartilage

Cartilage is known for its superior low-friction properties but is also often described as a "spongy shock absorber" that protects the joint from high impact loads. In the human body, e.g., in the hip joint, cartilage experiences contact pressures of up to 10 MPa during normal activities²⁴. Under physiological conditions, cartilage is exposed to a combination of compressive, tensile and shear stresses at different frequencies. It is important to realize that the mechanical properties of articular cartilage vary depending on the species, age, joint, location in the joint and zone in the tissue.

With every joint movement, interstitial fluid is pressed out of the cartilage and soaked back into the tissue during unloading. This mechanism is an ongoing process as the contact point migrates over the cartilage surface. The dominant load support mechanism is interstitial fluid pressurization, which influences mainly the compressive properties of cartilage. The compressive load is dissipated due to frictional drag of the interstitial fluid trapped in the aggrecan network. Compressive Young's moduli between 0.24 and 0.85 MPa are reported for cartilage^{31,32}. Cartilage tension occurs as a side effect to compression when the surrounding regions are pulled towards the point of loading. The tensile properties are dominated by the collagen fibers, especially due to their arcadic alignment, and are nonlinear: At small deformations, the collagen fibers realign in the loading direction, whereas, at higher deformations, the crosslinked fibers begin to stretch, resulting in a higher tissue stiffness at larger strains. The tensile modulus of human articular cartilage varies between 5 and 25 MPa²⁴. The shear properties of cartilage depend on the interaction between the collagen fibers and the proteoglycan network. Especially the densely packed and horizontally orientated collagen fibers in the superficial zone optimize the resistance of the tissue towards shear forces. The shear storage modulus of cartilage varies between 0.2 and 2.5 MPa^{31,33}.

1.3.3. Tribology of articular cartilage

Friction and lubrication

The tribological properties of cartilage are outstanding and, mainly due to their multi-modal nature, not yet matched by any artificial system. To understand how a joint is able to function over several decades at ultra-low friction and with little wear, one has to consider the unique interplay between the material and the fluid phase constituents, especially in the boundary lubrication regime. At high speeds, in the elasto-hydrodynamic³⁴ and mixed regime, enough synovial fluid is available to form a thick lubricating fluid film.

However, at high contact pressures or decreasing sliding speeds, the fluid is slowly pressed out of the intra-articular space. As the lubricant can not instantly leave the gap due to viscous forces, pressure arises in the remaining fluid film and provides load support at least for a short duration. This process is called squeeze-film lubrication (Figure 1.7)³⁵.

Over time, a specific mechanism is necessary to maintain a continuous fluid layer between the joint surfaces to protect cartilage from high friction and wear. The highly hydrated articular cartilage itself does not dehydrate under ongoing loading due to interstitial fluid pressurization (Section 1.3.1). The tribological performance of cartilage depends on this process and the extent of exudation and rehydration³⁶ (biphasic lubrication). However, the microscopic phenomena leading to the formation of a thin hydrated protective layer on top of the material are still not fully understood. A variety of mechanisms have been described to compensate fluid that is squeezed out between the countering surfaces during loading (e.g., weeping³⁷ and boosted lubrication³⁸). Weeping lubrication assumes that pressurized fluid is slowly – due to interstitial fluid pressurization – pressed ("weeped") out of the cartilage matrix into the contact area. Boosted lubrication assumes that, due to joint loading, fluid is forced into the cartilage ECM, which effectively increases ("boosts") the concentration of boundary lubricant molecules confined at the articular surface.

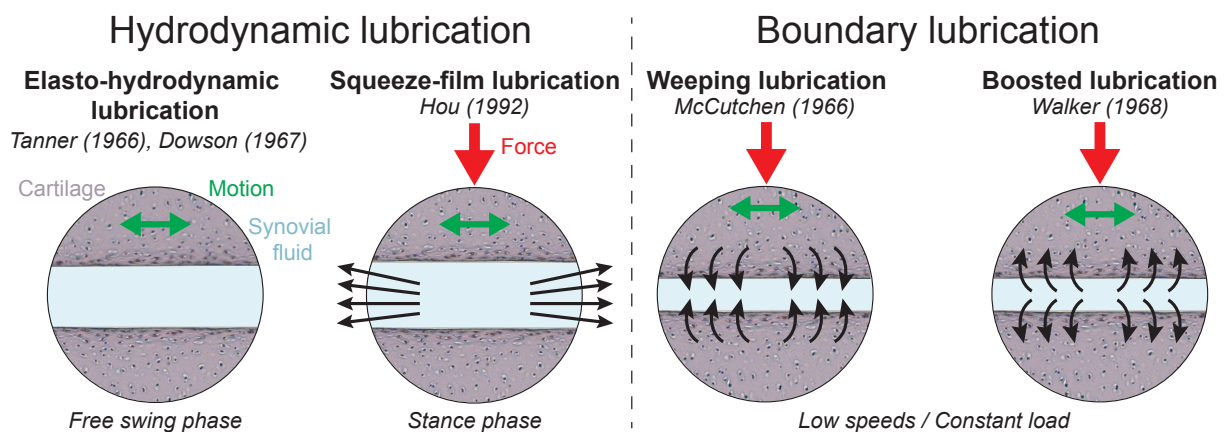


Figure 1.7.: Cartilage lubrication regimes: During a normal gait cycle, hydrodynamic lubrication³⁴ occurs at comparably high sliding speeds. In the free swing phase under low contact pressures, elasto-hydrodynamic lubrication dominates^{39,40}, whereas squeeze-film lubrication³⁵ occurs in the stance phase after heel strike when the contact pressure increases. Boundary lubrication⁴¹ is dominant at low sliding speeds, and different theories have been formulated to how a thin fluid film is maintained between the cartilage surfaces (weeping³⁷ and boosted lubrication³⁸).

In the long term, this process can only work efficiently as long as the fluid outflow is slowed down and the fluid film is stabilized at the surface. Therefore, a gel-like layer of adsorbed synovial fluid proteins, called lamina splendens (Section 1.3.1), is located at the cartilage surface, which is most likely stabilized by the polymer hyaluronic acid (HA). HA is not only the primary constituent of synovial fluid where it increases its viscosity, but has also been described to be able to entangle with the cartilage surface⁴², thus interacting with the collagen type II fibrils of the cartilage matrix⁴³. When trapped on the surface, HA facilitates the adsorption of proteins and phospholipids⁴⁴ from the fluid and solid phase (Figure 1.1b). The function of the adsorbed proteins, namely lubricin^{43,45}, fibronectin⁴⁶, collagen type II⁴³, aggrecan⁴⁷ and serum proteins^{36,48} (mostly albumin and globulin), has been widely discussed. The serum proteins have been described to regulate these adsorption processes⁴⁸. HA alone has been shown to be an insufficient

boundary lubricant⁴⁹ whereas the synergistic interaction of HA^{45,50} (potentially supported by fibronectin⁴⁶ and collagen type II⁴³) with cartilage proteoglycans (aggrecan and lubricin) seems to be a key mechanism in cartilage boundary lubrication. HA builds aggregates with aggrecans⁴⁷ and complexes with phospholipids⁴⁴. Moreover, HA films are known to collapse upon adsorption of lubricin as it physically crosslinks grafted HA⁵¹ and thereby acts as a surface-anchored protective layer⁵². The boundary lubrication potential of HA and lubricin was first reported at a latex-glass interface, where the presence of HA enabled lubricin to lubricate at higher contact pressures⁵³. Additionally, Seror *et al.*⁴⁷ found that aggrecan-HA complexes are much better boundary lubricants compared to HA alone.

There is increasing evidence^{36,47} that lubricin, aggrecans and phospholipids, stabilized at the cartilage surface by entangled HA and possibly fibronectin, mediate friction through hydration lubrication¹⁴ (Section 1.1.2, Figure 1.3). The proteoglycans and lipids trap water molecules at the surface. Under shear, energy can be dissipated by the exchange of these water molecules with free water molecules as well as by adsorption and desorption of the molecules themselves⁵⁴ (sacrificial layer mechanism⁵⁵). This theory is underlined by studies describing adsorbed synovial fluid components as a repulsive effective brush layer preventing interpenetration⁵¹ and adhesion⁵⁴ of the opposing surfaces under pressure⁴⁶. Klein *et al.*⁵⁶ described that especially the positively charged salt ions inside the hydration shell act as "ball bearings" as they are trapped between the negatively charged proteoglycan brushes and the negatively charged cartilage surfaces. The trapped fluid layer not only decreases the friction but also provides wear protection as it inhibits contact between surface aspirates and prevents potential cross-adsorption of molecules bridging the gap between the opposing surfaces. In summary, low friction and wear protection are established by a molecular system that is able to trap water at the surface, dissipates energy by adsorption and desorption under shear forces and protects the surfaces from each other by prohibiting cross-adhesion and interpenetration.

To explore the described lubrication mechanism of articular cartilage, measure friction coefficients under different conditions and explore the tribological properties of potential cartilage substitute materials, various test setups exist. Most setups are linear pin-on-disc tribometer operated with a reciprocal sliding motion (sliding length of $0 \text{ mm} < l < 35 \text{ mm}$ and sliding speeds of $0 \text{ mm s}^{-1} < v < 20 \text{ mm s}^{-1}$) at various contact pressures. Due to the viscoelastic nature of cartilage, mostly normal force controlled experiments are conducted. The two most commonly used material combinations are cartilage/cartilage and cartilage/glass. Tests are performed with either a constant or migrating contact point on the cartilage surface.^{48,57-60} Murakami *et al.*⁴⁸ performed a comparative study on the influence of the contact conditions on cartilage tribology. Reciprocating setups enable experiments on cartilage with a migrating contact and can therefore be used to simulate physiological condition. However, test setups with a stationary contact and continuous loading of the cartilage tissue can be used to evaluate the time-dependent changes of cartilage friction and, e.g., the effect of interstitial fluid pressurization on the tribological properties of cartilage. Moreover, this setup enables experiments over a broad range of sliding speeds compared to the reciprocating setup where inertia limits the sliding speed or rather large sliding length and large samples are necessary.

Wear

Cartilage wear can be subdivided into interfacial, fatigue and impact wear. In boundary lubrication, i.e., at direct contact between the opposing surfaces, interfacial wear arises mostly from two mechanisms: abrasion

and adhesion (Section 1.1.3)⁶¹. Compared to cartilage friction and lubrication, the origin and amount of cartilage wear is less investigated and understood¹⁸. Wear formation on articular cartilage surfaces is mostly reported based on the surface roughness, evaluated by confocal microscopy⁶² or atomic force microscopy⁶³. Friction measurements using immature bovine articular cartilage against alloys used in hip joint prostheses resulted in an increased cartilage surface roughness compared to tests against glass⁶⁴. However, after measurements against glass, delaminations in the cartilage surface (fatigue wear) were visible. Consistently, McGann *et al.*⁶⁵ reported that changes in surface roughness cannot be used as a predictable measure for cartilage wear.

The molecular mechanisms behind the wear resistance of cartilage have to date only been studied in model systems. Therefore, components of the synovial fluid, e.g., HA^{49,50,66} and fibronectin⁴⁶, were grafted or adsorbed to mica surfaces, and the interaction of these layers with other components, e.g., lubricin^{46,50}, HA⁴⁶ and serum proteins⁴⁶, was evaluated. The damage of the generated layers and tearing of the mica itself was thereby used as a measure for wear generation. Das *et al.*⁵⁰ reported that chemically grafted HA along with lubricin provided wear protection, whereas physisorbed HA in combination with lubricin was not able to reduce wear formation. Equiluz *et al.*⁴⁶ found that, although grafted fibronectin lubricated with equine synovial fluid resulted in the highest friction coefficient, it provided effective wear protection. However, lubrication with lubricin led to the most efficient wear protection of the mica surfaces and the lowest friction. Adhesive wear was described by Tadmor *et al.*⁴⁹; here, damage of the mica surfaces was observed when HA was physisorbed to both mica surfaces. In addition to the adsorption strength, the conformation of the lubricant molecule on the sliding surfaces has been reported to affect wear protection as lubrication with lubricin led to better wear protection on hydrophilic than on hydrophobic surfaces⁶⁷.

1.3.4. Osteoarthritis

Osteoarthritis (OA) is a joint disease that results in pathological degradation of articular cartilage and is worldwide the most frequent musculoskeletal condition. It has been suggested that the inflammation of the synovial membrane triggers a release of chondrotoxic proteins that leads to a progressive breakdown of cartilage tissue. Secondary causes of OA can be joint instabilities, meniscal lesions, malalignments, or genetic reasons. The most common symptoms of OA are joint pain and joint stiffness. Moreover, the resulting pain related functional impairment and limited perfusion can in turn accelerate the process of the disease.^{24,68}

In early (often subclinical) stages of OA, the fluid content of cartilage increases⁶⁹. Here, the aggregation ability and the concentration of proteoglycans decrease, which leads in combination with the loosening of the collagen network to a higher water content and tissue swelling²⁴. Hence, the fluid phase is no longer able to dissipate energy through interstitial fluid pressurization (Section 1.3), the physiological load support mechanism fails and the collagen matrix has to support the applied loads. This minimizes the resilience of the tissue and leads to an accelerated degradation of the collagen fibers during the onset of the disease. As side effects, the underlying subchondral bone changes as the fluid content increases and the degree of mineralization decreases. Cartilage degeneration can lead to inflammatory reactions of the synovium and the joint capsule as well as to fibrosis of the ligaments. Moreover, the impaired tribological function of cartilage often leads to damage of the menisci.²⁴

Treatment options of osteoarthritis include, in the early stages, nonsurgical interventions such as physical activity, behavioral and weight management as well as pain and anti-inflammatory medication. Viscosupplementation (Section 1.4.1), the administration of HA into the joint cavity, can be prescribed to treat mild to moderate OA. Surgical treatment strategies involve minimal invasive surgeries (debridement, microfracture, osteochondral autografting/mosaicplasty, autologous chondrocyte transplantation) and invasive surgeries (resurfacing implants, total joint replacements).^{24,68}

1.4. Macromolecular boundary lubricants

The joint cavity is filled with a viscous, shear-thinning, mostly acellular liquid called synovial fluid (~ 1 mL in a normal human knee joint). It is derived as an ultrafiltrate of blood plasma and provides nourishment, lubricity and waste removal. Synovial fluid maintains an ionic strength of around 140 mM⁷⁰ at a pH of 7.4⁷¹. It contains plasma proteins, e.g., albumin and globulin, the lubricant molecules HA, lubricin, fibronectin and surface-active phospholipids, proteolytic enzymes, inorganic salts and various other molecules, such as growth factors and cytokines.^{72–74}

The synovial fluid/cartilage system – though efficient – is not the most used lubrication system in the human body. On all epithelial surfaces, lubrication is mediated by mucus, a biopolymer-based hydrogel. Here, mucin, the main constituent of mucus and a glycoprotein similar to lubricin, is the lubricating molecule. In the following, key properties of all those lubricating macromolecules are summarized.

1.4.1. Hyaluronic acid

Hyaluronic acid (HA; also called hyaluronan, hyaluronate) is an anionic, non-sulfated, high-molecular weight glycosaminoglycan composed of D-glucuronic acid and N-acetyl-D-glucosamine. In contrast to other glycosaminoglycans, it is not synthesized in the Golgi apparatus but at the plasma membrane, which allows the production of chains with molecular weights exceeding 1 MDa²⁴. It has been reported that our body possesses an average total HA mass of 5 g with an one-third turn-over per day⁷⁵. HA is a component of the ECM and is involved in, e.g., the repair of skin tissue and the lubrication of joints.

In the synovial membrane, HA is secreted by fibroblast-like cells. Its physiological concentration in the synovial fluid ranges between 1 – 4 mg mL⁻¹ and the average molecular weight is 3 – 8 MDa. The high molecular weight influences the non-Newtonian properties of the synovial fluid and HA is the main reason for its high viscosity.^{76–80} In cartilage, HA is localized at the cartilage surface and can entangle with the collagen network, where it forms large proteoglycan aggregates together with aggrecan (Section 1.3). Moreover, it is concentrated around the lacunae of chondrocytes.^{24,81}

It has been reported that, under pathological conditions, synovial fluid has a reduced HA concentration (0.1 – 1.3 mg mL⁻¹)^{24,79} and partly also a decreased content of high molecular weight HA^{78,79}. Therefore, a non-surgical treatment option, called viscosupplementation, involves the administration of high molecular weight HA into the joint cavity. However, viscosupplementation of osteoarthritis has so far been approved by the U.S. Food and Drug Administration (FDA) only as a treatment option for knee joints⁸². This high-

lights the uncertainty of the success and exact mechanism behind this treatment. Many studies show that intra-articular injections can help relieve the symptoms, also when placebos such as saline are injected instead of HA solutions. Based on an analysis of overall 76 trials on the success of viscosupplementation, beneficial effects on pain, function and patient global assessment were prominent especially 5 to 13 weeks post injection⁸³. However, viscosupplementation with HA is regularly used during treatment of osteoarthritis in various joints although its benefit is highly disputed⁸⁴. Since *in vivo* HA complexes with proteins, e.g., lubricin, to build a viscoelastic network (Section 1.3.3)⁸⁵, recently cross-linked compounds became available and are clinically used.

1.4.2. Lubricin

Lubricin (proteoglycan 4; also called superficial zone protein), encoded by the *PRG4* gene, is a surface-active mucinous glycoprotein, which is expressed and localized on the articular cartilage surface and in the synovial fluid as well as in tendon, meniscus, lung, liver, heart, bone, muscular, ocular, and skin tissue. The protein has a molecular weight in the range of 227 – 345 kDa and contains a central region that is extensively modified by O-linked oligosaccharide side chains. At either side of the protein chain, globular unglycosylated domains are located (Figure 1.8a). In joints, lubricin is secreted by chondrocytes of the cartilage surface and synovial lining cells (synoviocytes). The concentration of lubricin in the synovial fluid is around $200 \mu\text{g mL}^{-1}$. As a coating on the cartilage surface and part of the lamina splendens (Section 1.3), it provides boundary lubrication and prevents cell and protein adhesion. Lubricin was found to bind specifically to the cartilage surface through its C-terminal (hemopexin-like) domain⁸⁶. However, lubricin is able to reduce friction not only between cartilage surfaces but also on synthetic surfaces, such as latex, mica and glass.^{87–90}

Reduced lubricin levels have been observed in synovial fluid from patients with anterior cruciate ligament injuries for up to 1 year post injury as well as in patients with established osteoarthritis^{87,91,92}. The recovery of the boundary lubrication function of synovial fluid through the supplementation with lubricin (tribosupplementation) has been shown *in vitro* with osteoarthritic synovial fluid⁹² and *in vivo* in an anterior cruciate ligament injury rat model⁹³. Tribosupplementation was also described to decrease the number of apoptotic chondrocytes, and to increase native lubricin expression compared to non-treated controls⁸⁷. These studies suggest lubricin as a therapeutic agent; however, it has so far only been tested clinically in eye drops treating the dry eye syndrome and tear film insufficiency^{94,95}.

1.4.3. Mucin

All wet epithelia in our body, including the eyes, lungs, gastrointestinal and urogenital tracts, are covered by a hydrogel called mucus. Its gel-forming building blocks are mucin glycoproteins. So far, around 20 mucin genes have been identified and can be divided into three groups: secreted gel-forming mucins, secreted non-gel-forming mucins and cell-surface mucins. Secreted gel-forming mucins, namely MUC2, MUC5AC, MUC5B, MUC6 and MUC19, are the major constituents of mucus and their concentrations can vary between 1 – 5 % wet wt., depending on the specific mucus localization and function⁹⁶. Secreted gel-forming mucins are produced by specialized epithelial cells and by glands located in the submucosal connective tissues^{97,98}.

They consist of a linear core molecule with a highly O-glycosylated central region, which contributes to its overall bottle-brush like structure (Figure 1.8b). The glycosylated region is flanked by cysteine-rich domains and a cysteine knot domain with non-repeating sequences at the C-terminus, and by von-Willebrand factor type D-like domains at the N-terminus. Whereas these domains are thought to be involved in blood clotting pathways, the C-terminal cysteine knot domain is believed to contribute to the dimer formation of the glycoprotein via a cystine (S–S) disulfide bond. The formed dimers further polymerize into larger oligomers, which increases the molecular weight from around 641 kDa⁹⁹ (monomer) to several MDa.^{97,98}

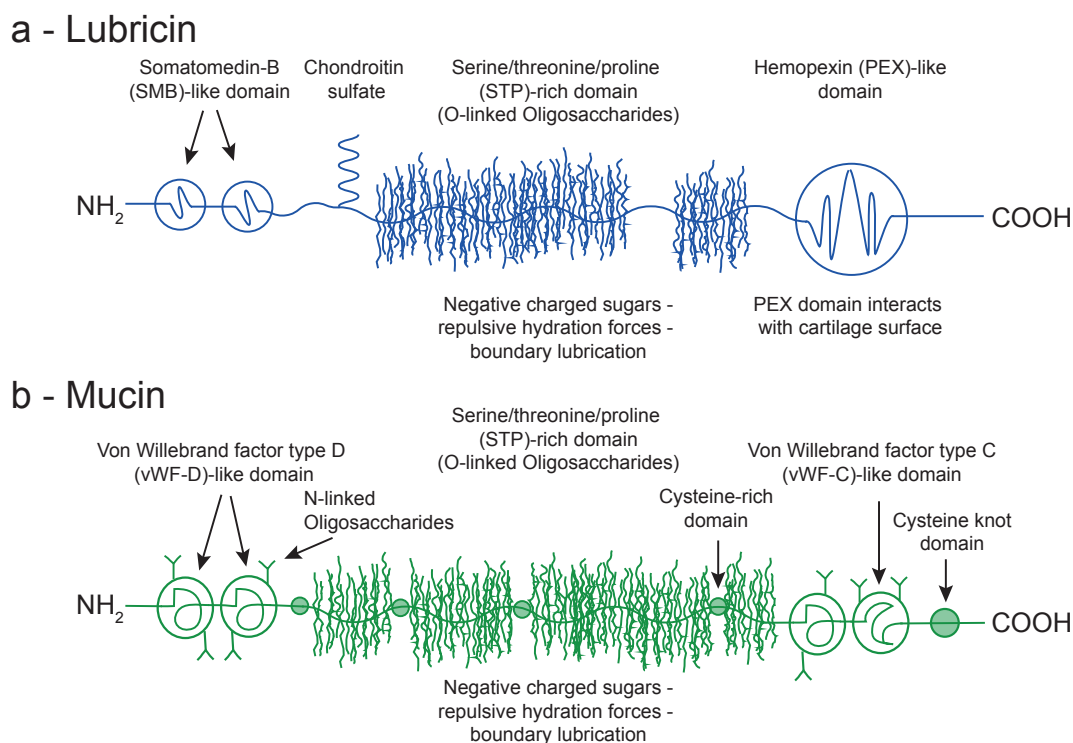


Figure 1.8.: Schematic structures of lubricin¹⁰⁰ and porcine gastric mucin⁹⁷. The two glycosylated proteins share a lot of similarities but also exhibit distinct differences. Specific to lubricin and important for its function as joint lubricant are, e.g., the chondroitin sulfate substitution site and the hemopexin-like domain, which is thought to mediate the interaction of lubricin with the cartilage surface. Mucins are secreted with a high molecular weight of around 641 kDa⁹⁹; in contrast, lubricin is with 227 – 345 kDa comparably smaller¹⁰¹.

Mucins can further form aggregates and the formation of gels (sol-gel transition) depends on the molecular weight and concentration of the polymer as well as on the temperature, pH and ionic strength of the surrounding medium. Porcine gastric mucin (PGM) contains two secreted mucins MUC5AC and MUC6 and purified PGM has been reported to form gels at concentrations above 10 mg mL^{-1} and at acidic pH ($\sim \text{pH } 4$)^{102,103}. PGM therefore shields the epithelial tissue from a typical $1 < \text{pH} < 2$ in the gastric lumen during active digestion¹⁰⁴. The viscoelastic non-Newtonian properties of mucin gels are crucial for their functionality: They build a protective layer against viruses¹⁰⁵, bacterial pathogens^{106,107} and toxic substances¹⁰⁸, act as a membrane for the exchange of gases and nutrients with the underlying epithelium, are involved in many disease processes, and finally lubricate and hydrate surfaces⁹⁸. The extensive glycosylation density of mucins enables especially the tribological functions of mucins. Mucin-associated glycans contribute up to 80 % of the molecular weight of the macromolecule and contain highly hydrated hydroxyl groups. Water typically accounts for up to 95 % of the total mass in a mucus gel. Shifts in the mucus water

content correlate with substantial changes of the mucus barrier function and result in important pathological disorders.^{97,98,109,110}

The ability of mucins to lubricate biological and synthetic surfaces¹¹¹ is facilitated by their tendency to adhere well to numerous materials, e.g., through electrostatic, hydrophobic, and H-bonding interactions¹⁰². Moreover, it has been reported for rat stomachs¹¹², that mucus comprises a loosely adherent outer layer and a firmly adherent layer attached to the epithelial surface. The shearing off of the outer layer during tissue loading might be, in addition to hydration lubrication (Section 1.1.2), a second energy dissipation mechanism to reduce friction (sacrificial layer mechanism), a process very similar to joint lubrication (Section 1.3.3).

1.5. Aims and objectives

The aim of this dissertation is to further the understanding of physiological lubrication strategies and specifically of the outstanding tribological properties of cartilage which are, up to now, unmatched by any artificial system. Therefore, the surface and bulk properties of cartilage are investigated as well as the fluid phase of the tissue, the lubricating fluid (synovial fluid) and their well-orchestrated interactions. These investigations are conducted by applying loss of function and consecutive gain of function principles to identify the crucial molecular components that are responsible for the extraordinary material properties of cartilage. A long-term motivation is to guide the path for the development of cartilage substitute materials or surface coatings for joint prostheses. Furthermore, new biomimetic materials, which are designed based on our understanding of physiological lubrication strategies, could further the development of bearings and various other material surfaces that undergo constant loaded movement, e.g., contact lenses.

To examine the properties of the cartilage bulk and fluid phase and to quantify the resilience of the tissue to ongoing loading, the tissue is dehydrated and consecutively rehydrated with fluids of different ionic strength (Section 3.2). The influence of the ionic strength of the interstitial fluid on cartilage friction and wear is further evaluated on different length scales using atomic force microscopy and macro-friction experiments (Section 3.3). HA solutions are used as a lubricant to assess the mechanism governing viscosupplementation.

To understand the microscopic mechanisms involved in hydration lubrication and specifically in mucin lubrication, the ability of porcine gastric mucin to hydrate synthetic surfaces and reduce friction is analyzed (Section 3.4). Mucins are examined in their native state as well as after complete deglycosylation and subsequent repair with lectin-PEG motifs. In a last step, the influence of different biopolymers present on the cartilage surface (hyaluronic acid and mucin) on cartilage friction and wear is investigated and it is asked whether mucin can act as a substitute lubricant in cartilage tribology (Section 3.5).

2. Materials & Methods

A number of the materials and methods discussed here have been described in detail in the methodology paper (Section 3.1).

2.1. Articular cartilage

Articular cartilage is a very complex structured material (Section 1.3.1) and varies depending on the species, type of joint and even depending on the location in the joint. The usage of human cartilage would have been optimal to ensure the knowledge transfer of results gained here to clinical practice. However, owing to the limited availability of human tissue, ovine cartilage was utilized as sheep are commonly used for large animal studies on cartilage repair^{113,114}. Ovine cartilage was obtained from reliable sources: Bayerische Landesanstalt für Landwirtschaft (LfL), Institut für Tierzucht (Grub/Poing, Germany) and the Metzgerei Boneberger (Freising, Germany). All tested samples originated hence from animals which were raised in a similar manner and had the same gender and age. This helped to keep the sample-to-sample variations relatively low and allowed for quantitative comparisons of tissue parameters. The knee joints (hinder legs) from 3 to 6 month old male lambs were obtained with closed articular joint capsules, frozen and stored at -20°C until further usage.

Since the cartilage-bone interface has been described to influence the properties of cartilage³⁶, all tests were conducted using osteochondral cylinders. Moreover, this allowed to test the cartilage surface in an unconfined geometry as the samples could be mounted by clamping the bone tissue. For sample preparation (Figure 2.1), the joints were thawed at 4°C overnight. The joint capsule was opened directly prior to sample preparation and the trochlear groove behind the patella was exposed. Osteochondral cylinders were harvested from both the lateral and medial side of the trochlear groove. A hollow cylindrical drill was used to drill osteochondral cylinder with diameters of either 5.5 mm or 8 mm perpendicular to the cartilage surface. The samples were detached from the underlying bone by performing horizontal cuts using an oscillating saw and, to ensure identical initial sample conditions, incubated for at least 1 h in either 20 mM HEPES

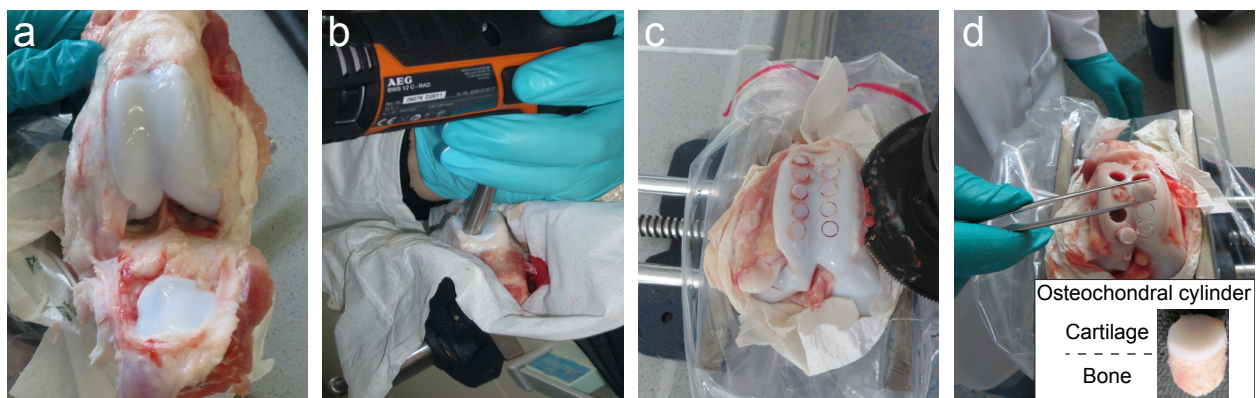


Figure 2.1.: Osteochondral cartilage preparation procedure: The closed knee joint was opened and the trochlear groove identified (a). Osteochondral cylinders were generated with a hollow drill (b) and removed from the joint using an oscillating saw (c). Finally, the samples were extracted with tweezers (d).

with 154 mM NaCl or in PBS.

The friction measurements between two cartilage surfaces were conducted at the University of Calgary in the laboratory of Prof. Tannin Schmidt. For these measurements, skeletally mature bovine knee joints were obtained and osteochondral cylinders were harvested from the trochlear groove according to a standard procedure described previously¹¹⁵. Briefly, annuli (diameter: inner = 3 mm, outer = 6.4 mm) and cores with a diameter of 12 mm were drilled using a drill press. Afterwards, they were rinsed overnight in PBS at 4 °C and frozen in PBS at –80 °C until further usage. Prior to testing, the samples were shaken overnight in PBS at 4 °C.

2.2. Lubricants

Different lubricants were tested on artificial materials and articular cartilage to investigate their ability to reduce friction and prevent wear. Synovial fluid components, specifically lubricin and hyaluronic acid, were compared to a commercial viscosupplement. Moreover, porcine gastric mucin, a glycoprotein and major component of mucus, was used. Mucins lubricate epithelial tissues but do not physiologically occur on joint surfaces or in the synovial fluid.

2.2.1. Lubricin

Lubricin (Section 1.4.2) was purified from fresh skeletally mature bovine knee joints (Calgary, Canada), as described previously¹¹⁵. Briefly, bovine cartilage discs were cultured in Dulbecco's Modified Eagle's Medium and purified using salt gradient diethylaminoethanol anion exchange chromatography. The purity of the solution was confirmed using 3 – 8 % Tris-acetate SDS-PAGE followed by a Simply Blue protein stain and densitometry analysis.

2.2.2. Hyaluronic acid

Hyaluronic acid (HA, Section 1.4.1) was purchased from Sigma-Aldrich (Hyaluronic acid sodium salt from *Streptococcus equi*, USA) with a molecular weight of 2 – 2.4 MDa.

2.2.3. Sinovial

One of the many commercially available viscosupplements (Section 1.4.1) is Sinovial (Humantis, Germany). It consists of 0.8 % (wt/vol) HA with a molecular weight between 0.8 and 1.2 MDa in a physiological sodium chloride solution. A meta-study investigating the effect of Sinovial claims that 3 to 5 weekly injections can reduce joint pain and disabilities¹¹⁶.

2.2.4. Porcine gastric mucin

Porcine gastric mucin (PGM, Section 1.4.3) was purified as described previously¹¹⁷ with the exception that the cesium chloride density gradient ultracentrifugation was omitted. Briefly, mucus was collected by scraping the surfaces of pig stomachs. The extracted mucus was dissolved in phosphate buffered saline (10 mM, 170 mM NaCl adjusted to pH 7.4) and purified by a series of centrifugation and size exclusion chromatography steps. Afterwards, the solution was concentrated and desalted by cross-flow dialysis until a conductance of less than 50 μS was reached. Finally, the obtained mucin MUC5AC was stored in lyophilized form at -80°C until further use. The successful purification of MUC5AC was verified with the same enzyme-linked immunosorbent assay as used for the adsorption measurements (Section 2.5.4).

2.3. Mechanical characterization

To investigate the complex viscoelastic material behavior of articular cartilage, a plethora of different mechanical characterization techniques is necessary. As a consequence, a broad range of applied testing strategies and utilized laboratory equipment is described in the literature so far. However, the experimental results are often highly dependent on the applied measurement technique, but only rarely identical techniques and measuring protocols are applied in more than one study. Here, a commercial shear rheometer (Figure 2.2b, MCR 302, Anton Paar, Austria) was adapted by in-house crafted sample holders and measuring heads in such a way that it can be used as a convenient platform to conduct a broad range of precise and well-defined material characterization tests in one single setup.

The rheometer consists of a lift drive, a drive unit, a measuring head and a measuring unit. The drive unit (Figure 2.2a) is comprised of an optical rotary encoder to measure angular displacements φ and calculate the shear strain γ , an EC motor to induce a torque M and apply a certain shear stress τ to the sample, and an air bearing that minimizes the internal friction and allows for very low torque applications. A force sensor is located in between the drive unit and the measuring head to measure the normal force F_n and calculate the compressive stress σ . The position of the measuring head in the vertical plane (gap g), and thereby the compressive strain ε applied to the sample, is controlled through the lift drive. The measuring head is chosen based on the measurement type. Different plate and cone geometries are commercially available, but the measuring head can also be customized by using a measuring head adapter (Figure 2.3a). The lower counter part to the measuring head is an exchangeable measuring unit. Depending on the application, either a simple plate or a more complex setup, e.g., the tribology cell, is utilized.

Prior to each measurement, the thickness of the cartilage layer d_0 was evaluated for every osteochondral cylinder on four points of the contour using a caliper (digital caliper, DIN 862). Moreover, the rheometer can be used to precisely track changes in cartilage thickness over time¹¹⁸.

2.3.1. Indentation measurements

For indentation measurements, the shear rheometer was equipped with a custom-made sample holder (Figure 2.2c), which can be mounted onto the rheometer bottom plate (P-PTD 200/56/AIR, Anton Paar, Austria).

A customized indenter (Figure 2.3a) with a diameter $d = 2r$ of 4.2 mm was inserted into the measuring head adapter (D-CP/PP 7, Anton Paar, Austria). The osteochondral cylinders were clamped inside the sample holder and were tested while being fully immersed. The measuring head was lowered with an indentation speed of $1 \mu\text{m s}^{-1}$, and each cartilage sample was indented until a time limit of 4 min or a force limit of $F_n = 40 \text{ N}$ was reached. The indentation stiffness E (Equation 2.3) was calculated using a linear fit to the acquired compressive stress σ (Equation 2.1) and strain ε (Equation 2.2, Figure 2.2c) data.

$$\sigma(t) = \frac{F_n(t)}{\pi r^2} \quad (2.1) \quad \varepsilon(t) = \frac{g_0 - g(t)}{d_0} \quad (2.2) \quad E = \frac{\sigma}{\varepsilon} \quad (2.3)$$

To investigate the viscoelastic compressive properties of cartilage, a dynamic experiment (Section 1.2) would be necessary. However, the rheometer is not equipped with a piezo element for oscillations in the vertical plane, which prevented dynamic indentation measurements.

2.3.2. Oscillatory shear measurements

Dynamic measurements using the rheometer are possible in the horizontal plane, as the rheometer is developed for rheological shear measurements and thus for very precise horizontal oscillations. The rheometer was equipped with a parallel plate measuring head with a diameter $d = 2r$ of 8 mm (PP08, Anton Paar, Austria) and the custom-made sample holder similar to the setup used for the indentation measurements (Figure 2.2c and Figure 2.3b). In oscillatory shear measurements, the elastic (storage modulus G' , Equation 2.8) and viscous (loss modulus G'' , Equation 2.9) material response was determined for different frequencies f . An oscillatory strain $\gamma(t)$ (Equation 2.6) was applied to the sample and the material response, the resulting shear stress $\tau(t)$ (Equation 2.7) and phase lag $\delta(f)$ (Figure 2.2c, inset), was measured. The shear stress is defined as the product of the torque and a geometry specific shape factor A (Equation 2.5).

$$\gamma_0 = \frac{r\phi}{g} \quad (2.4) \quad \tau_0 = MA = \frac{2M}{\pi r^3} \quad (2.5)$$

$$\gamma(t) = \gamma_0 \sin(2\pi ft) \quad (2.6) \quad \tau(t) = \tau_0 \sin(2\pi ft + \delta) \quad (2.7)$$

$$G'(f) = \frac{\tau_0}{\gamma_0} \cos(\delta) \quad (2.8) \quad G''(f) = \frac{\tau_0}{\gamma_0} \sin(\delta) \quad (2.9)$$

In a pre-measurement, the smallest shear strain amplitude γ_0 resolvable and controllable by the rheometer with the given setup was determined to ensure that further measurements are conducted in the linear-elastic regime. Therefore, a torque of $0.5 \mu\text{N m}$ was applied at a frequency of 1 Hz and the resulting strain was measured. Then, a slightly larger strain amplitude (typically $\gamma_0 = 0.001 \%$) was chosen for the main experiment, the frequency sweep, which was performed between 10 Hz and 0.1 Hz at room temperature and a normal force of 1 N. This normal force was chosen as the minimal force at which visual inspection of the sample/measuring head interface suggested full contact. Since cartilage exhibits creep (Section 1.2), a normal-force controlled measurement is necessary to ensure full contact between the sample surface and the

measuring head.

It is important to realize that the measured shear strain amplitude γ_0 depends on the gap g between the sample plate and the measuring head (Equation 2.4). For calculating the complex dynamic shear moduli (G^* , Equation 2.10), the software (Rheoplus, Anton Paar, Austria) assumes that this gap is equal to the sample thickness d , which does not hold true in our customized configuration. With our setup, the gap is equal to the sum of the sample holder height and the cartilage thickness (Figure 2.2c). Moreover, at a constant normal force, the tissue creeps and the cartilage thickness decreases over time. Accordingly, the shear strain amplitude needs to be corrected for each frequency, i.e., by multiplying it with the ratio of the actual cartilage thickness and the current gap position (Equation 2.11).

$$G^* = G' + iG'' \quad (2.10) \quad G_{\text{corrected}}^*(f) = G_{\text{uncorrected}}^*(f) \frac{d_0 - (g_0 - g(f))}{g(f)} \quad (2.11)$$

2.3.3. Viscosity measurements

The lubricant viscosities (η) were measured using a cone-plate setup on the rheometer (Figure 2.3c). Therefore, the planar bottom plate (P-PTD 200/56/AIR, Anton Paar, Austria) was combined with a conical measuring head ($d=25$ mm, $\alpha=1^\circ$, CP 25-1, Anton Paar, Austria). A volume of 80 μL was pipetted onto the measuring plate, and the measuring head was lowered to a gap of 50 μm . At this position, the gap between the plate and cone was completely filled with the test solution. Before the actual experiment, the measuring head was rotated at 1000 s^{-1} for 40 s. Afterwards, the viscosity was measured using a logarithmic speed ramp with rotational speeds n from 1000 s^{-1} to 1 s^{-1} with 5 measuring points per decade and a measuring point duration of 10 s. The applied torque was recorded and the viscosity calculated as the ratio of the shear stress τ and the shear rate $\dot{\gamma}$ (Equation 2.14). Here, the shear stress is defined as the product of the torque M and the geometry specific shape factor A for the cone-plate setup (Equation 2.12).

$$\tau = MA = \frac{3M}{2\pi r^3} \quad (2.12) \quad \dot{\gamma} = \frac{2\pi n}{\tan(\alpha)} \quad (2.13) \quad \eta = \frac{\tau}{\dot{\gamma}} \quad (2.14)$$

2.4. Tribology experiments

All friction measurements, except the cartilage/cartilage tests, and the experiments for wear generation, were conducted using the same instrument as utilized for the mechanical characterization experiments. Here, the shear rheometer (MCR 302, Anton Paar, Austria) was equipped with a tribology cell (T-PTD 200, Anton Paar, Austria). The friction coefficient μ is calculated as the ratio between the friction force F_f and the normal load F_1 (Equation 2.15, Section 1.1.1).

$$\mu = \frac{F_f}{F_1} \quad (2.15)$$

Friction experiments with both setups were conducted under constant contact conditions and the samples

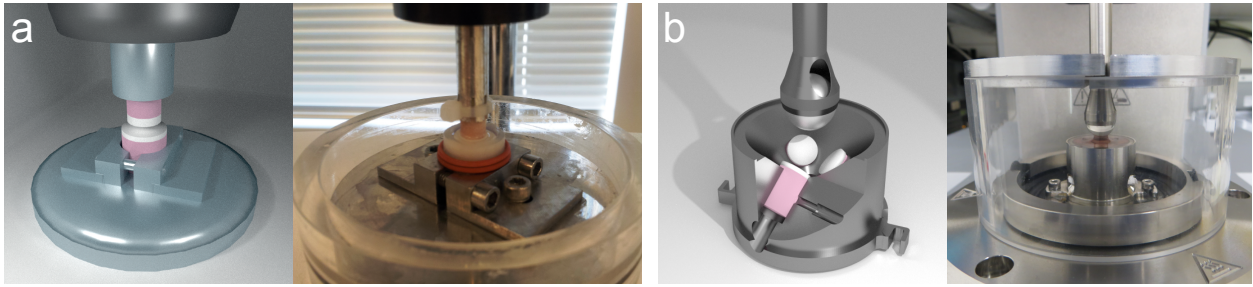


Figure 2.4.: Friction measurement setups: For the cartilage/cartilage friction tests (a), the bigger osteochondral cylinder was pressed into a plastic tube, which also holds the lubricant, and fixed with set screws. The smaller osteochondral cylinder was pressed into a metal tube and fixed with a lace. For glass/cartilage friction tests (b), the osteochondral cylinders were placed into the sample holder and fixed with set screws. The glass sphere was pressed into the measuring head.

were tested fully immersed. The constant contact condition was favored over the more physiological moving contact (established by linear tribology setups) as the boundary lubrication ability of lubricants over time can only be accessed with a constant contact (Section 1.3.3). To ensure comparability between the performed rotational measurements and other measurements performed with linear tribology setups, here the angular velocities (s^{-1}) are reported as "rotational speeds" reflecting the peripheral speeds of the spheres ($mm s^{-1}$). The time-dependent changes in cartilage friction were observed by conducting several measurements in a row, each with a constant rotational speed over a test period of 1 h. This measuring procedure was necessary because the friction coefficient of cartilage increases under constant contact over time owing to the decreasing interstitial fluid pressurization inside the cartilage tissue (Section 1.3). With synthetic material pairings, logarithmic speed ramps were performed to generate classical Stribeck curves (Section 1.1.2, Figure 1.2).

2.4.1. Cartilage/cartilage friction setup

Friction measurements between two cartilage surfaces were conducted using a previously described cartilage/cartilage friction test setup on a Bose ELF 320028 (TA Instruments, USA; Figure 2.4a). The samples were compressed to 18 % of the total thickness and allowed to stress-relax for 40 min. The friction test was then performed under displacement control at an effective velocity of 0.3 mm s^{-1} for ± 2 revolutions and a pre-sliding duration of 1.2 s between the rotations. The kinetic coefficient of friction was calculated from the second rotation in both the forward and backward direction. An effective radius r_{eff} of 2.44 mm, based on the inner radius r_i and outer radius r_o of the cartilage annuli, was used for the calculation of the friction coefficient (Equation 2.16). The samples were subjected to two friction tests on two consecutive days. Each sample set was first tested in PBS, as a negative control, then incubated in the test lubricant (i.e., either lubricin or mucin) overnight and measured again with this test lubricant. Three sample sets were tested for each lubricant.

$$r_{\text{eff}} = \frac{2}{3} \frac{(r_o^3 - r_i^3)}{(r_o^2 - r_i^2)} \quad (2.16)$$

$$F_f = \frac{M}{r_{\text{eff}}} \quad (2.17)$$

$$F_l = F_n \quad (2.18)$$

2.4.2. Glass/cartilage friction setup

Friction measurements using cartilage and glass as tribo-pairing were conducted using the shear rheometer. A glass sphere (diameter $d = 2r = 12.7$ mm, soda-lime glass, Kugel Pompel, Austria) was rotated on the cartilage surfaces of three osteochondral cylinders with a contact pressure of approximately 0.1 MPa (Figure 2.4b). The contact pressure was chosen based on literature values for *in vitro* friction tests^{30,55}. The physiological contact pressure in the trochlear groove is comparably higher, e.g., between 1.5 and 5 MPa during joint bending¹¹⁹. The friction coefficient was measured at rotational speeds of 0.01 mm s^{-1} , 0.1 mm s^{-1} , 1 mm s^{-1} , 10 mm s^{-1} and 50 mm s^{-1} in an arbitrary order over a time span of 1 h for each speed level with an unloading time of 30 min in between the measurements. For evaluation, the initial (averaged over the first 10 s of the measurement) and final friction coefficient (averaged over the last 10 s of the measurement) are reported. The friction coefficient was calculated as the ratio between the friction force F_f (Equation 2.19) and the normal load F_l (Equation 2.20), which are both corrected for the 45° angle α between the sample surfaces and the horizontal plane.

$$F_f = \frac{M}{r \sin(\alpha)} \quad (2.19)$$

$$F_l = \frac{F_n}{\cos(\alpha)} \quad (2.20)$$

2.4.3. Wear generation

To investigate wear generation on the cartilage surface, the glass/cartilage setup as described above was used and the glass sphere was rotated on top of three osteochondral cylinders with a rotational speed of 0.1 mm s^{-1} for 1 h. This speed level was chosen to investigate the performance of the lubricants in the boundary lubrication regime. The chosen rotational setup reduces the possibility of stick-slip friction (Section 1.1.1), mostly observed with oscillatory measurements, and thereby potential wear formation due to this particular phenomenon⁵².

2.4.4. Steel/PDMS friction setup

Friction measurements with PDMS and steel as a tribo-pairing were conducted using the same setup as described for the glass/cartilage tests. Instead of osteochondral cylinders, PDMS cylinders were manufactured by mixing PDMS (SYLGARD 184, Dow Corning, USA) in a 10:1 ratio with the curing agent and exposing the mixture to vacuum for 1 h to remove air bubbles before curing at 80°C for 1 h. Subsequently, the cylinders were punched out of the PDMS using a rotating hollow punch (diameter: 6.5 mm). The hollow punch was inserted into a press drill and rotated while punching the samples. This procedure ensured smooth lateral surfaces of the PDMS cylinders and prevented ruptures in the PDMS. Before each measurement, the cylinders were cleaned with 80 % ethanol and ddH₂O. During the measurement, a steel sphere with a diameter of 12.7 mm (stainless austenitic steel 1.4401, Kugel Pompel, Austria) was rotated on top of the cylinders with a contact pressure of approximately 0.1 MPa. Three consecutive logarithmic speed ramps were conducted by ramping the speed up or down between 1400 mm s^{-1} and 0.01 mm s^{-1} with a measuring point duration of 10 s and ten measuring points per decade.

2.5. Structural characterization

Different techniques were applied to quantify the structure of articular cartilage (Section 1.3.1): Histology was used to observe the overall tissue structure and the glycosaminoglycan content. A 1,9-dimethylmethylene blue assay was performed as a quantitative measure for the glycosaminoglycan content. Scanning electron microscopy and profilometric images were acquired to image the cartilage surface structure. Further surface analysis was conducted on all materials used for tribology: An enzyme-linked immunosorbent assay was used to determine the adsorption of mucin to different material surfaces.

2.5.1. Histology

Cartilage samples used for histological analysis were fixed in a 4 % buffered formalin solution (Roti-Histofix, Carl Roth, Germany) for 72 h, washed, decalcified in a 25 % EDTA solution for 48 h, dehydrated in an increasing ethanol series, and finally embedded in paraffin (Tissue-Tek TEC 5, EM E-2 5230, Sakura, USA). Histological sections with a thickness of 5 μm were sliced using a microtome (RM 2165, Leica, Germany) with a reusable knife (16 cm, profile c, Leica, Germany), transferred into a tissue floating bath, taken up onto microscopic slides (Superfrost Plus, Thermo Scientific, Germany), and dried on a heating plate overnight. Before staining, the slides were deparaffinized in Roti-Histol (Carl Roth, Germany) and rehydrated in a decreasing ethanol series. After staining, the slides were rinsed in ddH₂O, dehydrated in an increasing ethanol series followed by incubation in Roti-Histol for 5 min and 15 min, and sealed by covering them with Roti-Mount (Carl Roth, Germany) and a cover glass. Images were acquired using an Axioskop 2 plus (Zeiss, Germany).

Hematoxylin and eosin stain

Hematoxylin and eosin (H&E) stains (Figure 1.6b) were used to evaluate the overall tissue morphology and cell distribution. The staining colors collagen in pale pink, and cell nuclei in blue. The slides were incubated in Mayer's Hämalaun (Hemalum solution acid acc. to Mayer, Carl Roth, Germany) for 5 min, washed under running tap water for 13 min and incubated in Eosin Y (Carl Roth, Germany) for 5 min.

Safranin-O/fast green stain

Safranin-O/fast green stains (Figure 1.6b) were used to examine the glycosaminoglycan distribution. The staining colors proteoglycans in red, cytoplasm in green and cell nuclei in blue. The slides were incubated in Weigert's Iron Hämalaun (Hematoxylin solution A&B acc. to Weigert, Carl Roth, Germany) for 5 min, washed in ddH₂O four times for 3 min, and rinsed once in a 1 % acid-alcohol solution and three times in ddH₂O. Afterwards, the slides were incubated in Fast green FCF (Carl Roth, Germany) for 5 min, in a 1 % acetic-acid solution for 30 s, and in Safranin O (Carl Roth, Germany) for 30 min.

2.5.2. 1,9-Dimethylmethylene blue assay

A 1,9-dimethylmethylene blue (DMMB) assay²⁴ was used to quantitatively determine the sulfated glycosaminoglycan (sGAG) content of the cartilage samples. The dye complexes with sGAGs, which reduces the intensity of the two absorbency bands of the dye and creates a third absorbency band at 525 nm, the so called mu-band (Figure 2.5b). The intensity of the mu-band is within a certain range linear to the concentration of created complexes, allowing to quantify the sGAG concentration.

Following the procedure described in the manual of a commercial kit¹²⁰ (Biocolor Ltd, United Kingdom), the cartilage layer was dissected from the bone segment, and the tissue wet weight was determined. The sample was snap frozen and lyophilized, and the dry weight was measured. Subsequently, each specimen was immersed in 2 mL of papain solution (papain from papaya latex, Sigma-Aldrich, USA) for 18 h at 60 °C and stored at −80 °C. The cartilage digestion by papain was necessary as the cartilage extracellular matrix is a dense network and not accessible for the dye. Papain is an unspecific cystein protease. By cleaving the link protein, it fully separates the aggrecan from the hyaluronic backbone. Furthermore, the collagen network and the HA molecules are fragmented, which facilitates the binding of the dye to the sulfated glycosaminoglycans of aggrecan. After the digestion step, the sample solution was added to the DMMB solution, mixed, and the absorption was measured at 525 nm (Specord 210, Analytic Jena, Germany). Dilutions of chondroitin-6-sulfate sodium salt (Chondroitin sulfate sodium salt from shark cartilage, Sigma-Aldrich, USA) were used as standards (S_1 – S_5 , Figure 2.5b).

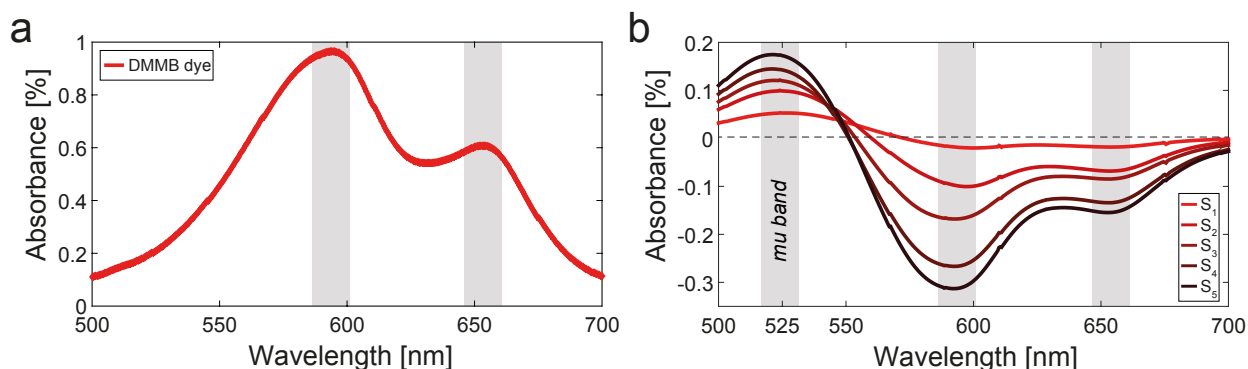


Figure 2.5.: Absorption spectra of the DMMB assay. Two distinct bands (maxima) are visible in the absorption spectra of the DMMB dye (a). The deviations in absorption between the spectrum of the dye and the spectrum of the five standard solutions (S_1 – S_5), with increasing chondroitin sulfate concentrations, are depicted in (b). Here, the third band, the so called “mu band”, is visible.

2.5.3. Scanning electron microscopy

Scanning electron microscopy (SEM; JEOL–JSM–6060LV, Jeol, Germany) was used to qualitatively evaluate changes in the sample surface structure. Before imaging, samples were fixed in 2.5 % glutaraldehyde in 0.05 M HEPES (pH 7) for 2 d, washed, dehydrated in an increasing ethanol series, critical-point dried (EPD 030, BAL–TEC, Liechtenstein), and sputtered with gold (MED 020, BAL–TEC, Liechtenstein). Images were acquired at an acceleration voltage of 5 kV and a spot size of 30 nm.

2.5.4. Adsorption measurements

Mucin adsorption to the different material surfaces used during the tribological measurements was quantified via an enzyme-linked immunosorbent assay (ELISA). Therefore, small glass (soda-lime glass), steel (stainless austenitic steel 1.4401) and PDMS (SYLGARD 184, Dow Corning, USA) platelets with a length of 10 mm, a width of 5 mm and a height of 1 – 3 mm were manufactured and small cartilage pieces were harvested as described before (Section 2.1). The samples were incubated in a 0.1 % (wt/vol) mucin solution for 1 h, washed extensively in PBS-TWEEN (1 % (wt/vol) TWEEN 20) and incubated in blocking buffer containing 5 % (wt/vol) powdered milk (Carl Roth, Germany) in PBS-TWEEN, at 4 °C overnight. Afterwards, the platelets were incubated for 1 h in either the mucin antibody (anti-MUC5AC, oligomeric mucus/gel-forming, antibodies–online, Germany) or the isotype control (IgG1 isotype control from murine myeloma, Sigma-Aldrich, USA). As a secondary antibody, goat anti-mouse (Murine) IgG (Heavy & Light Chain) antibody HRP (antibodies–online, Germany) labeled with horseradish peroxidase was used (2 h incubation time). Subsequently, o-phenylenediamine (Sigma-Aldrich, USA) was added to this mix and converted by the horseradish peroxidase. The reaction product was determined spectrophotometrically (Victor 3, PerkinElmer, USA). The measured absorption was corrected for the slightly different surface areas of the test platelets.

2.5.5. Profilometer measurements

Following the friction tests for wear generation (Section 2.4.3), the cartilage surfaces were investigated using an optical profilometer (μ surf custom, nanofocus, Germany) with a 20x objective (Zeiss, Germany).

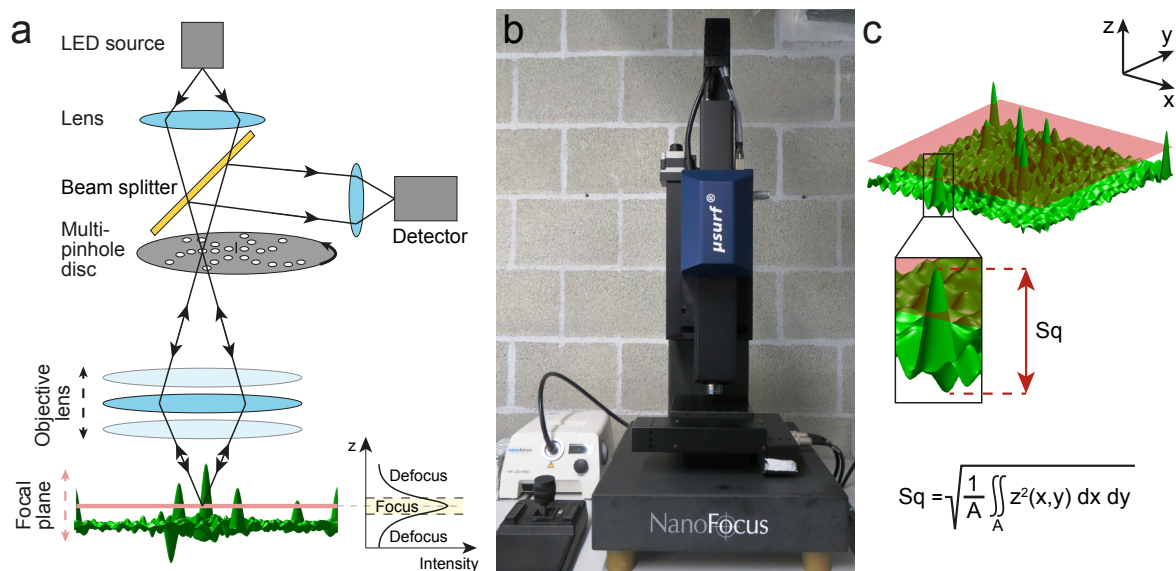


Figure 2.6.: Optical profilometer: measuring principle, setup and quantitative image analysis. The μ surf custom profilometer (b) is equipped with a multi-pinhole disc, which enables fast and precise imaging of the sample surface (a). The focal plain is determined by moving the objective lens in the vertical plane and measuring the maxima of the reflected light intensity. The collected images contain 3-dimensional data (x,y,z), which enable a quantitative image analysis of the surface topography (c). The root mean square roughness (Sq) is a standard parameter to compare the roughness of surfaces.

The profilometer comprises a LED light source, a rotating multi-pinhole disc, an objective lens with a piezo drive, and a CCD camera (Figure 2.6a). The LED light is focused onto the sample surface through the multi-pinhole disc and the objective lens. The multi-pinhole disc is a disc with a large number of pinholes arranged in a special pattern. Only light reflected by objects in focus can pass the pinholes of the rotating disc and is detected by the CCD camera. This enables a vertical resolution in the nanometer range as scattered light is eliminated. The sample surface in focus is scanned in the horizontal direction by rotating the multi-pinhole disc. Compared to the classical line-scanning technique, as, e.g., applied in scanning electron microscopy, this approach is faster and leads to less artifacts. To capture a three-dimensional image of the sample surface (Figure 2.6c), the focal plane can be shifted by moving the objective lens in the vertical direction.¹²¹

For imaging, samples were removed from the lubricant and carefully rinsed in PBS. Afterwards, the samples were exposed to air for approximately 10 min until the surface was mostly free of water droplets. For each sample three images were acquired at arbitrary locations where no or only few droplets were visible in the microscopic image. Image analysis was therefore performed on a total of 27 images for each lubricant. The resolution of the images was $1.56\ \mu\text{m}$ in horizontal and $0.22\ \mu\text{m}$ in vertical direction. After the measurements, the images were corrected for sample tilt by applying a linear polynomial correction (μsoft version 6.0, nanofocus, Germany).

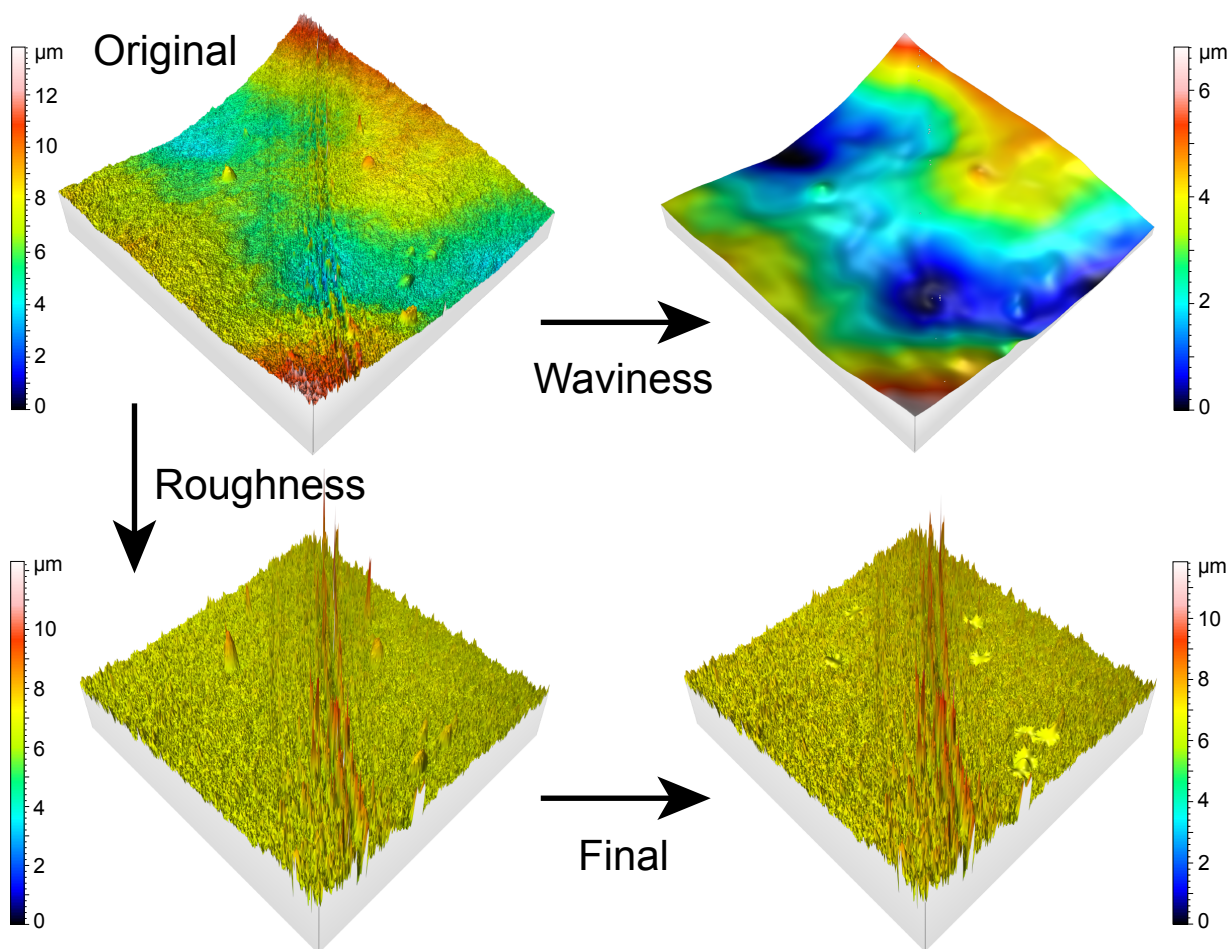


Figure 2.7.: 3D images of surface topography: after imaging, filtering and adjustments. The original image is shown after correction for sample tilt. Next, a Gaussian filter is applied and the waviness and roughness profiles are separated. Finally, the roughness profile is corrected for water bubbles and void points.

Image analysis (Figure 2.7) was performed using the software μ soft analysis extended V7 (nanofocus, Germany). To analyze surface features generated by the friction measurement, the surface waviness of the samples was removed by applying a Gaussian filter (ISO 16610–61) with a cut-off wavelength of 80 μm . The image was cropped after filtering to remove generated edge artifacts. In a second step, the void points in the image were automatically filled by the software. A manual step was necessary to remove some remaining water bubbles, which should not be considered as sample surface features. Therefore, corresponding spots on the image were manually smoothed. Finally, surface parameters were calculated from the resulting topographical image. The following ISO 25178–2 parameters were chosen for surface evaluation^{122–124}:

The root mean square roughness (Sq , Equation 2.21) was calculated as it is a standard parameter to compare the roughness of surfaces.

$$Sq = \sqrt{\frac{1}{A} \iint_A z^2(x, y) \, dx \, dy} \quad (2.21)$$

Another parameter taking into account the surface height is the ten-point height ($S10z$, Equation 2.22). It is defined as the average height of the five highest local maxima z_{pi} plus the average height of the five lowest local minima z_{vi} .

$$S10z = \frac{\sum_{i=1}^5 |z_{pi}| + \sum_{i=1}^5 |z_{vi}|}{5} \quad (2.22)$$

Since the $S10z$ parameter relies on height information of only 10 single peaks, two volumetric parameters were chosen to additionally examine these local surface features. Through image segmentation into motifs (dales and hills) using the watersheds method¹²⁴, the closed dales volume (Sdv) and closed hills volume (Shv) were evaluated. In addition to local wear features, wear tracks were visible on the surfaces and could be quantified by a spatial parameter: the isotropy of the surface (Str). An anisotropic surface is directionally structured whereas an isotropic surface is randomly structured. Wear tracks should therefore lead to a decrease in the surface isotropy. The surface isotropy is determined based on the autocorrelation function (ACF, Equation 2.23).

$$ACF(\tau_x, \tau_y) = \frac{\iint z(x, y)z(x - \tau_x, y - \tau_y) \, dx \, dy}{\iint_A z^2(x, y) \, dx \, dy} \quad (2.23)$$

A surface profile (z) in one direction is compared with surface profile lines along the given direction at different positions (x, y) and the correlation length between the profile lines is calculated. The isotropy of the surface is defined as the ratio of the minimum autocorrelation length in any direction divided by the maximum autocorrelation length in any direction. By integration of the Fourier spectrum of the autocorrelation length per direction into polar coordinates, the principal direction of the surface structures can be determined and the anisotropy quantified.

3. Summaries of publications

3.1. Adapting a commercial shear rheometer for applications in cartilage research

K. Boettcher, S. Grumbein, U. Winkler, J. Nachtsheim, and O. Lieleg

Articular cartilage is a material of great interest from several perspectives. First, osteoarthritis is a painful joint disease that mostly affects cartilage – the tissue lining our joint surfaces. The disease prevalence is increasing and the knee cartilage repair market volume on its own is tremendous. Second, the durability and low friction properties of cartilage are outstanding and not yet matched by any artificial material. Therefore, material scientists are interested to understand these unique properties and mimic them in bionic materials. The interdisciplinary and fast-paced cartilage research has led to a plethora of different mechanical and structural characterization techniques. These are necessary to investigate such a complex material, however, the obtained results are often highly dependent on the applied measurement technique, and only rarely the identical technique and measuring protocol is applied in more than one study.

This article describes how a commercial shear rheometer (MCR 102/302, Anton Paar, Austria) is adapted in such a way that a broad range of material characterization experiments can be performed on a single instrument. For a comprehensive analysis of the mechanical properties, the cartilage thickness can be determined and indentation, creep and shear measurements can be conducted. A customized sample holder is designed to accommodate osteochondral cylinders with a diameter of 8 mm. This sample holder can be screwed on top of the measuring cell bottom plate of the rheometer.

For the thickness and indentation measurements, a measuring head with a diameter of 4.2 mm is crafted, which can be lowered onto the surface and into the cartilage tissue. Due to the precise control of the measurement parameters by the rheometer, measurements can be performed both in displacement- or force-controlled mode. Force-controlled experiments enable not only creep measurements but are in general advantageous with viscoelastic materials such as cartilage as they ensure constant contact conditions. Dynamic measurements are possible in shear, as the rheometer is developed for rheological shear measurements and thus for very precise oscillations in the horizontal plane. An 8 mm measuring head is used for the shear measurements, and frequency sweeps are performed between 0.1 Hz and 10 Hz.

In addition to the mechanical experiments, friction tests can be conducted using the same instrument by simply exchanging the measuring cell of the rheometer. Here, a custom-made sample holder is developed to accommodate three osteochondral cylinders, which can then be probed with a sphere that is inserted into the measuring head. This setup enables force controlled and lubricated friction measurements with a constant contact area over a broad range of rotational speeds (0.001 to 1000 mm s^{-1}).

Whereas this article focuses on the demonstration of measurements with osteochondral cylinders, other cylindrical samples can be inserted into the presented sample holder geometries as well. This enables the examination of synthetic or bioengineered materials, envisioned to be used as future cartilage substitute materials, in the exactly same measurement setup as its biological template.

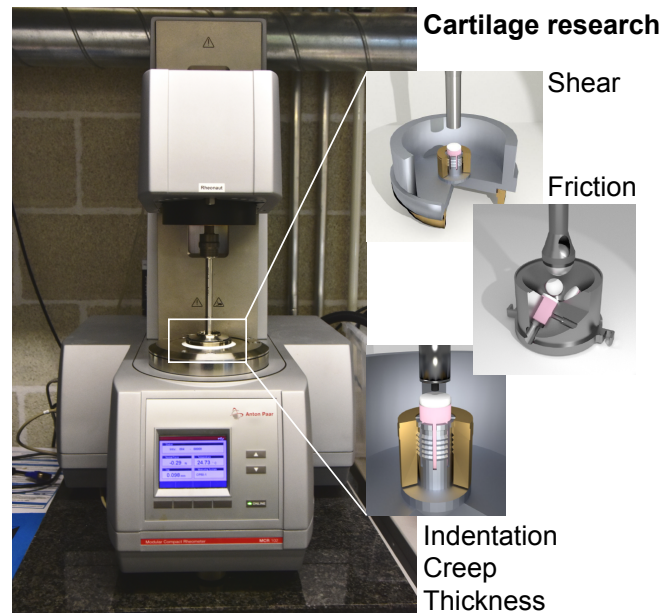


Figure 3.1.: Table of Content Graphic: Here it is described, how five different measurement types, which are all highly relevant for cartilage research, can be performed with a single commercial shear rheometer.

Individual contributions of the candidate: This article¹¹⁸ (Appendix A.1) was published in the international peer-reviewed journal *Review of Scientific Instruments*. I established the friction testing technique, designed the test protocols, performed the cartilage harvesting and the thickness, shear and friction measurements and supervised the indentation experiments. Moreover, I contributed to the design of the sample holders and measuring heads. Finally, I analyzed the measurements and wrote the article.

3.2. The structure and mechanical properties of articular cartilage are highly resilient towards transient dehydration

K. Boettcher, S. Kienle, J. Nachtsheim, R. Burgkart, T. Hugel, and O. Lieleg

Articular cartilage is a complex biomaterial which combines well-orchestrated viscoelastic properties and ultra-low friction behavior. Although maintaining those properties over decades is key to allow for painless joint mobility, cartilage lacks the ability to regenerate itself after injury or damage. Nevertheless, cartilage can perform its function for the greater part of a human lifetime. How this is achieved by the tissue remains enigmatic. The unique material properties of cartilage are attributed to the interaction of the synovial and interstitial fluid with the solid tissue phase, i.e., chondrocytes embedded in an extracellular matrix. Highly negatively charged glycosaminoglycans inside the extracellular matrix attract mobile counterions from the fluid phase, and the resulting imbalance of mobile ions inside and outside of the tissue leads to an osmotic pressure, a process called interstitial fluid pressurization. Through this process, the fluid phase is thought to protect the solid phase from damage.

To extend our current understanding of the material properties of articular cartilage, specifically the interaction between the fluid and solid phase, the material properties of ovine articular cartilage before and after dehydration are quantified in a multi-perspective approach combining rheology, tribology, AFM, SEM and histology. Thereby, the biomaterial is challenged with dehydration beyond physiological levels and rehydration is performed by using fluids with different ionic strength (no salt, 154 mM NaCl, 2 M NaCl).

Visually, the fresh and rehydrated samples cannot be distinguished whereas samples in the dehydrated state appear red, rough and inhomogeneous. Accordingly, the samples regain their initial thickness and fluid content upon rehydration independent of the fluid ionic strength. However, the hypertonic fluid (2 M NaCl) is soaked back into the tissue at a considerably slower speed compared to a fluid with physiological ionic strength (154 mM NaCl). The opposite effect, a faster kinetic, is observed with the hypotonic (no salt) fluid. The mechanical characterization shows that cartilage can recover its compressive and shear stiffness after rehydration with a fluid with physiological ionic strength. Moreover, an inverse relationship is observed between the shear stiffness and the fluid ionic strength. No structural changes in the overall tissue are observed in histology. However, the SEM and AFM pictures reveal a slightly altered surface structure after rehydration. Surprisingly, these changes do not entail distinct changes in the friction properties of cartilage when rehydration is performed at physiological ionic strength.

In conclusion, a broad range of mechanical and structural properties of cartilage can be restored after de- and rehydration provided that a physiological salt solution is used for rehydration. This finding suggests that the high lifetime of the tissue is, at least in part, based on its supreme ability to quickly and completely reabsorb fluid that has been pressed out of the tissue, e.g., during joint loading. This robust recovery of the material is an unexpected property for a complex tissue and therefore one could speculate if the high resilience of the tissue might minimize the risk of irreversible material failure and compensate for its poor regenerative abilities. Tissue engineering approaches should thus not only reproduce the correct tissue mechanics but also its pronounced sturdiness to guarantee a similar longevity.

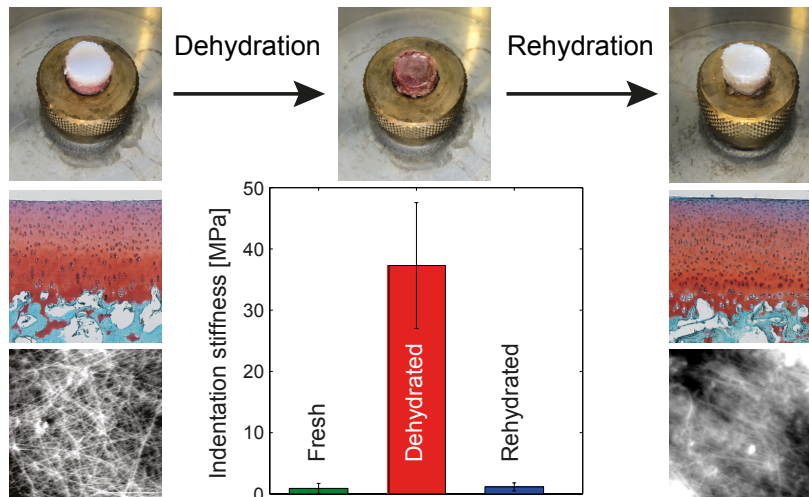


Figure 3.2.: Table of Content Graphic: Here, the sturdiness of articular cartilage towards changes in fluid content is demonstrated and it is shown that articular cartilage recovers a broad range of its material properties after dehydration.

Individual contributions of the candidate: This article¹²⁵ (Appendix A.2) was published in the international peer-reviewed journal *Acta Biomaterialia*. I performed all experiments except for the atomic force microscopy, I supervised the completion of the DMMB assay and analyzed the data from all measurements. I contributed to the conception and design of the study and wrote the article.

3.3. Comparison of friction and wear of articular cartilage on different length scales

Sandra Kienle, Kathrin Boettcher, Lorenz Wiegleb, Joanna Urban, Rainer Burgkart, Oliver Lieleg, and Thorsten Hugel

In joint tribology, low friction and wear protection are not the result of a single lubrication mechanism; rather, the mechanism adapts depending on the load, shear stress and sliding rate. At low sliding speeds, in the boundary lubrication regime, the tribological properties of articular cartilage are mediated by lubricants such as HA and lubricin. A therapeutic strategy to recover this mechanism in diseased joints, e.g., during early osteoarthritis, involves the administration of hyaluronic acid (viscosupplementation). Another lubrication mechanism depends on interstitial fluid pressurization, a process resulting out of the osmotic gradient between the highly negatively charged collagen-proteoglycan cartilage matrix and the surrounding fluid.

In the work presented here, it is investigated how changing the lubricating fluid affects friction and wear of cartilage, and the study is thereby focused on boundary and mixed lubrication as well as interstitial fluid pressurization. Therefore, lubricants with different salt ionic strength are compared with Sinovial, a commercially available viscosupplement. Different length and time scales are probed by combining AFM based friction force microscopy with macro-friction experiments. Wear formation on the cartilage surface is analyzed through AFM imaging and optical profilometry.

AFM images of the cartilage surface show that the network appears less dense with decreasing salt concentration. This can be explained with changes in the electrostatic shielding of the proteoglycan charges by the ionic strength of the fluid. Consistently, a decreasing friction coefficient with decreasing fluid ionic strength is measured with the AFM in the boundary lubrication regime. With decreasing salt concentration more water is drawn into the tissue, the collagen fiber network swells, the contact area between the AFM sphere and the solid matrix decreases and, consequently, the friction coefficient is reduced. Lubrication with Sinovial leads to a friction coefficient lower than for 2 M NaCl but higher than with ddH₂O and 154 mM NaCl. Macro-friction measurements with a rotational tribometer reveal, in contrast to the AFM friction measurements, an increasing friction coefficient with decreasing salt concentration, which is consistent with results previously described in the literature. Explanations for the different results obtained with the AFM and rotational tribology could be the different counter materials used for the measurements (AFM: polystyrene sphere, rotational tribology: glass sphere) or simply the different length scales probed by these techniques. However, Sinovial does not significantly lower the friction coefficient in either of these setups. Cartilage wear is investigated after 1 h friction measurements. Whereas after lubrication with ddH₂O no individual collagen fibers are visible anymore, samples lubricated with salt solutions show an improved wear resistance. However, the best preserved network is observed after lubrication with Sinovial.

In conclusion, this study demonstrates that the ionic strength of the lubricant changes the frictional behavior and the wear resistance of articular cartilage. Lubrication with Sinovial has no significant impact on the friction coefficient, but reduces wear in the utilized setup. Moreover this study confirms the previous notion that friction and wear are not correlated in articular cartilage tribology and suggests that the main role of hyaluronic acid might be to provide wear protection.



Figure 3.3.: Table of Content Graphic: This study demonstrates the previous notion that friction and wear are not correlated. It is shown that the ionic strength of the lubricant changes the frictional behavior and the wear resistance of cartilage and found that Sinovial does not lower friction but provides wear protection.

Individual contributions of the candidate: This article¹²⁶ (article: Appendix A.3, SI: Appendix B.1) was published in the international peer-reviewed journal *Journal of Biomechanics*. I contributed to the conception and design of the study. I performed the rotational tribology and profilometry measurements and analyzed the data of these experiments. I contributed to the discussion of the overall results and wrote parts of the article.

3.4. Modulating mucin hydration and lubrication by deglycosylation and polyethylene glycol binding

Thomas Crouzier[#], Kathrin Boettcher[#], Anthony R. Geonnotti, Nicole L. Kavanaugh, Julie B. Hirsch, Katharina Ribbeck, and Oliver Lieleg. (#: equal contribution)

All wet epithelia in our body, e.g., in the eye, lung, gastrointestinal and urogenital tract, are covered by a hydrogel called mucus. Its gel-forming building blocks are secreted mucin glycoproteins, a family of high molecular weight and highly glycosylated biopolymers. Mucin-associated glycans contribute up to 80 % of the molecular weight of mucins and contain highly hydrated hydroxyl groups. A key property of mucins is their exceptional capacity to hydrate and lubricate surfaces. Water typically accounts for up to 95 % of the total mass in a mucus gel. Shifts in the mucus water content correlate with substantial changes of the mucus barrier function and result in important pathological disorders.

This study explores the role of glycosylation in mucus hydration and lubricity, using mucin coatings as a simplified model system for mucus gels. To evaluate the contribution of mucin-associated glycans, these are either completely or partially chemically removed, and deglycosylated mucins are repaired through a lectin conjugated repair-motive.

For the hydration measurements, the native and deglycosylated mucins are adsorbed to gold surfaces and the coatings are analyzed with a quartz crystal microbalance with dissipation. Whereas with native mucin coatings surface hydration levels similar to those found in mucus gels are reached, the removal of mucin glycans results in a 3.5-fold decrease in hydration. Friction measurements using rotational tribology show that native mucins can effectively lubricate PDMS surfaces over a broad range of sliding speeds. Consent with the hydration measurements, deglycosylation of the mucins leads to an increase in friction by two orders of magnitude and friction coefficients as high as without any mucin. Mucins may achieve energy dissipation and thus friction reduction by two independent mechanisms: First, surface bound mucin can provide hydration lubrication which is based on an exchange of trapped water molecules with free water molecules in the fluid. Second, shearing off whole adsorbed mucin macromolecules from the surface may additionally contribute to the observed reduction in friction.

As a next step, a repair strategy is developed by substituting the removed glycans with polyethylene glycol (PEG) polymer chains. PEG is therefore conjugated to wheat germ agglutinin (WGA), a lectin-type protein, added to partially deglycosylated mucin coatings, and the resulting hydration and lubricity of the coating is measured. Although the simple addition of PEG to the coatings has no effect, the addition of immobilized WGA-PEG to the adsorbed mucins greatly enhances hydration and lubrication.

This work provides a more detailed insight to the origin of mucin-mediated hydration and lubrication. It demonstrates that glycans control the hydration and lubrication ability of mucins. Moreover, this study shows that the substitution of mucin-bound glycans with synthetic polymers can, to a large extent, restore mucin hydration and lubricity. This could prove to be a useful new treatment strategy for patients with poor mucus coverage, defective mucus production, or glycosylation as caused by Sjögren syndrome, dry eye, or certain bacterial infections.

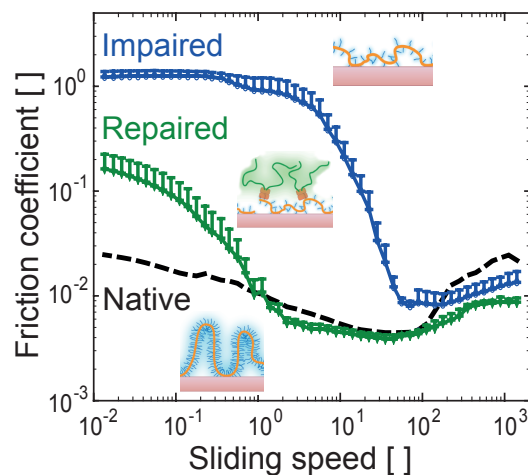


Figure 3.4.: Table of Content Graphic: Mucin biopolymers efficiently lubricate our eyes, gastrointestinal tract, and female reproductive tract. It is found that removing mucin-associated glycans eliminates their lubrication potential and correlates with the structural collapse and dehydration of mucin coatings. Both hydration and lubrication properties of defective mucins can be restored by grafting polyethylene glycol molecules onto them through the binding of lectins to residual glycans.

Individual contributions of the candidate: This article¹²⁷ (article: Appendix A.4, SI: Appendix B.2) was published in the international peer-reviewed journal *Advanced Materials Interfaces* with a shared first authorship. I performed and analyzed the friction measurements. I contributed to the design of the study, the discussion of the results and wrote parts of the article.

3.5. Porcine gastric mucins reduce friction and wear in cartilage boundary lubrication

K. Boettcher, S.G. Dorosz, T.A. Schmidt and, O. Lieleg

Mucin glycoproteins are the main component of mucus, a hydrogel covering the wet epithelia of our body. Mucins combine a multitude of important functions on biological interfaces: they protect, hydrate and lubricate, for instance, the eye and gastrointestinal tract. For joint lubrication, however, nature employs a different but related mucinous glycoprotein: lubricin. Together with other macromolecules, e.g., hyaluronic acid (HA), lubricin serves as a boundary lubricant and is thought to play a major role in friction reduction and wear protection on articular cartilage – especially at low sliding speeds.

This study examines if mucin can take over the functions of lubricin and/or HA in cartilage tribology, and, i.e., whether mucin is able to reduce friction and wear between cartilage surfaces to similar extents.

The gained results show that purified gastric mucin is able to reduce friction between two cartilage surfaces. However, when rotational tribology is used and the lubricants are tested between cartilage and glass surfaces, only lubricin is able to reduce friction, whereas HA and mucin do not decrease the friction over the broad range of tested sliding speeds. An explanation could be that mucin adsorbs to glass reasonably well and only weakly to cartilage, strong adsorption is however necessary for efficient hydration lubrication.

To systematically evaluate wear formation, a quantitative method is established based on ISO25178–2 parameters. The cartilage surfaces are examined with optical profilometry after 1 h friction measurements (glass/cartilage tribology setup) and the surface topography of the captured 3-dimensional images is analyzed. No differences in the root mean square roughness (Sq) are observed between the examined groups, but visually it is found that lubrication with HA leads to an increased amount of wear pits and asperities whereas lubricin generates features that can be described as wear tracks.

In general, cartilage wear can be subdivided into interfacial, fatigue and impact wear. In boundary lubrication, i.e., under direct contact between the opposing surfaces, interfacial wear can occur due to two mechanisms: abrasion and adhesion. Adhesive wear is quantified by evaluating the minimal and maximal peaks of the surface (S10z) and it is found that this parameter is significantly increased after lubrication with HA. This result is in agreement with previous reports where lubrication of mica surfaces with HA led to surface damage due to bridging of the surfaces during shear. The visual wear tracks generated after lubrication with lubricin are categorized as abrasive wear and quantified by calculating the isotropy of the surface. In contrast to HA and lubricin, mucin is able to prevent wear on cartilage. Although mucins are large enough to potentially bridge the opposing surfaces during cartilage tribology similar to HA, mucin adsorbs only weakly to the cartilage surfaces, thus possibly preventing the formation of molecular cross-bridges.

In conclusion, these results advance the understanding of why, *in vivo*, multiple biopolymers are present in the synovial fluid to achieve optimal friction reduction and wear protection at sliding interfaces. Also, these findings show that in contrast to HA and lubricin, mucin – when used as a single molecular component in a lubricant – reduces friction in cartilage/cartilage tribology equally well as lubricin and also seems to be sufficient to prevent wear on cartilage when probed with a glass sphere. This study therefore demonstrates the great potential of purified mucins as ingredients for tribosupplements in osteoarthritis treatment.

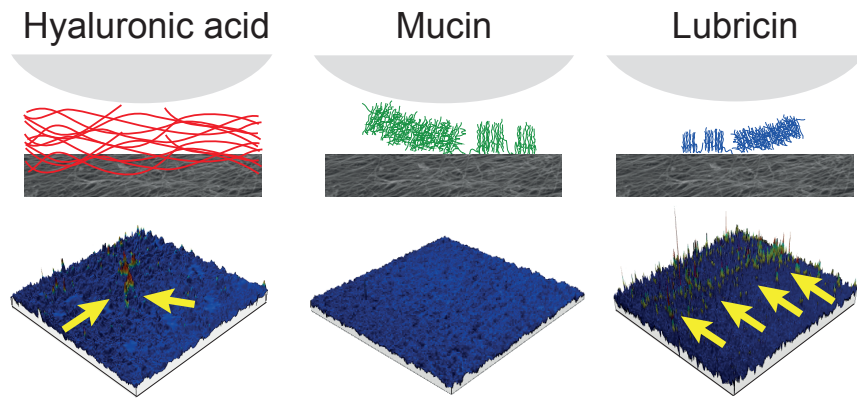


Figure 3.5.: Table of Content Graphic: Lubrication with mucin protects cartilage against wear, whereas hyaluronic acid leads to adhesive wear and lubricin generates abrasive wear in a glass/cartilage tribology setup. All lubricants reduce friction between two cartilage surfaces, but only lubricin is able to reduce friction in a glass/cartilage setup. Thus mucin could potentially be used in tribosupplementation or in coatings on implant materials for joint replacement.

Individual contributions of the candidate: This article (manuscript: Appendix A.5, SI: Appendix B.3) has been submitted to an international peer-reviewed journal. I contributed to the conception of the study, designed the experiments and conducted the measurements. I analyzed the data, performed the statistical evaluation and wrote the article.

4. Discussion & Outlook

The overall aim of this thesis is to achieve an enhanced understanding of physiological lubrication strategies and specifically the tribological properties of articular cartilage. Therefore, not only the tribological but also the biomechanical and structural tissue properties were studied here.

The first part of this thesis is focused on the interaction between the solid and fluid phase of the tissue. Therefore, cartilage was subjected to dehydration and consecutive rehydration and the fluid ionic strength was varied. The following key results were obtained and will be discussed below:

- In its native state, the ionic strength of the lubricant changed the frictional behavior and wear resistance of cartilage, and the examined differences varied depending on the observed length scale.
- A broad range of mechanical and structural properties of articular cartilage could be restored after de- and rehydration provided that a physiological salt solution was used for rehydration.
- The ionic strength of the buffer used for cartilage rehydration influenced the rehydration kinetics and surface structure as well as the creep, shear and friction properties of cartilage.

Articular cartilage withstands numerous loading cycles each day and is thereby compressed and decompressed thousands of times. It seems unlikely that the tissue would endure such an ongoing burden without damage – but it does, which is striking considering the fact that the tissue itself is not able to regenerate and compensate for occurring wear or injuries. To understand this outstanding durability of articular cartilage, the tissue was subjected not to millions of load cycles but to overnight dehydration in Section 3.2 and the recovery of the tissue was investigated. This material science approach of a drastic and unphysiological tissue modification has been used before: e.g., the complete enzymatic removal of glycosaminoglycans from cartilage^{52, 128, 129} has clearly advanced our understanding on how the material properties of articular cartilage are established on a molecular scale. After dehydration, the cartilage samples were rehydrated and could regain their initial water content, thickness, bulk structure and mechanical properties. Only the surface structure seemed considerably changed, however, without any perceivable impact on the tribological properties. So far, this is the only study that performed and characterized rehydration of dehydrated articular cartilage. Meyer *et al.*¹³⁰ investigated elastic cartilage samples, which only reached a maximum rehydration level of 80 % of their initial weight after partial dehydration. Next to articular cartilage, there are two other types of cartilaginous tissues: elastic cartilage and fibrocartilage. The inability of elastic cartilage to completely rehydrate is unexpected as the water content of elastic cartilage (70 % – 75 %)¹³¹ is only slightly lower compared to articular cartilage (70 % – 80 %)²⁴. However, there are some obvious structural differences between these cartilage types: e.g., elastic cartilage possesses no distinct hierarchical structure but contains elastic fibers, which are distributed throughout the extracellular matrix and compact the arrangement of the chondrocytes. These elastic fibers provide elastic cartilage with the ability to withstand repeated bending. Possibly, the difference in mechanical loading could be the reason for the observed inability of elastic cartilage to regain its water content after partial dehydration. Elastic cartilage can be found in the epiglottis and the auricula/pinnae where it does not have to withstand continuous load cycles under high contact pressures as articular cartilage. Overall, there are only few studies investigating the structural and mechanical properties of elastic cartilage and further experiments comparing the different cartilage types have to be conducted.

The third cartilage type, fibrocartilage, differs strongly from articular and elastic cartilage as it contains type I collagen fibers. Fibrocartilage can be found, e.g., in the annulus fibrosus, menisci, and the temporomandibular joint but is also formed in case of severe articular cartilage degradation. As soon as the bone underneath the cartilage is damaged, blood enters the cartilage defect site and fibrocartilage is formed inside the lesion as a substitution for articular cartilage. However, fibrocartilage has a slightly lower water content compared to articular cartilage, ranging between 70 % – 78 %, and proteoglycans constitute less than 10 % of its dry weight¹³². There are up to now no studies on the de- and rehydration kinetics of fibrocartilage. It would be interesting to investigate fibrocartilage as, for instance, the meniscus is a fibrocartilaginous tissue and has to withstand comparable mechanical stresses and strains in joints as articular cartilage. Similar to articular cartilage, interstitial fluid pressurization has been reported as the main load support mechanism in meniscus tissue¹³³. However, in other fibrocartilage tissues, e.g., the temporomandibular joint, interstitial fluid lubrication seems to play a minor role for load support and lubrication¹³⁴.

Interstitial fluid pressurization is known to influence the mechanical and tribological properties of articular cartilage. Therefore, as expected, the ionic strength of the rehydration fluid influenced the rehydration kinetic as well as the tissue properties after complete rehydration of articular cartilage (Section 3.2). Moreover, distinct changes were especially observable in the surface structure after rehydration with a hypotonic (no salt) or hypertonic (2 M NaCl) buffer. Interestingly, these alterations did not lead to functional changes in the friction coefficient or wear formations. A dependency of the friction coefficient on the ionic strength of the lubricant was not only observed in Section 3.2 for rehydrated samples but also in Section 3.3 for fresh articular cartilage samples. A distinct comparison of these studies is, however, difficult as in Section 3.2 physiologically buffered solutions (pH 7) and in Section 3.3 unbuffered aqueous solutions were used. The pH of aqueous solutions (ultrapure water) ranges between 4.5 and 5 and is therefore slightly acidic. The interstitial fluid in cartilage tissue has a pH around 7. A lower pH can entail an increased positive charge in the solid matrix of cartilage due to the protonation of amino acids. As interstitial fluid pressurization depends on the negative fixed charge density in the cartilage tissue, the strength of this mechanism will be influenced by a change in pH. Moreover, such a pH-induced amino acid protonation can also lead to protein aggregation, degradation, and tissue denaturation.

In Section 3.3, the friction coefficient was not only evaluated as a function of the ionic strength of the lubricant but also on different measuring length scales. In macro-friction measurements, the friction coefficient decreased with increasing ionic strength as described before by Ateshian *et al.*¹³⁵. However, in friction measurements conducted with an AFM, the friction coefficient showed the opposite trend. A reason for this scale-dependency of the friction coefficient could be that although interstitial fluid pressurization is the key process influencing cartilage friction, it might not dominate the friction behavior when cartilage is probed on the nano-scale. Here, other parameters, e.g., the collagen tension, orientation and extracellular matrix mesh size might have a major impact. The finding that certain cartilage alterations are only measurable when the correct scale is probed could suggest that also early structural cartilage changes due to osteoarthritis might be detectable by measurement techniques probing the correct length-scale. In fact, early cartilage tissue degradation due to osteoarthritis was observed through variations in the frequency-dependent stiffness and hydraulic permeability in a frequency range that is even well beyond the capabilities of typical AFMs and therefore rarely probed¹³⁶. Similarly, the functional changes due to the variations in the surface structure of rehydrated cartilage samples in Section 3.2 might only be detectable on the nano-scale and were therefore

not measurable by the performed macro-friction experiments. In turn, the scale-dependency of cartilage material properties should be considered in future studies when choosing a specific measurement technique. This finding also underlines the importance of a broad cartilage material characterization over various length and time scales with the same setup as, e.g., presented in Section 3.1.

A challenge in achieving this goal is to conduct this *in vitro* characterization by only changing one specific parameter while keeping all other influences constant. As an example, different opposing materials were used during the macro-friction (glass) and AFM (polystyrene) friction measurements, which limits the comparability of the obtained results. The surface topography and roughness as well as the chemistry of these synthetic materials differs, which could influence their interaction with lubricating molecules and the cartilage surface and therefore the measured friction coefficient. However, not only in these studies but in the whole research community a broad variety of test setups is used, as discussed in Section 3.1, which makes it challenging to compare the results obtained in different studies. In addition to differences in the opposing material, different contact pressures and contact modalities (migrating vs. constant contact) are frequently used, which often leads to contradicting results. An example is the still open question if and how hyaluronic acid (HA) acts as a boundary lubricant on cartilage surfaces. While HA alone has been reported to be a poor boundary lubricant between cartilage and glass^{90,137} (which is consistent with the results obtained in Section 3.3 and Section 3.5), HA has shown good lubricity between two cartilage surfaces¹¹⁵. Contradictory results were also reported for the synergistic effect of lubricin and HA. Chang *et al.*¹³⁸ did not find an enhanced tribological performance of HA in combination with lubricin on hydrophobic (methyl-terminated) and hydrophilic (hydroxyl-terminated) self-assembled monolayer surfaces. However, Lee *et al.*⁶⁶ and Das *et al.*⁵⁰ observed that grafted HA in combination with lubricin reduces friction and enhanced wear protection between mica surfaces. Moreover, Greene *et al.*⁴² reported similar findings in a cartilage/glass setup. Hence, it is obvious that the utilized counterface materials have a strong impact on the tribological performance of lubricants¹³⁷. Therefore, variations of the setup and the measurement parameter in *in vitro* studies should be minimized. Moreover, their influence needs to be considered carefully when proposing specific mechanisms in cartilage tribology.

The newly gained mechanistic insights into cartilage, specifically the high resilience of the tissue due to the fluid-solid phase interactions and the scale-dependency of the mechanical properties, can be transferred in a next step from basic research to clinical applications (Figure 4.1). As an example, new cartilage substitute materials can be developed through the adaptation of their composition and structure under biomimetic aspects and in such a way that they can interact with the surrounding biological system. As cartilage lacks the ability to regenerate, external interference is necessary after injury or as a treatment of degenerative diseases. The gold standard surgical treatment option has not changed during decades and cartilage defects are still widely treated with partial or total joint arthroplasty. The first artificial joints were implanted by the German surgeon Themistocles Gluck (1853 – 1942), who also repaired a fractured femur by using steel plates. Steel was the predominately used implant material, as experiments with other materials, e.g., rubber, glass, wax, and celluloid, resulted in poor outcome. A special metal alloy for orthopaedic applications called vitallium – a mixture of cobalt, chromium and molybdenum – was introduced by Reiner Erdle and Charles Prange in 1932. It is, especially in combination with ultra high molecular weight polyethylene (UHMWPE), still used extensively, e.g., in hip prosthesis^{139,140}. In addition to that, metal on metal and ceramic on ceramic combinations are on the market. These synthetic non-degradable materials are mainly used owing to their

high load-bearing properties, low friction, wear resistance and long-term durability. Indeed, as described in Section 3.2, high resilience is a key feature of articular cartilage. However, in addition to this, no further cartilage properties are mimicked by these standard materials, nor do they interact with the physiological surrounding, e.g., ions or macromolecules in the synovial fluid.

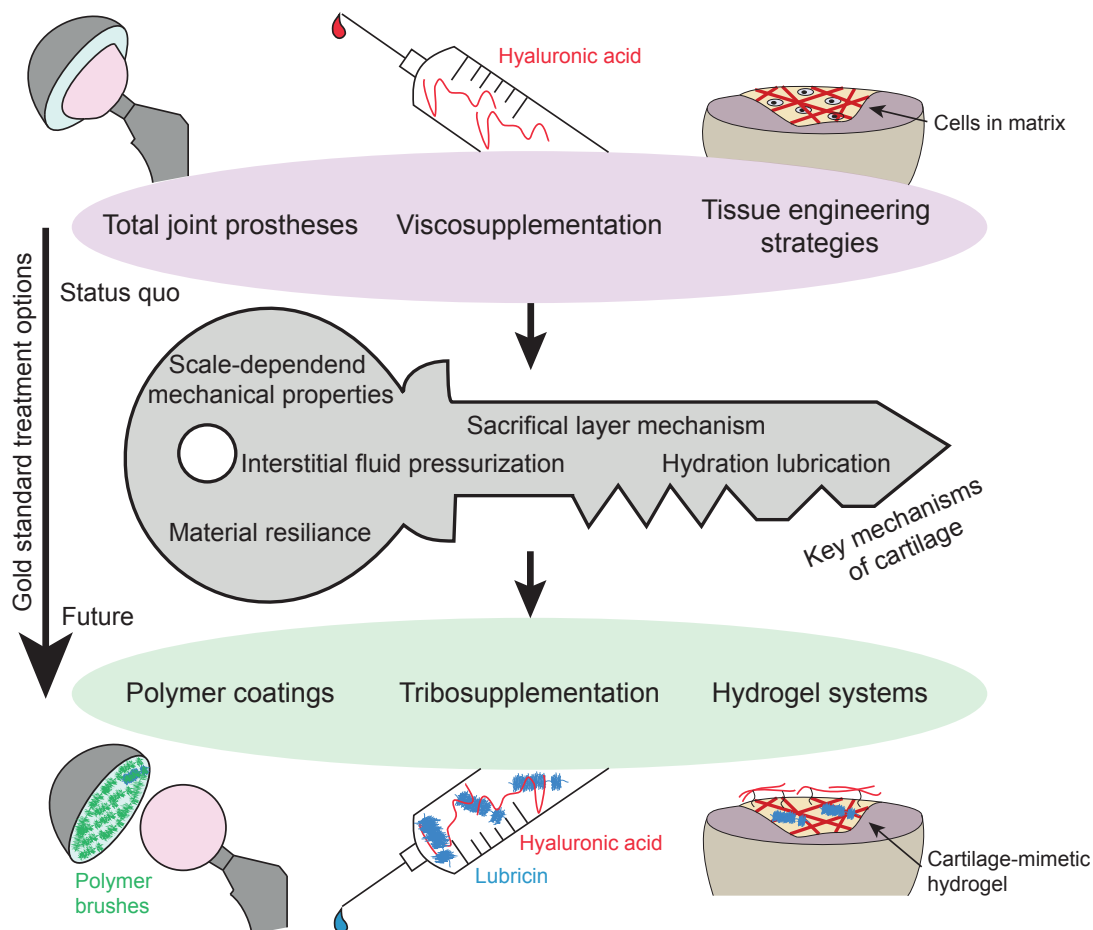


Figure 4.1.: Cartilage treatment strategies evolve over time. Total joint prostheses, viscosupplementation and tissue engineering strategies, e.g., MACI, are gold standard treatment options for different grades of cartilage degeneration. Through the conducted research and thus advanced knowledge of the key mechanisms responsible for the outstanding mechanical and tribological properties of cartilage tissue, these treatment options could be improved. Some of these biomimetic solutions are already tested in clinical trails (polymer coatings of acetabular liners in total hip prostheses), others are still under investigation in applied research studies as, e.g., injection-compounds containing hyaluronic acid and lubricin, or cartilage-mimetic hydrogel systems.

Recent strategies to treat cartilage defects try to tackle this problem by applying tissue engineering strategies. On the first glance, cartilage seemed easy to reproduce by tissue engineering approaches. Its extracellular matrix composition is rather simple and only one cell type, chondrocytes, resides in the matrix. However, tissue engineers are up to now struggling to mimic the complex interplay of the cartilage components as the biological template is still not fully understood. Moreover, cartilage tissue proved to be very heterogeneous with varying thickness and mechanical properties even depending on the location in a specific joint¹⁴¹. Intuitively the best solution would be to stimulate the regenerative potential of cartilage. Microfracture is a clinical repair strategy that relies on penetration of the subchondral bone to induce bleeding and stimulate

regeneration by cell invasion into the cartilage defect. Although this technique leads to newly formed cartilaginous tissue, the outcome is not always reproducible and the tissue structure deviates from articular cartilage as it seems to resemble fibrocartilage rather than articular cartilage. As discussed previously, fibrocartilage lacks the ability to fully rehydrate after partial dehydration and does not utilize interstitial fluid pressurization to facilitate lubricity. Yet, the ability of articular cartilage to rehydrate as well as interstitial fluid pressurization have been proven in Section 3.2 to be key material properties. An adequate *in vivo* articular cartilage regeneration seems therefore difficult. Further research activities focused on *in vitro* cultivation of cartilage tissue. Autologous chondrocyte transplantation is performed by harvesting an articular cartilage sample from a low weight-bearing region in the joint of the patient in a first arthroscopic operation. Next, the chondrocytes are expanded *in vitro*, implanted in a second operation into the cartilage defect and covered by a periosteal flap, porcine membrane, or a HA scaffold. A major drawback is the potential hypertrophy of the periosteal flap, or immune reaction to the allogeneic scaffold as well as the dedifferentiation of the delivered cells into fibrochondrocytes. Moreover, autologous chondrocyte transplantation entails a long recovery time (6 – 12 months) to ensure neotissue maturation and to protect the newly formed fragile tissue against damage resulting from loading.¹⁴²

To overcome graft instability, a major limitation of the listed tissue engineering approaches, scaffold based treatment strategies were introduced. Moreover, the scaffold can be used to provide the correct chemo-mechanical environment for matrix synthesis and prevent the formation of fibrocartilage instead of articular cartilage. Matrix-induced autologous chondrocyte implantation (MACI) is currently the most frequently used scaffold-based tissue engineering approach in cartilage repair. Here, the harvested chondrocytes are cultured *in vitro* for three days on a porcine-derived collagen membrane prior to implantation. The scaffold is implanted with the cell loaded side facing the subchondral bone and the "low-friction surface" towards the intra-articular space and fixed with fibrin glue¹⁴². Until now, the superiority of MACI over existing cartilage repair techniques remains unproven, and in clinical practice the microfracture technique is still often chosen over MACI owing to its simplicity. Similarly, other scaffold based approaches, such as autologous matrix-induced chondrogenesis (AMIC), techniques using bone marrow derived mesenchymal stem cells, or other natural or synthetic scaffolds¹⁴³, are not yet established in clinical practice.^{141, 142, 144}

Owing to the discussed limitations of current tissue engineering strategies, the focus in scaffold design approaches recently shifted from structural recreation of cartilage to an adequate adaptation of the mechanical properties. Liao *et al.*¹⁴⁵ developed a poly(ϵ -caprolactone) fiber-reinforced scaffold filled with an alginate and polyacrylamide hydrogel that partly resembles the load-bearing and tribological properties of articular cartilage. Moreover, an increasing number of studies investigates scaffold-based cell-free strategies with non-degradable hydrogels for cartilage repair. This might seem like a step backwards but could lead to treatment strategies with near-term clinical translation. Here, the final aim is not tissue regeneration but a durable functional rehabilitation by using an artificial material that leads to reproducible success and is easy to use. Compared to degradable scaffolds, non-degradable materials bear the possibility to implement biomimetic aspects discussed in this thesis, e.g., the high resilience of the tissue and the scale-dependency of the mechanical properties.

A vast majority of hydrogel types has been investigated so far for the development of such a cartilage-mimetic material^{146–149}. Recently, many research groups focus on polyvinyl alcohol (PVA) and polyethylene glycol (PEG) hydrogels as their material properties can be adapted to be comparable to articular cartilage,

e.g., by different crosslink procedures or coblending^{147,150}. Both hydrogel types are favored over other polymer-based systems due to their high water absorbency and bioinert behavior. PVA and PEG hydrogels are already used in medical applications and have been approved by the U.S. Food and Drug Administration (FDA) for clinical uses in humans^{146,150,151}. ReSure Sealent is a PEG hydrogel for sealing clear corneal incisions following cataract surgery (FDA approval: 2014)¹⁵². Cartiva SCI is a PVA hydrogel available for clinical usage as a cartilage substitute material in Canada, Europe and South America¹⁵³. For a similar PVA hydrogel product, SaluCartilage, long term failure owing to dislocation as a result of inadequate fixation was reported after an *in vivo* study¹⁵⁴. Both products are anchored through press-fit fixation into the defect site. Other fixation mechanisms have been evaluated as well: Ushio *et al.*¹⁵⁵ combined a PVA hydrogel with a titanium fiber mesh for bone fixation.

Another approach to mimic the properties and lubricity of articular cartilage was recently introduced by Greene *et al.*¹⁵⁶. They mimicked the functional interplay of the cartilage solid phase, specifically the glycosaminoglycans, with the interstitial fluid, using a reconstituted network of highly interconnected cellulose fibers with immobilized carboxymethylcellulose-polyethylene glycol molecules. It was suggested that the purely synthetic scaffold was able to support load by interstitial fluid pressurization and that the gradual dissipation of fluid pressure dampened high impact loads. However, Greene *et al.*¹⁵⁶ did not report the compression or shear modulus of the scaffold. Regarding the tribological properties, the scaffold exhibited a time dependent friction response and wear resistance reminiscent to that of cartilage tissue, especially when the scaffold was lubricated with a boundary lubricant, e.g., carboxymethylcellulose-polyethylene glycol. The study thereby demonstrated the possibility of improving a cartilage substitute material by not only implementing a cartilage-mimetic solid-fluid interaction into the scaffold bulk structure but utilizing the adsorption of boundary lubricants onto the material surface to improve the tribological properties of the material.

The second part of this thesis is focused on the cartilage surface and its interaction with macromolecules in the lubricating fluid. To understand the lubricating ability of polymers at sliding interfaces, the hydration and lubrication ability of native and chemically modified mucin coatings on synthetic surfaces was investigated. Next, this knowledge was utilized to analyze friction and wear on articular cartilage as a function of the macromolecules in the lubricant. The following key results were obtained and will be discussed below:

- Lubrication with Sinovial, a commercially available viscosupplement, has no significant impact on the friction coefficient but reduces wear formation.
- Mucin glycans control the hydration and lubrication ability of mucins.
- Lectin conjugated polyethylene glycol (PEG) can be used to restore mucin hydration and the lubricity of partially deglycosylated mucins.
- Mucin reduces friction in cartilage/cartilage tribology equally well as lubricin.
- Mucin is, in contrast to HA and lubricin, able to prevent wear on cartilage as a single molecular component.

As discussed above, the lubricity of HA highly depends on its ability to adsorb to the sliding surfaces. It was described in Section 3.3 that Sinovial, a viscosupplement containing 0.8 % (wt/vol) HA with a molecular

weight between 0.8 and 1.2 MDa, and in Section 3.5 that a 0.1 % (wt/vol) HA solution with a molecular weight between 2 and 2.4 MDa were not able to reduce the friction coefficient in a glass/cartilage setup. In addition to friction, wear formation was investigated, and it was shown in Section 3.3 that Sinovial was able to reduce wear formation, whereas in Section 3.5 lubrication with a 0.1 % (wt/vol) HA solution caused adhesive wear. A reason for this (on the first glance contradictory) finding could be the different polymer content and molecular weight of HA on the one hand or simply the wear analysis method on the other hand. Whereas a qualitative wear analysis was performed in Section 3.3, a quantitative analysis was introduced in Section 3.5. Of course, the different polymer content of the lubricants entailed different viscosities. For Sinovial, a viscosity of 0.6 Pas was reported¹⁵⁷, whereas for the 0.1 % (wt/vol) HA solution a viscosity of 0.01 Pas was measured in Section 3.5. As the experiments were conducted at the same sliding speed (0.1 mm s^{-1}) and contact pressure (0.1 MPa), the Sommerfeld number is higher for Sinovial compared to the 0.1 % (wt/vol) HA solution. Therefore, the film thickness under Sinovial lubrication might have been thicker, protecting the cartilage surfaces from wear. However, this comparison of the Sommerfeld numbers has to be performed with care as HA solutions are non-Newtonian fluids (Section 1.1.2). Consistent with the finding discussed in Section 3.5, Das *et al.*⁵⁰ reported that HA alone is not able to reduce wear. They stated that immobilization of HA by chemical grafting is necessary to protect the surface from abrasive wear and that the addition of lubricin can further increase the wear resistance. Similarly, Lee *et al.*⁶⁶ reported the highest wear protection for grafted HA in combination with lubricin. Moreover, they stated that increasing the molecular weight from 0.05 to 2.6 MDa increases the wear protection which could be another reason for the differences observed in the framework of this thesis.

Although HA is able to lubricate two cartilage surfaces to a certain degree⁷⁹, multiple biopolymers seem to be necessary to provide wear protection and low friction coefficients at physiological levels. In the presence of other macromolecules, HA is known to form aggregates and build a surface-anchored protective layer on the cartilage surface (see Section 1.3.3). Singh *et al.*¹⁵⁸ recently developed a tissue surface modification strategy to trap HA on the cartilage surface in joints. They introduced an HA-binding peptide that can be covalently anchored onto the tissue surface through collagen-binding peptides and non-covalently binds HA from the synovial fluid. Instead of repetitive viscosupplement injections, which are necessary owing to the low residual time of injected HA in the joint cavity, this approach offers a permanent solution through a one-time treatment. The presented tissue modification option is similar to the mucin repair strategy introduced in Section 3.4 as both aim at a synthetic regeneration of molecular processes mediating physiological lubrication. However, these novel chemical tissue modification procedures still have to pass the clinical approval process and have not yet been tested *in vivo*. For now, a clinically available solution is given by crosslinked HA compounds that can be used for viscosupplementation as they show longer residence times in joints compared to simple HA solution¹⁵⁹. However, Jevsevar *et al.*¹⁶⁰ reported in a meta-analysis of double-blinded, sham-controlled clinical trials that there were no obvious clinically important advantages for both viscosupplement types compared to placebos.

As a consequence of our increasing understanding of physiological lubrication strategies, the injection of lubricin instead or in combination with HA is discussed and called tribosupplementation. This term was first introduced in a patent in 1999, describing the administration of lubricin directly to the injured or arthritic joint¹⁶¹. The efficiency of this treatment was evaluated in an *in vivo* study in rats: here, the main finding was that intra-articular lubricin injections following anterior cruciate ligament injuries reduced cartilage damage

and collagen type II degradation and might therefore retard cartilage degeneration and the development of posttraumatic osteoarthritis⁹³. The usage of a mixture of lubricin with HA or glycosaminoglycans to treat cartilage damage *in vivo* was first patented by Synthes GmbH (USA) in 2004¹⁶². A patent directly related to the lubricity of the mixture was filed by Lubris BioPharma, Llc (USA) in 2013¹⁶³. They disclosed that mixed solutions of HA and lubricin with controlled rheological properties can be used for various medical and cosmetic applications. It was specifically stated that such a mixture can be applied for viscosupplementation purposes and is advantageous due to its higher viscosity, which enhances both the residual time of HA in the joint capsule and the cushioning effects of HA. Moreover, the mixture is thought to improve hydrodynamic as well as boundary lubrication mechanisms. Until now, no related product is clinically available, and a product of Lubris BioPharma is still in the pre-IND phase prior to clinical trials for FDA approval⁹⁵. The only approved clinical product based on lubricin are eye drops (Dry Eye, Lubris BioPharma, USA) for treatment of the dry eye syndrome and tear film insufficiency. However, physiologically, on the eye not lubricin but mucin is the lubricating molecule.

The molecular principle governing the ability of mucins to hydrate and lubricate was analyzed in Section 3.4. It was shown that glycans control these properties and that deglycosylation leads to a loss in hydration and lubricity of mucin coatings. Repair motifs can however be used to regain the functions of partially deglycosylated mucins. This finding might, in addition to the injection of lubricin and HA, pave the way for a future treatment strategy for patients with defective mucus production or mucin glycosylation as caused by Sjögren syndrome, dry eye or certain bacterial infections.

In addition to the eye, mucins lubricate a broad range of body surfaces including the nasal and oral cavities as well as the respiratory, gastrointestinal and, female genital tract. Thus it seems surprising that in joints, a rather complicated multi-component system is used instead. If mucins would be able to lubricate cartilage surfaces efficiently, native mucin, novel mucin-mimetics, or other polymer brushes could be used to supplement the synovial fluid and repair or coat a diseased/degraded cartilage surface. Such a biomimetic repair approach would be less complex, cheaper and have a higher availability.

The ability of mucin to lubricate cartilage surfaces was analyzed in Section 3.5. There, it was shown that mucin is in fact able to reduce friction between cartilage surfaces to a similar degree as lubricin ($\mu \sim 0.1$), and is able to prevent wear in a cartilage/glass setup. However, only lubricin reduced friction between cartilage and glass surfaces. So far, no wear analysis between two cartilage surfaces was performed. Concluding, as stated above for HA, the ability to adhere to the different surfaces as well as the adsorption strength and conformation of the polymer determine the lubricity of boundary lubricants in general. It is possible that the interaction of lubricin with other macromolecules is necessary to enable friction reduction to physiological values ($\mu < 0.01$) and sufficient wear protection. Future studies are necessary to reveal the exact interaction of different macromolecules on cartilage surfaces. The quantitative wear analysis established in Section 3.5 can be used to evaluate wear formation and not only friction reduction. So far, the interaction of different molecules present in the synovial fluid has only been tested on mica surfaces as discussed in Section 1.3.3. Another study on mica surfaces was conducted by Seror *et al.*⁴⁴. However, they coated the mica surfaces with HA (which, to some extent, mimics the cartilage surface) and found that HA grafted on mica surfaces and complexed with aggrecan did not lead to physiologically relevant friction coefficients under high contact pressures. The authors contributed this observation to the weakly hydrated SO_3^- of the chondroitin sulfate moieties exposed by the aggrecan brushes and concluded that the utilized components are not sufficient

to model cartilage lubrication. They found, however, that phosphatidylcholine lipids in combination with HA were able to efficiently lubricate under high contact pressures. This demonstrates that there are indeed molecular combinations that can mimic the performance and interaction of synovial fluid compounds, and can be used for bioinspired lubrication strategies even under harsh mechanical contact conditions.

The load-environment is a measurement parameter that needs to be considered more closely in future studies. Whereas high contact pressures are present in joints, mucins seem to reduce friction mostly in low load environments. In the studies presented here, the contact pressure was fixed to a value frequently used for *in vitro* cartilage friction tests (0.1 MPa, see Section 2.4.2), but is certainly lower than contact pressures reached during normal activities, e.g., in the hip joint (up to 10 MPa). As presented in Section 3.3, mucin is able to lubricate at this intermediate contact pressure level, and is therefore also applicable outside low contact pressure environments as they occur, for example, in the eye (3 – 5 kPa)¹⁶⁴.

A unique approach of this thesis is the combined analysis of general physiological lubrication strategies and cartilage lubrication at fixed parameters, as just discussed for the contact pressure. Together with existing publications, the findings presented here underline that lubrication in the human body is mediated through different molecules but similar processes: hydration lubrication and self-sacrificial layers. The gained results create the gateway to develop optimized implant coatings, supplements or repair strategies for lubricating body fluids and tissues, for instance, if a malfunction is caused by a pathologically altered lubrication.

When searching for molecules that are able to perform hydration lubrication, important selection criteria are their water solubility, ability to adsorb, and their hydration strength¹⁵. So far, polyethylene oxide (PEO) and polyethylene glycol (PEG) have been investigated in various studies. However, PEO for example only adsorbs to mica surfaces from solutions containing potassium and cesium ions but not when sodium or lithium ions are present, which inhibits its usage in physiological fluids¹⁶⁵. Poly-L-lysine-g-PEG was found to adsorb to mica via its positively charge PLL backbone and as a result, the bottle-brush-like PEG chains are exposed into the lubricating fluid. This configuration is optimal for hydration lubrication and results in physiologically low friction coefficients even under high contact pressures¹⁶⁶. This finding was confirmed by the results discussed in Section 3.4, where deglycosylated mucins were successfully repaired with lectin-PEG. The lubricity of mucin coatings could be thereby restored because the conjugated PEGs were able to functionally substitute the removed glycans and mediate hydration lubrication by themselves. Another promising approach was reported by Chen *et al.*¹⁶⁷, where they showed that poly(2-methacryloyloxyethyl phosphorylcholine) (polyMPC), grown from the surface of mica sheets, led to friction coefficients as low as 0.001 in aqueous media – even under high contact pressures. Although these results are very promising, for those polymeric lubricants to be used *in vivo*, they need to adsorb adequately to physiological tissue or implant surfaces instead of mica. Until now, only few studies have tested the lubrication and adsorption ability of synthetic polymer lubricants directly on physiological surfaces. Shi *et al.*⁶⁰ investigated the lubrication of bovine cartilage surfaces with PEG dissolved in PBS with a pin-on-disk tribometer (using alumina as a counter material) and found that the PEG lubricant reduced the friction coefficient by 40 % compared to lubrication with PBS. Wathier *et al.*¹⁶⁸ reported a friction reduction of up to 50 % between two cartilage surfaces through lubrication with a large-molecular-weight polyanion. However, neither of these studies investigated the adhesion of the lubricants to the surfaces nor their *in vivo* performance. Moreover, the residual time of those molecules in the joint cavity is unknown as none of these polymers are chemically grafted on the cartilage surface.

Several studies investigated polymer coatings on implant surfaces especially regarding their wear properties. Aseptic loosening, owing to an inflammatory response initiated through wear particles, is still a main failure reason of total hip prostheses. Recently, polyMPC covalently grafted onto the surface of ultra-high molecular weight polyethylene (UHMWPE), a common material used for hip prostheses, was suggested as an improved bearing material^{169,170}. The polyMPC layer increases the hydrophilicity of the material and mimics physiological lubrication as the polyMPC polymer brushes reduce friction through hydration lubrication even under high contact pressures as discussed above. Kyomoto *et al.* showed that hip prosthesis cups with a high density of polyMPC grafted chains exhibit both low friction in ball-on-plate friction tests¹⁷⁰ and a significantly reduced wear rate compared to untreated cups in a hip simulator wear test using Co-Cr-Mo alloy balls¹⁷¹. They stated, that the polyMPC coating forms a 100 – 200 nm hydration layer on top of the surface of the material and thereby reduces friction and wear through hydration lubrication. When the proposed system was tested in a physiologically relevant environment, it was reported that lubrication with HA reduced the start-up friction whereas additional macromolecules from the synovial fluid might adsorb and increase the shear resistance of the polyMPC layer and thereby diminish its lubricity¹⁷². The latter effect has to be evaluated further, but might be reduced during physiological walking cycles owing to the constant de- and rehydration of the polymer layer. Moreover, surface modification with polyMPC is a promising approach as the clinical usage of MPC polymers, e.g., in soft contact lenses (omafilcon A, Proclear, CooperVision, USA) is already authorized by the FDA¹⁷³ and polyMPC-grafted acetabular liners in artificial hip joints have been approved for clinical use in Japan since 2011¹⁷⁰. First clinical data of the polyMPC-grafted liners (minimum of three years follow-up assessment and 22,000 clinical applications, Japan's UMIN-CTR: UMIN000003681¹⁷⁴) suggest an excellent *in vivo* performance, and neither wear nor osteolysis have been observed so far¹⁷⁵. This product might be a first clinically used permanent treatment option for cartilage defects that integrates a bioinspired lubrication strategy and was developed based on the extensive research conducted in the field of biotribology.

Whereas with the polyMPC coatings a physiological lubrication mechanism was mimicked with synthetic materials, one could also imagine that a biological molecule purified from one tissue can substitute the function of another molecule which is physiologically found in a different tissue. Indeed, it was demonstrated in this thesis that mucins are able to lubricate materials on which they do not occur physiologically, e.g., artificial interfaces such as steel/PDMS, glass/PDMS and polytetrafluorethylen (PTFE)/PDMS, and mucins also reduce friction and wear on cartilage surfaces. Therefore, they could potentially be used as alternative tribosupplements. For this application, the interaction of mucin with other synovial fluid molecules has to be evaluated in future studies, as well as the immunotoxicity of xenogeneic mucin, e.g., porcine gastric mucin, when brought in contact with human tissue. However, porcine gastric mucin is already clinically used in an artificial saliva substitute spray (Saliva Orthana, A.S Pharma, United Kingdom)¹⁷⁶, but seems not to provide an increased symptomatic relief of oral dryness over a mucin-free placebo spray¹⁷⁷. Certainly, the reason for this is unclear and could be due to an inadequate mucin purification process, as an irreversibly altered mucin structure, suppressed mucin-mucin interactions and significant deglycosylation have been suggested for Orthana mucin samples and other commercially available porcine gastric mucins (M2378/M1778, Sigma-Aldrich, USA)¹⁷⁸. A loss of lubricity due to deglycosylation was demonstrated in Section 3.4 and could be restored by suitable repair motifs. Therefore, properly purified porcine gastric mucin may be a promising ingredient not only for artificial saliva substitute sprays but also for eye drops, contact lens coatings or coatings on other sliding interfaces, e.g., in total joint prostheses, or on cartilage

substitute materials. It is likely that the purification efficiency of functional mucins can be increased in the future, which would enable the utilization of mucin as an aqueous lubricant beyond biomedical applications, for instance, as a durable super-lubricant in small bearing systems.

Appendix

This appendix is comprised of:

- A. The five journal articles summarized in this thesis
- B. The supplemental information of the featured articles
- C. The licenses of the publishers to use the articles for this thesis
- D. A publication list

A. Publications

A.1. Adapting a commercial shear rheometer for applications in cartilage research

REVIEW OF SCIENTIFIC INSTRUMENTS **85**, 093903 (2014)



Adapting a commercial shear rheometer for applications in cartilage research

K. Boettcher,^{1,2} S. Grumbein,^{1,2} U. Winkler,^{1,2} J. Nachtsheim,^{1,2} and O. Lieleg^{1,2,a)}

¹Zentralinstitut für Medizintechnik, Technische Universität München, 85748 Garching, Germany

²Fakultät für Maschinenwesen, Technische Universität München, 85748 Garching, Germany

(Received 13 June 2014; accepted 25 August 2014; published online 11 September 2014)

Cartilage research typically requires a broad range of experimental characterization techniques and thus various testing setups. Here, we describe how several of those tests can be performed with a single experimental platform, i.e. a commercial shear rheometer. Although primarily designed for shear experiments, such a rheometer can be equipped with different adapters to perform indentation and creep measurements, quantify alterations in the sample thickness, and conduct friction measurements in addition to shear rheology. Beyond combining four distinct experimental methods into one setup, the modified rheometer allows for performing material characterizations over a broad range of time scales, frequencies, and normal loads. © 2014 AIP Publishing LLC. [<http://dx.doi.org/10.1063/1.4894820>]

I. INTRODUCTION

Cartilage research might be one of the most dynamic and challenging research fields in biomedical engineering. One reason is the high prevalence of articular cartilage damage, as osteoarthritis alone is diagnosed for 22.7% of adult American citizens.¹ The knee cartilage repair market volume on its own is tremendous. However, cartilage regeneration methods cannot be adopted from other musculoskeletal research areas, since – in contrast to other tissues – the self-healing abilities of cartilage are very limited. This is due to the fact that cartilage tissue is devoid of neurons and blood vessels. Articular cartilage is composed of 80% water, with only one cell type (chondrocytes) residing inside the cartilage biopolymer matrix which is mainly composed of collagen II.² Although the material composition of articular cartilage is rather simple, the biomaterial poses many challenges for the development of a biomimetic substitute material. First, cartilage establishes a durable, low-friction surface in joints that has to withstand direct and continuous mechanical loading. Second, the structure of the natural material is highly complex and the structure-function relationships dictating the material properties of cartilage are not yet fully understood. Regarding the interplay of the different material components with each other and with the environment, a lot of consecutive theories have been published. For describing the bulk mechanical properties, the viscoelastic theory³ was further developed into the biphasic theory⁴ and later extended into the triphasic theory.⁵ For rationalizing the surface properties of cartilage, various mechanisms have been proposed as summarized by Neu *et al.*⁶ and McNary *et al.*⁷

The large variety of studies, theories, and mechanisms described in the literature can be, at least in part, attributed to the technical challenges in cartilage characterization. A plethora of different mechanical and structural characteriza-

tion techniques is necessary to investigate the complex material behavior of cartilage which leads to a broad range of applied testing strategies and utilized laboratory equipment. Therefore, the experimental results are often highly dependent on the applied measurement technique and only rarely the identical technique and measuring protocol is applied in more than one study.

Already the determination of cartilage thickness as well as observing its osmotic swelling behavior is performed with a multitude of techniques. Methods described in the literature include a digital micrometer, high frequency ultrasound,^{8,9} a laser-based system,¹⁰ a confined chamber,¹¹ and a needle probe measurement.¹² All of these techniques come with certain advantages and disadvantages. However, mechanical characterization techniques require the correct determination of cartilage thickness as an input parameter for calculating the material stiffness. In order to compare studies, it is important to employ techniques with an equal accuracy.

For evaluating the compressive properties of cartilage, macroscopic compression tests either in confined¹¹ or unconfined¹³ geometries are used in addition to indentation measurements with porous and solid indenters. These indenters can have sizes ranging from the macro-scale¹⁴ down to the μm scale, e.g., when atomic force microscopes¹⁵ or nanoindenters¹⁶ are used. Whereas macroscopic experiments mostly rely on static tests, AFM and nanoindenters can evaluate the dynamic compressive mechanical properties in an oscillatory manner covering a range of frequencies. Similarly, cartilage shear properties are usually evaluated over a frequency spectrum of typically 0.01–10 Hz using custom made setups¹⁷ or commercial rheometers.¹⁸

An even broader variety of test setups and protocols can be found for the determination of cartilage friction. In the joint, cartilage is loaded via an oscillatory movement with a migrating contact. This can be best simulated by a linearly reciprocating tribometer with a defined stroke length and sliding speed. Here, stainless steel, glass, or cartilage itself is used as a counterpart material for performing the friction

^{a)} Author to whom correspondence should be addressed. Electronic mail: oliver.lieleg@tum.de

measurement. However, these linear tribometers are limited to a rather small velocity range around a few mm/s,^{19,20} whereas the naturally occurring speed regime in the joint ranges from a few mm/s up to 200 mm/s.²¹ During the last years, AFM techniques were established to measure friction on cartilage surfaces at small sliding velocities but cannot reach into the speed range of linear tribometers or above. Therefore, a technique which enables the characterization of cartilage over its whole biomedically relevant speed regime would be highly beneficial for this field of research. In general, a versatile, cartilage-compatible testing system that incorporates the various experimental approaches described above into one setup would enable a more time-efficient, standardized, and comprehensive material characterization.

We here demonstrate how a commercial shear rheometer can be adapted by in-house crafted sample holders and measuring heads to perform four different measurement types that are highly relevant in cartilage research: measuring changes in cartilage thickness, indentation experiments, frequency dependent shear experiments, and cartilage tribology. We explain how cylindrical samples can be obtained from the joints of lambs, how those cylindrical samples can be used for the whole range of experiments by employing suitable sample holders, and we discuss example measurements for all of those measurement types.

II. EXPERIMENTAL SETUP

In the following, we describe the modification of a commercial stress-controlled rheometer from Anton Paar (Graz, Austria). Of course, the adapter fixing our in-house crafted sample holder onto the rheometer plate is adapted for this particular rheometer. However, we envision that similar adapter solutions can be easily found for other commercially available rheometers. All experiments shown here were conducted on a Physica Modular Compact Rheometer MCR 102 equipped with TruStrain control and the Tack/Squeeze/Normal Force extension package. The TruStrain control package lowers the minimal oscillation torque limit, whereas the Tack/Squeeze/Normal Force package enables normal force controlled measurements. The latter is required for cartilage compression and creep tests, as

well as for surface detection and determining the material relaxation under normal load. When choosing a rheometer for reproducing the measurements we describe here, it is important to make sure that it has a sufficiently refined normal force control implemented into its configuration.

A. Sample preparation

Osteochondral cylinders were harvested from both the lateral and medial side of the patella-femoral groove of lamb knee joints (hinder leg). The joints were obtained with closed articular joint capsules from a local slaughterhouse, frozen and stored at -20°C until further usage. For sample preparation, the joints were thawed at 4°C . The region of interest is the *Facies patellaris femoris* which is the area behind the knee cap. Figure 1 shows the preparation process of osteochondral cylinders from this area, starting from the closed joint. The joint is clamped in a vise and opened with a scalpel. Within the opened joint capsule, the *facies patellaris femoris* is identified (Fig. 1(a)) and a hollow, cylindrical drill is used to cut perpendicular through the articular surface into the bone (Fig. 1(b)). An oscillating saw is used to perform a horizontal cut into the bone from the side to detach the drilled cylinders from the rest of the joint (Fig. 1(c)). Afterwards, the cylindrical sample can be extracted from the bone with a lever tool and tweezers (Fig. 1(d)). For the experiments described below, relatively flat cartilage surfaces are required. However, the joint possesses an intrinsic curvature which limits both the size of an individual sample obtained by this drilling process and the number of samples that can be obtained from a given joint. For cartilage indentation experiments, dynamic shear measurements and for determining changes in the thickness of the cartilage layer during dehydration, we chose cylindrical samples with diameters of $2r = 8$ mm. In contrast, for cartilage tribology, samples with smaller diameters are sufficient when the ball-on-cylinder measuring setup we describe here is used (see Sec. II C 1). Thus, cylindrical drillings with a diameter of $2r = 5.5$ mm were used for our tribology experiments.

After sample extraction, the osteochondral cylinders were stored in 20 mM HEPES buffer (pH adjusted to 7.0 and supplemented with 154 mM NaCl) for at least 1 h before any

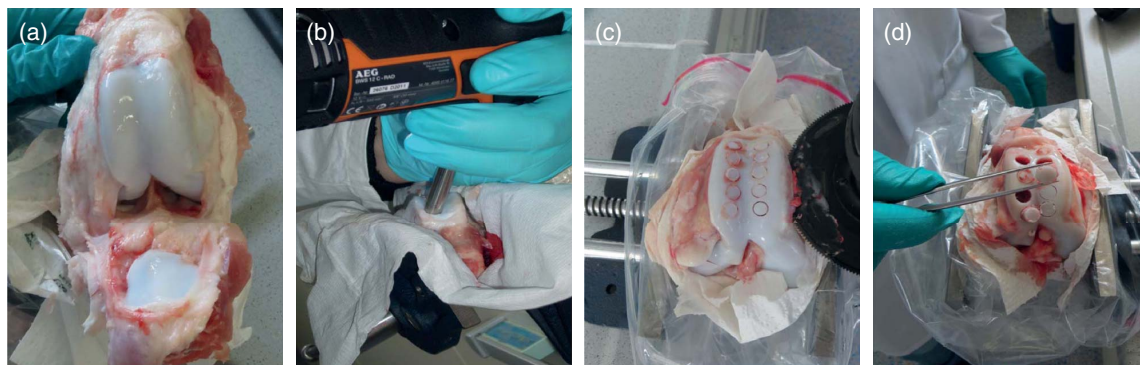


FIG. 1. Sample preparation procedure. The closed knee joint is opened and the *Facies patellaris femoris* is identified (a). Osteochondral cylinders are generated with a hollow drill (b) and removed from the joint using an oscillating saw (c). Finally, the samples are extracted with tweezers (d).

measurements were conducted. This procedure ensures comparable starting conditions as the cartilage samples are subjected to partial dehydration during the preparation process. For each measurement type shown in this article, only the bone segment of the cylindrical sample was used for fixation. As a consequence, the cartilage layer could always be probed without lateral confinement by the sample holder geometry.

B. Measuring setup for determining changes in cartilage thickness, indentation-creep measurements, and cartilage shear rheology

1. Sample holder geometry

For performing indentation experiments with the cylindrical samples, we crafted a customized sample holder geometry as depicted in Figure 2(a). This sample holder can also be used for measuring changes in the thickness of the cartilage layer, e.g., during dehydration, or for conducting dynamic shear experiments.

The core unit of this sample holder is a jaw chuck into which the cylindrical sample can be inserted. The sample is then fixed by adding a screw cap onto the jaw chuck and tightening the unit. Since this cap has a hole that is slightly larger than the sample diameter, the osteochondral cylinder can be inserted into the jaw chuck in such a way that the cartilage layer located on top of the cylinder is exposed.

The jaw chuck unit, in turn, is then mounted onto a hollow cylinder crafted from aluminum which has an inner diameter of 60 mm (Fig. 2(b)). The fixed sample can then be approached by a rheometer measuring head from above. The aluminum cylinder can be flooded with a liquid so that the cartilage sample is prevented from drying during the experiment. If a valuable liquid is used for the experiment, the volume of this aluminum cylinder can be reduced by inserting a cylindrical inset (Fig. 2(c)). In our case, we crafted this second cylinder from teflon. For fixing this sample holding unit onto the rheometer, a customized solution needs to be found depending on the type and geometry of the rheometer bottom plate that is normally used for sample deposition. In the case of Anton Paar rheometers from the MCR series, this can

be achieved by an adapter ring which is fixed to the sides of the rheometer sample plate (P-PTD200/56/AIR, Anton Paar, Graz, Austria) by three screws. This adapter ring was generated with a winding into which the aluminum cylinder can be screwed tight. This allows for working with several sample holders in parallel and to quickly switch sample holders without the need of opening the jaw chuck and removing the old sample first.

All the experiments described here were conducted at room temperature. However, if all adapter parts were crafted from suitable metals, the temperature-controlling abilities of the peltier element integrated into the rheometer sample plate could be harnessed to achieve a certain level of temperature control.

2. Determining changes in cartilage thickness

For strongly hydrated materials such as cartilage, the fluid flux into or out of the material and thus its dynamic swelling and shrinkage behavior is of great interest. We now describe how a change in cartilage thickness triggered by a loss of water can be traced by following the cartilage surface during the dehydration process. This protocol can also be used to investigate the influence of environmental conditions (e.g., temperature, humidity, osmotic pressure) on the cartilage hydration state and thus its thickness, or to examine the inverse process, i.e., cartilage (re)hydration and the ensuing increase in cartilage thickness.

For detecting the cartilage surface of the osteochondral cylinders, the measuring head of the rheometer was lowered from a retracted position ~ 20 mm above the sample surface at a speed of $100 \mu\text{m/s}$ and a data acquisition time of 0.05 s until a normal force of 0.05 N was reached. At this point, the gap position was recorded (which allows for calculating relative changes in the thickness of the cartilage layer) and the measurement head was retracted. In the example measurements shown in Figure 3, the protocol was applied over a time period of 10 h and a measuring point was acquired every 10 min.

Initially, the measuring head diameter was chosen to match to the cartilage sample diameter ($2r = 8$ mm). However, some specimens developed elevated areas on the

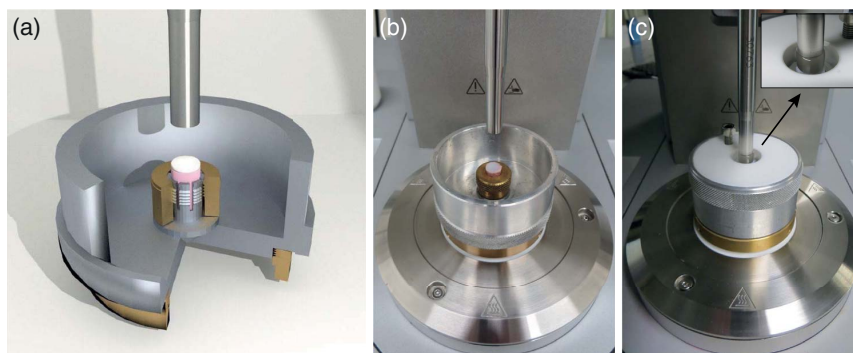


FIG. 2. Sample holder setup. The core unit of the sample holder (a) is a jaw chuck into which the osteochondral cylinder is inserted. The sample holder, in turn, is fixed onto the sample plate of the rheometer via an adapter ring (b). For measurements where the sample needs to be immersed into a valuable liquid, the volume of the sample holder can be reduced by inserting a second cylinder (c). The close-up view in subfigure (c) shows the lowered measuring head which is partially immersed into the fluid during the measurement, the cartilage surface is located ~ 1 cm below the liquid/air interface.

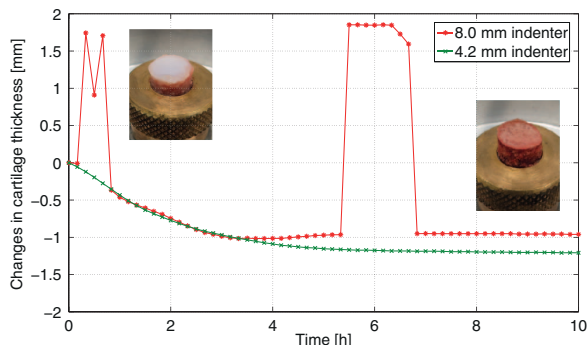


FIG. 3. Alterations in the thickness of a cartilage layer during dehydration. Whereas an indenter size equal to the sample diameter ($d = 8$ mm, red circles) leads to artifacts in the measurement, a smaller indenter ($d = 4.2$ mm, green crosses) was successfully used to trace the changes in cartilage thickness over time. The small pictures visualize the sample state at the starting and end point of the measurement.

circular edge of the sample during the dehydration process. Those elevated areas on the sample edge lead to artifacts when the measuring head approaches the sample surface (red curve in Fig. 3). This demonstrated that a measuring head with a thinner tip is required for such a measurement. As a measuring head with a diameter of 8 mm is the smallest commercial measuring system available for this rheometer, a customized solution was developed. Therefore, a measuring head adapter available for single-use plates (D-CP/PP 7, Anton Paar, Graz, Austria) was combined with an in-house crafted indenter that exhibits a tip with a diameter of $2r = 4.2$ mm (Fig. 4).

Owing to the smaller diameter of the indenter, the artifacts generated by the elevated edges of the dehydrated samples were eliminated and the continuous changes in cartilage thickness during dehydration were successfully recorded (green curve in Fig. 3). Overall, the cartilage layer thickness decreased by 1.2 mm during ~ 6 h. After this time, no significant changes were detected anymore. During the first 1.5 h, the thickness reduction was approximately linear in time whereas the shrinkage rate decreased afterwards. With an initial cartilage layer thickness of 1.8 mm (as determined

with a caliper), the thickness of this particular cartilage sample decreased by approximately 67% during dehydration.

3. Cartilage indentation and creep experiments

For an appropriate characterization of a viscoelastic bio-material such as cartilage, various considerations and decisions have to be made prior to any experiments. For instance, full sample hydration needs to be ensured during the measurement and the indenter type and size should be chosen carefully. For viscoelastic materials, flat indenters are frequently chosen as they ensure a constant and well-known contact area independent of the displacement. When defining the indenter diameter, one has to consider that a large indenter might not get in full contact with the slightly curved surface of cartilage, whereas a smaller indenter may lead to increasing edge effects around the indenter.¹⁶

When performing an indentation experiment, it is important to realize that cartilage is a viscoelastic material that exhibits relaxation and creep behavior at constant displacement or load, respectively. Therefore, normal force controlled test protocols should be favored over displacement controlled procedures. Here, for a static indentation test, the surface was first approached from a retracted position at a speed of $25 \mu\text{m/s}$ until a normal force $F_N > 0.05$ N was detected. Afterwards, an indentation speed of $1 \mu\text{m/s}$ and a data acquisition time of 0.1 s were chosen, and the sample was indented until the creep force (Fig. 5(a): F_{creep}, t_1) was reached. For the following creep test, the force was kept constant at a creep force of 3 N or 7 N, respectively, for 2 h (Fig. 5(a): t_2). To evaluate the influence of the indenter size, the indentation test was conducted with three different indenter sizes: $2r = 1.5$ mm, 4.2 mm, and 8 mm. The two smaller indenters were crafted in-house and were used with the same sample holder and adapter geometry as described in Sec. II B 1. The indentation data are shown in Figure 5(b) for the first 15% strain. Young's moduli were calculated as $E = \text{stress/strain}$ between 1% and 10% strain. The obtained values ranged from 0.3 MPa to 9.4 MPa and increased with decreasing indenter size which is consistent with previously published data.²²

During the unconfined compression test (8 mm indenter), the measured mechanical behavior is insensitive towards

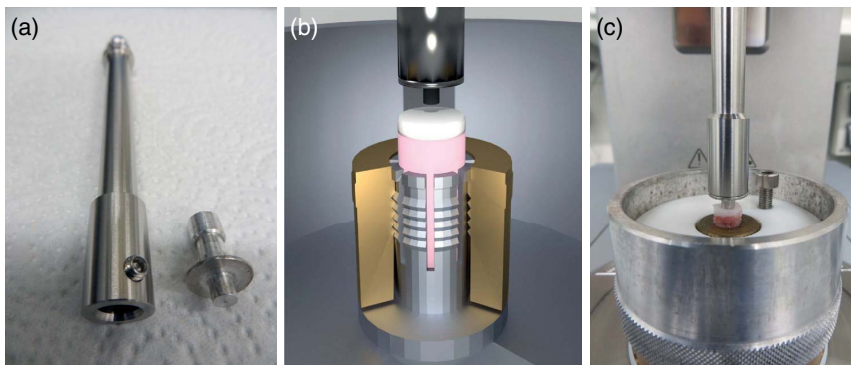


FIG. 4. Indentation setup. The customized indenter can be inserted into the commercial measuring head adapter (a). During the measurement, this indenter is lowered onto the osteochondral cylinder (b) which is mounted into the sample holder (c) as described in the main text.

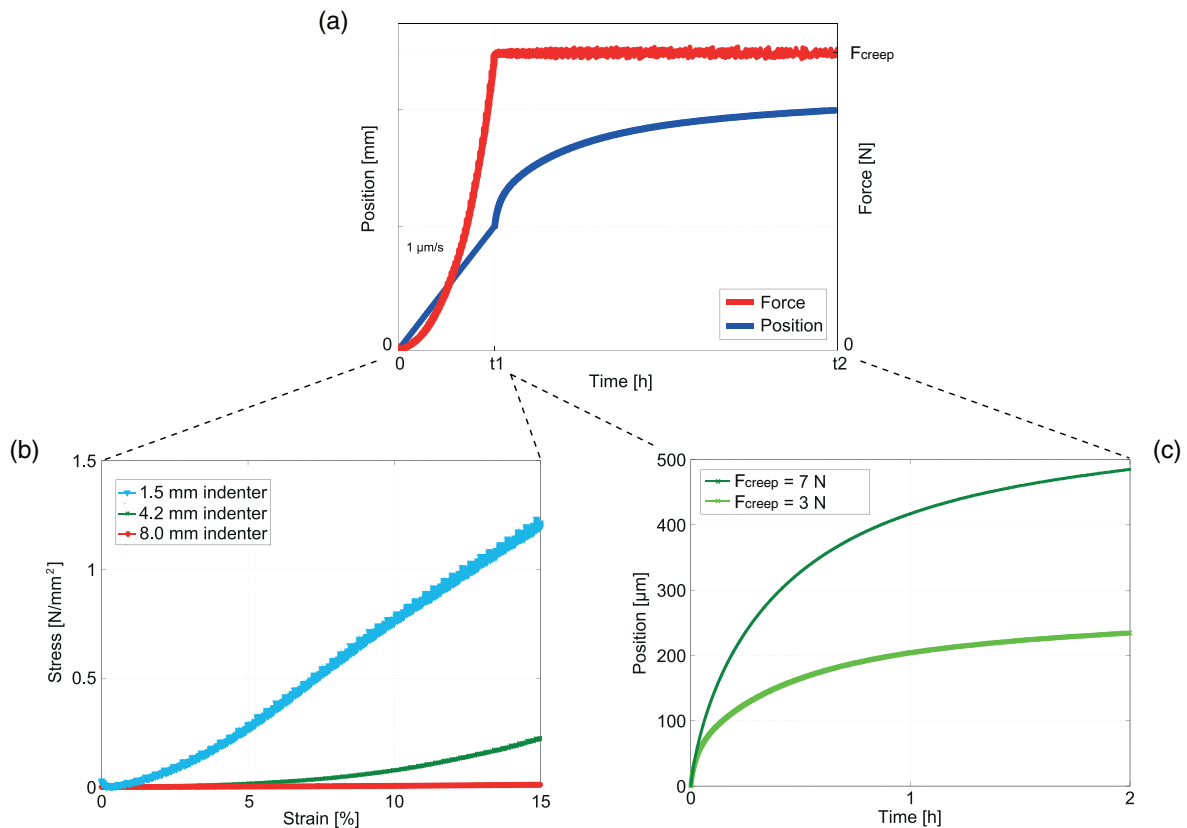


FIG. 5. Indentation-creep measurements performed (a) at a constant indentation speed (b) and a constant creep force (c). For both measurements, the osteochondral sample was immersed in 20 mM HEPES buffer supplemented with 154 mM NaCl.

local sample variations. However, the sample surface curvature might prevent full contact between the sample and the measuring head and thereby lead to an underestimation of the modulus. In contrast, using smaller indenters corresponds to a confined testing setup with increasing edge problems and an increasing sensitivity to local sample inhomogeneities. Moreover, cartilage is a viscoelastic tissue and thereby its material properties cannot be fully described by a Young's modulus as this would neglect the viscous part of the material behavior. A dynamic analysis is necessary to determine both the elastic (storage modulus) and viscous (loss modulus) component at different frequencies and load amplitudes. Such a dynamic, oscillating measuring protocol requires a high resolution in the vertical movement. However, the utilized rheometer is equipped with a step motor developed for switching between different positions in the vertical direction. Precise oscillations are typically only performed in the horizontal plane (see Sec. II B 4) and controlled via a second, independent motor. Oscillatory indentation experiments might be possible with the newest rheometer generation (e.g., the MCR 702 Twin-Drive (Anton Paar) equipped with a "IsoLign Piezo flange" which enables a stepless gap control down to sizes of 10 nm) but are difficult to perform with the rheometer used here.

The creep measurements were conducted with the $2r = 4.2$ mm indenter at two different creep force levels

(3 N and 7 N) corresponding to normal stresses of 0.22 MPa and 0.5 MPa. As expected, the observed creep is smaller for the smaller normal force, resulting in a total creep deformation of $220 \mu\text{m}$. For the higher creep force, a creep displacement of $500 \mu\text{m}$ is reached. The equilibrium creep strain is 28% at 3 N and 48% at 7 N, respectively. Thus, our result agrees very well with the creep strain of $(55 \pm 3)\%$ measured by Basalo *et al.* under similar conditions.²³

4. Cartilage shear rheology

Dynamic shear measurements were performed using a parallel plate measuring head with a diameter of 8 mm (PP08, Anton Paar, Graz, Austria). The osteochondral samples were placed into the customized sample holder and fully covered with fluid to prevent sample drying. For determining the storage and loss modulus of the sample, a frequency sweep was performed at room temperature over a frequency range of 10 Hz to 1 mHz. A normal force of 1 N was applied and kept constant during the measurement. This value was chosen as the minimal normal force at which visual inspection of the sample/measuring head interface suggested full contact. We observed an increase of the measured shear modulus and stronger sample creep with increasing normal force (data

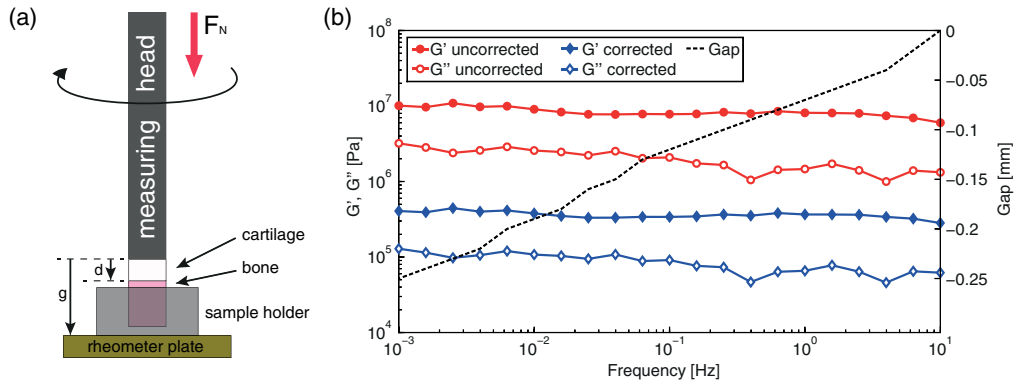


FIG. 6. Analysis of the cartilage shear rheology data. A schematic illustration of the relevant dimensions required for data correction is depicted in (a). The shear moduli calculated by the rheometer (red) are based on the measured gap, g , and need to be corrected for the initial sample thickness, d_0 , and the cartilage thickness decrease due to relaxation as indicated by the dashed curve in (b). As a consequence, both moduli are shifted to lower absolute values and the artificial increase of the storage modulus at low frequencies is eliminated (b). See main text for details.

not shown). A normal-force controlled measurement is necessary since cartilage exhibits significant creep which makes deformation-controlled frequency sweeps difficult. Owing to the fact that the osteochondral cylinders are inserted into the adapter where they are fixed manually, the position of the cartilage surface will slightly vary between experiments. Furthermore, the gap recorded by the instrument will not correspond to the sample thickness. As a consequence, the shear strain amplitude γ calculated by the rheometer will not correctly return the amount of shear that is actually applied to the cartilage layer. We now briefly describe how this can be accounted for in the data analysis.

To ensure linear response, a pre-measurement using a torque of $M = 1 \mu\text{Nm}$ and a frequency of $f = 1 \text{ Hz}$ was performed to determine the deformation γ_0 the rheometer can successfully control for the given cartilage sample (here: $\gamma_0 = 0.0003\%$ at a plate separation of $\sim 35 \text{ mm}$). For the following frequency sweep, a nominal shear strain amplitude slightly larger than this amplitude was chosen, i.e., $\gamma = 0.001\%$. It is important to realize that, in the rheometer software (Rheoplus, Anton Paar, Graz, Austria), this shear strain amplitude is defined as the ratio between the angular displacement φ and the gap g between the sample plate and the measuring head. For calculating the dynamic shear moduli, the software assumes that this gap is equal to the sample thickness d , which does not hold true anymore in our customized configuration (Fig. 6(a)). Accordingly, the shear strain amplitude needs to be corrected with the ratio of the measured gap ($\sim 35 \text{ mm}$) and the sample thickness ($\sim 1.5 \text{ mm}$), and we obtain an effective shear strain amplitude of 0.023% . Similarly, the shear moduli calculated by the software need to be corrected by the same ratio:

$$G_{\text{corrected}}^* = \frac{\text{stress}}{\text{strain}} = \frac{2 Mg}{\pi r^4 \varphi} \times \frac{d}{g} = G_{\text{uncorrected}}^* \times \frac{d}{g}.$$

Here, r denotes the radius of the cylindrical sample. The initial cartilage layer thickness d_0 was evaluated for each fresh sample on four points along the contour using a caliper. If only a single measuring point is recorded, this simple correction is sufficient, and at a frequency of 1 Hz we measure corrected

storage moduli in the range of $0.4\text{--}0.6 \text{ MPa}$ which agrees well with literature values.¹⁷

However, when an extended frequency spectrum is recorded over several orders of magnitude in frequencies, it is important to realize that the cartilage layer thickness decreases over time. This is due to the necessity of performing the shear measurements with a constant normal force which induces vertical cartilage creep (see Sec. II B 3). To correct for this time dependent change in the cartilage layer thickness, it is necessary to read out the current gap position $g(f)$ for each measurement point. These updated thickness values $d(f)$ then need to be used for the calculation of the dynamic shear moduli. As a consequence, the previous equation is slightly modified to

$$\begin{aligned} G_{\text{corrected}}^*(f) &= G_{\text{uncorrected}}^*(f) \times \frac{d(f)}{g(f)} \\ &= G_{\text{uncorrected}}^*(f) \times \frac{d_0 - [g_0 - g(f)]}{g(f)}, \end{aligned}$$

where g_0 denotes the gap recorded at the beginning of the frequency sweep. An example how the recorded frequency spectrum of a cylindrical cartilage sample changes after this correction is depicted in Figure 6(b). Although the frequency dependence of both viscoelastic moduli is weak, the artificial increase of the storage modulus with decreasing frequencies is removed when the correction is applied. In our example, we obtain a loss factor of ~ 0.2 which underscores the highly elastic properties of cartilage reported in the literature.²⁴

C. Measuring setup for performing cartilage friction measurements

1. Sample holder geometry and tribology unit

The measuring setup we describe here for performing tribology experiments on osteochondral cylinders is a modification of a classical ball-on-3-plates setup (T-PTD 200, Anton Paar, Graz, Austria) and the sample holder for this application was developed together with Anton Paar (Fig. 7(a)).

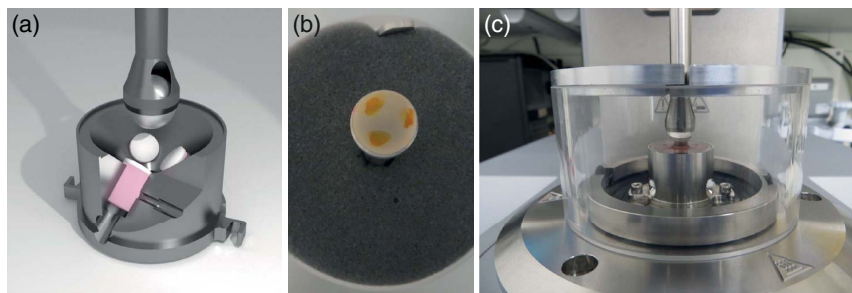


FIG. 7. Schematic illustration of the tribological test setup probing a set of three osteochondral cylinders with a 1/2 in. glass sphere (a). An equal force distribution on each of the three cylindrical samples is verified by evaluating the contact area between each cartilage surface and the glass sphere (b). The assembled tribology setup with mounted sample holder, covering hood and lowered measuring head is depicted in (c).

This setup combines a cylindrical measuring head which can hold spheres with diameters of 1/2 in. (BC 12.7, Anton Paar, Graz, Austria) with a sample holder unit into which three cylindrical samples can be inserted (Fig. 8(a)). For performing tribological measurements, spheres crafted from a broad range of materials can be used. We have mostly focused on spheres made of glass or steel (Kugel Pompel, Wien, Austria). However, depending on the application, other materials such as ceramics or polymer spheres might be interesting as tribological measuring heads as well.

The vertical position of the cylindrical samples that are inserted into the sample holder can be individually adjusted by three screws which reach into the cylindrical drillings of the sample holder from below (Fig. 8(b)). In addition, we have integrated a second set of three screws which allow for the lateral fixation of the inserted samples (Fig. 8(c)). This modification avoids lateral sample movement during friction measurements and prevents unwanted sample extraction from the sample holder between distinct measurements, i.e., when the measuring head holding the tribology-sphere is pulled back in vertical direction.

The commercial tribology-unit supporting the sample holder (T-PTD 200, Anton Paar, Graz, Austria) comprises a lateral spring system which ensures that an applied normal force is evenly distributed onto the three cylindrical samples so that lateral shear is minimized. For the measurements described here, a normal force of 6 N was applied to the sample set, resulting in a force of 2.8 N acting normally to each specimen surface. An even force distribution was experimentally verified by obtaining colored imprints of stained

cartilage samples onto the glass sphere (Fig. 7(b)). We also observed that, with this normal force, almost full contact between the tribo-glass sphere and the surface of the osteochondral cylinders is achieved. To fully lubricate the samples in this sample holder, a volume of approximately 1 ml is necessary, and a covering hood was designed to minimize fluid evaporation during long-term measurements (Fig. 7(c)).

2. Cartilage friction measurements

When determining the friction coefficient on cartilage samples, it is important to realize that cartilage exhibits a time-dependent friction behavior which is based on the triphasic nature of the strongly hydrated cartilage biopolymer matrix. At short loading times, the tribological behavior is dominated by a fluid film that is generated on the surface of the cartilage layer, and this fluid film is, to a great extent, responsible for the very low friction properties of cartilage. If the mechanical load persists, increasing amounts of the applied normal force are carried by the cartilage biopolymer matrix which leads to an increasing friction coefficient. At extended probing times, the friction coefficient is reported to saturate and reaches a plateau. The absolute value of the measured friction coefficient will depend on both, the material used for probing the tribological properties of cartilage and the detailed setup of the tribology measuring system. This time-dependent friction behavior should occur for most if not all tribological techniques. Indeed, as depicted in Figure 9, we observe this time-dependent friction behavior in our rotational tribology setup

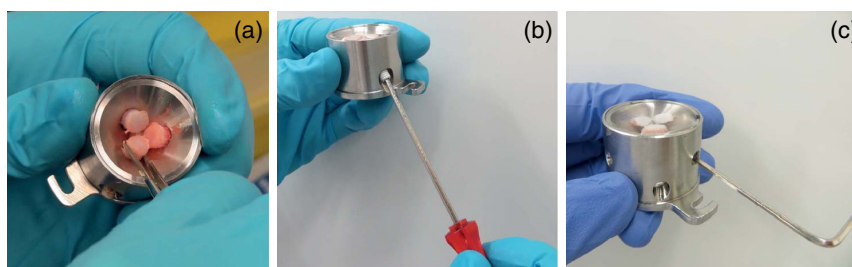


FIG. 8. Sample holder setup for cartilage tribology. Three cylindrical samples are placed into the sample holder (a) and their vertical position is adjusted with set screws (b). Lateral sample displacement is suppressed by a third set of screws (c) which fix the bone segment of the osteochondral cylinder in the sample holder.

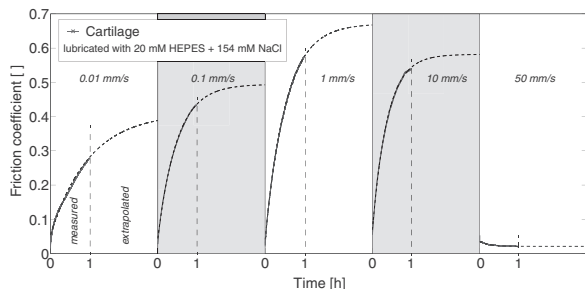


FIG. 9. Increase of the friction coefficient over time at different rotational speeds as determined for a measuring time of 1 h. The data points were then fitted with an exponential rise (see main text) to obtain the plateau friction coefficient for each speed level.

at low and intermediate rotation speeds. Different from linear tribology setups, where the accessible range of sliding velocities is rather limited due to inertia effects, rotational tribology offers the possibility to analyze a broad range of friction speeds. In fact, the shear rheometer used here can control rotation speeds in the range of 1 $\mu\text{m/s}$ to 100 mm/s very well. Within this accessible range of rotation speeds, only at the highest rotation speed tested, i.e., at 50 mm/s, we observed a qualitatively different time-dependent friction behavior.

Here, the friction coefficient continuously decreases over time. Whereas this behavior is highly reproducible, its microscopic origin is still unclear. It can be seen from the individual friction measurements depicted in Figure 9, that within a measurement time of 1 h, none of the curves reaches its plateau friction value. However, by fitting an exponential rise to the data (see dashed lines in Fig. 9), we can extrapolate this plateau friction coefficient (μ_{plateau}):

$$\mu(t) = \mu_{\text{plateau}} - b \times e^{-ct}.$$

The 1 h sliding speed-measurements were conducted with a normal force of 6 N in an arbitrary order with 30 min of relaxation time in between the measurements. Therefore, a complete measurement on one sample set lasted 7 h in total (5 h measurement time). The data acquisition rate for these measurements was set to 1 point/s.

Next, we compare those plateau friction values obtained at different constant sliding speeds to the friction coefficients obtained from a different experiment type, i.e., speed ramp measurements. In those speed ramps, the rotation speed is continuously increased and the friction coefficient is determined at each passing speed level. In such an experiment, the total measurement time is significantly lower than for the measurements at constant speed levels, but the measuring time per speed level is rather short. Thereby, the acquisition time per data point can be tuned and, as a consequence, different regimes of the time-dependent friction behavior will be probed for speed ramps with short and long acquisition times. Thus, one would expect that a speed ramp with a higher acquisition time will return larger friction coefficients than a speed ramp with a shorter acquisition time. Indeed, we observe such a behavior (Fig. 10).

When comparing the two different measuring protocols, we also find that the plateau friction values, obtained as shown

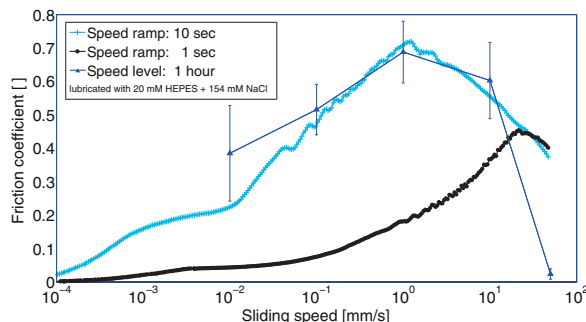


FIG. 10. Comparison of the plateau friction coefficient obtained at distinct rotation speeds (dark blue triangles, 1 h total measurement duration, data from Fig. 9) with results obtained with speed ramp measurements performed with different data acquisition times and 50 data points per decade (black circles: 1 s; light blue crosses: 10 s).

in Figure 9, nicely coincide with the 10 s speed ramp (which is surprising given the large differences in the corresponding time scales). We note that further measurements will be needed to differentiate between effects which are due to the acceleration of the tribology head (which is prominent in speed ramp measurements) and intrinsic material behavior at specific sliding speeds.

III. CONCLUSION

We here have described how four different measurement types which are all highly relevant for cartilage research can be performed with a single commercial shear rheometer. Most of the modifications that are necessary to conduct those measurements are quick and easy and require only adapters that can be crafted in an in-house workshop. The only exception is the tribology unit which is needed to minimize lateral shear during a rotational friction force measurement. All the measurements described can be performed with immersed samples, and the volume of the required hydration liquid is low in all cases, i.e., in the range of a few ml. Whereas we have focused on demonstration measurements with osteochondral cylinders, other cylindrical samples can of course be inserted into the presented sample holder geometries as well. Any synthetic or bioengineered material which is envisioned to be used as a cartilage substitute in the future can thus be tested in the exactly same measurement setup as its biological template. In conclusion, the modifications we describe here might provide a convenient platform to conduct a broad range of precise and well-defined material characterization tests in one single setup.

ACKNOWLEDGMENTS

The authors thank Rudolf Lehrhuber for crafting the adapters and sample holders and the Bayerische Landesanstalt für Landwirtschaft (LfL) Institut für Tierzucht Grub/Poing (Albert Steiner and Marcel Bowenz) for providing the lamb joints. This project was supported by the International Graduate School of Science and Engineering (IGSSE) in the framework of the focus area “Biomaterials.” Additional support

093903-9 Boettcher *et al.*Rev. Sci. Instrum. **85**, 093903 (2014)

from the Deutsche Forschungsgemeinschaft through SFB 863 is acknowledged as well.

- ¹K. E. Barbour, C. G. Helmick, K. A. Theis, L. B. Murphy, J. M. Hootman, T. J. Brady, and Y. J. Cheng, *MMWR Morb. Mortal Wkly. Rep.* **62**, 869–873 (2013).
- ²J. S. Temenoff and A. G. Mikos, *Biomaterials* **21**, 431–440 (2000).
- ³J. Parsons and J. Black, *J. Biomech.* **10**, 21–29 (1977).
- ⁴V. Mow, S. Kuei, W. Lai, and C. Armstrong, *J. Biomech. Eng.* **102**, 73–84 (1980).
- ⁵W. M. Lai, J. S. Hou, and V. C. Mow, *J. Biomech. Eng.* **113**, 245–258 (1991).
- ⁶C. P. Neu, K. Komvopoulos, and A. H. Reddi, *Tissue Eng. Part B* **14**, 235–247 (2008).
- ⁷S. M. McNary, K. A. Athanasiou, and A. H. Reddi, *Tissue Eng. Part B* **18**, 88–100 (2012).
- ⁸Q. Wang, Y.-Y. Yang, H.-J. Niu, W.-J. Zhang, Q.-J. Feng, and W.-F. Chen, *BMC Musculoskelet. Disord.* **14**, 289 (2013).
- ⁹Q. Wang, Y. P. Zheng, G. Leung, W. L. Lam, X. Guo, H. B. Lu, L. Qin, and A. F. T. Mak, *Phys. Med. Biol.* **53**, 2537–2552 (2008).
- ¹⁰A. Pham and M. Hull, *J. Biomech.* **40**, 3223–3229 (2007).
- ¹¹S. R. Eisenberg and A. J. Grodzinsky, *J. Orthop. Res.* **3**, 148–159 (1985).
- ¹²J. S. Jurvelin, T. Räsänen, P. Kolmonens, and T. Lyyra, *J. Biomech.* **28**, 231–235 (1995).
- ¹³I. M. Basalo, R. L. Mauck, T.-A. N. Kelly, S. B. Nicoll, F. H. Chen, C. T. Hung, and G. A. Ateshian, *J. Biomech. Eng.* **126**, 779 (2004).
- ¹⁴V. Mow, M. Gibbs, W. Lai, W. Zhu, and K. Athanasiou, *J. Biomech.* **22**, 853–861 (1989).
- ¹⁵L. Han, E. H. Frank, J. J. Greene, H.-Y. Lee, H.-H. K. Hung, A. J. Grodzinsky, and C. Ortiz, *Biophys. J.* **100**, 1846–1854 (2011).
- ¹⁶O. Franke, M. Göken, M. A. Meyers, K. Durst, and A. M. Hodge, *Mater. Sci. Eng. C* **31**, 789 (2011).
- ¹⁷M. Jin and A. J. Grodzinsky, *Macromolecules* **34**, 8330–8339 (2001).
- ¹⁸A. M. Nguyen and M. E. Levenston, *J. Orthop. Res.* **30**, 95–102 (2012).
- ¹⁹I. M. Basalo, D. Raj, R. Krishnan, F. H. Chen, C. T. Hung, and G. A. Ateshian, *J. Biomech.* **38**, 1343–1349 (2005).
- ²⁰L. Shi, V. I. Sikavitsas, and A. Striolo, *Ann. Biomed. Eng.* **39**, 132–146 (2011).
- ²¹J. H. Dumbleton, *Tribology of Natural and Artificial Joints* (Elsevier Scientific Pub. Co., Amsterdam, 1981), Vol. 3.
- ²²R. Korhonen, M. Laasanen, J. Töyräs, J. Rieppo, J. Hirvonen, H. Helminen, and J. Jurvelin, *J. Biomech.* **35**, 903–909 (2002).
- ²³I. M. Basalo, F. H. Chen, C. T. Hung, and G. A. Ateshian, *J. Biomech. Eng.* **128**, 131–134 (2006).
- ²⁴W. Zhu, V. C. Mow, T. J. Koob, and D. R. Eyre, *J. Orthop. Res.* **11**, 771–781 (1993).

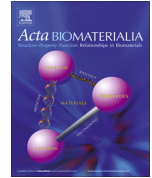
A.2. The structure and mechanical properties of articular cartilage are highly resilient towards transient dehydration

Acta Biomaterialia 29 (2016) 180–187



Contents lists available at ScienceDirect

Acta Biomaterialia

journal homepage: www.elsevier.com/locate/actabiomat

The structure and mechanical properties of articular cartilage are highly resilient towards transient dehydration

K. Boettcher^a, S. Kienle^b, J. Nachtsheim^a, R. Burgkart^c, T. Hugel^{b,d}, O. Lielég^{a,*}^a Institute of Medical Engineering IMETUM and Department of Mechanical Engineering, Technische Universität München, Boltzmannstraße 11, 85748 Garching, Germany^b Institute of Medical Engineering IMETUM and Physics Department, Technische Universität München, Boltzmannstraße 11, 85748 Garching, Germany^c Clinic of Orthopaedics and Sportsorthopaedics, Klinikum rechts der Isar, Technische Universität München, Ismaninger Str. 22, 81675 Munich, Germany^d Institute of Physical Chemistry, University of Freiburg, Albertstr. 23a, 79104 Freiburg, Germany

ARTICLE INFO

Article history:

Received 31 March 2015

Received in revised form 7 September 2015

Accepted 28 September 2015

Available online 30 September 2015

Keywords:

Dehydration

Tribology

Histology

Rheology

SEM

AFM

ABSTRACT

Articular cartilage is a mechanically highly challenged material with very limited regenerative ability. In contrast to elastic cartilage, articular cartilage is exposed to recurring partial dehydration owing to ongoing compression but maintains its functionality over decades. To extend our current understanding of the material properties of articular cartilage, specifically the interaction between the fluid and solid phase, we here analyze the reversibility of tissue dehydration. We perform an artificial dehydration that extends beyond naturally occurring levels and quantify material recovery as a function of the ionic strength of the rehydration buffer. Mechanical (indentation, compression, shear, and friction) measurements are used to evaluate the influence of de- and rehydration on the viscoelastic properties of cartilage. The structure and composition of native and de/rehydrated cartilage are analyzed using histology, scanning electron microscopy, and atomic force microscopy along with a 1,9-dimethylmethylene blue (DMMB) assay. A broad range of mechanical and structural properties of cartilage can be restored after de- and rehydration provided that a physiological salt solution is used for rehydration. We detect only minor alterations in the microarchitecture of rehydrated cartilage in the superficial zone and find that these alterations do not interfere with the viscoelastic and tribological properties of the tissue.

Statement of Significance

We here demonstrate the sturdiness of articular cartilage towards changes in fluid content and show that articular cartilage recovers a broad range of its material properties after dehydration. We analyze the reversibility of tissue dehydration to extend our current understanding of how the material properties of cartilage are established, focusing on the interaction between the fluid and solid phase. Our findings suggest that the high resilience of the tissue minimizes the risk of irreversible material failure and thus compensates, at least in part, its poor regenerative abilities. Tissue engineering approaches should thus not only reproduce the correct tissue mechanics but also its pronounced sturdiness to guarantee a similar longevity.

© 2015 Acta Materialia Inc. Published by Elsevier Ltd. All rights reserved.

1. Introduction

Articular cartilage differs from other tissues owing to its extraordinary ability to withstand high loads along with its opti-

mized friction properties. Cartilage possesses a poor self-renewal capacity, which also distinguishes this particular tissue from other tissue types. To ensure its function over a lifetime and under extreme situations, various mechanisms are in place to distribute loads and dissipate energy, thereby protecting the network structure from damage. Understanding the detailed structure–function relationships in articular cartilage has proved to be challenging [1,2]; however, such an understanding would not only help to create suitable cartilage surrogate materials but also facilitate the development of numerous biomimetic approaches. The unique material properties of cartilage are thought to be attributed to

* Corresponding author at: Zentralinstitut für Medizintechnik der Technischen Universität München, Boltzmannstraße 11, 85748 Garching, Germany.

E-mail addresses: kathrin.boettcher@tum.de (K. Boettcher), kienle.sandra@gmail.com (S. Kienle), j.nachtsheim@hotmail.de (J. Nachtsheim), burgkart@tum.de (R. Burgkart), thorsten.hugel@physchem.uni-freiburg.de (T. Hugel), oliver.lieleg@tum.de (O. Lielég).

<http://dx.doi.org/10.1016/j.actbio.2015.09.034>

1742-7061/© 2015 Acta Materialia Inc. Published by Elsevier Ltd. All rights reserved.

the interactions of the synovial fluid and interstitial fluid with the solid tissue phase. The solid phase of articular cartilage contains a single cell type (chondrocytes) embedded in an extracellular matrix (ECM) [3,4], which can be subdivided into the type II collagen fiber network and glycosaminoglycans (GAGs). These GAGs establish a highly negative fixed charge density in the cartilage ECM and thereby govern the interplay between the solid and fluid phase. This negative net charge attracts mobile counterions (e.g., Na^+ , Ca^{2+}) from the fluid phase to maintain electroneutrality inside the tissue. The resulting imbalance of mobile ions inside and outside the tissue leads to an osmotic pressure (Donnan pressure); this process is called interstitial fluid pressurization and can be described by triphasic theory [5].

Cartilage is known for its superior low-friction properties but is often described as a “spongy shock absorber” that protects the joint from impact loads. With every joint movement, interstitial fluid is pressed out of the cartilage and soaked back into the tissue during unloading. This mechanism occurs constantly as the contact point migrates over the joint surfaces and is established by the negatively charged GAGs [6]. During short mechanical loading, over 95% of the load is supported by the fluid phase [7]. Early stages of cartilage degeneration are accompanied by a decrease in the GAG content, and thus by a decreased ability of cartilage to strongly bind water, which counterintuitively leads to an increased water content [8]. Consequently, an external mechanical load must be carried mostly by the solid phase instead of by the fluid phase.

For a better understanding of the material behavior of articular cartilage, previous studies have exposed the tissue to various extreme situations. For example, decreasing the GAG content or changing the ionic strength of cartilage interstitial fluid to non-physiological levels through dialysis was observed to alter the structural [9,10], compressive [11], tensile [12], and shear properties [9,13,14] along with the friction behavior [15] of cartilage. Although these tissue modifications are generally more drastic than changes that occur *in vivo*, they have provided valuable insights into how the material properties of cartilage are established on a molecular scale. To date, few studies have investigated the degree to which cartilage tissue can recover its microstructure [6] and mechanical properties after dehydration [16,17] and how this process depends on the ionic strength of the rehydration fluid. This is especially interesting because partial dehydration of cartilage can occur during complex, long-lasting surgical procedures (e.g., mosaicplasty and allotransplantation) or develop because of GAG loss during early arthritis or long-term loading. Indeed, long-term joint loading can stimulate GAG synthesis [18], which indicates that the human body tries to counteract the recurring partial dehydration events by increasing the ability of cartilage to pressurize the interstitial fluid, thus preventing irreversible damage. When studying material failure, one possible approach to estimate the long-term endurance of a material is to mimic the physiological loading as closely as possible and study the material over extended time periods. A complementary strategy that is often used in engineering science is to apply a drastically increased, non-physiological challenge over a shorter time period, on the assumption that this will yield a comparable outcome (accelerated life testing) [19].

In this study, we chose a materials science approach and studied the material properties of articular cartilage by examining its response to de- and rehydration. We challenged the biomaterial with dehydration beyond physiological levels and performed rehydration with different fluids to gain a better understanding of the interaction between the solid and fluid phase of the tissue. We systematically compared the structural, topological, mechanical, and tribological properties of articular cartilage in both its fresh state and after complete de- and rehydration as a function of the NaCl

concentration in the rehydration buffer. With this approach, we were able to demonstrate the high resilience of articular cartilage towards transient water loss.

2. Experimental

2.1. Specimen preparation and treatment

Articular cartilage tissue was harvested from 3 to 6 month old male lambs as described in Boettcher et al. [20]. Osteochondral cylinders with diameters of either 5.5 or 8 mm were drilled out of the patellofemoral grooves. The dissected samples were incubated for 1 h in 20 mM 4-(2-hydroxyethyl)-1-piperazineethanesulfonic acid (HEPES) with 154 mM NaCl to ensure identical initial sample conditions. Samples were dehydrated overnight at room temperature (25 °C) and a humidity of 49%. To minimize sample degradation and potential GAG loss, rehydration and sample storage were performed at 9 °C and a humidity of 70% overnight. As rehydration solutions we chose 20 mM HEPES buffer (pH 7), either without additional salt (hypotonic), or supplemented with 154 mM NaCl (physiological/isotonic) or 2 M NaCl (hypertonic), respectively. All measurements were performed and repeated on samples from at least two different lambs.

2.2. De- and rehydration process

Sample shrinkage and swelling were observed at room temperature for at least 5 h by mounting the sample onto a rheometer (MCR 102, Anton Paar, Graz, Austria) in a custom-made sample holder [20]. The sample surface was approached with a flat-ended cylindrical measuring head (\varnothing 4.2 mm) at a rate of 100 $\mu\text{m/s}$ every 5 min. During the rehydration process, the samples were fully immersed in the solutions mentioned above. Three samples were observed for each experimental condition.

2.3. Water content

Cartilage tissue was carefully removed from the underlying bone, excess fluid was removed, and samples were weighed on an analytical electronic balance (CP225D, Sartorius, Göttingen, Germany). Subsequently, the samples were incubated for 1 h in 20 mM HEPES with 154 mM NaCl and then de- and rehydrated as described above. After each step, the sample mass was determined. To determine dry weight (m_{dry}), the samples were snap-frozen and lyophilized. The water content (wc) of each sample was calculated as $\text{wc} = [(m - m_{\text{dry}})/m]$. Nine samples were measured in the fresh and dehydrated state (three samples for each rehydration fluid).

2.4. Indentation measurements

The rheometer was equipped with a cylindrical flat-ended solid indenter (\varnothing 4.2 mm) [20]. Samples were fully immersed into the test fluid, and measurements were conducted at room temperature with an indentation speed of 1 $\mu\text{m/s}$. Each cartilage sample was indented until a time limit of 4 min or a force limit of 40 N was reached. With this indentation protocol, all three material states (fresh, dehydrated, rehydrated) could be characterized. The indentation stiffness was calculated using a linear fit to the acquired stress-strain data. The thickness of the cartilage layer was evaluated for each fresh sample on four points of the contour using a caliper (digital caliper DIN 862, accuracy = 0.01 mm). For the rehydrated conditions, the measured initial sample thickness was used. This approach is justified by our restoration that all of our rehydration procedures almost fully restored the initial thickness of

the cartilage samples. Four samples were measured for each of the five experimental conditions.

2.5. Dynamic shear measurements

The rheometer was equipped with a parallel plate measuring head (\varnothing 8 mm, PP08, Anton Paar, Graz, Austria) [20]. A frequency sweep was performed between 10 Hz and 0.1 Hz at room temperature, and a normal force of 1 N was applied to ensure full contact between the plate and the sample surface. Sample thickness was determined as described above, and 24 samples were measured in the fresh condition (six samples for each rehydration fluid).

2.6. 1,9-Dimethylmethylene blue assay

A 1,9-dimethylmethylene blue (DMMB) assay [21] was used to quantitatively determine the GAG contents of the cartilage samples. Following the procedure described in reference [22] (Biocolour Ltd., Carrickfergus, UK), the cartilage layer was dissected from the bone segment, and the tissue wet weight was determined. The sample was snap frozen and lyophilized, and the dry weight was measured. Subsequently, each specimen was immersed in 2 mL papain solution for 18 h at 60 °C and stored at –80 °C. The absorbance of the DMMB/sample solution was measured at 525 nm (Specord 210, Analytic Jena AG, Jena, Germany). Chondroitin 6-sulfate sodium salt (C4384, Sigma–Aldrich, Schnellendorf, Germany) was used as a standard. Six samples were measured for each experimental condition.

2.7. Histology

All cartilage samples used for histological analysis were fixed in a 4% buffered formalin solution (Roti-Histofix, Carl Roth, Karlsruhe, Germany) decalcified in a 25% EDTA solution, and then embedded in paraffin. Hematoxylin and eosin (H&E) stains were used to evaluate the overall tissue morphology and cell distribution. Safranin-O/fast green stains were used to examine the GAG distribution. Images were acquired using an Axioskop 2 plus (Zeiss, Jena, Germany).

2.8. Scanning electron microscopy

Scanning electron microscopy (SEM; JEOL-JSM-6060LV, Jeol, Eching, Germany) was used to qualitatively evaluate changes in sample surface structure. Before imaging, 2 samples per condition were fixed in 2.5% glutaraldehyde in 0.05 M HEPES (pH 7), critical-point dried, and sputtered with gold (BAL-TEC MED020, Balzers, Liechtenstein). Images were acquired at an acceleration voltage of 5 kV and a spot size of 30 nm.

2.9. Atomic force microscopy

Atomic force microscopy (AFM; MFP-3D SA, Asylum Research, Santa Barbara, USA) images were acquired in constant force mode at a scan rate of 1 Hz. Fresh and rehydrated cartilage samples were examined using a triangular cantilever with a nominal spring constant of $k = 0.01$ N/m (MLCT, Bruker, Camarillo, USA), whereas a rectangular cantilever with $k = 0.3$ N/m (CSC37a/AL BS, Mikromasch, Wetzlar, Germany) was used for dehydrated samples. For each condition at least two samples from two different joints were imaged and for each sample images were acquired from at least three different spots. With exception of the dehydrated samples, all samples were imaged in the respective incubation fluid. During the measurement, the samples were clamped in a cylindrical bore inside a custom-built fluid cell.

2.10. Friction measurements

The rheometer was equipped with a tribology unit (Anton Paar, Graz, Austria), and the measurements were performed as described in [20]. For each measurement, the incubation solution was used as a lubricant. Owing to the constant contact between the cartilage specimens and the glass sphere, the friction coefficient increased over time [23]. Thus, the initial (averaged over the first 10 s of the measurement) and final friction coefficient (averaged over the last 10 s of the measurement) of friction measurements with a total duration of 1 h are reported. Three samples were measured for each experimental condition.

2.11. Statistical analysis

To detect significant differences between the examined groups, one-way ANOVAs and Tukey post hoc tests were carried out. The assumptions of normal distribution and homogeneity of variances were verified using the Shapiro–Wilk test of normality and Levene's test for homogeneity of variances, respectively. All statistical analyses were performed using R (Foundation for Statistical Computing). We used $p < 0.05$ for statistical significance.

3. Results

All fresh articular cartilage samples had a smooth, white appearance (Fig. 1a). When these samples were dehydrated, the thickness of the cartilage layer significantly decreased ($p < 0.001$), and the cartilage's morphology changed. The material appeared red, rough, and inhomogeneous (Fig. 1a). After rehydration with a buffer solution (20 mM HEPES without additional salt, with 154 mM NaCl or 2 M NaCl), the cartilage recovered its initial appearance (Fig. 1a), and it was difficult to distinguish the rehydrated sample from a fresh one by simple visual inspection.

3.1. De- and rehydration kinetics and water content

To assess the de- and rehydration kinetics, changes in cartilage thickness were measured (Fig. 1b). The rate of decrease in thickness due to dehydration was $\sim 15\%$ per hour, and the decrease in thickness appears overall exponential and nearly linear during the first 3 h. After approximately 8 h, no further substantial decrease in thickness was observed. As an equilibrium cartilage thickness was reached after this time span, the strongest possible dehydration under the given circumstances (room temperature, humidity) was assumed, and the samples were covered with physiological buffer solution. The surface of the cartilage layer was then tracked during the rehydration process. A constant cartilage thickness was achieved after 3–4 h of rehydration, and the final thickness of the rehydrated cartilage layer was not significantly different ($p > 0.9$) from that of the initial specimen (Fig. 1b). Measurements of the wet and dry weights of cartilage samples showed that the initial water content (80 wet wt%) was significantly reduced ($p < 0.001$) to 20 wet wt% after dehydration. However, this water content could be completely restored to the initial value of 80 wet wt% ($p = 0.992$) when the samples were rehydrated in the saline solution (Fig. 1c).

We next considered whether such a complete reversal of the dehydration procedure could only be achieved with a physiological rehydration fluid (20 mM HEPES with 154 mM NaCl). When a hypotonic (20 mM HEPES) or a hypertonic (20 mM HEPES with 2 M NaCl) rehydration medium was used, both the dynamics of the rehydration process as well as the equilibrium thickness of the cartilage samples depended on the ionic strength of the rehydration buffer (Fig. 1b). For all rehydration fluids, the sample

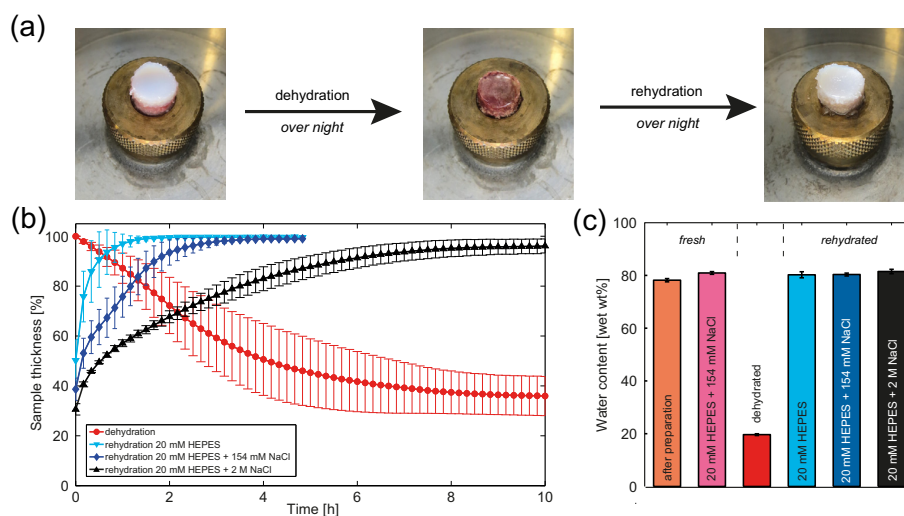


Fig. 1. Cartilage appearance, thickness and water content recovered upon rehydration. (a) Images of fresh, dehydrated and rehydrated cartilage. The de- and rehydration kinetics in different rehydration fluids is shown in (b) and the water content in (c). The error bars denote the standard deviation.

thickness approached a plateau over time, whereas the time needed to reach equilibrium strongly depended on the ionic strength of the solution. The hypertonic fluid was soaked back into the tissue at a considerably slower speed. Under this condition, full hydration required 8–10 h, similar to the time needed for complete dehydration. The opposite effect (i.e., a clearly faster rehydration than under physiological conditions) was observed for the hypotonic solution. The equilibrium thicknesses of samples rehydrated under hypotonic conditions slightly exceeded those of fresh samples. In contrast, final sample thicknesses were slightly decreased when rehydration was performed using hypertonic solutions. However, these differences in sample thickness were not significant ($p > 0.9$) and did not manifest themselves in different water contents (Fig. 1c).

3.2. Mechanical properties

On the basis of the differences in the macroscopic morphology and water content observed between the fresh and the dehydrated samples, one would anticipate similarly strong differences in the mechanical properties. Indeed, indentation measurements (Fig. 2a) showed a significantly increased ($p < 0.001$) indentation stiffness of 37.3 ± 10.3 MPa for the dehydrated samples compared to that of the fresh samples (0.9 ± 0.8 MPa). Interestingly, rehydrating the cartilage samples in physiological buffer (20 mM HEPES with 154 mM NaCl) fully restored the stiffness of the sample; the indentation stiffness of the rehydrated sample was 1.1 ± 0.7 MPa and therefore not significantly different from that of fresh cartilage ($p = 0.998$).

During joint movement, articular cartilage is not only subjected to compressive forces, but also to shear loading, which occurs at different frequencies [24]. Thus, we repeated our comparison of fresh and rehydrated cartilage with oscillatory shear measurements to probe the mechanics of cartilage under shear load and over a range of physiologically relevant frequencies (i.e., between 0.1 and 10 Hz). In the linear elastic regime and under low compressive strain, the material was dominated by elasticity and both, the storage modulus $G'(f)$ and loss modulus $G''(f)$ only weakly depended on the frequency, i.e., a pronounced plateau was observed (Fig. 2b). Therefore, the storage modulus at a frequency of 1 Hz was chosen for further quantification and comparison of

the different groups. For fresh samples, an average storage modulus of 0.4 ± 0.16 MPa was measured at an intermediate frequency of 1 Hz. After de- and rehydration in physiological buffer, the storage modulus (0.5 ± 0.18 MPa) was not significantly different from its initial value ($p = 0.701$), which agreed with our indentation results. We next tested whether hypo- or hypertonic rehydration would produce a different outcome. No difference was observed for rehydration with the hypotonic solution (0.4 ± 0.14 MPa) compared to the physiological solution ($p = 0.464$), but rehydration with the hypertonic solution (0.2 ± 0.04 MPa) decreased the shear modulus significantly compared to the fresh state ($p = 0.028$), determined at a shear frequency of 1 Hz.

3.3. Structure and GAG content

Thus far, we have found that articular cartilage can recover its initial appearance, thickness, compressive stiffness, and shear stiffness after rehydration. However, sample dehydration might still have an irreversible impact on the cartilage microstructure. For example, sample dehydration might affect the general structure of the tissue or alter the GAG content or distribution.

H&E stains were used to evaluate the overall tissue structures of fresh and rehydrated samples (Fig. 3a). Neither the chondrocyte distribution nor the overall structure of the tissue was qualitatively changed after rehydration, and no differences between the three rehydration fluids were observed. For the rehydrated tissue samples, safranin-O/fast green stains (Fig. 3b) revealed a small GAG loss, which was mainly located in the superficial zone. These visible changes in the GAG content were quantified using a DMMB assay. For fresh samples, an average GAG level of 202 ± 28 $\mu\text{g}/\text{mg}$ dry weight was determined. After rehydration in physiological buffer, the GAG concentration was slightly but not significantly decreased ($p = 0.140$) to an average of 169 ± 41 $\mu\text{g}/\text{mg}$ dry weight, which corresponds to 87% of its initial value. This slight decrease agreed with the obtained histology result.

Next, the surfaces of fresh, dehydrated, and rehydrated cartilage samples were compared using SEM and AFM. In the SEM images shown in Fig. 4a, the collagen fiber structure in the superficial zone of fresh samples can be clearly seen. The AFM images shown in Fig. 4b underscored this impression and showed a regularly spaced network with randomly orientated, straight fibers. Dehydration

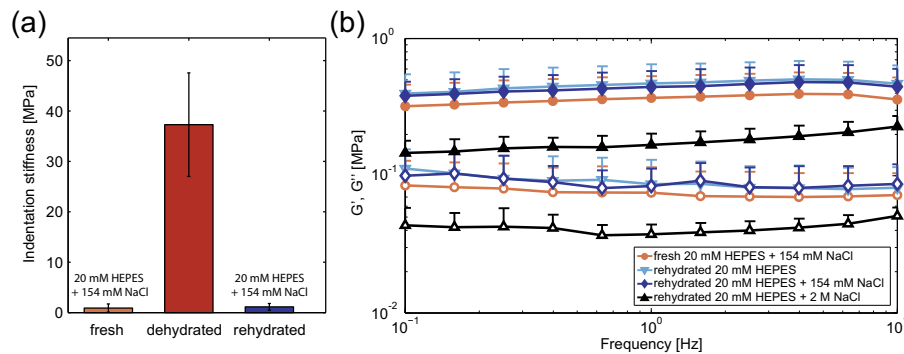


Fig. 2. Cartilage mechanical properties recovered upon rehydration. Indentation measurements (a) showed a significantly increased indentation stiffness for dehydrated cartilage. The dynamic shear moduli (b), i.e., the storage (filled symbols) and loss modulus (open symbols), were only significantly altered for hypertonic rehydration (black upright triangles) compared to fresh samples. The error bars denote the standard deviation.

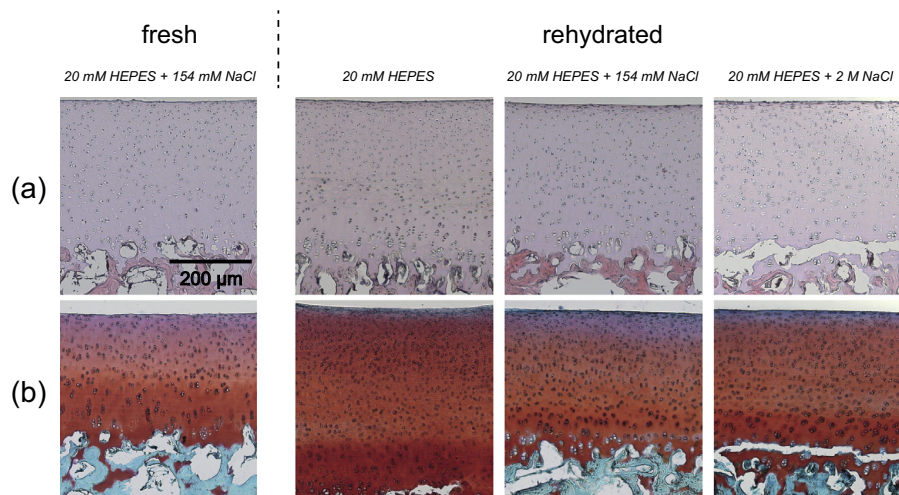


Fig. 3. Cartilage morphology and GAG distribution were overall unaffected by the dehydration/rehydration procedure. H&E stains (upper row, a) showed a similar tissue structure and cell distribution for all conditions. Safranin-O/fast green stains (lower row, b) revealed a slightly reduced GAG concentration (indicated by a lower intensity of red dye) in the superficial zone of all rehydrated samples. The scale bar applies to all images. (For interpretation of the references to color in this figure legend, the reader is referred to the web version of this article.)

clearly affected the fiber network. As one might expect, the network appeared denser, and the AFM image indicated an increased surface waviness. After rehydration in physiological buffer, the fiber density returned to a level similar to that observed in fresh samples. The fiber density seemed to increase with increasing ionic strength of the rehydration fluid. However, the surface appeared to be somewhat clogged in the SEM images and, compared to the fresh state, the fiber network is not as clearly visible. This was reflected in the AFM images by the slightly blurred appearance of the rehydrated fiber networks. Thus, both imaging techniques revealed a clear difference between the surfaces before and after dehydration.

3.4. Friction

The superficial zone of articular cartilage is a highly complex system, and its role in ensuring low friction in joints is highly discussed [25–27]. An altered surface morphology of cartilage could entail a distinct change in the tribological properties of cartilage. Thus, we compared the tribological behaviors of fresh and rehydrated articular cartilage samples using a rotational tribology

setup at a contact pressure of 0.1 MPa. As a consequence of this normal load, the cartilage samples exhibited creep during the measurement. This creep, which is depicted in Fig. 5a, is another measure of the mechanical properties of the cartilage samples. Physiological rehydration resulted in creep similar to that in fresh cartilage samples. However, at low sliding speeds, the creep displacement was significantly decreased for the hypotonic ($v = 0.01$ mm/s: $p = 0.021$, $v = 0.1$ mm/s: $p = 0.026$) and slightly but not significantly decreased for the hypertonic ($v = 0.01$ mm/s: $p = 0.053$, $v = 0.1$ mm/s: $p = 0.050$) conditions.

Only small changes were observed when the friction coefficient was analyzed for fresh and rehydrated samples. Fig. 5b depicts the initial and final friction coefficients for different rehydration fluids. The fresh samples showed a nearly constant friction coefficient for rotational speeds smaller than 10 mm/s. For hypotonic rehydration, the initial and final friction coefficients were significantly increased for all but the slowest sliding speed ($p < 0.050$). Rehydration with physiological and hypertonic solutions resulted in significantly decreased final friction coefficients at intermediate sliding speeds ($v = 1$ mm/s: $p < 0.002$) and a slight decrease in the initial friction coefficients.

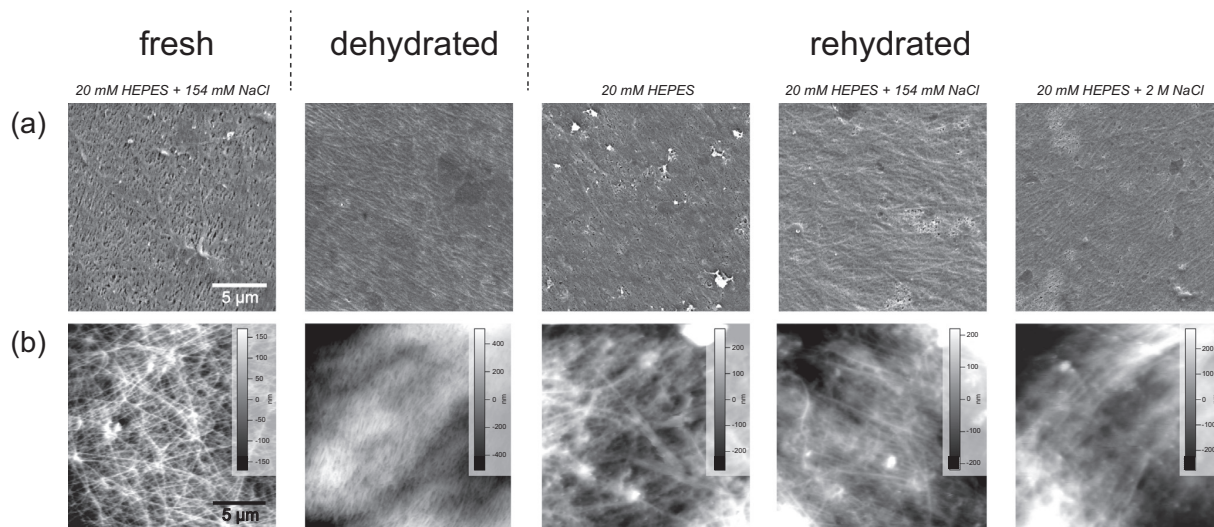


Fig. 4. Recovery of the cartilage surface structure after rehydration depended on the ionic strength of the rehydration solution. SEM (upper row, a) and AFM (lower row, b) pictures revealed a denser collagen structure in the dehydrated state. The surface of all rehydrated samples seemed somewhat clogged, i.e., the collagen fibers were not as clearly visible. The scale bars apply to all images in each row.

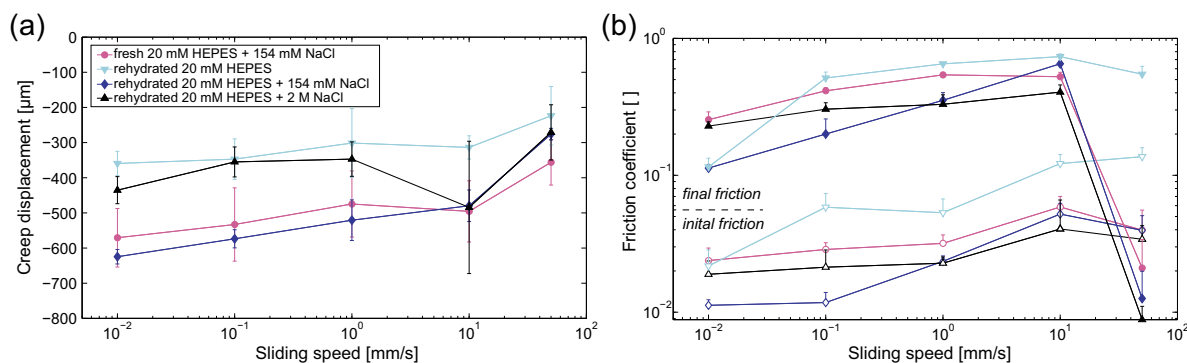


Fig. 5. Cartilage friction and creep depended slightly on the ionic strength of the rehydration/lubrication solution but was not significantly changed after rehydration. The total creep displacement is shown in (a). For samples rehydrated in physiological buffer, the creep displacement was virtually identical to that of fresh samples. The initial (open symbols) and final (closed symbols) friction coefficients are depicted for a speed range of 0.01–50 mm/s (b). The error bars denote the standard deviation. The legend in subfigure (a) also applies to the data shown in (b).

4. Discussion

Here, we describe how articular cartilage can recover a broad range of its material properties after strong dehydration, provided that the correct buffer conditions are used for rehydration.

To our knowledge, this is the first study investigating the reversibility of strong dehydration of articular cartilage. The ability of the material to completely restore its mechanical and structural properties after dehydration is surprising considering the drastic challenge that dehydration presents. The initial speed of the dehydration process observed here compares well to the dehydration rate reported for human cadaveric articular cartilage [28]; however, that study did not observe dehydration until equilibrium or the rehydration behavior of the tissue. For a closely related tissue (i.e., elastic cartilage from porcine ears) both de- and rehydration was performed, but different behaviors were observed [16]; rehydration in a 0.9% saline solution was tracked by consecutive mass measurements, and an exponential increase in sample mass was found during the first 1–2 h. These findings compare well to the findings of the present study; however, full rehydration could

not be achieved for dehydrated elastic cartilage samples, with the maximum rehydration level only reaching 80% of the initial weight. In addition, complete rehydration is not observed for lung, skin, muscle, and tendon tissue [16].

Articular cartilage may outperform those other tissues in terms of its rehydration abilities owing to its very high content of polyanionic GAGs. The concentration of GAGs in articular cartilage is four times higher than in elastic cartilage [29]. These GAGs regulate the swelling and shrinkage behavior of articular cartilage via the electrostatic interactions of the cartilage matrix macromolecules with ions in the hydration solution [1]. Therefore, one would expect different kinetics when rehydration of dehydrated cartilage is performed with a hypotonic or a hypertonic rehydration medium. Indeed, we showed that the hypertonic fluid was soaked back into the tissue at a considerably slower speed, which can be attributed to the increased shielding of the fixed charge density of the GAGs and the resulting decrease in the Donnan osmotic pressure [11,12]. This effect was also reflected in the thickness of the rehydrated cartilage samples; rehydration with a hypertonic solution led to a slightly decreased thickness compared to rehydration with

a physiological solution. Hypotonic rehydration was not only faster, but also led to a slightly increased equilibrium thickness. We attribute this observation to the stronger repulsive forces between negative charges in the matrix, resulting in an increased swelling pressure, a higher water content, and a larger collagen tension in the cartilage matrix [9]. However, these slight differences in sample thickness did not manifest themselves in the measured water content, which is most likely due to the limited sensitivity of the weighing procedure.

It seems reasonable to assume that the incomplete rehydration of a tissue will result in altered mechanical properties of the biomaterial. Indeed, for ligaments, where the tissue creep behavior depends on the water content [30], insufficient tissue rehydration has been reported together with altered creep after rehydration [31]. In contrast, articular cartilage was not only able to fully regain its initial water content, but could also restore a broad spectrum of physiologically relevant biomechanical properties after rehydration. This underscores the extraordinary sturdiness of articular cartilage. Herein, we quantified a subset of those biomechanical properties by performing indentation and shear measurements with fresh and rehydrated cartilage samples. The results obtained from these two techniques agreed well and reinforced our visual impression that the biomaterial was strongly altered after dehydration but recovered its material properties upon rehydration. Moreover, the shear moduli of freshly harvested cartilage samples measured herein were in the range of those reported by others [13,32]. We compared different rehydration solutions using shear measurements as this technique allowed us to detect differences between samples with higher accuracy compared to indentation measurements performed with our shear rheometer.

For rehydrated samples, we observed an inverse relationship between shear stiffness and fluid salt concentration. This dependence is consistent with previous studies [13,14], where the mechanical properties of fresh cartilage were analyzed after the interstitial fluid of the tissue had been gently exchanged by dialysis. The shear properties of articular cartilage are, to a great extent, determined by the pre-tension of collagen fibers in the superficial and middle zone [32]. This pre-tension is generated by an osmotic swelling pressure in the tissue. A higher ionic strength in the interstitial fluid would directly decrease this osmotic swelling pressure. Alternatively, a reduced GAG density in the superficial zone of rehydrated cartilage samples could also result in a lower osmotic swelling pressure. The average GAG level we determined for fresh samples compares well to previously published data [33]. However, for rehydrated samples, we observed a slightly reduced GAG concentration in the superficial zone. A control experiment revealed that this slight loss of GAGs can be attributed to the overnight sample storage. This slight GAG loss in the superficial zone might explain the insensitivity of the shear modulus to hypotonic rehydration solutions.

NMR studies on the bulk organization of articular cartilage have suggested that the microarchitecture of the tissue is not permanently altered after dehydration and subsequent rehydration [6]. In this study, we confirmed this notion using histology as we detected almost no differences between fresh and rehydrated samples. In addition, the AFM results suggested a reversible collapse of the superficial collagen network of dehydrated articular cartilage [34]. In AFM and SEM images, we observed such a collapsed fiber network in the dehydrated samples as a consequence of the fluid removal. In contrast, the full recovery of the mechanical properties of our treated cartilage samples suggested that the network structure may recover after sample rehydration, although this was not fully true for the superficial zone. In the superficial zone, we detected permanent alterations as the surface appeared less porous after rehydration, and the fiber network was not as prominent as in the fresh state. Surprisingly, these localized alterations did

not manifest themselves in the creep and friction behaviors of the samples when rehydration was performed at physiological ionic strength. However, both hypo- and hypertonic buffer solutions led to reduced sample creep after rehydration. For hypotonic rehydration, the initial and final friction coefficients were significantly increased, and the boundary friction regime appeared to be prolonged. We speculate that this reduced lubricity at high friction speeds could also be a consequence of the altered Donnan pressure at low ionic strength. At hypotonic conditions, the charged GAGs may trap water more strongly in the tissue, thus delaying the build-up of a lubricating fluid film. Altogether, our friction experiments also underscore our previous notion that a physiological rehydration buffer is most suitable to restore the material properties of dehydrated cartilage.

5. Conclusions

Our results demonstrate the high robustness of articular cartilage towards transient dehydration. Overall, the best approximation of native cartilage behavior was achieved when rehydration was performed with a buffer solution at physiological ionic strength. This robust recovery of the material is an unexpected property for a complex tissue, and the rehydrated cartilage even maintains its sensitivity towards the ionic strength of the tissue fluid.

Our findings suggest that the inability of cartilage to repair itself might be largely compensated by its high endurance and robustness. We therefore speculate that the high resilience of the tissue might minimize the risk of irreversible material failure, lower the need for repair, and compensate for its poor regenerative abilities to a certain degree. Tissue engineering approaches that aim at mimicking the material properties of articular cartilage should thus not only reproduce the correct mechanics of the tissue, but also its pronounced sturdiness towards dynamic changes in fluid content, to guarantee a similar longevity.

Acknowledgments

The work was supported by the International Graduate School of Science and Engineering (IGSSE) in the framework of the focus area “Biomaterials”. We would like to thank the Bayerische Landesanstalt für Landwirtschaft (LfL) Institut für Tierzucht Grub/ Poing and the Metzgerei Boneberger for providing the lamb joints, Prof. Alan Grodzinsky, Joanna Urban, and Peter Föhr for helpful discussions, Ulrike Winkler and Lorenz Wiegler for conducting pilot experiments, and Tina Bidmon and Sabine Günzkofer for their support.

References

- [1] V.C. Mow, X.E. Guo, Mechano-electrochemical properties of articular cartilage: their inhomogeneities and anisotropies, *Annu. Rev. Biomed. Eng.* 4 (2002) 175–209.
- [2] D.J. Huey, J.C. Hu, K.A. Athanasiou, Unlike bone, cartilage regeneration remains elusive, *Science* 338 (2012) 917–921.
- [3] J.A. Buckwalter, H.J. Mankin, A.J. Grodzinsky, Articular cartilage and osteoarthritis, *Instr. Course Lect.* 54 (2005) 465–480.
- [4] S. Fox, A.J.A. Bedi, S.A. Rodeo, The basic science of articular cartilage: structure, composition, and function, *Sports Health* 1 (2009) 461–468.
- [5] W.M. Lai, J.S. Hou, V.C. Mow, A triphasic theory for the swelling and deformation behaviors of articular cartilage, *J. Biomech. Eng.* 113 (1991) 245–258.
- [6] J. Xu, P. Zhu, M.D. Morris, A. Ramamoorthy, Solid-state NMR spectroscopy provides atomic-level insights into the dehydration of cartilage, *J. Phys. Chem. B* 115 (2011) 9948–9954.
- [7] M.A. Soltz, G.A. Ateshian, Experimental verification and theoretical prediction of cartilage interstitial fluid pressurization at an impermeable contact interface in confined compression, *J. Biomech.* 31 (1998) 927–934.

- [8] H.B. Henninger, C.J. Underwood, G.A. Ateshian, J.A. Weiss, Effect of sulfated glycosaminoglycan digestion on the transverse permeability of medial collateral ligament, *J. Biomech.* 43 (2010) 2567–2573.
- [9] J.R. Parsons, J. Black, Mechanical behavior of articular cartilage: quantitative changes with alteration of ionic environment, *J. Biomech.* 12 (1979) 765–773.
- [10] S. Wang, Y. Huang, S. Saarakkala, Y. Zheng, Quantitative assessment of articular cartilage with morphologic, acoustic and mechanical properties obtained using high-frequency ultrasound, *Ultrasound Med. Biol.* 36 (2010) 512–527.
- [11] S.R. Eisenberg, A.J. Grodzinsky, Swelling of articular cartilage and other connective tissues: electromechanochemical forces, *J. Orthop. Res.* 3 (1985) 148–159.
- [12] R.K. Korhonen, J.S. Jurvelin, Compressive and tensile properties of articular cartilage in axial loading are modulated differently by osmotic environment, *Med. Eng. Phys.* 32 (2010) 155–160.
- [13] M. Jin, A.J. Grodzinsky, Effect of electrostatic interactions between glycosaminoglycans on the shear stiffness of cartilage: a molecular model and experiments, *Macromolecules* 34 (2001) 8330–8339.
- [14] A.M. Nguyen, M.E. Levenston, Comparison of osmotic swelling influences on meniscal fibrocartilage and articular cartilage tissue mechanics in compression and shear, *J. Orthop. Res.* 30 (2012) 95–102.
- [15] G. Ateshian, M. Soltz, R. Mauck, I. Basalo, C. Hung, W.M. Lai, The role of osmotic pressure and tension-compression nonlinearity in the frictional response of articular cartilage, *Transp. Porous Media* 50 (2003) 5–33.
- [16] J.P. Meyer, K.E. McAvoy, J. Jiang, J.P. Brody, Rehydration capacities and rates for various porcine tissues after dehydration, *PLoS One* 8 (2013) e72573.
- [17] M. Schwarz, B. Schneider-Wald, A. Kruse, W. Richter, G. Reising, M. Kreinest, et al., Tribologische Messungen am Gelenkknorpel, *Orthopäde* 41 (2012) 827–836.
- [18] E. Saadat, H. Lan, S. Majumdar, D. Rempel, K. King, Long-term cyclical *in vivo* loading increases cartilage proteoglycan content in a spatially specific manner: an infrared microspectroscopic imaging and polarized light microscopy study, *Arthritis Research & Therapy* 8 (2006) R147.
- [19] Y. Lee, M.E. Barkey, Development of accelerated life test criteria, in: Y. Lee, J. Pan, R.B. Hathaway M.E. Barkey (Eds.), *Fatigue Testing and Analysis*, Burlington, 2005, p. 313–336.
- [20] K. Boettcher, S. Grumbein, U. Winkler, J. Nachtsheim, O. Lieleg, Adapting a commercial shear rheometer for applications in cartilage research, *Rev. Sci. Instrum.* 85 (2014) 093903.
- [21] K.A. Athanasiou, E.M. Darling, G.D. DuRaine, J.C. Hu, A.H. Reddi, *Articular Cartilage*, first ed., CRC Press, 2013.
- [22] Biocolor Ltd., *Blyscan Sulfated Glycosaminoglycan Assay*, [November 17, 2014]; Available from: <<http://www.biocolor.co.uk/manuals/blyscan.pdf>>.
- [23] M. Caligaris, G.A. Ateshian, Effects of sustained interstitial fluid pressurization under migrating contact area and boundary lubrication by synovial fluid on cartilage friction, *Osteoarthritis Cartilage* 16 (2008) 1220–1227.
- [24] R. Cross, Standing, walking, running, and jumping on a force plate, *Am. J. Phys.* 67 (1999) 304–309.
- [25] J. Katta, Z. Jin, E. Ingham, J. Fisher, Biotribology of articular cartilage – a review of the recent advances, *Med. Eng. Phys.* 30 (2008) 1349–1363.
- [26] S.M. McNary, K.A. Athanasiou, A.H. Reddi, Engineering lubrication in articular cartilage, *Tissue Eng. Part B Rev* 18 (2012) 88–100.
- [27] P. Kumar, M. Oka, J. Toguchida, M. Kobayashi, E. Uchida, T. Nakamura, et al., Role of uppermost superficial surface layer of articular cartilage in the lubrication mechanism of joints, *J. Anat.* 199 (2001) 241–250.
- [28] A. Pham, M. Hull, Dehydration rates of meniscus and articular cartilage *in vitro* using a fast and accurate laser-based coordinate digitizing system, *J. Biomech.* 40 (2007) 3223–3229.
- [29] A. Naumann, J.E. Dennis, A. Awadallah, D.A. Carrino, J.M. Mansour, E. Kastenbauer, et al., Immunochemical and mechanical characterization of cartilage subtypes in rabbit, *J. Histochem. Cytochem.* 50 (2002) 1049–1058.
- [30] G.M. Thornton, N.G. Shrive, C.B. Frank, Altering ligament water content affects ligament pre-stress and creep behavior, *J. Orthop. Res.* 19 (2001) 845–851.
- [31] A.H. Hoffman, D.R. Robichaud, J.J. Duquette, P. Grigg, Determining the effect of hydration upon the properties of ligaments using pseudo Gaussian stress stimuli, *J. Biomech.* 38 (2005) 1636–1642.
- [32] W. Zhu, V.C. Mow, T.J. Koob, D.R. Eyre, Viscoelastic shear properties of articular cartilage and the effects of glycosidase treatments, *J. Orthop. Res.* 11 (1993) 771–781.
- [33] D. Burkhardt, S. Hwa, P. Ghosh, A novel microassay for the quantitation of the sulfated glycosaminoglycan content of histological sections: its application to determine the effects of Diacerein on cartilage in an ovine model of osteoarthritis, *Osteoarthritis Cartilage* 9 (2001) 238–247.
- [34] P. Zhu, M. Fang, Nano-morphology of cartilage in hydrated and dehydrated conditions revealed by atomic force microscopy, *J. Phys. Chem. Biophys.* 02 (2012) 106.

A.3. Comparison of friction and wear of articular cartilage on different length scales

Journal of Biomechanics 48 (2015) 3052–3058



Contents lists available at [ScienceDirect](#)

Journal of Biomechanics

journal homepage: www.elsevier.com/locate/jbiomech
www.JBiomech.com



Comparison of friction and wear of articular cartilage on different length scales



Sandra Kienle^a, Kathrin Boettcher^b, Lorenz Wiegleb^a, Joanna Urban^d, Rainer Burgkart^c,
Oliver Lieleg^b, Thorsten Hugel^{a,d,*}

^a Physics Department and Institute for Medical Engineering, IMETUM, Technische Universität München, Boltzmannstr. 11, 85748 Garching, Germany

^b Department for Mechanical Engineering and Institute for Medical Engineering, IMETUM, Technische Universität München, Boltzmannstr. 11, 85748 Garching, Germany

^c Klinik für Orthopädie und Sportorthopädie, Klinikum Rechts der Isar, Technische Universität München, Ismaninger Straße 22, 81675 München, Germany

^d Institute of Physical Chemistry, University of Freiburg, Albertstr. 23a, 79104 Freiburg, Germany

ARTICLE INFO

Article history:
Accepted 23 July 2015

Keywords:
Atomic force microscopy
Tribometer
Hyaluronic acid
Wear protection
Friction
Lubrication

ABSTRACT

The exceptional tribological properties of articular cartilage are still far from being fully understood. Articular cartilage is able to withstand high loads and provide exceptionally low friction. Although the regeneration abilities of the tissue are very limited, it can last for many decades. These biomechanical properties are realized by an interplay of different lubrication and wear protection mechanisms. The deterioration of cartilage due to aging or injury leads to the development of osteoarthritis. A current treatment strategy focuses on supplementing the intra-articular fluid with a saline solution containing hyaluronic acid. In the work presented here, we investigated how changing the lubricating fluid affects friction and wear of articular cartilage, focusing on the boundary and mixed lubrication as well as interstitial fluid pressurization mechanisms. Different length and time scales were probed by atomic force microscopy, tribology and profilometry. We compared aqueous solutions with different NaCl concentrations to a viscosupplement containing hyaluronic acid (HA). In particular, we found that the presence of ions changes the frictional behavior and the wear resistance. In contrast, hyaluronic acid showed no significant impact on the friction coefficient, but considerably reduced wear. This study confirms the previous notion that friction and wear are not necessarily correlated in articular cartilage tribology and that the main role of HA might be to provide wear protection for the articular surface.

© 2015 Elsevier Ltd. All rights reserved.

1. Introduction

Articular cartilage is an exceptional biological material that covers the end of bones and forms the intercalating surfaces in joints. Its main function is to withstand high loads and to provide low friction, in particular while tolerating permanent changes of moving direction (Athanasίου et al., 2013). In cartilage, low friction and good wear protection are not the result of a single lubrication mechanism: rather, the mechanism adapts to changing load, shear stress or sliding rate. At low sliding speeds in the presence of a molecularly thin fluid film, the tribological properties are governed by the interactions between contact asperities. This is known as the boundary lubrication regime. The very efficient

boundary lubrication mechanism in cartilage is mediated by lubricants such as PRG4 (proteoglycan 4 or lubricin), hyaluronic acid and SAPL (surface-active phospholipids) present at the articular surface (Chang et al., 2014; Coles et al., 2010; Seror et al., 2015). Another very important lubrication mechanism is the interstitial fluid pressurization (Athanasίου et al., 2013). Cartilage can be described as a triphasic material composed of: (i) the solid, porous network composed of collagen type II and charged proteoglycans, (ii) a fluid phase and (iii) ions. The fluid phase is the main component of cartilage (70–80%). The negatively charged proteoglycans draw water into the matrix (“Donnan effect”) and cause the network to swell. Together with the low hydraulic permeability of cartilage, this produces a high interstitial fluid pressure which is counterbalanced by the collagen network. If cartilage is loaded, most of the load is supported by the fluid and not by the solid matrix (Ateshian, 2009; Bonnevie et al., 2011; Forster and Fisher, 1999). If the contact continuously migrates over the cartilage surface, the friction force remains low and constant (Caligaris

* Corresponding author at: Institute of Physical Chemistry, University of Freiburg, Albertstr. 23a, 79104 Freiburg, Germany. Tel.: +49 761 203 6192, fax: +49 761 203 6189.

E-mail address: TH@physchem.uni-freiburg.de (T. Hugel).

<http://dx.doi.org/10.1016/j.jbiomech.2015.07.027>
0021-9290/© 2015 Elsevier Ltd. All rights reserved.

and Ateshian, 2008; Chan et al., 2010). However, if one region is loaded permanently, the fraction of load supported by the fluid decreases as the fluid is squeezed out of the matrix. Such a static contact causes an increase of the friction coefficient from an initial value to a plateau friction coefficient (Mow et al., 1984; Soltz and Ateshian, 1998). The time until equilibrium is reached depends on the contact area and the permeability of the tissue (Mow et al., 1980; Park et al., 2004).

Although healthy cartilage lasts for decades without losing its function, with advanced age it often starts to deteriorate leading to the development of osteoarthritis. Osteoarthritis can have a genetic basis, but may also be induced by injuries or wear caused by age or malalignment of the joint (Andriacchi et al., 2009; Athanasiou et al., 2013). The onset of the disease is associated with a loss of mechanical properties on the micro- and macroscale (Wilusz et al., 2013). These changes can be attributed to a decrease in proteoglycan content and an increased fraction of water in the tissue (Malemud, 1991), which alters the interstitial fluid pressure and therefore directly the frictional properties. Furthermore, the molecular weight and the concentration of hyaluronic acid in the synovial fluid decrease. This reduces the wear resistance capability and can lead to further damage, also under normal loading conditions (Dahl et al., 1985).

As it is not yet possible to artificially recreate cartilage, most of the treatment strategies for osteoarthritis focus on pain reduction and maintenance of joint functionality. One such strategy are intra-articular hyaluronic acid injections (Felson et al., 2000; Pelletier et al., 2001), which are believed to increase the viscosity of synovial fluid back to its original level (viscosupplementation) and therefore improve the joint function and diminish pain (Gigante and Callegari, 2011).

One of the many commercially available viscosupplements is Sinovial¹ (Humantis, Köln, Germany). It consists of 0.8% hyaluronic acid with a molecular weight between 800 and 1200 kDa in a physiological sodium chloride solution (Gigante and Callegari, 2011). A meta-study investigating the effect of Sinovial claims that 3–5 weekly injections can reduce the pain in the joints and disabilities. However, controversial results on the impact of viscosupplementation can be found in the literature. Many studies show that intra-articular injections can help relieve the symptoms, also when placebos such as saline are injected. In some studies, almost 80% of the pain relief is accounted for by the placebo effect. Although its benefits are disputed, viscosupplementation with hyaluronic acid is regularly used during treatment of osteoarthritis and is still beneficial for some patients due to the reduction of pain.

Here, we addressed the mechanistic principle of how Sinovial influences lubrication, wear and frictional properties of articular cartilage in the boundary lubrication regime on the micro- and macroscale. We chose two complementary methods: atomic force microscopy (AFM) and a rotational tribology setup (Boettcher et al., 2014). Owing to the small contact area, the AFM allows to probe boundary lubrication (Park et al., 2004) whereas with the static contact of the tribometer the effect of the interstitial fluid pressurization can be investigated (Caligaris and Ateshian, 2008). We compared Sinovial with aqueous solutions containing different NaCl concentrations and evaluated their lubricating abilities. Finally, lubricant dependent resistance against wear was characterized using AFM and a profilometer. The different investigated lubricants showed no significant effect on the friction coefficient, but Sinovial did considerably improve the wear protection in cartilage. It is very likely that another viscosupplement containing hyaluronic acid in a similar concentration and molecular weight would lead to comparable results.

¹ Sinovial was chosen randomly for our study and we did not receive any kind of funding from Humantis.

2. Results and discussions

2.1. Surface characterization

First, we started with the characterization of the cartilage surface. We imaged the surface of freshly prepared ovine cartilage samples with an atomic force microscope in contact mode using a cantilever with a sharp tip (Fig. 1A, B and C). Directly after preparation, the samples were incubated in the lubricant of interest. As lubricants, we chose ddH₂O, 154 mM NaCl solution (physiological concentration) and 2 M NaCl solution. The cartilage network was clearly visible for all lubricants. No deposits or damage of the structure were observed. With increasing salt concentration, the network appeared denser (Fig. 1). This can be explained with changes of the electrostatic shielding of the proteoglycan charges with the ionic strength. Cartilage samples incubated in 2 M NaCl shrink due to loss of water whereas the volume of cartilage in ddH₂O increases (Ateshian et al., 2003; Eisenberg and Grodzinsky, 1985; Parsons and Black, 1979). A similar effect can be observed in osteoarthritis: The amount of water in the tissue increases in the early (often subclinical) stages of the disease (Eckstein and Wirth, 2011). The aggregation ability and the concentration of proteoglycans decrease, which in combination with the loosening of the collagen network leads to more free interstitial space filled with water (Athanasiou et al., 2013). Thus, the network in the early stages of the disease might bear resemblance to the structure of healthy cartilage incubated in ddH₂O observed by us in this study.

In addition, we imaged the surface of fresh, healthy cartilage with a profilometer (Fig. 1D). Owing to the larger scale of the image (800 μ m), the individual fibers were not visible, but a smooth surface without any signs of wear was observed (Fig. 1D).

2.2. AFM-based friction force microscopy

In the next step, AFM-based friction force measurements were performed using a rectangular cantilever with a polystyrene sphere attached (Fig. 2A, inset). Articular cartilage samples were freshly prepared, anchored in a custom-built fluid cell and incubated in one of the four lubricants: ddH₂O, 154 mM NaCl, 2 M NaCl or the viscosupplement Sinovial (physiological NaCl concentration). The contact pressure during an AFM experiment can be estimated as several 100 Pa. For the parameters used here (see Section 4), we can estimate using the formula given in Park et al. (2004) (p.1684) that the interstitial fluid pressure will relax on the timescale of several ms. Therefore we can assume that only boundary lubrication is probed during an AFM experiment (Coles et al., 2008; Zeng, 2013).

Trace and retrace were recorded (Fig. 2A) and averaged to obtain the friction force F_R (Fig. 2B) and the friction coefficient μ (see Section 4 for more details on the evaluation). In Fig. 2C the velocity dependence of μ in the different lubricants is shown. No dependence on scan velocity was observed for any of the lubricants, as expected for the boundary lubrication regime (Coles et al., 2008). The lowest friction coefficients were measured in ddH₂O whereas the highest μ corresponds to the measurements in 2 M NaCl, and μ increased with increasing salt concentration. The p values obtained from Tukey test indicate that the difference in μ between ddH₂O and 2 M NaCl was significant for all velocities ($p < 0.005$). We observed a significant difference in the friction coefficient between a physiological NaCl concentration and 2 M NaCl for the two intermediate velocities ($\nu = 1$ Hz: $p = 0.005$, $\nu = 2$ Hz: $p = 0.038$). The friction coefficient measured for Sinovial was significantly larger for the lowest sliding speed compared to ddH₂O ($p < 0.01$). For the lowest speed there was also a significant difference in μ between ddH₂O and physiological NaCl concentration. Other differences were not significant (see Supplemental material). These results can be explained considering boundary lubrication,

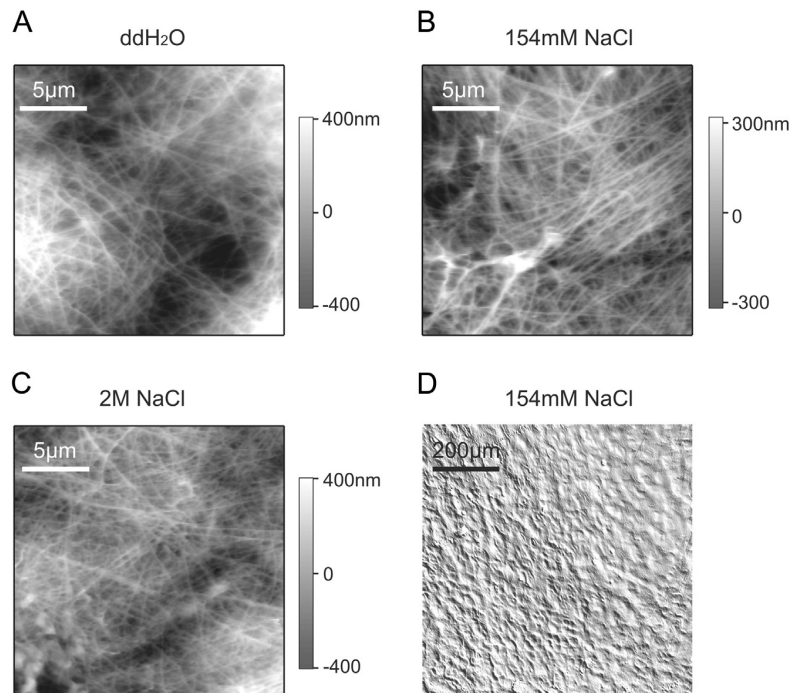


Fig. 1. AFM images of fresh ovine cartilage in (A) ddH₂O, (B) 154 mM NaCl and (C) 2 M NaCl. (D) Profilometer image of a fresh cartilage sample in 154 mM NaCl.

where the contact area between the sphere and the solid matrix is responsible for the measured friction coefficient. With decreasing salt concentration more water is drawn into the tissue and the network swells. This could mean that less fibers are in contact with the polystyrene sphere during a friction force experiment in ddH₂O. Consequently, the measured friction coefficient in pure water is lower than in solutions containing salt.

It has been suggested that the hyaluronic acid present in Sinovial is adsorbed onto the cartilage surface and contributes to boundary lubrication (Greene et al., 2011; Jay et al., 2007; Seror et al., 2015). Surprisingly, this mechanism seems to have no significant impact on the friction coefficient observed here: for Sinovial, μ was lower than in 2 M NaCl but higher than in ddH₂O and in 154 mM NaCl. Therefore, we conclude that, in the boundary lubrication regime, a low friction coefficient might not be a key factor for joint function and does not necessarily correlate with good wear protection. In addition, it should be noted that the molecular weight of the hyaluronic acid present in native cartilage is much higher (i.e. 20 MDa (Athanasios et al., 2013)) than in Sinovial (around 1 MDa). As a consequence, the hyaluronic acid variant used in Sinovial might not be as efficiently trapped at the cartilage surface as the native variant. Furthermore, some studies report that hyaluronic acid on its own actually increases the friction coefficient (Seror et al., 2015), and significantly decreased friction is only observed in combination with PRG4 or phospholipids (Jay et al., 2007; Schmidt et al., 2007; Seror et al., 2015; Yu et al., 2012). It has been observed that lubricin itself does not significantly reduce the friction coefficient, although it helps to preserve the surface structure (Coles et al., 2010).

2.3. Macro-friction experiments

In the human body, friction on articular cartilage surfaces occurs on a macroscopic scale and over a broad range of sliding speeds. We next repeated our comparison of different lubricants with a macroscopic method, i.e. a rotational macrotribometer (see

Boettcher et al., 2014 for more details). Here, a glass sphere in contact with three cartilage samples was rotated with a constant velocity (Fig. 3A, inset).

The contact pressure was 0.1 MPa, much higher than during an AFM experiment. Therefore, a different lubrication regime is probed and boundary and mixed lubrication as well as the effect of the interstitial fluid pressurization can be investigated in the macro-friction experiment: At the beginning of each measurement, most of the load is supported by the fluid. Due to the static contact during the experiment, the fluid is squeezed out of the loaded area, and more load is supported by the solid matrix. This is reflected by an increase of the friction coefficient with time (Fig. 3A). After a certain time, an equilibrium plateau friction coefficient is reached. However, in most of our tribometer experiments the plateau friction coefficient μ_{plateau} has not yet been reached after 1 h of measurement. Thus, the plateau friction coefficient was estimated by fitting the data with an exponential function:

$$\mu(t) = \mu_{\text{plateau}} - b \cdot e^{-ct}$$

where b and c are free fit parameters. Again, the friction coefficients were measured in the four lubricants: ddH₂O, 154 mM NaCl, 2 M NaCl and Sinovial. For each lubricant, a new set of cartilage samples was used. Fig. 3A shows the measured time dependence of the friction coefficients for the four lubricants at four different velocities as well as the fitted functions. Fig. 3B shows the plateau friction values obtained from those fits as a function of velocity.

Contrary to the results obtained by atomic force microscopy where μ slightly increased with increasing salt concentration, the average friction coefficient measured with the tribometer for sliding speeds > 0.1 mm/s decreased with increasing salt concentration. A similar effect was observed by Ateshian et al. who determined friction forces between a glass plate and bovine cartilage samples at different salt concentrations (Ateshian et al., 2003). It was later suggested that this effect could be caused by hydrated ions that attach to the negatively charged glass surface and reduce the friction

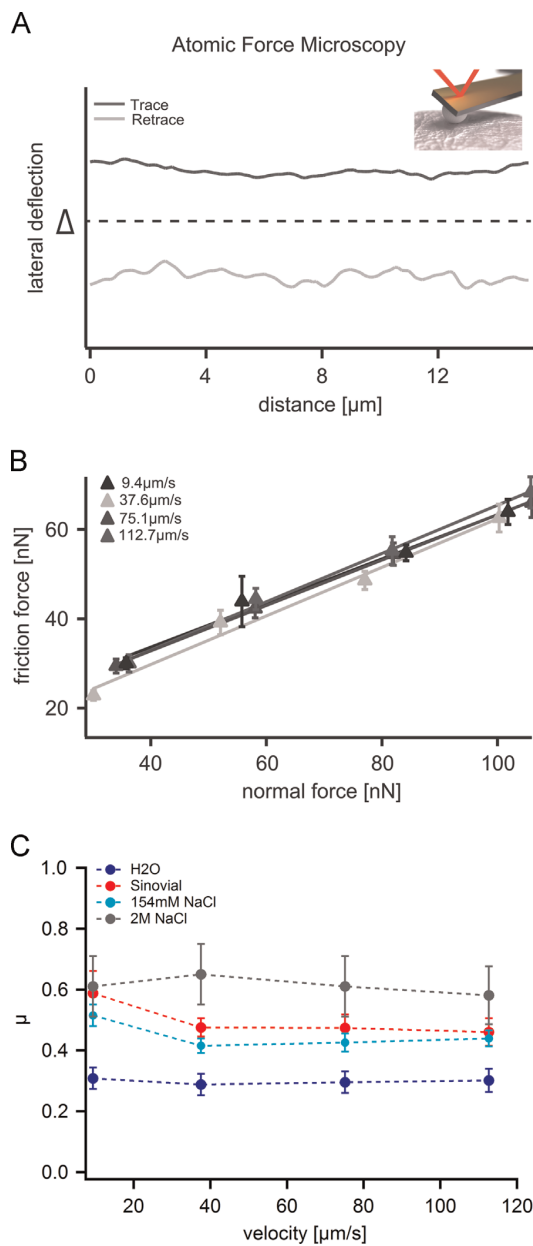


Fig. 2. (A) Friction loop (trace and retrace) of a scan line during a friction measurement with an AFM in 154 mM NaCl. Inset: Schematic illustration of the AFM setup. (B) Measured friction force for different normal forces and scan velocities. The solid lines correspond to a linear fit to the data with the friction coefficient being the slope of the line. (C) Friction coefficient for measurements in ddH₂O (dark blue), 154 mM NaCl (light blue), 2 M NaCl (grey) and Sinovial (red) with the atomic force microscope at different velocities. At least 8 samples were probed for each lubricant. Error bars denote the standard deviation of the mean value. (For interpretation of the references to color in this figure legend, the reader is referred to the web version of this article.)

force (Klein, 2006). The same explanation could be applied to our experiment as both the glass sphere and the cartilage surface are negatively charged. Nevertheless, measurements performed with the AFM and the tribometer consistently show that Sinovial does not significantly lower the friction coefficient compared to ddH₂O and NaCl solutions in the velocity range between 0.01 mm/s and 1 mm/s. Tribometer measurements at 10 mm/s showed significantly reduced

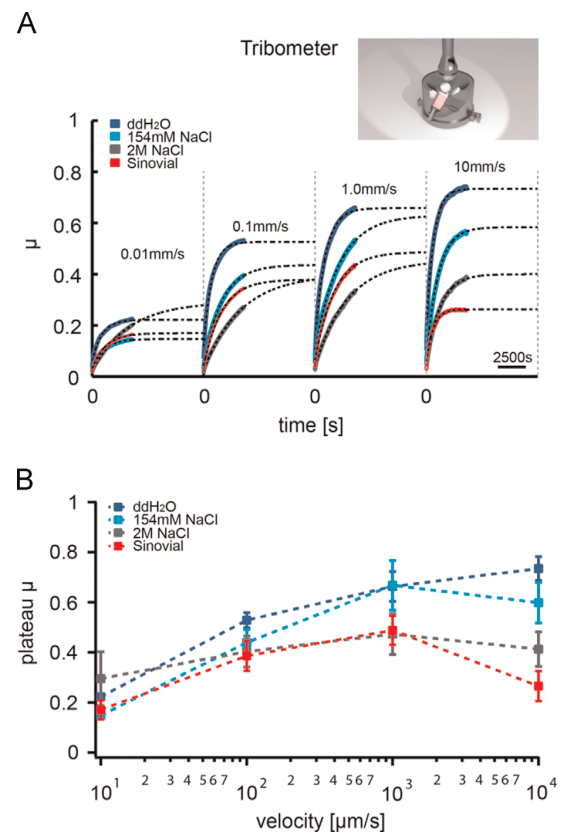


Fig. 3. (A) Time and velocity dependent friction coefficient for measurements in ddH₂O (dark blue), Sinovial (red), 154 mM NaCl (light blue) and 2 M NaCl (grey) with the rotational tribometer. The dotted line corresponds to the fit of the data using equation 1. Inset: Schematic illustration of the tribometer setup. (B) Plateau and friction coefficient for different velocities and different lubricants, namely ddH₂O (dark blue), Sinovial (red), 154 mM NaCl (light blue), and 2 M NaCl (grey). 4 sample sets were probed in each lubricant. The error bars represent the standard deviation.

friction coefficients for 2 M NaCl ($p < 0.035$) and Sinovial ($p < 0.001$) compared to the other lubricants. At 0.1 mm/s the friction coefficient for Sinovial was significantly decreased compared to ddH₂O ($p < 0.043$). All other differences were not significant (Supplemental material). The reason for this is not clear and could be due to the higher viscosity of Sinovial influencing the friction in the mixed lubrication regime. This behavior was confirmed using a linear tribometer on cartilage in Sinovial and 154 mM NaCl lubricants in the velocity range of 10–600 μm/s. There, we even compared the friction of cartilage on cartilage with cartilage on polystyrene and did not observe any significant difference (Supplemental material).

2.4. Wear protection

The relation between friction and wear in articular cartilage is still under debate. It is often observed that friction and wear are directly related (Oungoulian et al., 2015). Nevertheless, it has also been suggested that a low friction coefficient does not automatically result in low wear (Coles et al., 2010; Greene et al., 2011; Lizhang et al., 2011). To directly investigate how the choice of lubricant affects cartilage wear, we imaged the surface after tribometer friction experiments. Here, the load exerted on the cartilage samples in the tribological setup can be treated as a model for prolonged increased loads occurring in a misaligned joint, leading to the development of

osteoarthritis (Andriacchi et al., 2009; Athanasiou et al., 2013). Tribometer measurements were performed for 1 h at two different velocities: 0.1 mm/s and 10 mm/s. We chose these two velocities since, at 10 mm/s, the friction coefficient measured in Sinovial was significantly lower compared to the other lubricants whereas at 0.1 mm/s no difference was observed. Again, ddH₂O, 154 mM NaCl, 2 M NaCl and Sinovial were used as lubricants. Surface characterization after tribological treatment was performed both with an atomic force microscope in contact mode (image size 20 $\mu\text{m} \times 20 \mu\text{m}$) and with a profilometer (image size 800 $\mu\text{m} \times 800 \mu\text{m}$).

AFM images of fresh samples showed distinct fiber structure (Fig. 1). In contrast, images taken after the tribometer experiments clearly showed that the cartilage surface was affected by the measurement (Fig. 4). Especially after measurements in ddH₂O, neither a clear network structure nor individual fibers were visible anymore (Fig. 4, first row). This holds true for both velocities (0.1 mm/s and 10 mm/s) and could be due to two effects: the superficial layer of the network could be worn away by the glass sphere and debris formed by the eroded material might be deposited on the surface forming a layer on top of the natural cartilage network. Samples in salt solutions (154 mM and 2 M NaCl) showed improved wear resistance. Although the network

was not fully intact, fibers were visible. Debris was observed on the sample surface especially after tribometer measurements at 0.1 mm/s. These observations were confirmed with images obtained by profilometry. Here, the cartilage samples lubricated with ddH₂O showed the most prominent wear tracks and debris deposition, both being signs of abrasive wear. Surfaces lubricated with solutions containing NaCl exhibited better wear protection.

AFM images of samples after tribological treatment with Sinovial as a lubricant showed that the network is less damaged compared to samples probed in the other lubricants for both scan velocities (0.1 mm/s and 10 mm/s). To quantify this impression, an observer-blinded study was performed, where AFM images of samples in the four lubricants were shown to observers who were not involved in the AFM measurements performed for this study. The participants rated the different images based on the degree of preservation of the network, assigning four points for a very well preserved network, three and two points for samples with an increasing level of damage and one point for an image without any visible network. The average ratings for the two velocities and the four lubricants are presented in Table 1. For both velocities and each lubricant six images from different samples were used in the study (see Supplemental material).

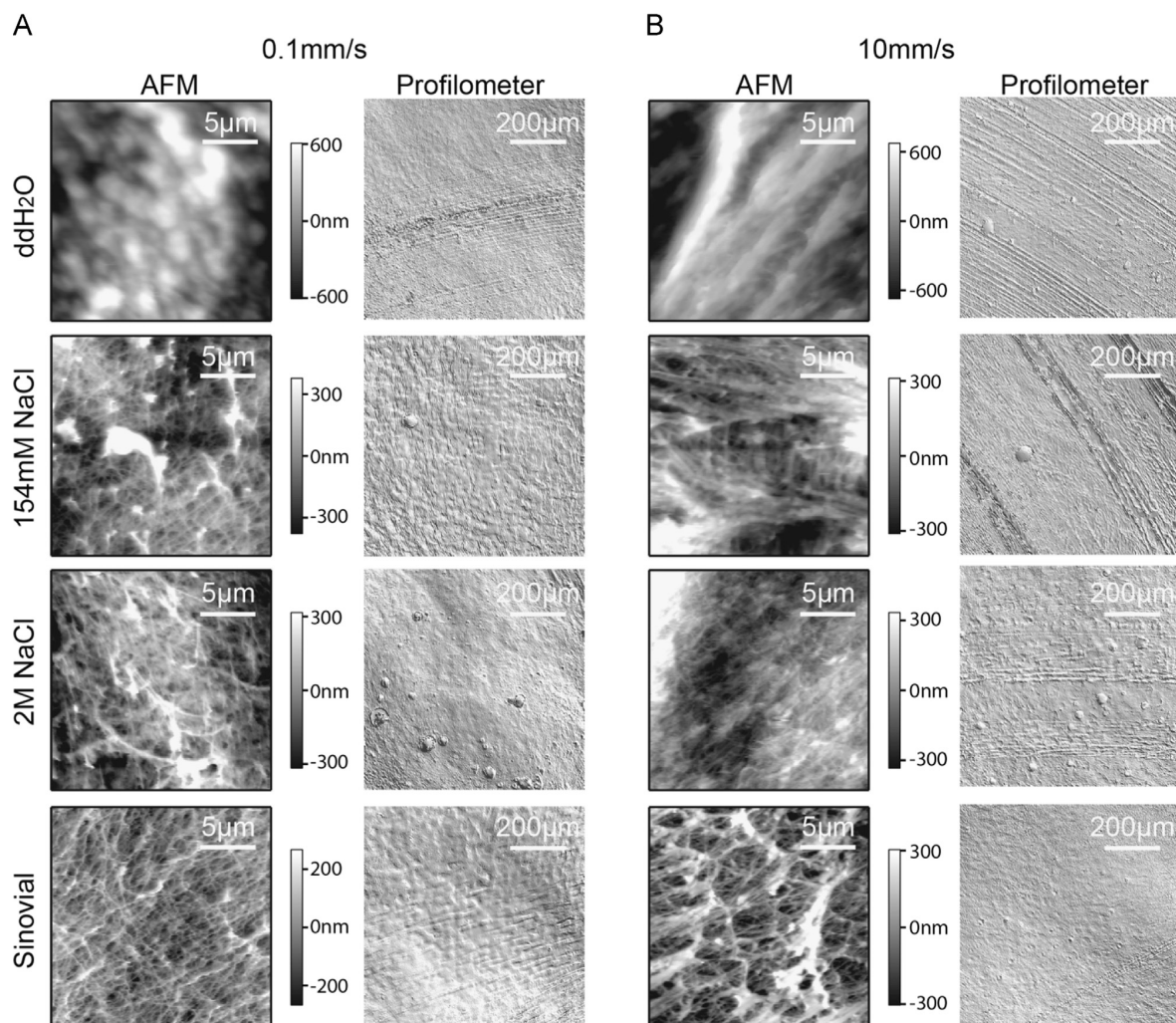


Fig. 4. Surface structure of cartilage samples after an 1 h tribometer experiment in either ddH₂O, 154 mM NaCl, 2 M NaCl or Sinovial at two different rotation speeds (0.1 mm/s and 10 mm/s). The surface was imaged with an atomic force microscope and with a profilometer.

Table 1

Nine participants rated the AFM images taken in the four lubricants after tribometer experiments. Here, the average of the points together with the standard deviation of the average of all nine participants is presented.

| | ddH ₂ O | 154 mM NaCl | 2 M NaCl | Sinovial |
|----------|--------------------|-------------|-----------|-----------|
| 0.1 mm/s | 1.0 ± 0.0 | 3.1 ± 0.8 | 2.0 ± 0.0 | 3.8 ± 0.5 |
| 10 mm/s | 1.0 ± 0.0 | 2.4 ± 0.7 | 2.9 ± 0.7 | 3.8 ± 0.4 |

For both velocities the observers rated the images taken in Sinovial as the ones with the most intact network. The observations were confirmed by the profilometer results, where fewer signs of wear were visible after tribological treatment in Sinovial.

Our data fit well with previously published results where the enzymatic digestion of hyaluronic acid significantly decreased the wear resistance of articular cartilage but, at the same time, only slightly increased the friction coefficient (Lee et al., 2013). This suggests that hyaluronic acid – both free in synovial fluid as well as adsorbed and bound on the articular surface – can improve the wear resistance of the tissue without necessarily affecting the friction coefficient.

3. Conclusion

In this study, we investigated friction and wear protection mechanisms in articular cartilage using AFM based friction force microscopy and tribology as well as surface imaging by AFM and profilometry. The results indicate that a low friction coefficient, which is widely regarded as the key factor for the engineering of cartilage-mimetic materials, does not directly correlate with low wear. In particular, we find that the presence of hyaluronic acid in the lubricating liquid has no strong impact on the friction coefficient over a wide range of velocities but significantly reduces wear. This suggests that intra-articular hyaluronic acid injections can improve the wear resistance of articular cartilage *in vivo*, at least for a certain time.

4. Materials and methods

4.1. Cartilage samples

The cartilage samples were harvested from the knee joint of the hinder leg of either lambs (3–6 months old) or elderly sheep. The samples obtained from sheep were only used for the measurements with the linear tribometer (Supplemental material). The joints were obtained from a local slaughter house the day after animal sacrifice and stored frozen until further usage. Before the measurement, the joints were slowly defrosted overnight in the refrigerator. Osteochondral cylinders with a diameter of 5–10 mm were drilled out of the patellofemoral groove. Prior to measurements the samples were usually stored in the lubricant for at least 1 h. The samples from sheep were prepared directly after receiving them from the slaughter house and frozen individually in PBS until the day of the measurements.

4.2. Atomic force microscopy

The imaging of cartilage samples in liquid environment was performed in contact mode. A sharp cantilever with a low spring constant (MLCT, Bruker AFM Probes, USA, nominal tip radius 20 nm) was chosen to avoid damage to the surface. The images of untreated samples show a distinct collagen meshwork, as expected for cartilage imaged with a sharp tip (Stolz et al., 2009). The observed collagen network structure remained unchanged for imaging over a range of setpoints, as well as during prolonged imaging of the same area. This indicated that no substantial damage to the sample occurred during imaging.

To measure friction forces with the atomic force microscope (AFM) rectangular cantilevers (Novascan, USA) with a polystyrene sphere (diameter 10 μm) attached were used. The cartilage samples (5 mm diameter) were anchored in a custom-built fluid cell which was then filled with the lubricant of interest (ultrapure water (ddH₂O, Biochrom, Germany), 154 mM NaCl, 2 M NaCl or Sinovial (Humantis,

Germany)). The AFM (MFP-3D SA, Asylum Research, an Oxford Instruments Company, CA, USA) was operated in contact mode with normal forces F_N ranging between 30 and 110 nN and scan velocities between 9 and 113 μm/s over a period of about 45 min for the whole measurement. For each velocity, measurements were performed for a series of normal loads. The load was kept constant while the lateral deflection was recorded during trace and retrace of one scan line (15 μm). To obtain the friction force, the lateral deflection during trace and retrace was averaged and multiplied by the lateral sensitivity of the cantilever, which was calibrated prior to the measurement using the diamagnetic levitation force calibrator (DLFC) (Li et al., 2006). The scanning axis was chosen perpendicular to the long axis of the cantilever to assure the cantilever deflected symmetrically during trace and retrace. For each measurement, a single line was scanned at least 64 times. The contact area was estimated to be around 5 μm and the contact pressure as a few 100 Pa. The lateral force F_R was plotted versus the normal force F_N and fitted with a straight line, the slope of which is the friction coefficient μ .

4.3. Rotational tribometer

The macrotribology measurements were performed using a rheometer (MCR 102, Anton Paar, Graz, Austria) equipped with a tribology measuring cell (T-PTD 200, Anton Paar, Graz, Austria). The test procedure was described in detail by Boettcher et al. (2014). In short, a glass sphere with a diameter of ½ in. was lowered onto three osteochondral cylinders fixed inside a custom made sample holder, and the samples were fully submerged by adding 1 ml of the lubricant. During the measurements, a normal force of 6 N was applied resulting in a contact pressure of approximately 0.1 MPa. Each sample was subjected to four friction tests at rotational velocities of 0.01, 0.1, 1 and 10 mm/s in an arbitrary order with 30 min of relaxation time between the measurements. For each test, the friction coefficient was measured over a period of 1 h with a measuring point duration of 1 s.

For wear evaluation tests, friction measurements were performed with the setup described above at a velocity of 0.1 mm/s or 10 mm/s for 1 h. Afterwards the samples were kept in the lubricant and imaged using first the AFM and directly afterwards the profilometer.

4.4. Profilometer

Images were acquired using an optical profilometer (μsurf custom, nanofocus, Oberhausen, Germany). Samples were removed from the lubricant and carefully rinsed in ddH₂O, especially to remove residual Sinovial from the surface. Afterwards, the samples were exposed to air for approximately 10 min until the surface was mostly free of water droplets and could be imaged. Three images per sample were recorded at arbitrary locations. To correct for sample tilt and curvature, a linear polynomial correction was applied (μsoft version 6.0, nanofocus, Oberhausen, Germany) to the images.

4.5. Statistical analysis

To detect significant differences between the examined groups, one-way ANOVAs and Tukey post-hoc tests were carried out. The assumptions of normal distribution and homogeneity of variances were verified using the Shapiro-Wilk test of normality and Levene test for homogeneity of variances, respectively. All statistical analyses were performed using R (Foundation for Statistical Computing). We used $p < 0.05$ for statistical significance.

Acknowledgments

The authors thank Julius Braun and Prof. Dr. Oliver Betz for the help with the linear tribometer measurements (Institute of Evolution and Ecology, Tübingen) and the Bayerische Landesanstalt für Landwirtschaft (LfL) Institut für Tierzucht Grub/Poing (Albert Steiner and Marcel Bowenz) for providing the lamb joints. This Project was supported by the International Graduate School of Science and Engineering (IGSSE) in the framework of the focus area “Biomaterials”, “BioMat02-LURACS”. The study was partially supported by the German Federal Ministry of Education and Research (BMBF) Grant (0315577C) to R.B.

Appendix A. Supplementary material

Supplementary data associated with this article can be found in the online version at <http://doi:10.1016/j.jbiomech.2015.07.027>.

References

- Andriacchi, T.P., Koo, S., Scanlan, S.F., 2009. Gait mechanics influence healthy cartilage morphology and osteoarthritis of the knee. *J. Bone J. Surg.* 91 (Suppl. 1), S95–S101.
- Ateshian, G.A., 2009. The role of interstitial fluid pressurization in articular cartilage lubrication. *J. Biomech.* 42, 1163–1176.
- Ateshian, G.A., Soltz, M.A., Mauck, R.L., Basalo, I.M., Hung, C.T., Michael Lai, W., 2003. The role of osmotic pressure and tension-compression nonlinearity in the frictional response of articular cartilage. *Transp. Porous Media* 50, 5–33.
- Athanasios, K.A., Darling, E.M., Duraine, G.D., Hu, J.C., Reddi, A.H., 2013. *Cartilage*. CRC Press, Boca Raton.
- Boettcher, K., Grumbein, S., Winkler, U., Nachtsheim, J., Lielig, O., 2014. Adapting a commercial shear rheometer for applications in cartilage research. *Rev. Sci. Instrum.* 85, 093903.
- Bonnevie, E.D., Baro, V., Wang, L., Burris, D.L., 2011. In-situ studies of cartilage microtribology: roles of speed and contact area. *Tribol. Lett.* 41, 83–95.
- Caligaris, M., Ateshian, G.A., 2008. Effects of sustained interstitial fluid pressurization under migrating contact area, and boundary lubrication by synovial fluid, on cartilage friction. *Osteoarthr. Cartil.* 16, 1220–1227.
- Chan, S.M., Neu, C.P., Duraine, G., Komvopoulos, K., Reddi, A.H., 2010. Atomic force microscope investigation of the boundary-lubricant layer in articular cartilage. *Osteoarthr. Cartil.* 18, 956–963.
- Chang, D.P., Guilak, F., Jay, G.D., Zauscher, S., 2014. Interaction of lubricin with type II collagen surfaces: adsorption, friction, and normal forces. *J. Biomech.* 47, 659–666.
- Coles, J.M., Blum, J.J., Jay, G.D., Darling, E.M., Guilak, F., Zauscher, S., 2008. In situ friction measurement on murine cartilage by atomic force microscopy. *J. Biomech.* 41, 541–548.
- Coles, J.M., Zhang, L., Blum, J.J., Warman, M.L., Jay, G.D., Guilak, F., Zauscher, S., 2010. Loss of cartilage structure, stiffness, and frictional properties in mice lacking PRG4. *Arthritis Rheum.* 62, 1666–1674.
- Dahl, L.B., Dahl, I.M., Engstrom-Laurent, A., Granath, K., 1985. Concentration and molecular weight of sodium hyaluronate in synovial fluid from patients with rheumatoid arthritis and other arthropathies. *Ann. Rheum. Dis.* 44, 817–822.
- Eckstein, F., Wirth, W., 2011. Quantitative cartilage imaging in knee. *Arthritis* 2011, 475684.
- Eisenberg, S.R., Grodzinsky, A.J., 1985. Swelling of articular cartilage and other connective tissues: electromechanochemical forces. *J. Orthop. Res.* 3, 148–159.
- Felson, D.T., Lawrence, R.C., Hochberg, M.C., McAlindon, T., Dieppe, P.A., Minor, M.A., Blair, S.N., Berman, B.M., Fries, J.F., Weinberger, M., Lorig, K.R., Jacobs, J.J., Goldberg, V., 2000. Osteoarthritis: new insights. Part 2: treatment approaches. *Ann. Intern. Med.* 133, 726–737.
- Forster, H., Fisher, J., 1999. The influence of continuous sliding and subsequent surface wear on the friction of articular cartilage. *Proc. Inst. Mech. Eng.* 213, 329–345.
- Gigante, A., Callegari, L., 2011. The role of intra-articular hyaluronan (Synovial) in the treatment of osteoarthritis. *Rheum. Int.* 31, 427–444.
- Greene, G.W., Banquy, X., Lee, D.W., Lowrey, D.D., Yu, J., Israelachvili, J.N., 2011. Adaptive mechanically controlled lubrication mechanism found in articular joints. *Proc. Natl. Acad. Sci.* 108, 5255–5259.
- Jay, G.D., Torres, J.R., Warman, M.L., Laderer, M.C., Breuer, K.C., 2007. The role of lubricin in the mechanical behavior of synovial fluid. *Proc. Natl. Acad. Sci.* 104, 6194–6199.
- Klein, J., 2006. Molecular mechanisms of synovial joint lubrication. *Proc. Inst. Mech. Eng.* 220, 691–710.
- Lee, D.W., Banquy, X., Israelachvili, J.N., 2013. Stick-slip friction and wear of articular joints. *Proc. Natl. Acad. Sci. USA* 110, E567–E574.
- Li, Q., Kim, K.S., Rydberg, A., 2006. Lateral force calibration of an atomic force microscope with a diamagnetic levitation spring system. *Rev. Sci. Instrum.* 77, 065105.
- Lizhang, J., Fisher, J., Jin, Z., Burton, A., Williams, S., 2011. The effect of contact stress on cartilage friction, deformation and wear. *Proc. Inst. Mech. Eng.* 225, 461–475.
- Malemud, C.J., 1991. Changes in proteoglycans in osteoarthritis: biochemistry, ultrastructure and biosynthetic processing. *J. Rheumatol. Suppl.* 27, 60–62.
- Mow, V.C., Holmes, M.H., Lai, W.M., 1984. Fluid transport and mechanical properties of articular cartilage: a review. *J. Biomech.* 17, 377–394.
- Mow, V.C., Kuei, S.C., Lai, W.M., Armstrong, C.G., 1980. Biphasic creep and stress relaxation of articular cartilage in compression? Theory and experiments. *J. Biomech. Eng.* 102, 73–84.
- Oungoulian, S.R., Durney, K.M., Jones, B.K., Ahmed, C.S., Hung, C.T., Ateshian, G.A., 2015. Wear and damage of articular cartilage with friction against orthopedic implant materials. *J. Biomech.* 48, 1957–1964.
- Park, S., Costa, K.D., Ateshian, G.A., 2004. Microscale frictional response of bovine articular cartilage from atomic force microscopy. *J. Biomech.* 37, 1679–1687.
- Parsons, J.R., Black, J., 1979. Mechanical behavior of articular cartilage: Quantitative changes with alteration of ionic environment. *J. Biomech.* 12, 765–773.
- Pelletier, J.P., Martel-Pelletier, J., Abramson, S.B., 2001. Osteoarthritis, an inflammatory disease: potential implication for the selection of new therapeutic targets. *Arthritis Rheum.* 44, 1237–1247.
- Schmidt, T.A., Gastelum, N.S., Nguyen, Q.T., Schumacher, B.L., Sah, R.L., 2007. Boundary lubrication of articular cartilage: role of synovial fluid constituents. *Arthritis Rheum.* 56, 882–891.
- Seror, J., Zhu, L., Goldberg, R., Day, A.J., Klein, J., 2015. Supramolecular synergy in the boundary lubrication of synovial joints. *Nat. Commun.* 6, 6497.
- Soltz, M.A., Ateshian, G.A., 1998. Experimental verification and theoretical prediction of cartilage interstitial fluid pressurization at an impermeable contact interface in confined compression. *J. Biomech.* 31, 927–934.
- Stolz, M., Gottardi, R., Raiteri, R., Miot, S., Martin, I., Imer, R., Staufer, U., Raducanu, A., Duggelin, M., Baschong, W., Daniels, A.U., Friederich, N.F., Aszodi, A., Aebi, U., 2009. Early detection of aging cartilage and osteoarthritis in mice and patient samples using atomic force microscopy. *Nat. Nanotechnol.* 4, 186–192.
- Wilusz, R.E., Zauscher, S., Guilak, F., 2013. Micromechanical mapping of early osteoarthritic changes in the pericellular matrix of human articular cartilage. *Osteoarthr. Cartil.* 21, 1895–1903.
- Yu, J., Banquy, X., Greene, G.W., Lowrey, D.D., Israelachvili, J.N., 2012. The boundary lubrication of chemically grafted and cross-linked hyaluronic acid in phosphate buffered saline and lipid solutions measured by the surface forces apparatus. *Langmuir* 28, 2244–2250.
- Zeng, H., 2013. *Polymer adhesion, friction, and lubrication*. John Wiley & Sons, Inc, Hoboken.

A.4. Modulating mucin hydration and lubrication by deglycosylation and polyethylene glycol binding

Materials
Views

www.MaterialsViews.com

ADVANCED
MATERIALS
INTERFACES
www.advmatinterfaces.de

Modulating Mucin Hydration and Lubrication by Deglycosylation and Polyethylene Glycol Binding

Thomas Crouzier, Kathrin Boettcher, Anthony R. Geonnotti, Nicole L. Kavanaugh, Julie B. Hirsch, Katharina Ribbeck,* and Oliver Lieleg*

A key property of mucin glycoproteins is their exceptional capacity to hydrate and lubricate surfaces. In vivo, mucins assemble into mucus hydrogels that cover the epithelium and protect it from dehydration and shear stress. A better understanding of the origin of these properties could lead to new treatment strategies for patients with poor mucus coverage, defective mucus production, or glycosylation as caused by Sjögren syndrome, dry eye, or in the case of certain bacterial infections. In this work, mucin coatings are used to show that mucin-associated glycans are essential for the formation of such hydrated and lubricating layers. Native mucins are compared with deglycosylated mucins by analyzing their hydration and it is shown that their lubricative potential in the boundary and mixed lubrication regime is linked to the hydration. The removal of glycans from the mucin results in a 3.5-fold decrease in hydration and an increase in friction by two orders of magnitude. This loss of function is countered by grafting polyethylene glycol (PEG) molecules to defective mucins through lectin–glycan interactions. This lectin-PEG conjugation restores hydration and improves lubrication of the partially deglycosylated mucin coatings. Thus, local complementation of defective mucus layers could prove to be a useful new treatment strategy.

and they reduce bacterial adhesion to surfaces.^[2,3] Mucins also form highly hydrated and lubricative layers that protect the underlying epithelium from dehydration and shear stress that emerge during eye blinking or when swallowing food. Water typically accounts for up to 95% of the total mass in the mucus gel.^[4,5] Shifts in the mucus water content correlate with substantial changes of the mucus barrier function^[6–8] and result in important pathological disorders such as dry mouth^[9] and dry eye.^[10] Mucin-associated glycans contribute up to 80% of the molecular weight of mucins^[11] and contain highly hydrated hydroxyl groups. Differences in the amount and composition of glycans from mucins extracted from pig stomachs and mucins from bovine submaxillary glands correlate with their capacity to adsorb water.^[12] However, other properties such as protein composition also differ between these two mucin species, precluding the establishment of a definitive link between

1. Introduction

Mucus is a hydrogel that covers all wet epithelia in our body, including the eyes, lungs, gastrointestinal and urogenital tracts. Its gel-forming building blocks are secreted mucin glycoproteins, a family of high molecular weight and densely glycosylated biopolymers. Those mucins can act as an infection shield by trapping various viruses in the biopolymer matrix^[1]

the presence of mucin glycans and hydration.

Mucins, and other well-hydrated molecules such as zwitterionic polymers, polysaccharides, and polyelectrolytes are generally good boundary lubricants when adsorbed^[13,14] or assembled in brush structures^[15–18] on surfaces. Hence, mucin-associated glycans could also be essential for the lubricative function of mucus. In a related system, the mucin-like macromolecule lubricin showed a significant decrease in lubricity when its associated glycans were removed.^[19] Moreover, the lubricity of salivary films, which contain mucins, has also been correlated with the total amount of glycosylation present in the film. However, also here, the complexity of saliva composition precluded the identification of the specific role of mucin glycosylation.^[20] Hence, there is a need for a more defined experimental system to determine if mucin glycosylation is essential to the hydration and lubrication properties of mucins.

This study explores the role of glycosylation in mucin hydration and lubricity, using mucin coatings as a simplified model system. Such mucin coatings can reconstitute levels of surface hydration^[21,22] and lubrication^[23–25] similar to those found in native mucus. Our data show that the removal of mucin-bound glycans results in a significant reduction in hydration and lubricity of the mucin-coated surface. We show that the hydration and lubricity of deglycosylated mucins can be partially

Dr. T. Crouzier, Dr. N. L. Kavanaugh, Prof. K. Ribbeck
Massachusetts Institute of Technology
77 Massachusetts Avenue, Cambridge, MA 02139, USA
E-mail: ribbeck@mit.edu

K. Boettcher, Prof. O. Lieleg
Department of Mechanical Engineering and Institute
of Medical Engineering IMETUM
Technische Universität München
Boltzmannstrasse 11, Garching 85748, Germany
E-mail: oliver.lieleg@tum.de

Dr. A. R. Geonnotti, J. B. Hirsch
Oral and Topical Healthcare R&D
Innovation Platforms Johnson and Johnson Family of Consumer
Companies
199 Grandview Road, Skillman, NJ 08558, USA

DOI: 10.1002/admi.201500308



restored by sequestering polyethylene glycol (PEG) polymers to the mucins. Together, this work provides a more detailed insight to the origin of mucus-mediated hydration and lubrication. It also shows that the substitution of mucin-bound glycans with synthetic polymers can, to a large extent, restore mucin hydration and lubricity.

2. Results and Discussion

2.1. Native and Deglycosylated Mucins Form Coatings with Different Quartz Crystal Microbalance with Dissipation (QCM-D) Signatures

To investigate the potential of mucin-bound glycans for hydration and lubrication, we used mucin coatings as a simplified model system. Mucin coatings were generated by adsorbing mucins onto gold surfaces. An analysis of the coating by QCM-D showed that the mucins formed voluminous and highly viscoelastic layers on the surface, as suggested by the high frequency shift and dissipation values recorded (Figure 1A,D). Moreover, the coatings appeared to be homogeneous at the microscopic scale when inspected by fluorescence microscopy (Figure 1A, inset). To evaluate the contribution of mucin-associated glycans to the properties of mucin coatings, these were chemically removed either completely (ApoMucin) or partially (pApoMucin), and coatings were generated from the deglycosylated mucins (Figure 1E). The reduction in glycan content

following deglycosylation was confirmed by a periodic acid-Schiff assay and lectin staining for the mucin solutions and the resulting coatings, respectively (Figure S1, Supporting Information). QCM-D analysis showed that partially deglycosylated mucins formed coatings with lower QCM-D dissipation values than fully glycosylated mucins, suggesting a more collapsed and stiff layer (Figure 1B). To account for slight variations in adsorbed mass between mucin and pApoMucin, we normalized the dissipation (D , related to the mechanical properties) to the frequency shift (Δf , related to the mass adsorbed) (Figure 1C). A coating with native mucin resulted in a higher slope of the $D/\Delta f$ curve than a coating with pApoMucin. This confirmed that pApoMucin formed stiffer coatings per adsorbed unit mass than native mucin coatings.

2.2. Mucin Deglycosylation Results in Dehydrated and Poorly Lubricating Coatings

To analyze the role of mucin-bound glycans for hydration of the mucin coating, we measured the hydration of native and deglycosylated mucin coatings. The hydration of the coatings (Figure 2A) was determined by comparing their hydrated mass, obtained via QCM-D, with their dry mass, obtained by drying the same samples then subjecting them to ellipsometry measurements. To best isolate the contribution of mucin glycans and since the hydration of mucin coatings did not seem to be sensitive to changes in NaCl concentrations (Figure S2, Supporting

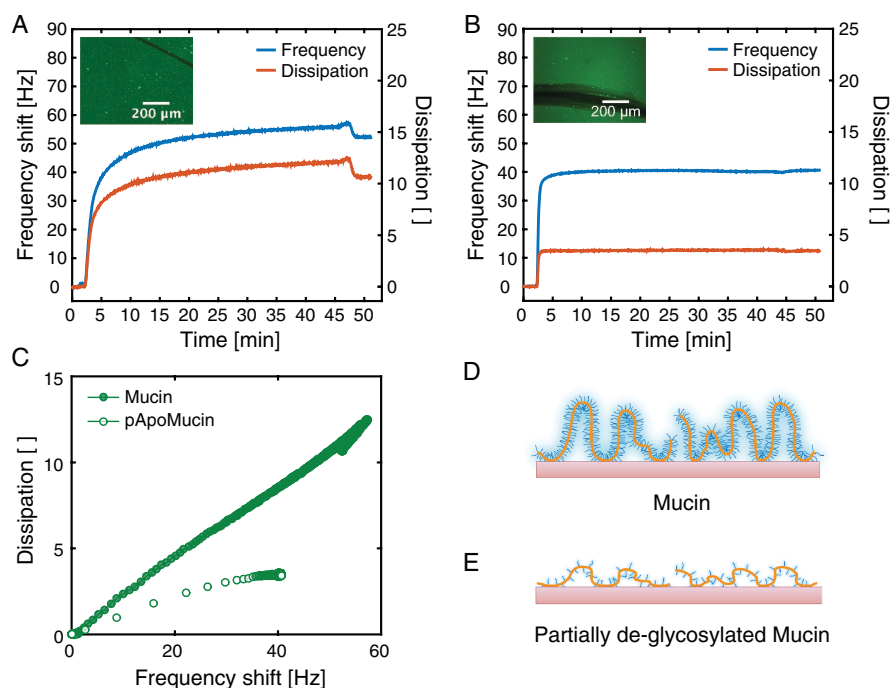


Figure 1. Native and deglycosylated mucin coatings. Quartz crystal microbalance frequency shift and dissipation measurement due to the adsorption of A) native mucin and B) partially deglycosylated mucin to a gold surface. The inset pictures show fluorescence microscopy images of the coatings with a scratch to enhance contrast. C) Changes in dissipation and frequency shift during adsorption. Schematic depiction of D) native mucin coating and E) partially deglycosylated mucin coatings.

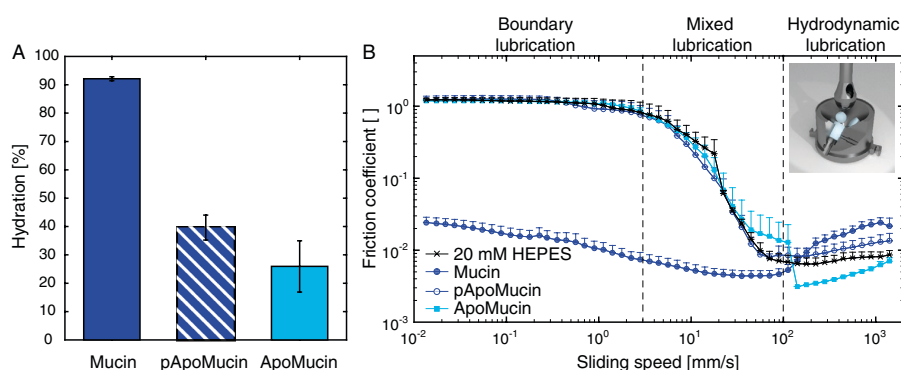


Figure 2. Mucin deglycosylation results in coating dehydration and loss of lubricity. A) Hydration of native mucin, partially deglycosylated (pApoMucin) and fully deglycosylated (ApoMucin) mucin coatings. The error bars denote the standard deviation to the mean of at least seven independent experiments. B) Lubrication of PDMS surfaces by native mucin, pApoMucin, and ApoMucin compared to aqueous buffer (HEPES). The error bars denote the error of the mean as obtained from three independent experiments. The inset depicts a schematic representation of the tribological setup used for friction measurements.

Information), we kept the pH and ionic strength of mucin adsorption and wash buffers constant for our experiments. The removal of mucin glycans resulted in a sharp drop of hydration ($p < 0.001$), from $92 \pm 1\%$ to $40 \pm 4\%$ and $26 \pm 9\%$ for partially and fully deglycosylated mucin, respectively. Similar to native mucins, both partial and fully deglycosylated mucins adsorbed to polydimethylsiloxane (PDMS) surfaces used for tribological measurements and formed coatings of comparable surface density to those on gold as judged by fluorescence measurements (Table S1, Supporting Information).

Since mucus layers experience a variety of different sliding speeds, contact pressures, and diverse lubricant viscosities, it is important to characterize the lubricating potential of mucins over a broad range of velocities. For instance, in the ileum a sliding speed of 2.3 mm s^{-1} was measured whereas in the jejunum the corresponding value is with 20.2 mm s^{-1} one order of magnitude higher.^[26] During eye blinking, a friction speed of 150 mm s^{-1} was reported.^[27] Our tribological results show that native mucins can effectively lubricate PDMS surfaces over a broad range of sliding speeds (Figure 2B), primarily in the boundary and mixed lubrication regime. Here, the mucin coating reduced the friction coefficient by two orders of magnitude.

Mucins may achieve energy dissipation and thus friction reduction by two independent mechanisms: First, surface bound mucin can provide hydration lubrication which is based on an exchange of trapped water molecules with free water molecules in the fluid.^[28] Second, shearing off whole adsorbed mucin macromolecules from either the PDMS or the steel surface may additionally contribute to the observed reduction in friction.^[24]

When coatings were built from partially or fully deglycosylated mucins, the friction coefficient was as high as without any mucin coating. This effect can result from a combination of multiple phenomena: The loss of hydration upon mucin deglycosylation can affect the hydration lubrication at the molecular scale. It can also influence the coating structure, which has been shown to impact mucin coating lubricity.^[24] In addition, molecular interactions between the deglycosylated mucins and the two surfaces can bind the opposing surfaces together and increase friction.

Such bridging effects have indeed been demonstrated with porcine gastric mucins at high contact pressures (several MPa) and at the nanoscale.^[29] Finally, also the adsorption efficiency and adsorption strength of the different mucin variants may be affected by altering the density of mucin glycans, and this could influence both the efficiency of mucin desorption from and re-adsorption to surfaces during a friction measurement.

Obviously, mucin-bound glycans play an important role in mediating hydration and lubrication, and an alteration of mucin glycosylation by pathogens or dysfunctional mucin expression is likely to result in dehydrated and poorly lubricating mucus. A molecular “repair” approach, which compensates the loss of mucin function triggered by deglycosylation, might open new avenues for the treatment of some mucus-related diseases.

2.3. PEG Can be Sequestered to Mucins by Conjugation to a Lectin

The mixing of polymers such as PEG,^[30] and other polymers^[31–33] to mucins has been used to alter the properties of mucinous systems. We here developed an alternative strategy by substituting the glycans with PEG polymer chains (Figure 3A). PEG was chosen for its known biocompatibility and the well-characterized hydration^[34,35] and lubrication^[36–39] capacity. Deglycosylation can decrease the molecular weight of mucins by up to 80%,^[40,41] thus relatively large 40 kDa PEG chains were chosen to compensate for that loss. PEG itself interacts only minimally with mucin coatings (Figure S3, Supporting Information). To facilitate mucin/PEG interaction, PEG was conjugated to wheat germ agglutinin (WGA), a lectin-type protein that binds sugars found in mucins and on cell surfaces.^[42,43] The conjugation reaction resulted in high molecular weight macromolecules (>135 kDa) consisting of three or more PEG chains associated per WGA monomer (Figure S4, Supporting Information). The bioconjugate (WGA-PEG) was able to adsorb to both coatings from native mucins and from partially deglycosylated mucins (Figure 3B) in a mucin concentration dependent manner, suggesting that the PEG grafting did not inhibit the sugar binding capacity of the lectin.

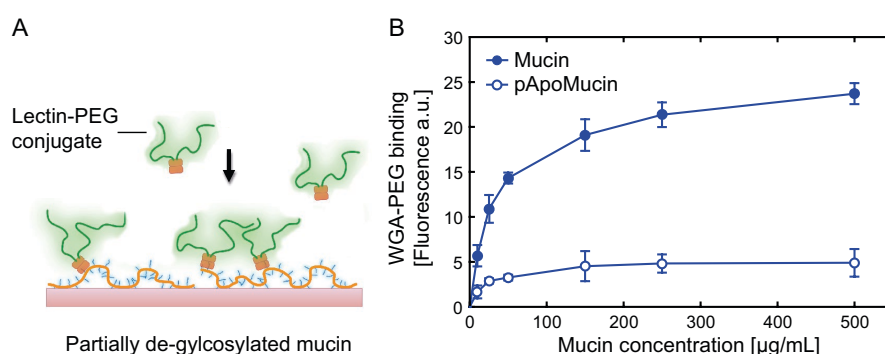


Figure 3. WGA-PEG conjugates can bind both mucins and partially deglycosylated mucins. A) Schematic illustration of our strategy to restore hydration and lubrication of deglycosylated mucin coatings by grafting PEG to mucins through mucin–lectin interactions. B) Fluorescence of FITC labeled WGA-PEG conjugates bound to immobilized native mucin and partially deglycosylated mucins (pApoMucin). The mucin concentration indicated is the concentration used to immobilize mucins to the surface. The error bars denote the standard deviation to the mean of three independent experiments.

2.4. Lectin-PEG Recovers Hydration and Lubrication of Deglycosylated Mucin Coatings

We added the PEG-WGA conjugates to partially deglycosylated mucin coatings and measured the resulting hydration of the coating. **Figure 4A** shows that the addition of PEG-WGA to deglycosylated mucin coatings resulted in a boost of hydration ($p < 0.001$) close to levels found in fully glycosylated mucins. For comparison, neither WGA nor PEG alone significantly ($p = 0.167$ and $p = 0.181$, respectively) impacted the hydration of the coating, which stagnated at around 50% of the hydration of unaltered mucins (Figure S5A, Supporting Information). As a second control, PEG conjugates were generated with Sambucus Nigra (SNA) lectin. SNA binds sialic acid residues,^[44] which are rare in the pig gastric mucin used for this study.^[45] As a consequence, SNA binding to mucin is weak (Figure S7, Supporting Information), and there was no significant impact of SNA-PEG on hydration ($p = 0.151$), confirming that binding of the PEG to the pApoMucin coating is necessary to restore hydration. If the hydration state of deglycosylated mucins can be brought back

to that of intact mucins, then the lubricating abilities of those “repaired mucins” might also approximate those of fully glycosylated mucins. We tested this hypothesis by quantifying the lubricating abilities of partially deglycosylated mucin coatings to which WGA-PEG was bound. Indeed, WGA-PEG binding to pApoMucin improved the lubricity of the coating both in the boundary and mixed lubrication regime (Figure 4B). In the latter, i.e., between friction speeds of 1 and 100 mm s^{-1} , pApoMucin + WGA-PEG layers were even equally efficient in reducing friction as intact mucin. Compared to the other lubricants (pApoMucin and pApoMucin + SNA-PEG), a significantly decreased friction was observed at sliding speeds smaller than 1.78 mm s^{-1} .

In contrast, adding just PEG alone did not alter the lubrication of the coating (Figure S5B, Supporting Information), suggesting that direct binding of the PEG to the mucin is critical to restore its lubricating properties. This was confirmed by a series of control experiments, which showed that the SNA-PEG variant added to pApoMucin coatings had no effect on hydration and lubrication. Similarly, no strong effect was measured

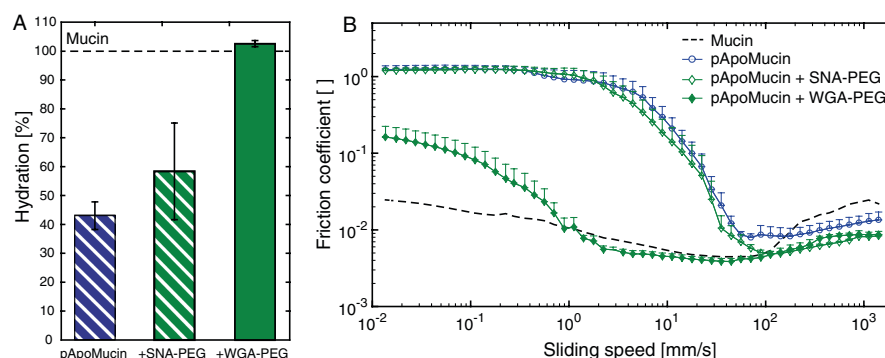


Figure 4. WGA-PEG restores hydration and lubrication of partially deglycosylated mucin coatings. A) Calculated hydration of partially deglycosylated mucin coatings treated with WGA-PEG or SNA-PEG. All values are normalized to the hydration state of native mucin coatings (=100%). The error bars denote the standard deviation to the mean of three independent experiments. B) The lubrication of partially deglycosylated mucin coatings treated with WGA-PEG or SNA-PEG is compared to native mucin coatings. The error bars denote the error of the mean as obtained from three independent experiments.

when WGA-PEG and SNA-PEG were added to ApoMucin coatings, presumably due to ApoMucin preventing nonspecific adsorption on the surface (Figure S5B, Supporting Information) while offering no glycan residues the lectin conjugates could bind to. When combining ApoMucin with either lectin-PEG conjugates, we found that the overall friction curve was shifted to the left (Figure S5B, Supporting Information), suggesting that the mixed and hydrodynamic regime is entered at smaller sliding speeds for those lubricants. Therefore, we speculate that this effect might be due to partial adsorption of lectin-PEG to the steel sphere or the PDMS cylinders. It might be possible that ApoMucin cannot fully block those surfaces thus granting partial access for lectin-PEG binding. Alternatively, differences in the lubricant viscosities could also explain the shifted onset of mixed lubrication. However, the viscosity of all lubricants is similar (Figure S8, Supporting Information) which is also consistent with our observation that no significant alteration of the hydrodynamic lubrication regime occurred for the various lubricants.

Together, these results show that the hydration and lubricative properties of PEG can be transferred to the mucin coating provided that the mucins are targeted by the correct lectin. However, although the improvement brought about by WGA-PEG could be satisfactory in certain cases, native mucin coatings still outperformed the WGA-PEG treated compromised mucin layers at very low friction speeds (Figure 4B). This highlights that the structural and chemical complexity of native mucins cannot be fully recovered by this simple substitute. Moreover, whereas the molecular repair approach demonstrated here can successfully restore the hydration capabilities of compromised mucins, it is unlikely that other mucin properties such as their antibacterial or antiviral activities can be equally rescued by grafting PEG molecules to defective mucins. PEG can only recapitulate some of the properties of the complex mixture of glycans present in native mucins. Future research may build on the strategy demonstrated here and explore other chemical grafting motifs thus addressing a broader range of mucin properties beyond hydration and lubricity. Accordingly, the design and production of fully synthetic mucins which can reproduce the broad spectrum of mucin properties is still an ongoing challenge.

3. Conclusions

In this study, we have shown the importance of mucin glycans in mucin hydration and lubrication. It implies that alterations to the glycans in vivo through dysfunctional post-translational processing or enzymatic digestion of mucin glycans can result in deficient mucus layers. Drugs such as rebamipide are currently investigated for their capacity to boost mucin production and help restore proper hydration of the mucosa,^[46] but a topical treatment of the mucus with polymers could be a viable alternative. We show that although the simple addition of PEG to the fluid phase of the lubricant has no effect, immobilizing PEG to the adsorbed mucins greatly enhances hydration and lubrication. Based on these results, one can speculate on the rationale for the natural design of mucins. Mucins-associated glycans hold water and confer an elongated structure to the

molecule, while the protein backbone provides the macroscopic structure of mucin assemblies and promotes adsorption to surfaces. Our results suggest a correlation between the presence of mucin-associated glycans, the structure of mucin coatings, coating hydration, and the lubricity of these surfaces.

4. Experimental Section

Materials and Reagents: Wheat germ agglutinin lectin (WGA, Vector Labs), fluorescently labeled WGA (FITC-WGA, Vector Labs), Sambucus Nigra lectin (SNA, Vector Labs), fluorescently labeled SNA (FITC-SNA, Vector Labs), and methoxy PEG succinimidyl carboxymethyl ester (40 kDa, mPEG-SCM, JenKem) were purchased. For control experiments using PEG, mPEG-SCM was inactivated by 20×10^{-3} M hydroxylamine (Sigma-Aldrich) at room temperature for 1 h. The hydroxylamine was then removed by centrifugation filtering (Pall, 10 kDa MWCO). Mucins were extracted from pig stomachs (pig gastric mucins, PGM) following a previously published protocol, omitting the cesium gradient density step.^[47] Briefly, the mucins were extracted by gently scraping the lumen of pig stomachs and dissolving the mucus in 200×10^{-3} M NaCl adjusted to pH 7.4. The mucins were then purified by a series of centrifugation and size exclusion chromatography separations. Mucin, partially deglycosylated mucins (pApoMucin) and fully deglycosylated mucins (ApoMucins) were fluorescently labeled by mixing a carboxylic acid succinimidyl ester amine-reactive derivative of the Alexa488 dye (Invitrogen) with the protein (at a 1:10 protein to dye ratio) in a carbonate-bicarbonate buffer (0.2 M, pH 8.5) for 1 h at room temperature. The excess dye was eliminated by centrifugation filtering (Pall, 10 kDa MWCO).

Mucin Deglycosylation: Partial deglycosylation (pApoMucins) was obtained by β -elimination of the glycans. In brief, mucins were dissolved in 500×10^{-3} M NaBH₄/50 $\times 10^{-3}$ M NaOH solution and incubated at 50 °C for 4 h. The reaction was quenched with ice-cold glacial acetic acid while keeping the sample on ice. The detached glycans were then separated from the protein via centrifugation filtering (Amicon, 30 kDa MWCO). The mucin was fully deglycosylated (ApoMucins) following a previously published protocol consisting of an acidic treatment using trifluoromethanesulfonic acid (TFMS) followed by the oxidation and β -elimination of the residual sugars.^[48] The relative glycan content of native mucins, partially deglycosylated mucins, fully deglycosylated mucins, and bovine serum albumin solutions as a negative control were assessed by a periodic acid-Schiff colorimetric assay following a previously published protocol.^[49] The decrease in sugar content of the coatings was revealed by an enzyme-linked lectin assay (ELLA) using fluorescently labeled WGA. In short, mucin, deglycosylated mucin, or bovine serum albumin coatings were generated in the wells of 96-well plates. A solution of FITC-WGA (50 $\mu\text{g mL}^{-1}$, in phosphate-buffered saline, PBS, pH 7.4) was introduced to the wells. After a 30 min incubation time the lectin solution was removed, and the coatings washed three times with 200 μL of PBS before the fluorescence of the wells was measured using a fluorescence plate reader (Spectramax M3, Molecular Device).

Mucin Coatings: Mucin, pApoMucin, or ApoMucin coatings were generated by incubating the surface for 1 h, with a 0.2 mg mL⁻¹ solution dissolved in 20×10^{-3} M HEPES, pH 7.4), except for the tribology experiments for which 1 mg mL⁻¹ solutions were used. Coatings of fluorescently labeled mucins on gold surfaces were observed using an Observer Z1 inverted fluorescent microscope (Zeiss) and a 10 \times 0.3 NA objective (Zeiss). To ensure similar coverage between mucin preparations on PDMS surfaces, the surface density of adsorbed protein was quantified. To do so, 96-well plates (351172, Becton Dickinson) were coated with PDMS by introducing 50 μL of PDMS (SYLGARD 184, 10% curing agent, Dow Corning) and rotating the plate to coat the wells. The PDMS was then cured overnight at 60 °C. Alexa488-pApoMucin or Alexa488-ApoMucin was then introduced into the well, incubated for 1 h, and residual mucin was washed off with 20×10^{-3} M HEPES solution,

pH 7.4. The resulting fluorescence was compared to a calibration curve performed in solution.

Lectin-PEG Conjugate Preparation: The lectin-PEG conjugates were synthesized by combining WGA, FITC-labeled WGA, or SNA lectins with 40 kDa mPEG-SCM (1:10 lectin to PEG ratio) in bicarbonate buffer (0.1 M, pH 8). The reaction was left for 2 h at room temperature with moderate shaking. The solution was then purified by multiple centrifugation filtering (100 kDa MWCO) removing free 40 kDa PEG and 36 kDa WGA. The resulting bioconjugate concentration was measured using bicinchoninic acid assays (Invitrogen) using WGA or SNA as standards. Quality control of the bioconjugation was performed by SDS-PAGE, where protein was stained using SimplyBlue stain (Invitrogen) and PEG was stained by soaking the gel in a 5 wt% barium chloride solution (Sigma) followed by a 0.1 M iodine solution (Sigma). The limited binding of SNA to mucins was demonstrated by incubating a polystyrene surface, a mucin coating, or an ApoMucin coating with an FITC-SNA solution (50 $\mu\text{g mL}^{-1}$ FITC-SNA in PBS, pH 7.4). After an incubation time of 30 min, the lectin solution was removed, and the coatings were washed three times with 200 μL of PBS before the fluorescence of surfaces/coatings was measured using a fluorescence plate reader (Spectramax M3, Molecular Device).

Mucin Binding of WGA-PEG: To test the WGA-PEG binding to mucin, WGA was first adsorbed on polystyrene 96-well plate (0.3 mg mL^{-1} in PBS for 30 min). The wells were then blocked with BSA (20 mg mL^{-1} in PBS for 1 h). The wells were coated with mucins or pApoMucin from solutions of various concentrations (0–1 mg mL^{-1} , in 20×10^{-3} M HEPES, pH 7.4, for 30 min) followed by extensive washing to remove unbound mucins. The fluorescently labeled WGA-PEG conjugate was then added (0.15 mg mL^{-1} in PBS for 30 min). Unbound WGA-PEG was removed by washing the wells with PBS. Finally, the fluorescence of the wells was measured using a fluorescence plate reader (Spectramax M3, Molecular Device).

Hydration Measurements: The hydration of the coatings was measured by combining QCM-D monitoring and ellipsometry measurements. A QCM-D instrument equipped with flow cells (E4 system, Q-Sense, Sweden) was used to measure the hydrated mass of the coatings. The crystals used (QX 301, Q-sense) were purchased, coated with gold, and cleaned by successively treating the surface with a detergent (0.1% sodium dodecyl sulfate, 10 min, 60 °C), acid (1 M HCl, 10 min, 60 °C), and 15 min in a UV-ozone cleaner. The protein solutions were pumped to fill the reservoir above the crystal surface, and then the flow was stopped to allow the coating to form. The crystal vibration was followed at its fundamental frequency (5 MHz) and six overtones (15, 25, 35, 45, 55, and 65 MHz). Changes in the resonance frequencies and in dissipation of the vibration once the excitation was stopped were followed at the seven frequencies. Shifts in frequency are related to changes in adsorbed mass whereas changes in dissipation reflect the mechanical properties of the adsorbed coating. Given the high dissipation values generated by mucin coatings, the Sauerbrey relation that ties frequency and adsorbed mass through a linear relationship did not apply. Thus, a Voigt-based model was used to accurately estimate the hydrated thickness.^[50] The density of the mucin coating was fixed at 1050 kg m^{-3} which is between that of pure water (1000 kg m^{-3}) and pure protein (1350 kg m^{-3}).^[51]

The dry thickness of mucin coatings was determined by spectroscopic ellipsometry using an XLS-100 ellipsometer (J.A. Woollam Co.). The measurements were performed at an angle of 70° and at wavelengths from 190 to 993 nm with 70 spectroscopic scans per measurements and four measurements per sample. The coatings previously generated on gold covered QCM-D crystals were rinsed with water and dried under nitrogen flow. A multilayer model composed of a silicon substrate (0.2 mm), a gold layer (75 nm), and a Cauchy layer of unknown thickness was used to calculate the mucin coating dry thickness (WVASE32 software, version 3.768). A density of 1200 kg m^{-3} was assumed to calculate the total mass.^[52] The level of hydration of the film was deduced from the dry and hydrated mass using the relationship

$$\text{Hydration (\%)} = \frac{\text{hydrated mass} - \text{dry mass}}{\text{hydrated mass}} \times 100 \quad (1)$$

Lubrication Measurements: For friction measurements, a commercial shear rheometer (MCR 302, Anton Paar) was equipped with a tribology unit (T-PTD 200, Anton Paar), and the measurements were performed in a ball-on-cylinder geometry as described in ref.^[53] and shown as an inset in Figure 2B. As friction partners in the tribology setup, PDMS cylinders and steel spheres with a diameter of 12.7 mm (Kugel Pompel) were chosen. The rationale for this choice was that, with this particular tribo pairing, the dynamic range between lubrication with simple HEPES buffer and lubrication with a solution of intact mucins was largest compared to when glass or Teflon spheres were used as friction probes (Figure S6, Supporting Information). This enabled to better distinguish intermediate levels of lubrication than with the other pairings. The PDMS cylinders were prepared by mixing PDMS (SYLGARD 184, Dow Corning) in a 10:1 ratio with the curing agent and exposing the mixture to vacuum for 1 h to remove air bubbles before curing at 80 °C for 1 h. Before each measurement, the cylinders were cleaned with 80% ethanol and ddH₂O. During the measurements, a normal force of 6 N was applied resulting in a contact pressure of ≈ 0.1 MPa. This normal force was chosen such that friction in the boundary, mixed, and hydrodynamic regime could be probed. However, here the boundary lubrication regime is focused on as the main aim of this study is to investigate the ability of mucins to act as boundary lubricants. The friction behavior was evaluated by performing a logarithmic speed ramp from 1000 to 0.01 mm s^{-1} and the friction coefficient was measured over 10 s per speed level. Before the first measuring point, the system was allowed to stabilize at the highest rotational speed for 10 s. All measurements were performed at room temperature and the PDMS cylinders were fully covered with lubricant during measurements. When native, partially, or fully deglycosylated mucin solutions (20×10^{-3} M HEPES, pH 7.4, 1 mg mL^{-1}) were used as lubricants, the PDMS cylinders were incubated in the lubricant for 1 h prior to the measurement. When lectin-PEG or PEG was used, the PDMS cylinders were incubated in the mucin solution (20×10^{-3} M HEPES, pH 7.4, 0.85 mg mL^{-1} , final concentration) for 60 min, with the addition of lectin-PEG (20×10^{-3} M HEPES, pH 7.4, 0.15 mg mL^{-1} , final concentration) after the first 30 min. Similarly, the incubation solution was afterward used as lubricant. Using mucin-free buffer as a lubricant after incubating the PDMS and/or steel surface was less efficient in reducing the friction coefficient in the boundary lubrication regime (Figure S9, Supporting Information) compared to when mucin was also present in the lubricating fluid.

Statistical Analysis: The statistical significance of variations in hydration measurements (five independent measurements per condition) was calculated by performing an unpaired *t*-test using SigmaPlot software (v13, Systat Software). The statistical significance of variations in the friction measurements (three independent measurements per condition) was calculated by performing one-way ANOVAs and Tukey post hoc tests. All statistical analyses were performed using R (Foundation for Statistical Computing). A *p*-value < 0.05 was used as a measure for statistical significance.

Supporting Information

Supporting Information is available from the Wiley Online Library or from the author.

Acknowledgements

T.C. and K.B. contributed equally to this work. The authors thank the Johnson and Johnson Corporate Office of Science and Technology that provided funding for this study. This work made use of the Institute for Soldier Nanotechnology facilities and of the MRSEC Shared Experiment Facilities supported by the National Science Foundation under Award No. DMR-819762. This work was made possible by a Marie Curie International Outgoing Fellowship “BIOMUC” (to T.C.). O.L. and K.B. acknowledge support from the Dean's Innovation Fund of the

Mechanical Engineering Department of TUM and from the Deutsche Forschungsgemeinschaft through SFB 1032, project B7.

Received: June 11, 2015

Revised: August 13, 2015

Published online:

- [1] O. Lieleg, C. Lieleg, J. Bloom, C. B. Buck, K. Ribbeck, *Biomacromolecules* **2012**, *13*, 1724.
- [2] L. Shi, R. Ardehali, K. D. Caldwell, P. Valint, *Colloids Surf., B* **2000**, *17*, 229.
- [3] Q. Pan, Y. Tian, X. Li, J. Ye, Y. Liu, L. Song, Y. Yang, R. Zhu, Y. He, L. Chen, W. Chen, X. Mao, Z. Peng, R. Wang, *J. Biol. Chem.* **2013**, *288*, 5407.
- [4] A. W. Larhed, P. Artursson, E. Björk, *Pharm. Res.* **1998**, *15*, 66.
- [5] J. Perez-Vilar, in *Oral Delivery of Macromolecular Drugs* (Ed: A. Bernkop-Schnürch), Springer US, New York, NY **2009**, pp. 21–48.
- [6] R. A. Cone, *Adv. Drug Delivery Rev.* **2009**, *61*, 75.
- [7] J. R. Turner, *Nat. Rev. Immunol.* **2009**, *9*, 799.
- [8] J. L. Bigelow, *Hum. Reprod.* **2004**, *19*, 889.
- [9] R. Pramanik, S. M. Osailan, S. J. Challacombe, D. Urquhart, G. B. Proctor, *Eur. J. Oral Sci.* **2010**, *118*, 245.
- [10] P. Ramamoorthy, J. J. Nichols, *Optom. Vis. Sci.* **2008**, *85*, E631.
- [11] R. Bansil, B. S. Turner, *Curr. Opin. Colloid Interface Sci.* **2006**, *11*, 164.
- [12] Y. Znamenskaya, J. Sotres, J. Engblom, T. Arnebrant, V. Kocherbitov, *J. Phys. Chem. B* **2012**, *116*, 5047.
- [13] B. Zappone, M. Ruths, G. W. Greene, G. D. Jay, J. N. Israelachvili, *Biophys. J.* **2007**, *92*, 1693.
- [14] N. Kampf, U. Raviv, J. Klein, *Macromolecules* **2004**, *37*, 1134.
- [15] T. Moro, Y. Takatori, K. Ishihara, T. Konno, Y. Takigawa, T. Matsushita, U.-I. Chung, K. Nakamura, H. Kawaguchi, *Nat. Mater.* **2004**, *3*, 829.
- [16] J. Klein, E. Kumacheva, D. Mahalu, D. Perahia, L. J. Fetters, *Nature* **1994**, *370*, 634.
- [17] M. Chen, W. H. Briscoe, S. P. Armes, J. Klein, *Science* **2009**, *323*, 1698.
- [18] K. Staudt, W. Böhme, W. Baumgartner, *J. Biomimetics, Biomater., Tissue Eng.* **2012**, *16*, 1.
- [19] G. D. Jay, D. A. Harris, C. J. Cha, *Glycoconjugate J.* **2001**, *18*, 807.
- [20] D. H. Veeregowda, H. C. van der Mei, J. de Vries, M. W. Rutland, J. J. Valle-Delgado, P. K. Sharma, H. J. Busscher, *Clin. Oral Invest.* **2012**, *16*, 1499.
- [21] O. Svensson, L. Lindh, M. Cardenas, T. Arnebrant, *J. Colloid Interface Sci.* **2006**, *299*, 608.
- [22] Y. Znamenskaya, J. Sotres, S. Gavryushov, J. Engblom, T. Arnebrant, V. Kocherbitov, *J. Phys. Chem. B* **2013**, *117*, 2554.
- [23] J. M. Coles, D. P. Chang, S. Zauscher, *Curr. Opin. Colloid Interface Sci.* **2010**, *15*, 406.
- [24] G. E. Yakubov, J. McColl, J. H. H. Bongaerts, J. J. Ramsden, *Langmuir* **2009**, *25*, 2313.
- [25] S. Lee, M. Müller, K. Rezwani, N. D. Spencer, *Langmuir* **2005**, *21*, 8344.
- [26] *Essentials of Experimental Surgery: Gastroenterology* (Ed: S. L. Jensen), Harwood Academic Publ, Amsterdam **1996**.
- [27] *Tribology for Scientists and Engineers: From Basics to Advanced Concepts* (Eds: P. L. Menezes, S. P. Ingole, M. Nosonovsky, S. V. Kailas, M. R. Lovell), Springer, New York **2013**.
- [28] L. Ma, A. Gaisinskaya-Kipnis, N. Kampf, J. Klein, *Nat. Commun.* **2015**, *6*, 6060.
- [29] N. M. Harvey, G. E. Yakubov, J. R. Stokes, J. Klein, *Biomacromolecules* **2011**, *12*, 1041.
- [30] R. K. Willits, W. M. Saltzman, *Biomaterials* **2001**, *22*, 445.
- [31] R. K. Willits, W. M. Saltzman, *Biomaterials* **2004**, *25*, 4563.
- [32] S. Rossi, F. Ferrari, M. C. Bonferoni, C. Caramella, *Eur. J. Pharm. Sci.* **2001**, *12*, 479.
- [33] D. H. Veeregowda, A. Kolbe, H. C. van der Mei, H. J. Busscher, A. Herrmann, P. K. Sharma, *Adv. Mater.* **2013**, *25*, 3426.
- [34] C. Branca, S. Magazù, G. Maisano, F. Migliardo, P. Migliardo, G. Romeo, *J. Phys. Chem. B* **2002**, *106*, 10272.
- [35] O. Tirosh, Y. Barenholz, J. Katzhendler, A. Prieve, *Biophys. J.* **1998**, *74*, 1371.
- [36] R. Heeb, S. Lee, N. V. Venkataraman, N. D. Spencer, *ACS Appl. Mater. Interfaces* **2009**, *1*, 1105.
- [37] T. Drobek, N. D. Spencer, *Langmuir* **2008**, *24*, 1484.
- [38] M. Müller, S. Lee, H. A. Spikes, N. D. Spencer, *Tribol. Lett.* **2003**, *15*, 395.
- [39] S. Liu, G. Tan, D. Wang, *Sci. China: Technol. Sci.* **2013**, *56*, 1709.
- [40] H. D. Hill, J. A. Reynolds, R. L. Hill, *J. Biol. Chem.* **1977**, *252*, 3791.
- [41] I. Carlstedt, A. Herrmann, H. Karlsson, J. Sheehan, L. A. Fransson, G. C. Hansson, *J. Biol. Chem.* **1993**, *268*, 18771.
- [42] M. Wirth, K. Gerhardt, C. Wurm, F. Gabor, *J. Controlled Release* **2002**, *79*, 183.
- [43] Y. Nagata, M. M. Burger, *J. Biol. Chem.* **1974**, *249*, 3116.
- [44] N. Shibuya, I. J. Goldstein, W. F. Broekaert, M. Nsimba-Lubaki, B. Peeters, W. J. Peumans, *J. Biol. Chem.* **1987**, *262*, 1596.
- [45] H. Nordman, J. R. Davies, A. Herrmann, N. G. Karlsson, G. C. Hansson, I. Carlstedt, *Biochem. J.* **1997**, *326*, 903.
- [46] Y. Takeji, H. Urashima, A. Aoki, H. Shinohara, *J. Ocul. Pharmacol. Ther.* **2012**, *28*, 259.
- [47] J. Celli, B. Gregor, B. Turner, N. H. Afdhal, R. Bansil, S. Erramilli, *Biomacromolecules* **2005**, *6*, 1329.
- [48] T. A. Gerken, R. Gupta, N. Jentoft, *Biochemistry* **1992**, *31*, 639.
- [49] M. Kilcoyne, J. Q. Gerlach, M. P. Farrell, V. P. Bhavanandan, L. Joshi, *Anal. Biochem.* **2011**, *416*, 18.
- [50] M. V. Voinova, M. Rodahl, M. Jonson, B. Kasemo, *Phys. Scr.* **1999**, *59*, 391.
- [51] N. Weber, H. P. Wendel, J. Kohn, *J. Biomed. Mater. Res. A* **2005**, *72A*, 420.
- [52] F. Caruso, D. N. Furlong, K. Ariga, I. Ichinose, T. Kunitake, *Langmuir* **1998**, *14*, 4559.
- [53] K. Boettcher, S. Grumbein, U. Winkler, J. Nachtsheim, O. Lieleg, *Rev. Sci. Instrum.* **2014**, *85*, 093903.

A.5. Porcine gastric mucins reduce friction and wear in cartilage boundary lubrication

Porcine gastric mucins reduce friction and wear in cartilage boundary lubrication

Kathrin Boettcher¹, Samuel G. Dorosz², Tannin A. Schmidt^{2,3}, Oliver Lieleg^{1,}*

¹ Institute of Medical Engineering IMETUM and Department of Mechanical Engineering, Technische Universität München, Boltzmannstraße 11, 85748 Garching, Germany

² Biomedical Engineering Graduate Program and ³ Faculty of Kinesiology, University of Calgary, Calgary, Alberta, Canada

KEYWORDS

tribology, MUC5AC, lubricin, PRG4, hyaluronic acid, optical profilometry

ABSTRACT

Mucin glycoproteins are the main component of mucus, a hydrogel covering the wet epithelia of our body. Mucins combine a multitude of important functions on biological interfaces: they hydrate and lubricate e.g., the eye and the gastrointestinal tract. For joint lubrication, however, nature employs a different but related mucinous glycoprotein: lubricin. Lubricin serves as a boundary lubricant to reduce friction and prevent wear on articular cartilage. Here we show that purified gastric mucin is able to reduce friction between cartilage surfaces to a similar extent as lubricin. Moreover, we find that mucin can prevent wear on cartilage in a glass/cartilage tribology setup and we compare these findings with the ability of mucins to adsorb to different surfaces. To systematically evaluate wear formation, we establish a new analysis method based on several quantitative parameters used in surface metrology. We then compare three macromolecular lubricants: hyaluronic acid, lubricin and mucin. Whereas mucin prevents wear, lubrication with hyaluronic acid leads to adhesive wear and lubricin generates abrasive wear on the cartilage surface. Our findings advance our understanding of why, *in vivo*, multiple biopolymers are present at the interface between the cartilage surface and the synovial fluid, and we demonstrate the great potential for mucin as a boundary lubricant in cartilage tribology.

INTRODUCTION

Joints in the human body are able to function over several decades at ultra-low friction and little wear. Especially because of their outstanding durability, they still outperform artificial joints. This durability can be mainly attributed to both articular cartilage, the tissue lining the joint surfaces, and synovial fluid within the joint. Especially the interplay between the solid and fluid phase of articular cartilage contributes to its outstanding material properties.

The cartilage matrix is mainly composed of a collagen type 2 matrix and aggrecan proteoglycans. These aggrecans consist of a core protein with attached glycosaminoglycans, which bind to hyaluronic acid (HA) polymer chains. HA is present throughout the cartilage matrix and interacts with the collagen type 2 fibrils¹. Glycosaminoglycans play an important role for cartilage hydration through a process called interstitial fluid pressurization²⁻⁴. The pressurized fluid phase inside the collagen matrix carries most of the load and is essential for the tissue durability as it protects the solid phase under stress.

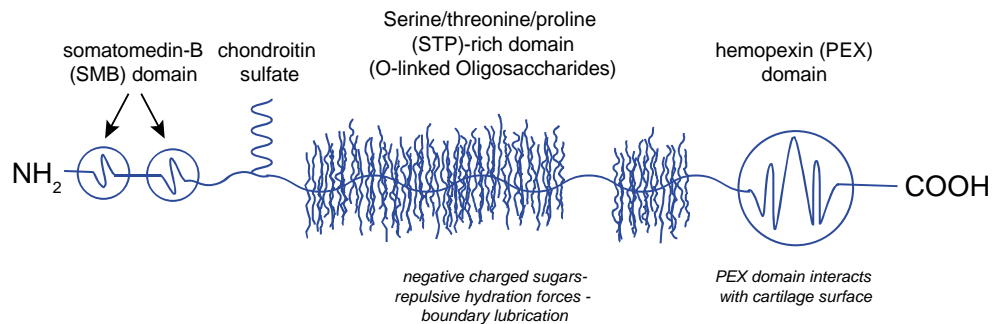
Whereas the function of the cartilage matrix components is mostly well understood, their interplay with the molecular components out of the fluid phase is still not fully clear. It also remains an open question why – despite its inability to regenerate – the cartilage surface can resist wear over several decades. HA is suggested to be important for wear resistance^{5,6}, whereas its role in friction reduction, especially at small rotational speeds in the boundary lubrication regime⁷, is highly discussed^{8,9} and seems to depend on the measurement setup and the two countering surfaces. It was recently shown that HA can entangle with other molecules on the cartilage surface¹⁰ and thereby act as a stabilizer for phospholipids¹¹ and smaller proteins such as lubricin^{1,12}, fibronectin (FN)¹³, collagen type 2¹, aggrecan¹⁴ and serum proteins^{15,16} (mostly albumin and globulin) from the fluid and solid

phase. HA films are known to collapse upon adsorption of lubricin as it physically crosslinks grafted HA¹⁷ and thereby act as surface-anchored protective layer¹⁸. Whereas there are no studies reporting on the wear protection properties of these layers, the boundary lubrication potential of HA and lubricin was first reported at a latex-glass interface, where the presence of HA enabled lubricin to lubricate at higher contact pressures¹⁹. Seror *et al.* found that, between two mica surfaces, aggrecan-HA complexes are much better boundary lubricants than HA alone¹⁴.

Evidence is increasing^{14,15} that lubricin, aggrecans and phospholipids, trapped by HA and possibly fibronectin¹³ and collagen type 2¹, mediate friction through hydration lubrication²⁰. The proteoglycans and lipids trap water molecules at the surface, and energy can be additionally dissipated by adsorption and desorption under shear²¹ (sacrificial layer mechanism²²). This is underscored by studies describing adsorbed synovial fluid components as a repulsive effective brush layer preventing interpenetration¹⁷ and adhesion²¹ of the opposing surfaces under pressure¹³. Klein *et al.*²³ described that especially positively charged salt ions inside the hydration shell can act as “ball bearings” when they are trapped between the negatively charged proteoglycan brushes and the negatively charged cartilage surfaces. Although friction and wear are not necessarily coupled, the trapped fluid layer does not only decrease friction but also provides wear protection as it inhibits contact between surface asperities (microscopic surface roughness) and potential cross-adsorption of molecules bridging the gap between the opposing surfaces.

Wear protection and friction reduction are not only essential between joint surfaces but also in between various other tissues in the human body. In general, the lubrication mechanism employed throughout the human body is similar and relies mainly on hydration lubrication. However, in contrast to joint lubrication, on epithelial surfaces

a - lubricin



b - mucin

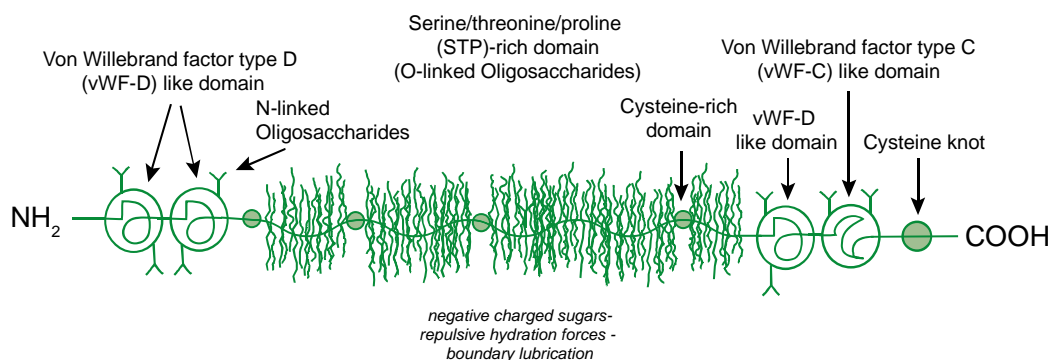


Figure 1. Schematic structures of lubricin²⁷ and porcine gastric mucin²⁸ (PGM). The two glycosylated proteins share a lot of similarities but also exhibit distinct differences. Specific to lubricin and important for its function as joint lubricant are e.g., the chondroitin sulfate substitution site and the hemopexin domain, which is thought to mediate the interaction of lubricin with the cartilage surface. Mucins are secreted with a high molecular weight of around 641 kDa²⁹, in contrast lubricin is with 227 – 345 kDa³⁰ comparably smaller.

hydration lubrication is mediated by a different molecule, namely mucin. All wet epithelia, e.g., ocular²⁴, oral and gastrointestinal tract surfaces, are covered with mucus, a biopolymer-based hydrogel. Mucin, a highly glycosylated glycoprotein, is the main component of mucus and known to reduce friction²⁵.

One could now ask why nature utilizes a unique and more complex lubrication mechanism in joints and if mucin could be able to mediate friction and wear also on articular cartilage and under higher contact pressures. Porcine gastric mucin (PGM) combines the molecular weight range of HA and the highly glycosylated domain of lubricin. Compared to lubricin, PGM does not possess a PEX-like domain, which lubricin

utilized to bind to cartilage surfaces²⁶ (Figure 1). However, it is known to adsorb to a wide variety of hydrophobic and hydrophilic surfaces and could possibly adsorb directly to the cartilage surface. Compared to lubricin, PGM is easier to purify in larger amounts.

The objectives of this study are to (1) test the suitability of porcine gastric mucin as a potential boundary lubricant in a cartilage/cartilage and glass/cartilage setup, (2) establish a quantitative method to systematically analyze different wear features on cartilage surfaces and (3) further clarify the tribological function of macromolecules present in synovial fluid by not only analyzing friction but also wear.

EXPERIMENTAL SECTION

Sample preparation

Knee joints from 3 - 6 month old lambs were obtained from local butchers and stored at $-20\text{ }^{\circ}\text{C}$ until further usage. On the day of experiments, osteochondral cylinders with a diameter of 5.5 mm were drilled out of the trochlear groove as described in Boettcher *et al.*³¹. The harvested samples were incubated for at least 0.5 h in PBS (Dulbecco's PBS, Lonza, Switzerland) to ensure identical initial sample conditions and afterwards incubated in the designated lubricant for 1 h prior to a measurement. All measurements were performed and repeated on samples from at least two different animals.

For the friction measurements between two cartilage surfaces, knee joints from skeletally mature bovine knee joints were obtained and osteochondral cylinders harvested from the trochlear groove as described previously³². Briefly, cores with a diameter of 12 mm and annuli (diameter: inner = 3 mm, outer = 6.4 mm) were drilled, rinsed overnight in PBS at $4\text{ }^{\circ}\text{C}$ and frozen in PBS at $-80\text{ }^{\circ}\text{C}$ until further usage. Prior to testing, the samples were shaken overnight in PBS at $4\text{ }^{\circ}\text{C}$.

Lubricants

The following lubricants were used throughout this study: PBS, 0.1 % (w/v) hyaluronic acid, 0.1 % mucin and 0.1 % lubricin solutions. All solutions were prepared in PBS (Dulbecco's PBS, Lonza, Switzerland).

Hyaluronic acid (HA) with a molecular weight of 2 – 2.4 MDa (Hyaluronic acid sodium salt from *Streptococcus equi.*) was purchased from Sigma Aldrich, USA.

Bovine lubricin was purified from fresh skeletally mature bovine knee joints, as described previously³². Briefly, cartilage discs were cultured in Dulbecco's Modified Eagle's Medium and purified using salt gradient diethylaminoethanol anion exchange

chromatography. The purity of the solution was confirmed using 3 – 8 % Tris-Acetate SDS-PAGE followed by Simply Blue protein stain and densitometry analysis.

Porcine gastric mucin was purified as described previously³³ with the exception that the cesium chloride density gradient ultracentrifugation was omitted. Briefly, mucus was collected by gently scraping the surface of pig stomachs. The extracted mucus was dissolved in phosphate buffered saline (10 mM, 170 mM NaCl adjusted to pH 7.4) and purified by a series of centrifugation and size exclusion chromatography steps. Subsequently, the solution was concentrated and desalted by cross-flow dialysis until a conductance of less than $50\text{ }\mu\text{S}$ was reached. Finally, the obtained mucin MUC5AC was stored in lyophilized form at $-80\text{ }^{\circ}\text{C}$ until further use. The successful purification of MUC5AC was verified with the same ELISA as used for the mucin adsorption measurements.

Viscosity measurements

The lubricant viscosities were measured using a shear rheometer (MCR 302, Anton Paar, Austria) equipped with a planar bottom plate (P-PTD 200/56/AIR, Anton Paar, Austria) and a conical measuring head ($\text{\O} 25\text{ mm}$, 1° angle, CP 25-1, Anton Paar, Austria). A volume of $80\text{ }\mu\text{l}$ was pipetted onto the measuring plate and the measuring head was lowered to a gap of $50\text{ }\mu\text{m}$. At this position, the gap between the plate and cone was completely filled with the test solution. Before the actual measurement, the measuring head was rotated at 1000 s^{-1} for 40 s. Afterwards, the viscosity was measured using a logarithmical speed ramp from 1000 s^{-1} to 1 s^{-1} with 5 measuring points per decade and a measuring point duration of 10 s.

Mucin adsorption

The ability of mucin to adsorb to the different materials used during the tribological measurements was quantified via an ELISA. Therefore, small glass (soda-lime glass), steel (stainless austenitic steel 1.4401) and PDMS (SYLGARD 184, Dow Corning, USA) platelets with a length of 10 mm, a width of 5 mm and a height of 1 – 3 mm were manufactured, incubated in a 0.1 % mucin solution ($n = 3$ for each material) for 1 h, washed extensively and then incubated in blocking buffer containing 5 % (w/v) powdered milk (Carl Roth, Germany) in PBS-TWEEN (1 % (w/v) TWEEN 20), the washing buffer, at 4 °C overnight. Subsequently, the plates were incubated for 1 h in either the mucin antibody (anti-MUC5AC, Oligomeric Mucus/gel-Forming, ABIN966608, antibodies-online, Germany) or the isotype control (IgG1 Isotype Control from murine myeloma, M5284, Sigma Aldrich, USA; $n = 2$ for each material). As a secondary antibody, Goat anti-Mouse (Murine) IgG (Heavy & Light Chain) antibody HRP (ABIN237501, antibodies-online, Germany) labelled with horseradish peroxidase was used (2 h incubation time). O-phenylenediamine (Sigma-Aldrich, USA) added to this mix afterwards was then converted by the horseradish peroxidase, and the reaction product was determined spectrophotometrically. The measured absorbance was corrected for the slightly different surface areas of the test platelets.

Tribology measurements

All friction measurements were conducted under constant contact conditions. This setup was favored over classical linear tribology setups as it is better suitable for the observation of the boundary lubrication ability of lubricants over time.

Friction measurements between two cartilage surfaces were conducted using a previously described cartilage/cartilage friction test setup on

a Bose ELF 3200³² (TA Instruments, USA; Figure S1a). The samples were compressed to 18 % of the total thickness and allowed to stress-relax for 40 min. The friction test was then conducted at an effective velocity of 0.3 mm/s for ± 2 revolutions and a pre-sliding duration of 1.2 s between the rotations. The kinetic coefficient of friction was calculated from the second rotation in both the forward and backward direction. The samples were subjected to two friction tests on two consecutive days. Each sample set was first tested in PBS, as a negative control, then incubated in the test lubricant (i.e., either lubricin or mucin) overnight and measured again with this test lubricant. Four sample sets were tested for each lubricant.

Friction measurements using cartilage and glass as tribo-pairing were conducted using a shear rheometer (MCR 302, Anton Paar, Austria) equipped with a tribology unit (T-PTD 200, Anton Paar, Austria). As described before³¹, a glass sphere (Kugel Pompel, Austria) was rotated on the cartilage surfaces of three osteochondral cylinders with a contact pressure of approximately 0.1 MPa (Figure S1b). The friction coefficient was measured at rotational speeds of 0.01 mm/s, 0.1 mm/s, 1 mm/s, 10 mm/s and 50 mm/s in an arbitrary order over a time span of 1 h for each speed level. For evaluation, the final friction coefficient (averaged over the last 10 s of the measurement) is reported. Three measurements were conducted with each lubricant.

To investigate wear generation, the same setup as described above was utilized and a glass sphere was rotated on top of three osteochondral cylinders with a rotational speed of 0.1 mm/s for 1 h. This speed level was chosen to investigate the performance of the lubricants in the boundary lubrication regime³⁴. The chosen rotational setup excludes the possibility of slip stick observed with oscillatory measurements and thereby potential wear formation due to this particular phenomenon¹⁸.

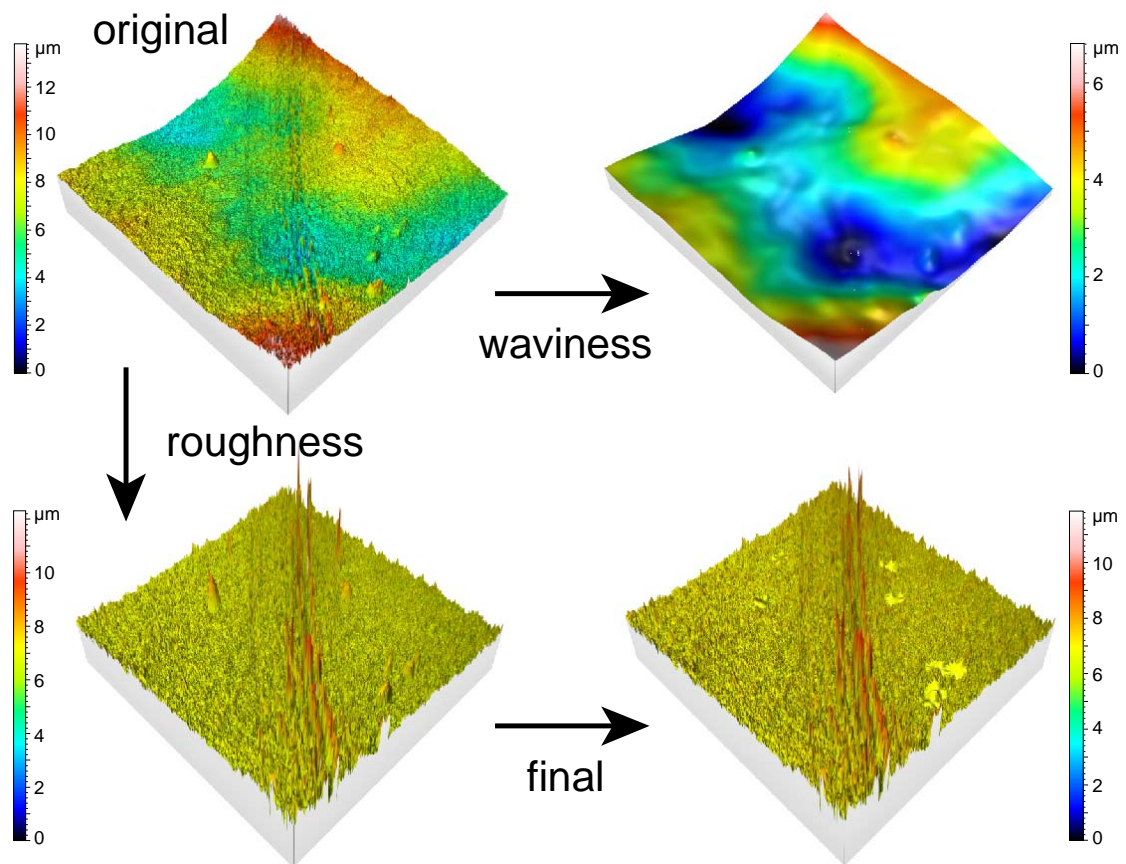


Figure 2. 3D images of surface topographies: after imaging, filtering and adjustments. The original image is shown after correction for sample tilt. Next, a Gaussian filter is applied and the waviness and roughness profiles are separated. Finally, the roughness profile is corrected for water bubbles and void points.

Three measurements were conducted with each lubricant and therefore a total of nine samples were tested for each experimental condition.

Profilometer measurements

Following the 1 h glass/cartilage friction tests, cartilage surfaces were investigated using an optical profilometer (μsurf custom, nanofocus, Germany) and a 20x objective (Zeiss, Germany). Samples were removed from the lubricant and carefully rinsed in PBS. Subsequently, the samples were exposed to air for approximately 10 min until the surface was mostly free of water droplets. Three images for each sample were acquired at arbitrary locations where no or only few droplets were visible in the microscopic

image. Image analysis was therefore performed on a total of 27 images for each lubricant. The resolution of the images was 1.56 μm in lateral and 0.22 μm in vertical direction. Directly after the measurement, the images were corrected for sample tilt by applying a linear polynomial correction (μsoft version 6.0, nanofocus, Germany) to the images.

Image analysis

Image analysis was performed using the software μsoft analysis extended V7 (nanofocus, Germany). To analyze surface features generated by the friction measurement, the surface waviness of the samples was removed by applying a Gaussian filter (ISO 16610-61) with a cut-off

wavelength of 80 μm (Figure 2). The image was cropped after filtering to remove generated edge artefacts. In a second step, the void points in the image were automatically filled by the software. A manual step was necessary to remove some remaining air bubbles, which should not be considered as sample surface features. Therefore, corresponding spots on the image were manually smoothed. Finally, surface parameters were calculated from the resulting topographical image. The following ISO 25178-2 parameters were chosen for surface evaluation³⁵⁻³⁷: The root mean square roughness (Sq, equation 1), which is related to the average roughness Sa (equation 2), was calculated as it is a standard parameter to compare the roughness of surfaces. Another parameter taking into account the surface height is the ten-point height (S10z, equation 3). It is defined as the average height of the five highest local maxima plus the average height of the five lowest local minima.

Since the S10z parameter relies on height information of only 10 single peaks, two volumetric parameters were chosen to additionally examine these local surface features. Through image segmentation into motifs (dales and hills) using the watersheds method, the closed dales volume (Sdv) and closed hills volume (Shv) were evaluated.

In addition to local wear features, wear tracks were visible on the surfaces and could be quantified by a spatial parameter: the isotropy of the surface (Str), which can be determined based on the autocorrelation function (ACF, equation 4). Here, a surface profile (z) in one direction is compared with surface profile lines in the same direction at different positions (x, y) and the correlation length between the profile lines is calculated. The isotropy of the surface is defined as the ratio of the minimum autocorrelation length in any direction divided by the maximum autocorrelation length in any direction. By integration of the Fourier spectrum of the autocorrelation length of each direction into polar

coordinates, the principal direction of the surface structures can be determined and the anisotropy quantified.

$$Sq = \sqrt{\iint_A (z(x, y))^2 dx dy} \quad (1)$$

$$Sa = \iint_A |z(x, y)| dx dy \quad (2)$$

$$S10z = \frac{\sum_{i=1}^5 |z_{pi}| + \sum_{i=1}^5 |z_{vi}|}{5} \quad (3)$$

$$ACF(\tau x, \tau y) = \frac{\iint_A z(x, y)z(x - \tau x, y - \tau y) dx dy}{\iint_A z^2(x, y) dx dy} \quad (4)$$

Statistical analysis

To detect significant differences between the examined groups, one-way ANOVAs and for all multiple comparisons (more than two groups) Tukey post-hoc tests were carried out³⁸. Since in the cartilage/cartilage setup the lubricants were compared by subjecting the sample sets to two consecutive tests, here, two-sample paired t-tests (one-tailed) were conducted.

For all tests, the homogeneity of variances was verified in boxplots and the normal distribution in Q-Q plot.

Since the wear data were not ideally normally distributed and the variances were initially not homogeneous, a box-cox transformation³⁹ was applied to these datasets. This transformation improved both, the normal distribution and the homogeneity of variances, and the transformed data met the assumptions for ANOVA.

Some of the analyzed wear parameters were local features and not present on all three images obtained for each sample. Therefore, only the mean value for one sample was considered for statistical analysis. This lead to a sample size of $n = 9$ instead of $n = 27$.

All statistical analyses were performed using the software R (Foundation for Statistical Computing).

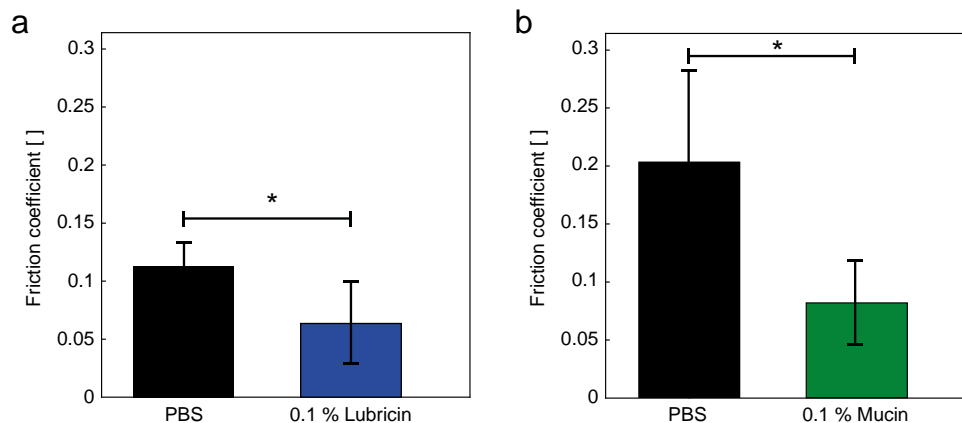


Figure 3. Lubricin and mucin decrease friction between cartilage surfaces. Measurements are conducted under constant contact conditions at a rotational speed of 0.3 mm/s on bovine trochlear cartilage. The error bars denote the standard deviation ($n = 4$).

We used $p < 0.05$ for statistical significance. The results are presented in boxplots. The bottom and top of the box represent the first and third quartile. The band inside the box is the median. The length of the whiskers is based on data within the 1.5 interquartile range of the upper and lower quartile. Data points outside of this range are denoted as outliers (dots).

RESULTS AND DISCUSSION

Influence of lubricin and mucin on cartilage friction

Mucins are glycoproteins and the main component of mucus, a slimy, viscoelastic layer covering various inner surfaces of the human body. Mucus is known for its protective and lubricative properties⁴⁰, e.g., in the gastrointestinal and vaginal tract. Mucins purified from mucus layers have been described as good boundary lubricants, with friction coefficients as low as 0.01^{25,41}. However in the knee joint, the comparably smaller mucinous glycoprotein lubricin is present. Friction measurements between two cartilage surfaces at a rotational speed of 0.3 mm/s show that a 0.1 % lubricin solution is able to reduce friction significantly ($p = 0.007$) compared to PBS (Figure 3a). This value is in general agreement with previously

published data with lower lubricin concentrations¹². For intact joints, a friction coefficient of $\mu = 0.001 - 0.01$ has been described²³. By using only a single macromolecule as lubricant, this ultra-low value is not reached as it probably requires the interaction between different synovial fluid constituents, present *in vivo*. Moreover, the friction coefficient is a system parameter and highly dependent on the *in vitro* measurement setup, its scale and the countering surfaces.

We now ask whether mucin can achieve a similar friction reduction between cartilage surfaces as lubricin. Indeed, lubrication with a 0.1 % mucin solution decreases the friction coefficient significantly compared to PBS ($p = 0.013$, Figure 3b) and to a similar extent as lubricin. A similar friction reduction has been described for HA as a lubricant in this measurement setup⁸.

The mucin concentration is chosen on the basis of previously published data reporting lubrication of a 0.1 % mucin solution between PDMS and steel²⁵, and lubricin was used at the same concentration, accordingly.

Lubricin reduces friction between cartilage and glass surfaces

In vitro the lubricity of different synovial fluid constituents is commonly evaluated between

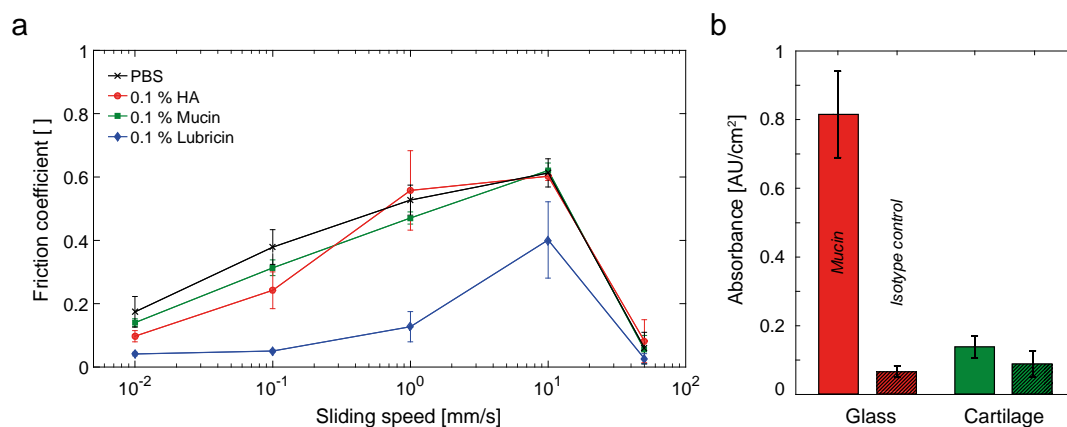


Figure 4. Lubricin, but neither mucin nor HA, decreases friction between glass/cartilage, especially at lower sliding speeds. Friction measurements are conducted over 1 h at each speed level and the final friction coefficient is reported (a). No difference in friction coefficient is observed using HA and mucin solutions compared to PBS as lubricant. Mucin adsorbs only weakly to cartilage compared to glass (b). The error bars denote the standard deviation ($n = 3$, $n = 2$ for the isotype control).

cartilage and an artificial material. These setups have the advantages of providing a defined countering surface and thus a defined contact area, which leads to cleaner data, as cartilage surfaces are naturally curved. Glass is frequently used as an opposing material in cartilage tribology^{42–44} and the adsorption properties of glass have been proposed to be similar to intact cartilage^{15,16}. However, it seems likely that glass cannot reproduce all physiological adsorption interactions with synovial fluid macromolecules. When rotating a glass sphere on top of osteochondral cylinders at different rotational speeds, lubrication with lubricin results in a significantly decreased friction ($p = 0.001$) at rotational speeds below 10 mm/s compared to PBS (Figure 4a). The measured friction coefficient of $\mu = 0.05$ (0.1 mm/s) is even lower compared to the friction coefficient of $\mu = 0.1$ (0.3 mm/s) obtained with the cartilage/cartilage setup. A reason for the slightly higher value for cartilage/cartilage might be the different species used for cartilage harvesting. The difference could also be attributed to the two not perfectly flat cartilage surfaces rotating on top

of each other. In contrast, in the glass/cartilage setup smaller sample dimensions can be used, which entails a more local sample/sample contact and thus a smoother cartilage area is probed by the glass sphere.

Similar to the cartilage/cartilage pairing, one would now assume that mucin reduces the friction to a similar extent in this glass/cartilage pairing. However, neither lubrication with mucin solutions nor with HA solutions reduces the friction coefficient significantly compared to PBS in the boundary lubrication regime ($p > 0.056$, Figure 4a). Although the viscosities of these lubricants are slightly different (Figure S2a), the friction coefficients are virtually identical over the observed speed range. One possible explanation could be that mucin adsorbs only weakly to the cartilage surface or glass sphere⁴⁵, and strong adsorption is necessary for efficient hydration lubrication. Indeed, adsorption measurements show that mucin can adsorb to glass reasonably well but only weakly to cartilage (Figure 4b). The mucins adsorb to steel and PDMS with much higher affinity than to glass (Figure S2b), which results in excellent

lubrication of a steel/PDMS surface pairing²⁵. However, this weak mucin absorption to cartilage seems to be sufficient to achieve mediocre boundary lubrication in cartilage/cartilage pairings as reflected by the measured friction coefficient of $\mu = 0.1$ (Figure 3b).

The poor boundary lubrication ability of HA in glass/cartilage setups has been discussed before, whereas HA is known to reduce friction in a cartilage/cartilage setup^{8,32} both alone and in combination with lubricin^{1,46}. Here, HA stabilizes the small protein on the cartilage surface under shear. It has been proposed that HA is mainly important to protect cartilage against wear¹⁰ and that higher molecular weight HA leads to better wear protection⁶. Therefore HA with a molecular weight of 2 MDa was chosen for this study.

In a next step, the wear generation is evaluated after subjecting the cartilage surfaces to friction measurements in the boundary lubrication regime using either HA, lubricin or mucin as lubricants.

Cartilage surface roughness does not correctly report wear

It has been confirmed by several studies that, although counterintuitive, wear and friction are not directly related^{13,18}. The wear protection properties of synovial components have been analyzed on mica surfaces by investigating wear tracks and delamination of mica by visual examinations^{6,13,17}. Studies, that directly assess wear on cartilage specimens, are mostly reporting the cartilage surface roughness as the only quantitative parameter^{42,47,48}. To our knowledge, there are only two studies using a quantitative approach on the basis of a broader range of parameters following ISO 25178-2 to evaluate changes in the surface topography of articular cartilage, and these studies focus on surface alterations owing to osteoarthritis^{49,50}.

We perform the wear analysis in the glass/cartilage setup and subject the osteochondral cylinders to a friction measurement at a rotational speed of 0.1 mm/s for 1 h.

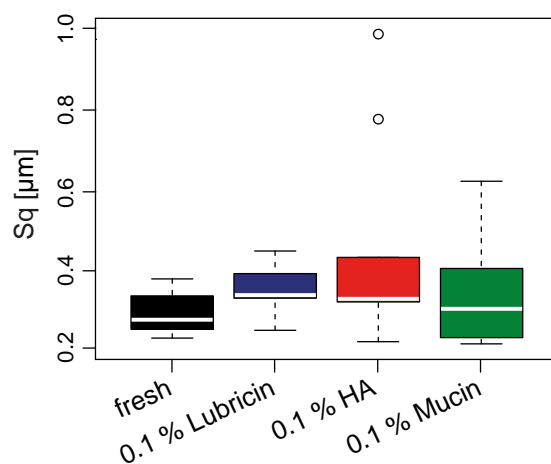


Figure 5. Roughness of untreated and treated cartilage surfaces. When lubricin, HA or mucin are used as a lubricant, the root mean square roughness (Sq) of the cartilage surface is not significantly altered compared to untreated cartilage. The whiskers denote the 1.5 IQR ($n = 9$).

As discussed above, an obvious parameter for a surface characterization is the roughness. Literature values on surface roughness of articular cartilage vary a lot between species and between different studies: $S_a = 0.07 \mu\text{m}$ (human)⁵¹, $S_a = 0.18 - 0.26 \mu\text{m}$ (bovine)⁵², $S_q = 2.34 \mu\text{m}$ (sheep)⁵³, $S_q = 5.32 \mu\text{m}$ (human)⁴⁹. Although the surface roughness seems to be useful to classify osteoarthritis degrees⁴⁹, the surface roughness is not a good measure for cartilage wear⁵⁴. Consistently, here we observe no differences in the root mean square roughness (Sq) between the examined groups (Figure 5, $p > 0.22$).

However, a microscopical examination of the cartilage surfaces clearly shows different wear features after lubrication with HA (Figure 6a) and lubricin (Figure 7a). Therefore, we next calculate other parameters to distinguish and quantify these features.

Lubrication with HA induces adhesive wear

In general, cartilage wear can be subdivided into interfacial, fatigue and impact wear⁵⁵.

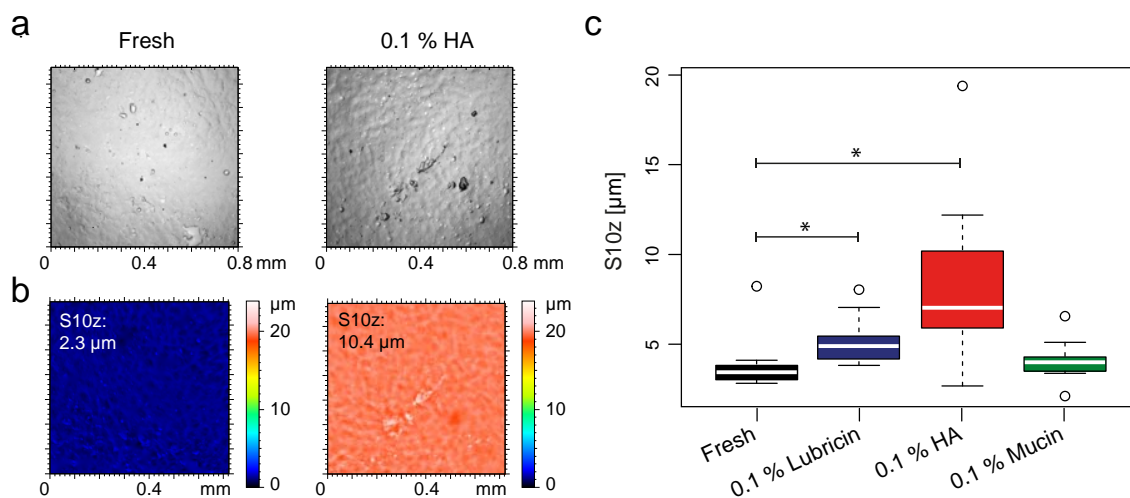


Figure 6. In the glass/cartilage tribology setup, lubrication with HA leads to localized adhesive wear on the cartilage surface. In the surface image (a) and the topographical image (b) wear features are clearly visible. When HA or lubricin solutions are used as lubricants, the ten point height (S10z), the average height of the five highest local maximums plus the average height of the five lowest local minima, is significantly increased compared to the surface of untreated cartilage. (c). When mucin is used as a lubricant, the surface topography is maintained. The whiskers denote the 1.5 IQR ($n = 9$).

In boundary lubrication, i.e. under direct contact between the opposing surfaces, interfacial wear can occur due to two mechanisms: abrasion and adhesion⁵⁶.

Adhesive wear can be generated by nonspecific binding of molecules to the opposing surface. The bridging of the surfaces leads to surface damage during shear as described for HA on mica surfaces^{7,13}. In agreement with these reports, we observe an increased amount of wear pits and asperities on our samples after lubricating the cartilage with HA. We quantify this effect by evaluating the minimal and maximal peaks of the surface (S10z). This parameter is significantly increased after lubrication with HA compared to fresh cartilage ($p = 0.003$, Figure 6c). The effect is apparent in the exemplary roughness profiles shown in Figure S3a.

After lubrication with HA, various peaks with a height of about 1 μm are visible. In contrast, a homogenous roughness with peak heights below 0.5 μm is observed for fresh cartilage. This finding is underlined by other parameters which also quantify these local surface alterations: The

closed hill (Shv) and dale volume (Sdv) are both significantly increased after lubrication with HA (Shv: $p = 0.003$, Sdv: $p = 0.007$, Figure S4).

In contrast, lubrication with mucin does not significantly increase any of these parameters (Figure S4 and Figure S5). After lubrication with lubricin, only the S10z parameter is significantly increased compared with fresh cartilage. However, adhesive wear is unlikely to be the reason for the increased S10z value obtained for lubricin because lubricin has a comparably low molecular weight and thus cannot easily bridge opposing surfaces as required for adhesive wear. Indeed, the optical appearance of wear features generated by lubrication with lubricin is distinctively different compared to the pits reported for adhesive wear (Figure 6a). These surface features can be described as wear tracks (Figure 7a).

Lubrication with lubricin induces abrasive wear

The observed wear tracks might be quantified through calculating the isotropy of the surface.

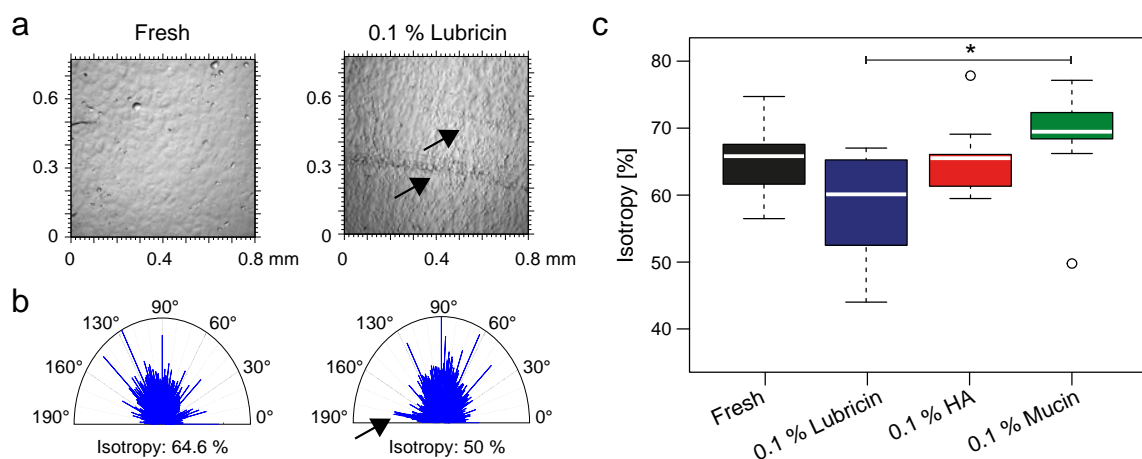


Figure 7. Lubrication with lubricin leads to wear tracks on the cartilage surface. The wear features observed in microscopy (a) are quantified by the isotropy parameter (b). Compared to the surface of untreated cartilage, lubrication with lubricin reduces the surface isotropy (c). The whiskers denote the 1.5 IQR ($n = 9$).

An anisotropic surface is directionally structured whereas an isotropic surface is randomly structured. Wear tracks should lead to a decrease in the surface isotropy and this is exactly what we find here (Figure 7c): We calculate a significantly decreased isotropy for surfaces lubricated with mucin compared to surfaces lubricated with lubricin ($p = 0.021$). This isotropy is visualized in a polar coordinate system (Figure 7b), displaying the self-similarity (autocorrelation length) of the profiles in each direction. The arrow in Figure 7b indicates the alterations due to the wear track.

However, owing to the small dimensions of the wear tracks with respect to the overall surface roughness, smaller wear tracks cannot be captured. This might be one reason why the isotropy is only slightly but not significantly decreased for lubricin compared to fresh surfaces. The wear track depth of approximately $2 \mu\text{m}$ is visualized in the profile shown in Figure S3b.

On some surfaces, the wear tracks are accompanied by slightly increased structures along the edges of these tracks (displaced material), which might also be reflected in the increased S10z value (Figure 6c) after lubricin lubrication. No significant difference in surface isotropy is observed for samples lubricated with

HA ($p = 0.992$) or mucin ($p = 0.496$, Figure 7c and Figure S5).

CONCLUSION

Our results advance our understanding of why, *in vivo*, multiple biopolymers are present in the synovial fluid to achieve optimal friction reduction and wear protection. In our *in vitro* testing setup, neither HA nor lubricin alone can reduce the friction between articular cartilage and glass to physiological levels and at the same time prevent wear formation. In contrast, mucin – when used as a single molecular component in a lubricant – reduces friction in cartilage/cartilage tribology equally well as lubricin and also seems to be sufficient to prevent wear on cartilage when probed with a glass sphere (Table 1): Neither distinct wear pits nor wear tracks are visible on the cartilage surface after lubrication with mucin. Although mucins are large enough to potentially bridge the opposing surfaces during cartilage tribology, mucin lubrication does not lead to adhesive wear in the glass/cartilage setup. One reason for this observation could be that, as shown here, mucins adsorb only weakly to the cartilage surface thus preventing the formation of

Table 1. Summary of friction reduction and wear protection properties of lubricin, HA and mucin. Lubricin and HA both lead to different types of wear. In contrast, mucin is fully able to protect the cartilage surface against damage. All substances can reduce the friction between two cartilage surfaces. However, only lubricin reduces friction between cartilage and glass.

| | Friction reduction | | Wear protection | |
|-----------------------|---------------------|-----------------|-----------------|---------------|
| | cartilage/cartilage | glass/cartilage | adhesive wear | abrasive wear |
| 0.1 % Lubricin | + | + | + | - |
| 0.1 % HA | + ^a | - | - | + |
| 0.1 % Mucin | + | - | + | + |

^a as measured in Kwiecinski *et al.*⁸

molecular cross-bridges. However, the weak mucin binding to cartilage surfaces seems to be sufficient to reduce friction between two cartilage surfaces, at least to intermediate lubricity levels. The wear-protection established by mucins could be different between two cartilage surfaces and at physiological conditions. Such an evaluation of the wear protection abilities of mucins is, however, much more complicated to perform. One complication will arise from the increased biological variance between experiments when performing a wear test in a tissue-on-tissue configuration, e.g., since the contact area between the two surfaces might become less defined thus reducing reproducibility of the results. Yet, the quantitative wear analysis procedure established here for a glass/cartilage setup might be an important stepping stone towards this physiological evaluation of mucin wear protection. Moreover, with the results and methodology introduced here, the wear protection properties of multi-component lubricants, i.e. HA in combination with lubricin or other synovial constituents, can be quantitatively evaluated in future experiments.

Our study demonstrates the importance of considering friction and wear as two independent phenomena. It highlights that the adsorption of lubricating molecules, and therefore the test counterface, needs to be considered when

discussing friction reduction and wear protection of molecular lubricants. This is not only important for *in vitro* experiments on articular cartilage or other biological surfaces but also for the design of artificial implant materials⁵⁷. The tribological performance of replacement joints could be significantly increased by implementing biomimetic lubrication strategies. One such strategy could be to apply coatings with substances, which interact with HA and lubricin, or to use coatings with synthetic polymer brushes⁵⁸. Moreover, one could consider the injection of biomimetic boundary lubricants, which are able to interact with the synthetic implant surfaces and take over the function of physiological lubricants. Our results show that although mucins are not present on the cartilage surface *in vivo*, they are able to reduce friction and prevent wear. Thus, either purified mucins or synthetic mucin-like macromolecules bear great potential as ingredients for tribosupplements⁵.

ASSOCIATED CONTENT

Supporting Information

Figure S1 shows schematics of the friction measurement setups. Figure S2 shows the lubricant viscosities and the mucin adsorption to different materials. Figure S3 shows exemplary roughness profiles across different surfaces.

Figure S4 shows boxplots of the wear parameter Sdv and Shv. Figure S5 shows a summary of the evaluated wear parameter after a 0.1 % mucin solution is used as lubricant. This material is available free of charge via the Internet at <http://pubs.acs.org>.

AUTHOR INFORMATION

Corresponding Author

*E-mail: oliver.lieleg@tum.de

Author Contributions

The manuscript was written through contributions of all authors. All authors have given approval to the final version of the manuscript.

Notes

The authors declare no competing financial interest.

ACKNOWLEDGMENT

The work was supported by the International Graduate School of Science and Engineering (IGSSE) in the framework of the focus area “Biomaterials”. Additional support from the Deutsche Forschungsgemeinschaft through project B 11 in the framework of SFB 863 (“Forces in Biomolecular Systems”), and the Natural Sciences and Engineering Research Council of Canada is gratefully acknowledged. We would like to thank the Bayerische Landesanstalt für Landwirtschaft (LfL) Institut für Tierzucht Grub/Poing and the Metzgerei Boneberger for providing the lamb joints, Julia Nachtsheim and Bensjamin Käs Dorf for helpful discussions and Dr. Stephan Haug from TUM|Stat for his advice on the statistical analysis.

REFERENCES

- (1) Majd, S. E., Kuijer, R., Köwitsch, A., Groth, T., Schmidt, T. A., Sharma, P. K., *Langmuir* **2014**, *30*, 14566–14572.
- (2) Caligaris, M., Ateshian, G. A., *Osteoarthritis and Cartilage* **2008**, *16*, 1220–1227.
- (3) Basalo, I. M., Mauck, R. L., Kelly, T.-A. N., Nicoll, S. B., Chen, F. H., Hung, C. T., Ateshian, G. A., *J. Biomech. Eng.* **2004**, *126*, 779.
- (4) Ateshian, G. A., *Journal of Biomechanics* **2009**, *42*, 1163–1176.
- (5) McNary, S. M., Athanasiou, K. A., Reddi, A. H., *Tissue Engineering Part B: Reviews* **2012**, *18*, 88–100.
- (6) Lee, D. W., Banquy, X., Das, S., Cadirov, N., Jay, G., Israelachvili, J., *Acta Biomaterialia* **2014**, *10*, 1817–1823.
- (7) Tadmor, R., Chen, N., Israelachvili, J., *Macromolecules* **2003**, *36*, 9519–9526.
- (8) Kwiecinski, J. J., Dorosz, S. G., Ludwig, T. E., Abubacker, S., Cowman, M. K., Schmidt, T. A., *Osteoarthritis and Cartilage* **2011**, *19*, 1356–1362.
- (9) Bonnevie, E. D., Galesso, D., Secchieri, C., Cohen, I., Bonassar, L. J., *PLoS ONE* **2015**, *10*, e0143415.
- (10) Greene, G. W., Banquy, X., Lee, D. W., Lowrey, D. D., Yu, J., Israelachvili, J. N., *Proceedings of the National Academy of Sciences* **2011**, *108*, 5255–5259.
- (11) Seror, J., Zhu, L., Goldberg, R., Day, A. J., Klein, J., *Nat Commun* **2015**, *6*.
- (12) Abubacker, S., Dorosz, S., Ponjevic, D., Jay, G., Matyas, J., Schmidt, T., *Annals of Biomedical Engineering* **2015**, 1–10.
- (13) Eguiluz, R. C., Cook, S. G., Brown, C. N., Wu, F., Pacifici, N. J., Bonassar, L. J., Gourdon, D., *Biomacromolecules* **2015**, *16*, 2884–2894.
- (14) Seror, J., Merkher, Y., Kampf, N., Collinson, L., Day, A. J., Maroudas, A., Klein, J., *Biomacromolecules* **2011**, *12*, 3432–3443.
- (15) Murakami, T., Nakashima, K., Yarimitsu, S., Sawae, Y., Sakai, N., *Proceedings of the Institution of Mechanical Engineers, Part J: Journal of Engineering Tribology* **2011**, *225*, 1174–1185.
- (16) Murakami, T., Yarimitsu, S., Nakashima, K., Sawae, Y., Sakai, N., *Friction* **2013**, *1*, 150–162.

- (17) Banquy, X., Lee, D. W., Das, S., Hogan, J., Israelachvili, J. N., *Advanced Functional Materials* **2014**, *24*, 3152–3161.
- (18) Lee, D. W., Banquy, X., Israelachvili, J. N., *Proceedings of the National Academy of Sciences* **2013**, *110*, E567.
- (19) Gregory, D. J., Lane, B. P., Sokoloff, L., *Connective Tissue Research* **1992**, *28*, 245–255.
- (20) Ma, L., Gaisinskaya-Kipnis, A., Kampf, N., Klein, J., *Nat Commun* **2015**, *6*.
- (21) Zappone, B., Ruths, M., Greene, G. W., Jay, G. D., Israelachvili, J. N., *Biophysical Journal* **2006**, *92*, 1693–1708.
- (22) Chan, S. M., Neu, C. P., DuRaine, G., Komvopoulos, K., Reddi, A. H., *Journal of Biomechanics* **2012**, *45*, 2426–2431.
- (23) Klein, J., *Proceedings of the Institution of Mechanical Engineers, Part J: Journal of Engineering Tribology* **2006**, *220*, 691–710.
- (24) Meloni, M., Servi, B. de, Marasco, D., Del Prete, S., *Molecular Vision* **2011**, *17*, 113–126.
- (25) Crouzier, T., Boettcher, K., Geonnotti, A. R., Kavanaugh, N. L., Hirsch, J. B., Ribbeck, K., Lieleg, O., *Adv. Mater. Interfaces* **2015**, 1500308.
- (26) Jones, A. R., Gleghorn, J. P., Hughes, C. E., Fitz, L. J., Zollner, R., Wainwright, S. D., Caterson, B., Morris, E. A., Bonassar, L. J., Flannery, C. R., *Journal of Orthopaedic Research* **2007**, *25*, 283–292.
- (27) Dédinaïté, A., *Soft Matter* **2012**, *8*, 273–284.
- (28) Bansil, R., Celli, J., Hardcastle, J., Turner, B., *Frontiers in Immunology* **2013**, *4*.
- (29) Mejías-Luque, R., Cobler, L., de Bolós C., *Atlas Genet Cytogenet Oncol* **2010**, *14*, 566–569.
- (30) Jay, G. D., *Current Opinion in Orthopaedics* **2004**, *15*, 355–359.
- (31) Boettcher, K., Grumbein, S., Winkler, U., Nachtsheim, J., Lieleg, O., *Rev Sci Instrum* **2014**, *85*, 093903.
- (32) Schmidt, T. A., Gastelum, N. S., Nguyen, Q. T., Schumacher, B. L., Sah, R. L., *Arthritis & Rheumatism* **2007**, *56*, 882–891.
- (33) Caldara, M., Friedlander, R. S., Kavanaugh, N. L., Aizenberg, J., Foster, K. R., Ribbeck, K., *Current biology CB* **2012**, *22*, 2325–2330.
- (34) Boettcher, K., Kienle, S., Nachtsheim, J., Burgkart, R., Hugel, T., Lieleg, O., *Acta Biomaterialia* **2015**.
- (35) *ISO 25178-2: 2012 Geometrical product specification (GPS) -- surface texture: Areal -- Part2: terms, definitions and surface texture parameters.*
- (36) Jiang, X., Scott, P., Whitehouse, D., Blunt, L., *Proceedings of the Royal Society of London A: Mathematical, Physical and Engineering Sciences* **2007**, *463*, 2071–2099.
- (37) Digital Surf. *μsoft analysis Manual: Surface imaging and Metrology software.* version 7.1.
- (38) Hothorn, T., Bretz, F., Westfall, P., *Biometrical journal* **2008**, *50*, 346–363.
- (39) Sakia, R. M., *Journal of the Royal Statistical Society. Series D (The Statistician)* **1992**, *41*, 169–178.
- (40) Cone, R. A., *Advanced Drug Delivery Reviews* **2009**, *61*, 75–85.
- (41) Lee, S., Müller, M., Rezwani, K., Spencer, N. D., *Langmuir* **2005**, *21*, 8344–8353.
- (42) Oungoulian, S. R., Hehir, K. E., Zhu, K., Willis, C. E., Marinescu, A. G., Merali, N., Ahmad, C. S., Hung, C. T., Ateshian, G. A., *Journal of Biomechanics* **2014**, *47*, 694–701.
- (43) Chan, S. M., Neu, C. P., Komvopoulos, K., Reddi, A. H., *Journal of Biomechanics* **2011**, *44*, 2015–2020.
- (44) Basalo, I. M., Chahine, N. O., Kaplun, M., Chen, F. H., Hung, C. T., Ateshian, G. A., *Journal of Biomechanics* **2007**, *40*, 1847–1854.
- (45) Crouzier, T., Jang, H., Ahn, J., Stocker, R., Ribbeck, K., *Biomacromolecules* **2013**, *14*, 3010–3016.
- (46) Das, S., Banquy, X., Zappone, B., Greene, G. W., Jay, G. D., Israelachvili, J. N., *Biomacromolecules* **2013**, *14*, 1669–1677.
- (47) Shekhawat, V. K., Laurent, M. P., Muehleman, C., Wimmer, M. A., *Osteoarthritis and Cartilage* **2009**, *17*, 1197–1203.
- (48) Graindorge, S., Ferrandez, W., Ingham, E., Jin, Z., Twigg, P., Fisher, J., *Proceedings of the Institution of Mechanical Engineers, Part H: Journal of Engineering in Medicine* **2006**, *220*, 597–607.
- (49) Baena, J. C., Peng, Z., *Wear* **2014**, *319*, 1–11.
- (50) Wang, M., Peng, Z., Wang, J., Jiang, X., *The International Conference on BioTribology 2011* **2013**, *63*, 235–242.
- (51) Peng, Z., Wang, M., *Wear of Materials 2013* **2013**, *301*, 210–217.

- (52) Ghosh, S., Bowen, J., Jiang, K., Espino, D. M., Shepherd, Duncan E. T., *Micron* **2013**, *44*, 179–184.
- (53) Tian, Y., Wang, J., Peng, Z., Jiang, X., *18th International Conference on Wear of Materials* **2011**, *271*, 2370–2378.
- (54) McGann, M. E., Vahdati, A., Wagner, D. R., *Proceedings of the Institution of Mechanical Engineers, Part H: Journal of Engineering in Medicine* **2012**, *226*, 612–622.
- (55) McGinty J. B., Burkhart S. S., Eds. *Basic Sciences: 5. Structure and Function of Diarthrodial Joints*, 3rd ed.; Lippincott Williams & Wilkins: Philadelphia, 2003.
- (56) Walker, P. S., Dowson, D., Longfield, M. D., Wright, V., *Annals of the Rheumatic Diseases* **1968**, *27*, 512–520.
- (57) Majd, S. E., Kuijer, R., Schmidt, T. A., Sharma, P. K., *Materials & Design* **2015**, *83*, 514–521.
- (58) Ishihara, K., *Polym J* **2015**, *47*, 585–597.

B. Supplemental information

B.1. Comparison of friction and wear of articular cartilage on different length scales

Supplement

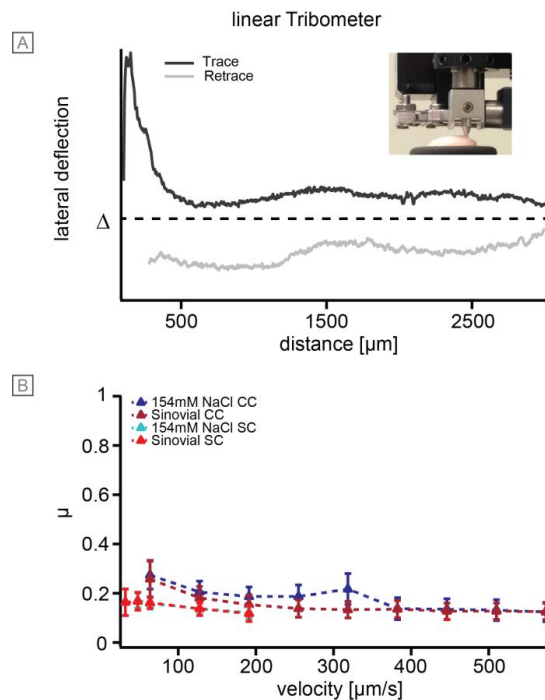


Fig. S 1 (A) Photograph of the linear tribometer setup with a polystyrene sphere as a probe and a friction loop (trace and retrace) measured during the scan of one line of a cartilage sample with a polystyrene sphere in 154 mM NaCl. (B) Friction coefficients for measurements in Sinovial (red) and 154 mM NaCl (blue) with the linear tribometer using a polystyrene sphere on cartilage (SC) and cartilage on cartilage (CC).

We used a linear Nano Tribometer (NTR) from CSM Instruments (Switzerland) with a pin on plate setup. The lateral and normal deflections were measured with capacitive sensors and were directly converted into the friction coefficient. Cartilage samples of a diameter of 10 mm were used as plate material and either a polystyrene sphere (diameter 750 μm) or a second cartilage sample (diameter 5 mm) as pin. The cartilage samples were glued with an instant adhesive onto the sample holder or the probe holder. The measurements were performed in either 154 mM NaCl or in Sinovial. The normal loads ranged between 2 and 6 mN and the velocities between 50 and 600 $\mu\text{m/s}$. For each parameter a line was scanned three to four times. Both trace and retrace were recorded and averaged to obtain the friction coefficient. At the beginning of each scan stiction could be observed. This was, together with the reversal points, neglected in the evaluation.

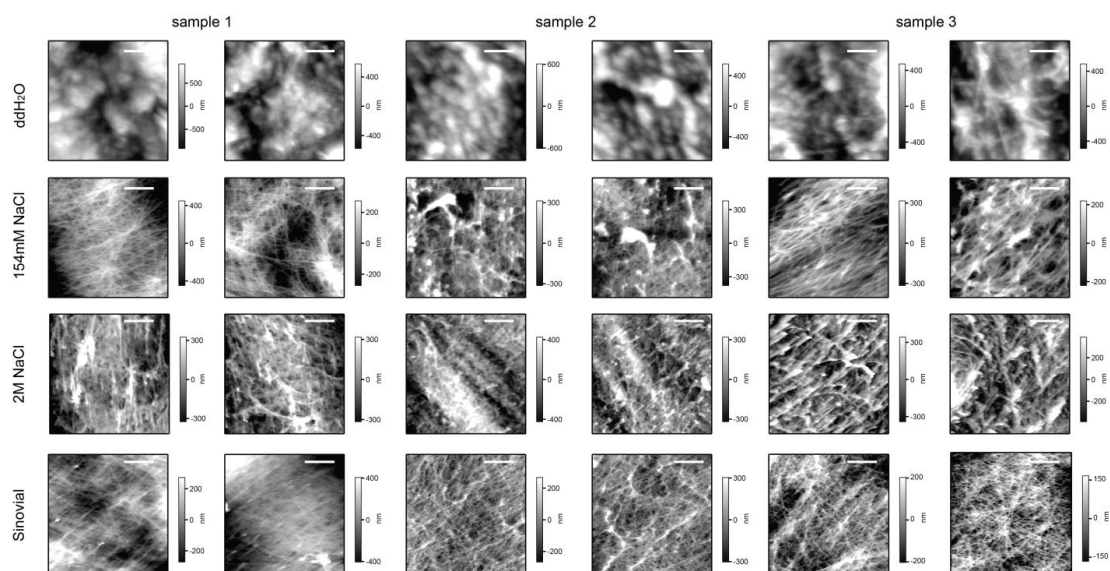


Fig. S 2 AFM images taken after tribological treatment performed for one hour at 0.1 mm/s in four lubricants (ddH₂O, 154 mM NaCl, 2 M NaCl, Sinovial). The images shown here were used for the observer-blinded study described in the main text. The scale bars correspond to 5 μm.

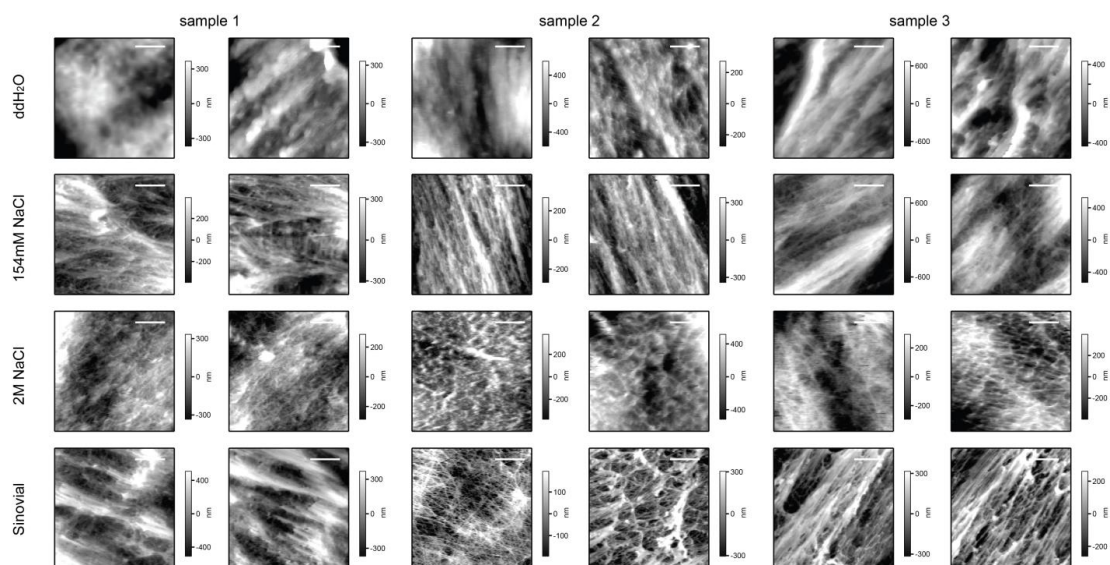


Fig. S 3 AFM images taken after tribological treatment performed for one hour at 10 mm/s in four lubricants (ddH₂O, 154 mM NaCl, 2 M NaCl, Sinovial). Three samples were imaged for each lubricant. The images shown here were used for the observer-blinded study described in the main text. The scale bars correspond to 5 μm.

Table S1. P-values obtained from the Tukey post-hoc test for different velocities for the AFM friction data: group 1 – ddH₂O, group 2 – 154 mM NaCl, group 3 – 2 M NaCl, group 4 – Sinovial. Values of p indicating a significant difference (p<0.05) are marked in red.

| groups | 9.4 $\mu\text{m/s}$ | 37.6 $\mu\text{m/s}$ | 75.1 $\mu\text{m/s}$ | 112.7 $\mu\text{m/s}$ |
|--------|---------------------|----------------------|----------------------|-----------------------|
| 2-1 | 0.023 | 0.14 | 0.12 | 0.097 |
| 3-1 | 0.0055 | 0.000041 | 0.00033 | 0.0017 |
| 4-1 | 0.010 | 0.053 | 0.063 | 0.13 |
| 3-2 | 0.66 | 0.0047 | 0.038 | 0.16 |
| 4-2 | 0.80 | 0.80 | 0.88 | 0.99 |
| 4-3 | 1.00 | 0.11 | 0.30 | 0.41 |

Table S2. P-values obtained from the Tukey post-hoc test for different velocities for the tribometer friction data: group 1 – ddH₂O, group 2 – 154 mM NaCl, group 3 – 2 M NaCl, group 4 – Sinovial. Values of p indicating a significant difference (p<0.05) are marked in red.

| groups | 0.01 mm/s | 0.1 mm/s | 1.0 mm/s | 10 mm/s |
|--------|-----------|--------------|----------|----------------|
| 2-1 | 0.54 | 0.24 | 1.00 | 0.12 |
| 3-1 | 0.56 | 0.076 | 0.062 | 0.0014 |
| 4-1 | 0.77 | 0.043 | 0.088 | 0.00010 |
| 3-2 | 0.095 | 0.84 | 0.056 | 0.035 |
| 4-2 | 0.97 | 0.63 | 0.080 | 0.0012 |
| 4-3 | 0.17 | 0.98 | 0.99 | 0.095 |

B.2. Modulating mucin hydration and lubrication by deglycosylation and polyethylene glycol binding

Supporting Information

Title: Modulating mucin hydration and lubrication by deglycosylation and polyethylene glycol binding

Author(s), and Corresponding Author(s)*: *Thomas Crouzier#, Kathrin Boettcher#, Anthony R. Geonnotti, Nicole L. Kavanaugh, Julie B. Hirsch, Katharina Ribbeck*, and Oliver Lieleg**

Table S1. Surface mass densities of mucin and deglycosylated mucins on gold coated QCM-D crystals and on PDMS surfaces estimated by ellipsometry and by fluorescence intensity measurements, respectively. Three samples were tested and the standard deviation of the mean is denoted.

| | Mass density on gold [mg/cm ²] | Mass density on PDMS [mg/cm ²] |
|-----------|---|---|
| Mucin | 3.5 ± 1.0 | 2.8 ± 0.3 |
| pApoMucin | 1.5 ± 0.4 | 2.2 ± 0.2 |
| ApoMucin | 2.8 ± 2.0 | 3.0 ± 0.1 |

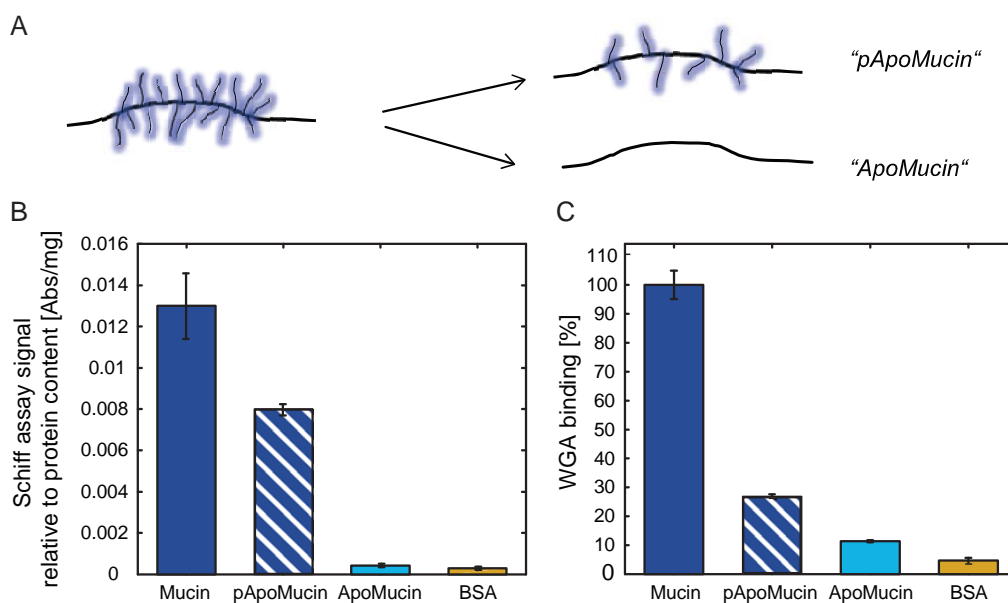


Figure S1. (A) Schematic representation of the mucin deglycosylation. (B) Schiff assay measurement on native and deglycosylated mucin solution. (C) Binding of the Wheat Germ Agglutinin (WGA) lectin on coatings of native mucin or deglycosylated mucins. Bovine serum albumin (BSA) containing no glycan was used as a negative control for both measurements. The error bars denote the standard deviation to the mean of three replicates of a single representative experiment.

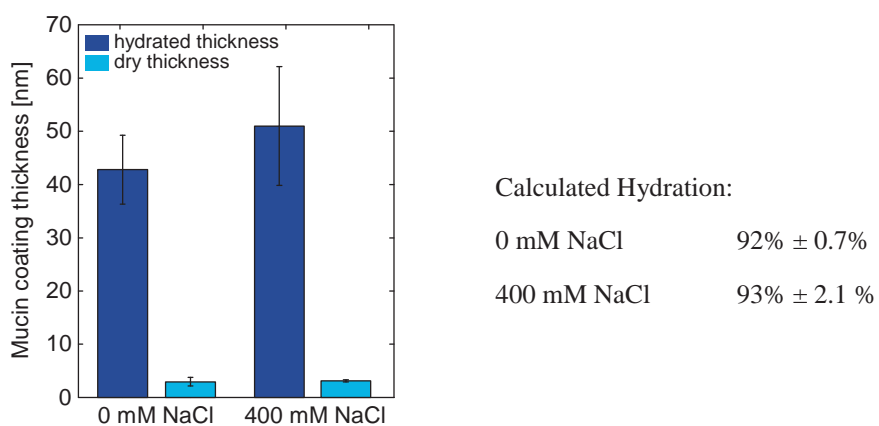


Figure S2. The effect of NaCl on mucin coating hydration is negligible. Mucin coating thickness as measured by Quartz Crystal Microbalance (in the hydrated state) or ellipsometry (in the dry state). The hydration of mucin coatings generated either in the absence of NaCl or in the presence of 400 mM NaCl (using 20 mM HEPES buffer, pH 7, in both cases) was calculated based on these values. The increase in salt concentration did not impact the mucin coating hydration.

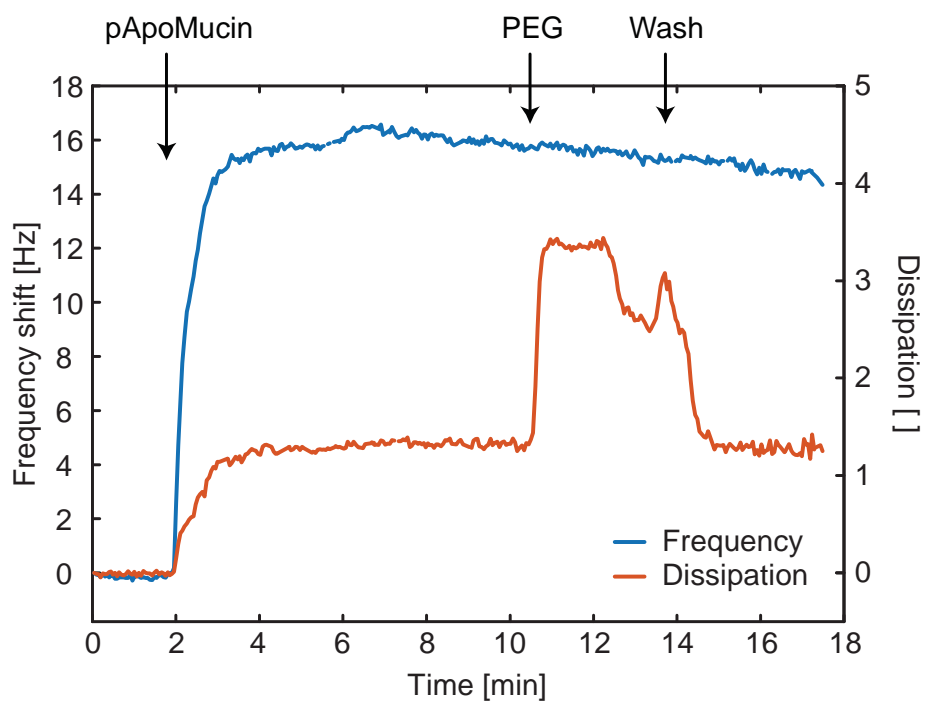


Figure S3. Quartz crystal microbalance with dissipation monitoring of the adsorption of partially deglycosylated mucin (pApoMucin) on a gold-coated quartz crystal, followed by exposure to a polyethylene glycol (PEG) solution.

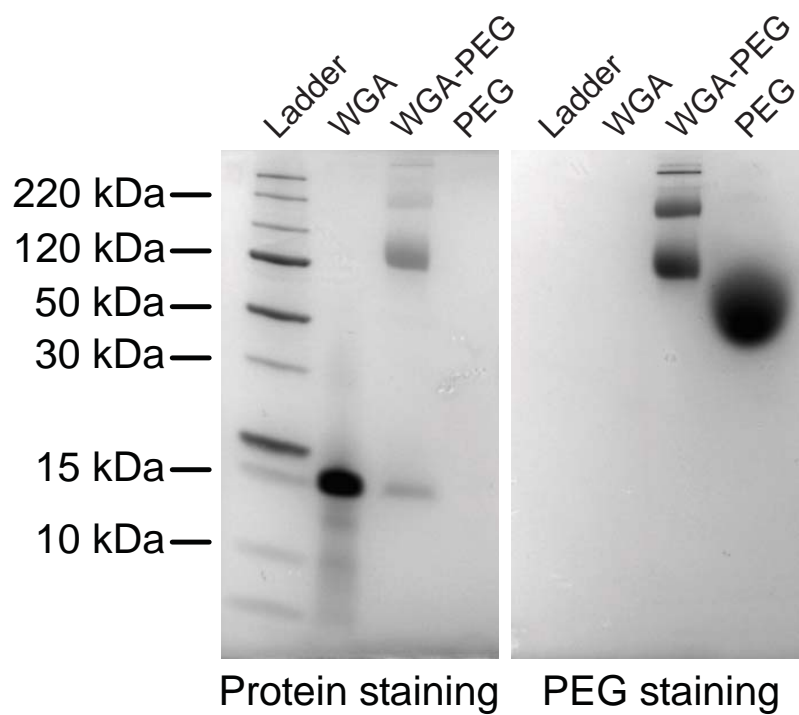


Figure S4. SDS-PAGE gel of Wheat Germ Agglutinin (WGA), polyetheneglycol (PEG) and WGA-PEG conjugate. The left gel was labeled for protein while the right gel was labeled for PEG.

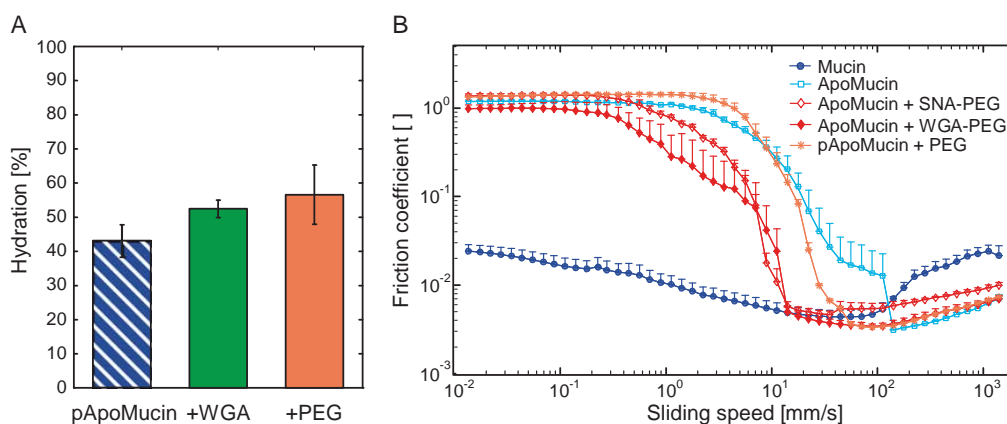


Figure S5. Binding of PEG to pApoMucin is required to restore mucin hydration and lubrication. (A) When added alone, neither WGA nor PEG restored the hydration of pApoMucin coatings. The error bars denote standard deviation to the mean of three independent experiments. (B) Without the lectin anchor, PEG could not restore the lubricity of pApoMucin coatings. And without any glycan residues to anchor to, the lectin-PEG could not restore the lubricating ability of ApoMucin coatings. The error bars denote the error of the mean as obtained from three independent experiments.

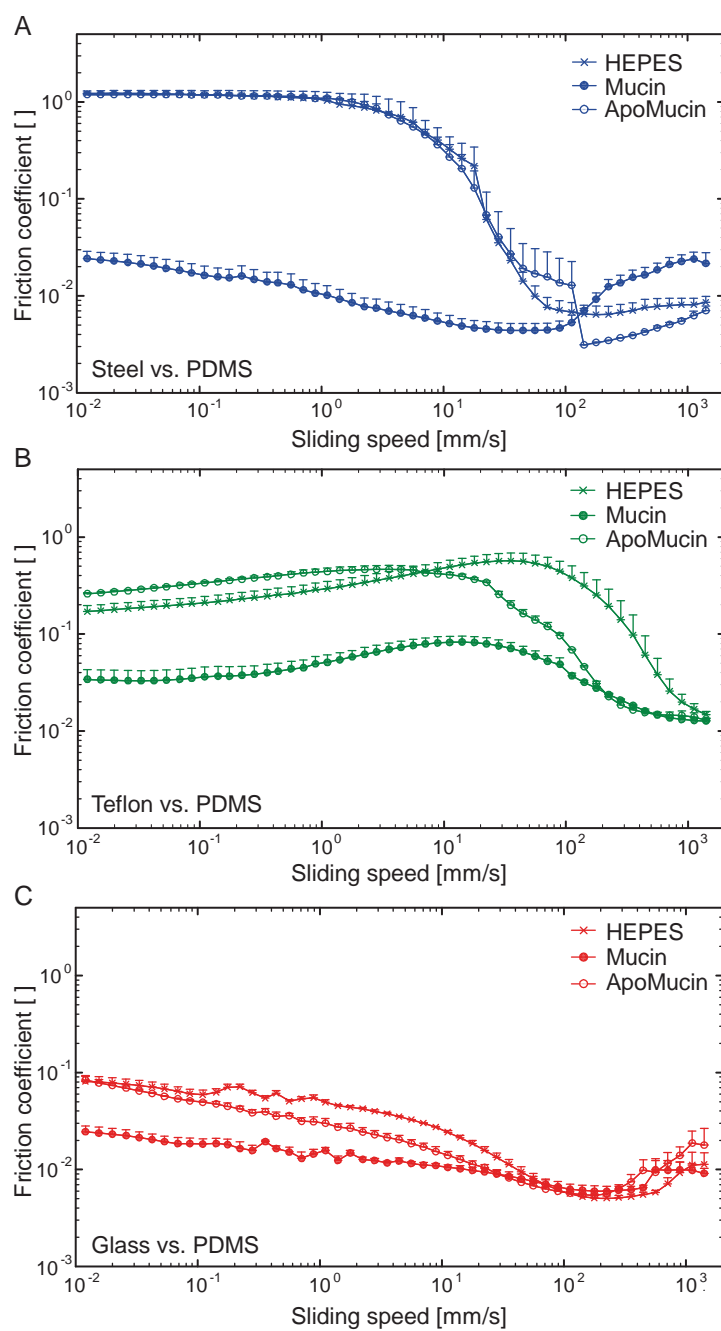


Figure S6. Stribeck curves obtained for different tribology pairings. The lubricity of HEPES buffer, mucin coatings and ApoMucin coatings deposited on PDMS are compared for different spherical friction probes made from (A) steel, (B) Teflon and (C) glass.

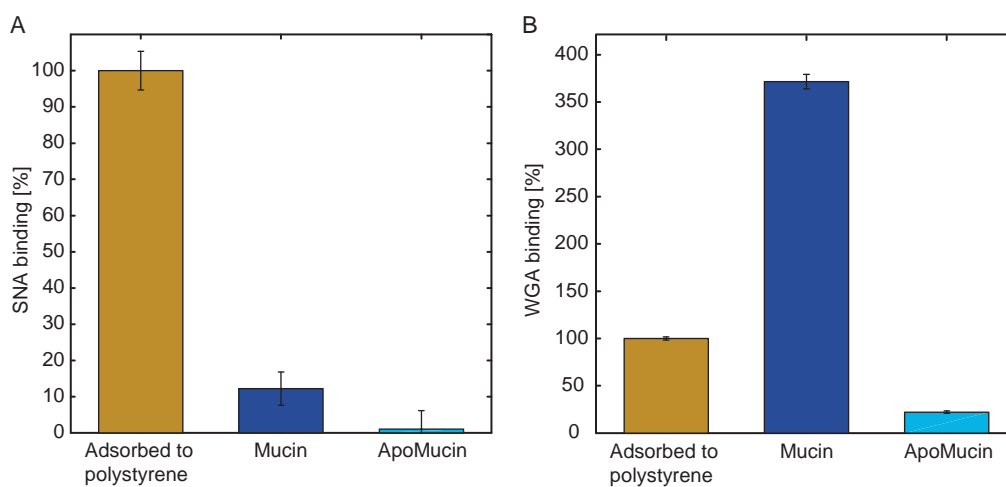


Figure S7. Binding of Sambucus Nigra lectin. Adsorption was observed on polystyrene and coatings of native mucin or deglycosylated mucins. The error bars denote the standard deviation to the mean of three replicates of a single representative experiment.

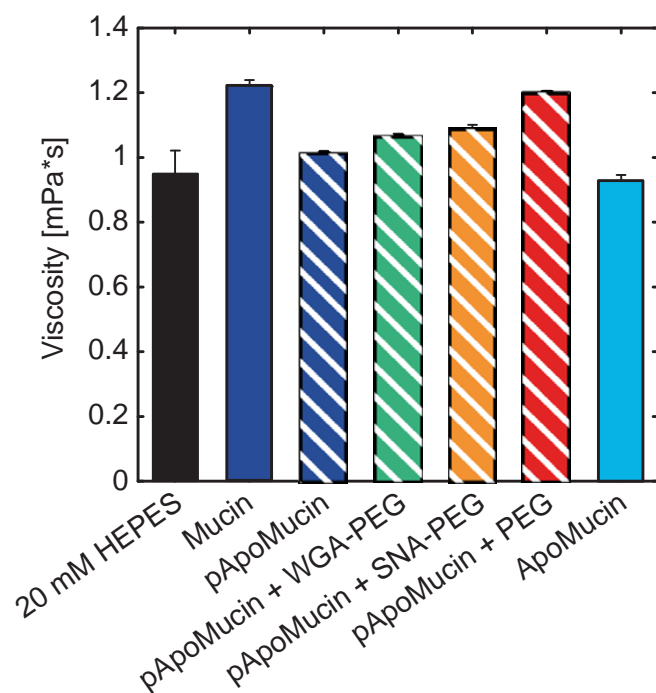


Figure S8: The viscosity of lubricants is frequency independent for shear rates corresponding to sliding speeds of 1 – 100 mm/s. The viscosity was averaged over this frequency range and the mean value was calculated for 3 measurements. The error bars represent the standard deviation.

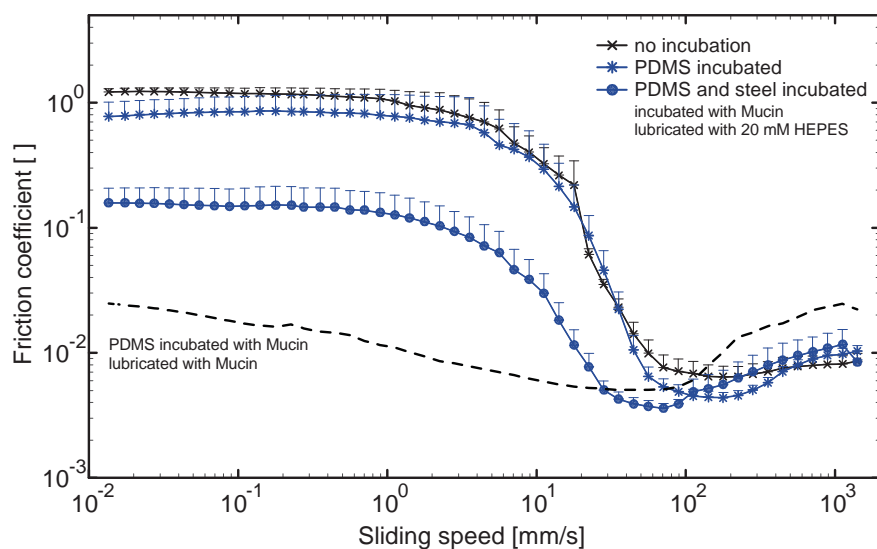


Figure S9: Comparison of different incubation procedures prior to the friction measurement. Incubation of both, the PDMS cylinders and the steel sphere with mucin prior to a friction measurement lubricated with HEPES reduces the friction coefficient in the boundary lubrication regime together with an earlier entry in the mixed lubrication regime.

B.3. Porcine gastric mucins reduce friction and wear in cartilage boundary lubrication

Supporting Information

Title: Porcine gastric mucins reduce friction and wear in cartilage boundary lubrication

Author(s), and Corresponding Author(s)*: Kathrin Boettcher¹, Samuel G. Dorosz², Tannin Schmidt^{2,3}, Oliver Lieleg^{1,*}

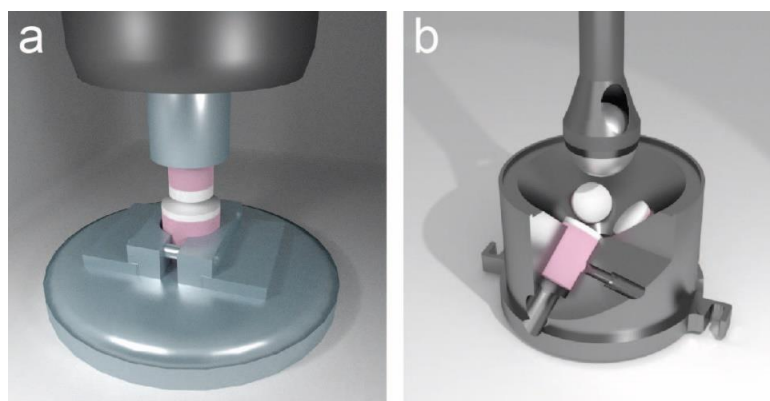


Figure S1. Experimental setups for friction measurements. In the cartilage/cartilage setup, the lower osteochondral cylinder is rotated against the upper osteochondral cylinder (a). In the cartilage/glass setup, a glass sphere is rotated against three osteochondral cylinders (b).

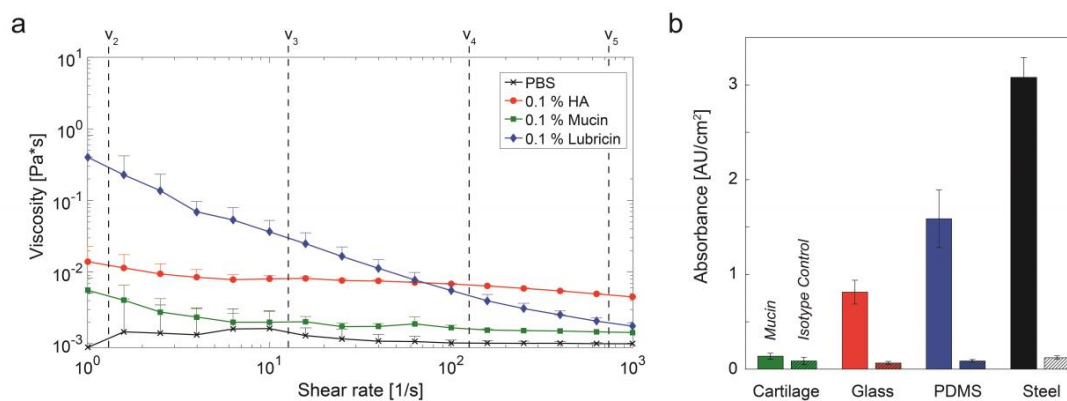


Figure S2. Viscosities of different lubricants and mucin adsorption to different materials. The viscosities of all lubricants are fairly similar. Only lubricin shows a slightly increasing viscosity with decreasing shear rates (a). Mucin adsorption is lowest on cartilage and highest on stainless steel.

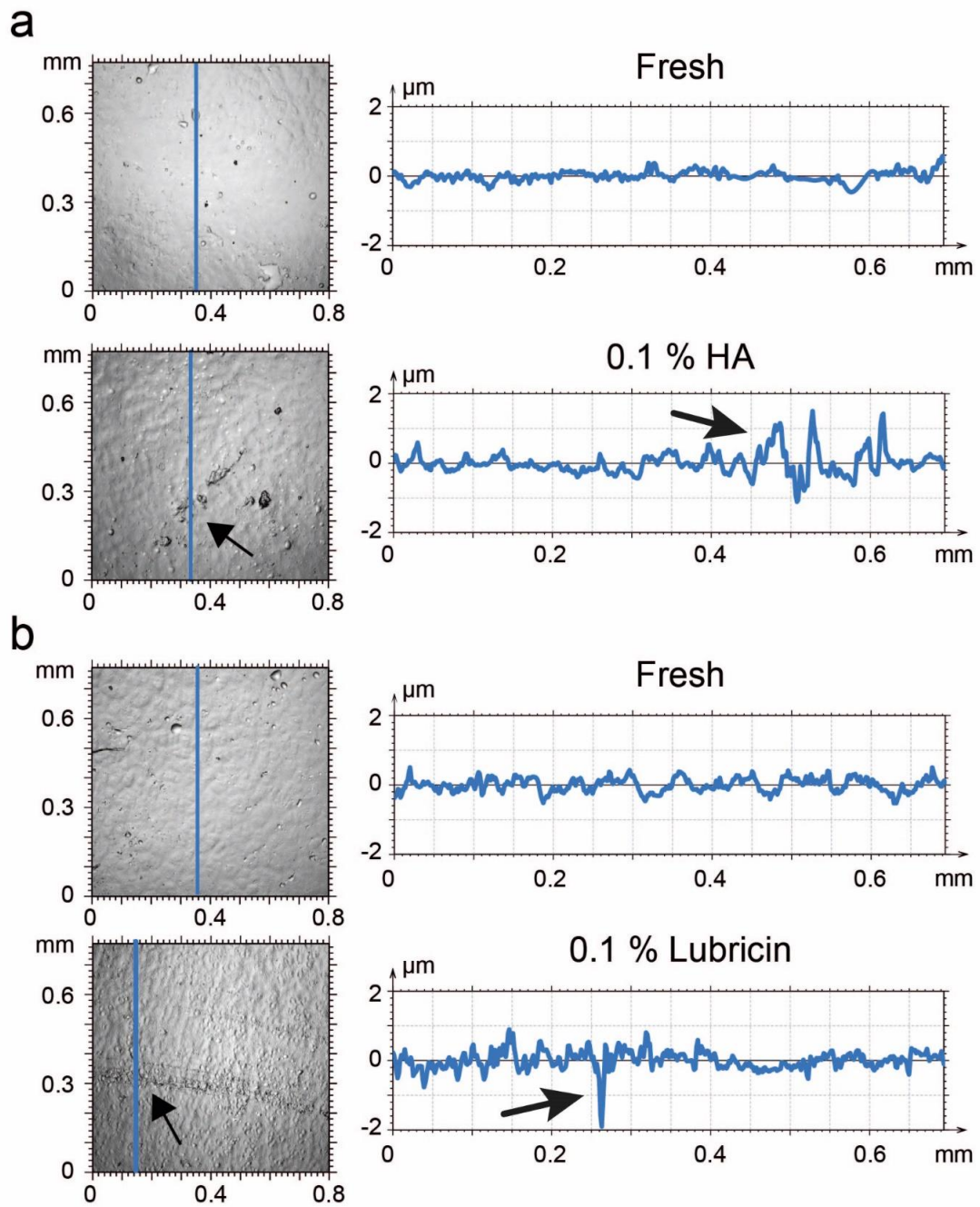


Figure S3. Profile lines along the blue lines depicted in the surface images. The adhesive wear hills and dales (a) and abrasive wear tracks (b) after lubrication with either 0.1 % HA or 0.1 % lubricin are visible, as well as the overall cartilage surface roughness.

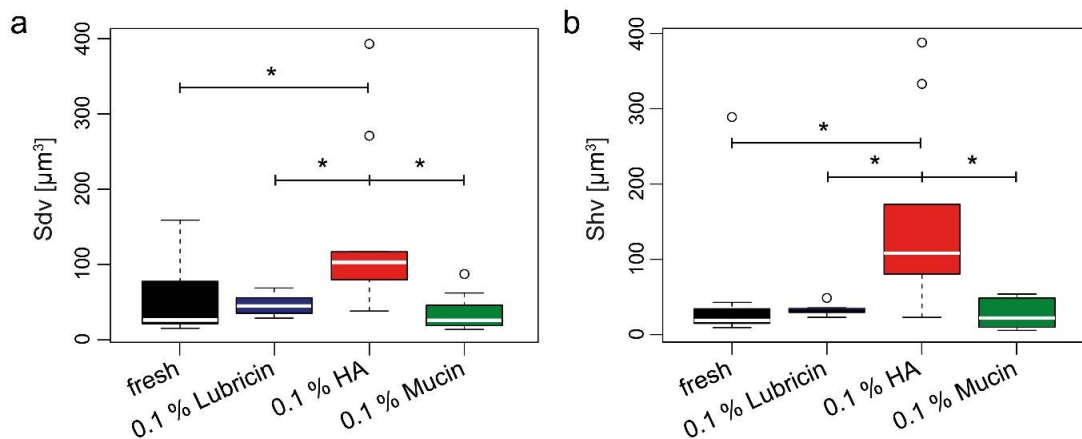


Figure S4. The changed topography due to lubrication with HA is also reflected in the mean dale volume (Sdv) and mean hill volume (Shv). This finding underlines the quantification of the observed alteration in cartilage surface topography using the S10z value.

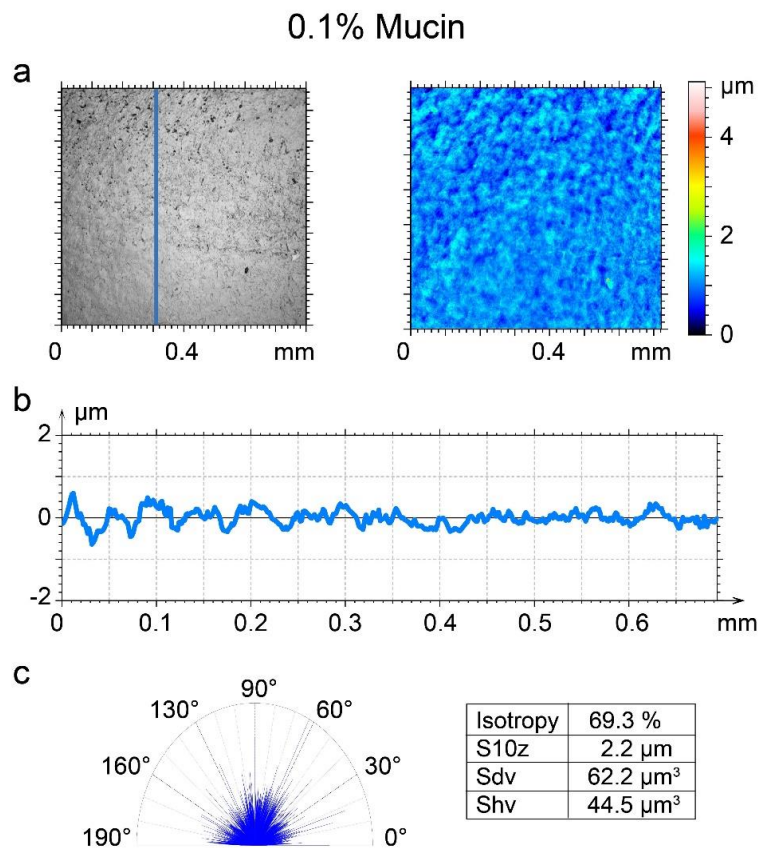


Figure S5. Lubrication with mucin preserves the cartilage surface and shows only minimal wear. Bright field microscopy as well as the topography images (a) show an unchanged surface compared to the fresh state. This is also reflected in the line profile (b) across such an image. The isotropy of the cartilage surfaces after friction measurements lubricated with mucin is similar or increased compared to the fresh cartilage surface (c).

C. Licenses for publications

C.1. Adapting a commercial shear rheometer for applications in cartilage research

AIP PUBLISHING LLC LICENSE TERMS AND CONDITIONS

Jan 08, 2016

All payments must be made in full to CCC. For payment instructions, please see information listed at the bottom of this form.

| | |
|-------------------------------------|--|
| License Number | 3784050569864 |
| Order Date | Jan 08, 2016 |
| Publisher | AIP Publishing LLC |
| Publication | Review of Scientific Instruments |
| Article Title | Adapting a commercial shear rheometer for applications in cartilage research |
| Author | K. Boettcher,S. Grumbein,U. Winkler, et al. |
| Online Publication Date | Sep 11, 2014 |
| Volume number | 85 |
| Issue number | 9 |
| Type of Use | Thesis/Dissertation |
| Requestor type | Author (original article) |
| Format | Print and electronic |
| Portion | Excerpt (> 800 words) |
| Will you be translating? | No |
| Title of your thesis / dissertation | Biotribology and biomechanics of articular cartilage |
| Expected completion date | Jul 2016 |
| Estimated size (number of pages) | 100 |
| Customer Tax ID | DE811193231 |
| Total | 0.00 EUR |

Terms and Conditions

AIP Publishing LLC -- Terms and Conditions: Permissions Uses

AIP Publishing LLC ("AIPP") hereby grants to you the non-exclusive right and license to use and/or distribute the Material according to the use specified in your order, on a one-time basis, for the specified term, with a maximum distribution equal to the number that you have ordered. Any links or other content accompanying the Material are not the subject of this license.

1. You agree to include the following copyright and permission notice with the reproduction of the Material: "Reprinted with permission from [FULL CITATION]. Copyright [PUBLICATION YEAR], AIP Publishing LLC." For an article, the copyright and permission notice must be printed on the first page of the article or book chapter. For photographs, covers, or tables, the copyright and permission notice may appear with the Material, in a footnote, or in the reference list.
2. If you have licensed reuse of a figure, photograph, cover, or table, it is your responsibility to ensure that the material is original to AIPP and does not contain the copyright of another entity, and that the copyright notice of the figure, photograph, cover, or table does not indicate that it was reprinted by AIPP, with permission, from another source. Under no circumstances does AIPP, purport or intend to grant permission to reuse material to which it does not hold copyright.
3. You may not alter or modify the Material in any manner. You may translate the Material into another language only if you have licensed translation rights. You may not use the Material for promotional purposes. AIPP reserves all rights not specifically granted herein.
4. The foregoing license shall not take effect unless and until AIPP or its agent, Copyright Clearance Center, receives the Payment in accordance with Copyright Clearance Center Billing and Payment Terms and Conditions, which are incorporated herein by reference.

APPENDIX C. LICENSES FOR PUBLICATIONS

5. AIPP or the Copyright Clearance Center may, within two business days of granting this license, revoke the license for any reason whatsoever, with a full refund payable to you. Should you violate the terms of this license at any time, AIPP, AIP Publishing LLC, or Copyright Clearance Center may revoke the license with no refund to you. Notice of such revocation will be made using the contact information provided by you. Failure to receive such notice will not nullify the revocation.
6. AIPP makes no representations or warranties with respect to the Material. You agree to indemnify and hold harmless AIPP, AIP Publishing LLC, and their officers, directors, employees or agents from and against any and all claims arising out of your use of the Material other than as specifically authorized herein.
7. The permission granted herein is personal to you and is not transferable or assignable without the prior written permission of AIPP. This license may not be amended except in a writing signed by the party to be charged.
8. If purchase orders, acknowledgments or check endorsements are issued on any forms containing terms and conditions which are inconsistent with these provisions, such inconsistent terms and conditions shall be of no force and effect. This document, including the CCC Billing and Payment Terms and Conditions, shall be the entire agreement between the parties relating to the subject matter hereof.

This Agreement shall be governed by and construed in accordance with the laws of the State of New York. Both parties hereby submit to the jurisdiction of the courts of New York County for purposes of resolving any disputes that may arise hereunder.

Questions? customercare@copyright.com or +1-855-239-3415 (toll free in the US) or +1-978-646-2777.

C.2. The structure and mechanical properties of articular cartilage are highly resilient towards transient dehydration

ELSEVIER LICENSE TERMS AND CONDITIONS

Jan 08, 2016

This is a License Agreement between Kathrin Boettcher ("You") and Elsevier ("Elsevier") provided by Copyright Clearance Center ("CCC"). The license consists of your order details, the terms and conditions provided by Elsevier, and the payment terms and conditions.

All payments must be made in full to CCC. For payment instructions, please see information listed at the bottom of this form.

| | |
|--|---|
| Supplier | Elsevier Limited The Boulevard, Langford Lane Kidlington, Oxford, OX5 1GB, UK |
| Registered Company Number | 1982084 |
| Customer name | Kathrin Boettcher |
| Customer address | Boltzmannstraße 11 Garching, 85748 |
| License number | 3784050936790 |
| License date | Jan 08, 2016 |
| Licensed content publisher | Elsevier |
| Licensed content publication | Acta Biomaterialia |
| Licensed content title | The structure and mechanical properties of articular cartilage are highly resilient towards transient dehydration |
| Licensed content author | K. Boettcher, S. Kienle, J. Nachtsheim, R. Burgkart, T. Hugel, O. Lieleg |
| Licensed content date | 1 January 2016 |
| Licensed content volume number | 29 |
| Licensed content issue number | n/a |
| Number of pages | 8 |
| Start Page | 180 |
| End Page | 187 |
| Type of Use | reuse in a thesis/dissertation |
| Intended publisher of new work | other |
| Portion | full article |
| Format | both print and electronic |
| Are you the author of this Elsevier article? | Yes |
| Will you be translating? | No |
| Title of your thesis/dissertation | Biotribology and biomechanics of articular cartilage |
| Expected completion date | Jul 2016 |
| Estimated size (number of pages) | 100 |

| | |
|---------------------|---------------------|
| Customer Tax ID | DE811193231 |
| Elsevier VAT number | GB 494 6272 12 |
| Permissions price | 0.00 EUR |
| VAT/Local Sales Tax | 0.00 EUR / 0.00 GBP |
| Total | 0.00 EUR |

Terms and Conditions

INTRODUCTION

1. The publisher for this copyrighted material is Elsevier. By clicking "accept" in connection with completing this licensing transaction, you agree that the following terms and conditions apply to this transaction (along with the Billing and Payment terms and conditions established by Copyright Clearance Center, Inc. ("CCC"), at the time that you opened your Rightslink account and that are available at any time at <http://myaccount.copyright.com>).

GENERAL TERMS

2. Elsevier hereby grants you permission to reproduce the aforementioned material subject to the terms and conditions indicated.

3. Acknowledgement: If any part of the material to be used (for example, figures) has appeared in our publication with credit or acknowledgement to another source, permission must also be sought from that source. If such permission is not obtained then that material may not be included in your publication/copies. Suitable acknowledgement to the source must be made, either as a footnote or in a reference list at the end of your publication, as follows:

"Reprinted from Publication title, Vol /edition number, Author(s), Title of article / title of chapter, Pages No., Copyright (Year), with permission from Elsevier [OR APPLICABLE SOCIETY COPYRIGHT OWNER]." Also Lancet special credit - "Reprinted from The Lancet, Vol. number, Author(s), Title of article, Pages No., Copyright (Year), with permission from Elsevier."

4. Reproduction of this material is confined to the purpose and/or media for which permission is hereby given.

5. Altering/Modifying Material: Not Permitted. However figures and illustrations may be altered/adapted minimally to serve your work. Any other abbreviations, additions, deletions and/or any other alterations shall be made only with prior written authorization of Elsevier Ltd. (Please contact Elsevier at permissions@elsevier.com)

6. If the permission fee for the requested use of our material is waived in this instance, please be advised that your future requests for Elsevier materials may attract a fee.

7. Reservation of Rights: Publisher reserves all rights not specifically granted in the combination of (i) the license details provided by you and accepted in the course of this licensing transaction, (ii) these terms and conditions and (iii) CCC's Billing and Payment terms and conditions.

8. License Contingent Upon Payment: While you may exercise the rights licensed immediately upon issuance of the license at the end of the licensing process for the transaction, provided that you have disclosed complete and accurate details of your proposed use, no license is finally effective unless and until full payment is received from you (either by publisher or by CCC) as provided in CCC's Billing and Payment terms and conditions. If full payment is not received on a timely basis, then any license preliminarily granted shall be deemed automatically revoked and shall be void as if never granted. Further, in the event that you breach any of these terms and conditions or any of CCC's Billing and Payment terms and conditions, the license is automatically revoked and shall be void as if never granted. Use of materials as described in a revoked license, as well as any use of the

materials beyond the scope of an unrevoked license, may constitute copyright infringement and publisher reserves the right to take any and all action to protect its copyright in the materials.

9. Warranties: Publisher makes no representations or warranties with respect to the licensed material.

10. Indemnity: You hereby indemnify and agree to hold harmless publisher and CCC, and their respective officers, directors, employees and agents, from and against any and all claims arising out of your use of the licensed material other than as specifically authorized pursuant to this license.

11. No Transfer of License: This license is personal to you and may not be sublicensed, assigned, or transferred by you to any other person without publisher's written permission.

12. No Amendment Except in Writing: This license may not be amended except in a writing signed by both parties (or, in the case of publisher, by CCC on publisher's behalf).

13. Objection to Contrary Terms: Publisher hereby objects to any terms contained in any purchase order, acknowledgment, check endorsement or other writing prepared by you, which terms are inconsistent with these terms and conditions or CCC's Billing and Payment terms and conditions. These terms and conditions, together with CCC's Billing and Payment terms and conditions (which are incorporated herein), comprise the entire agreement between you and publisher (and CCC) concerning this licensing transaction. In the event of any conflict between your obligations established by these terms and conditions and those established by CCC's Billing and Payment terms and conditions, these terms and conditions shall control.

14. Revocation: Elsevier or Copyright Clearance Center may deny the permissions described in this License at their sole discretion, for any reason or no reason, with a full refund payable to you. Notice of such denial will be made using the contact information provided by you. Failure to receive such notice will not alter or invalidate the denial. In no event will Elsevier or Copyright Clearance Center be responsible or liable for any costs, expenses or damage incurred by you as a result of a denial of your permission request, other than a refund of the amount(s) paid by you to Elsevier and/or Copyright Clearance Center for denied permissions.

LIMITED LICENSE

The following terms and conditions apply only to specific license types:

15. **Translation:** This permission is granted for non-exclusive world **English** rights only unless your license was granted for translation rights. If you licensed translation rights you may only translate this content into the languages you requested. A professional translator must perform all translations and reproduce the content word for word preserving the integrity of the article.

16. **Posting licensed content on any Website:** The following terms and conditions apply as follows: Licensing material from an Elsevier journal: All content posted to the web site must maintain the copyright information line on the bottom of each image; A hyper-text must be included to the Homepage of the journal from which you are licensing at <http://www.sciencedirect.com/science/journal/xxxxx> or the Elsevier homepage for books at <http://www.elsevier.com>; Central Storage: This license does not include permission for a scanned version of the material to be stored in a central repository such as that provided by Heron/XanEdu.

Licensing material from an Elsevier book: A hyper-text link must be included to the Elsevier homepage at <http://www.elsevier.com>. All content posted to the web site must maintain the copyright information line on the bottom of each image.

Posting licensed content on Electronic reserve: In addition to the above the following clauses are applicable: The web site must be password-protected and made available only to

bona fide students registered on a relevant course. This permission is granted for 1 year only. You may obtain a new license for future website posting.

17. **For journal authors:** the following clauses are applicable in addition to the above:

Preprints:

A preprint is an author's own write-up of research results and analysis, it has not been peer-reviewed, nor has it had any other value added to it by a publisher (such as formatting, copyright, technical enhancement etc.).

Authors can share their preprints anywhere at any time. Preprints should not be added to or enhanced in any way in order to appear more like, or to substitute for, the final versions of articles however authors can update their preprints on arXiv or RePEc with their Accepted Author Manuscript (see below).

If accepted for publication, we encourage authors to link from the preprint to their formal publication via its DOI. Millions of researchers have access to the formal publications on ScienceDirect, and so links will help users to find, access, cite and use the best available version. Please note that Cell Press, The Lancet and some society-owned have different preprint policies. Information on these policies is available on the journal homepage.

Accepted Author Manuscripts: An accepted author manuscript is the manuscript of an article that has been accepted for publication and which typically includes author-incorporated changes suggested during submission, peer review and editor-author communications.

Authors can share their accepted author manuscript:

- immediately
 - o via their non-commercial person homepage or blog
 - o by updating a preprint in arXiv or RePEc with the accepted manuscript
 - o via their research institute or institutional repository for internal institutional uses or as part of an invitation-only research collaboration work-group
 - o directly by providing copies to their students or to research collaborators for their personal use
 - o for private scholarly sharing as part of an invitation-only work group on commercial sites with which Elsevier has an agreement
- after the embargo period
 - o via non-commercial hosting platforms such as their institutional repository
 - o via commercial sites with which Elsevier has an agreement

In all cases accepted manuscripts should:

- link to the formal publication via its DOI
- bear a CC-BY-NC-ND license - this is easy to do
- if aggregated with other manuscripts, for example in a repository or other site, be shared in alignment with our hosting policy not be added to or enhanced in any way to appear more like, or to substitute for, the published journal article.

Published journal article (JPA): A published journal article (PJA) is the definitive final record of published research that appears or will appear in the journal and embodies all value-adding publishing activities including peer review co-ordination, copy-editing, formatting, (if relevant) pagination and online enrichment.

Policies for sharing publishing journal articles differ for subscription and gold open access articles:

Subscription Articles: If you are an author, please share a link to your article rather than the full-text. Millions of researchers have access to the formal publications on ScienceDirect,

and so links will help your users to find, access, cite, and use the best available version. Theses and dissertations which contain embedded PJAs as part of the formal submission can be posted publicly by the awarding institution with DOI links back to the formal publications on ScienceDirect.

If you are affiliated with a library that subscribes to ScienceDirect you have additional private sharing rights for others' research accessed under that agreement. This includes use for classroom teaching and internal training at the institution (including use in course packs and courseware programs), and inclusion of the article for grant funding purposes.

Gold Open Access Articles: May be shared according to the author-selected end-user license and should contain a [CrossMark logo](#), the end user license, and a DOI link to the formal publication on ScienceDirect.

Please refer to Elsevier's [posting policy](#) for further information.

18. **For book authors** the following clauses are applicable in addition to the above:

Authors are permitted to place a brief summary of their work online only. You are not allowed to download and post the published electronic version of your chapter, nor may you scan the printed edition to create an electronic version. **Posting to a repository:** Authors are permitted to post a summary of their chapter only in their institution's repository.

19. **Thesis/Dissertation:** If your license is for use in a thesis/dissertation your thesis may be submitted to your institution in either print or electronic form. Should your thesis be published commercially, please reapply for permission. These requirements include permission for the Library and Archives of Canada to supply single copies, on demand, of the complete thesis and include permission for Proquest/UMI to supply single copies, on demand, of the complete thesis. Should your thesis be published commercially, please reapply for permission. Theses and dissertations which contain embedded PJAs as part of the formal submission can be posted publicly by the awarding institution with DOI links back to the formal publications on ScienceDirect.

Elsevier Open Access Terms and Conditions

You can publish open access with Elsevier in hundreds of open access journals or in nearly 2000 established subscription journals that support open access publishing. Permitted third party re-use of these open access articles is defined by the author's choice of Creative Commons user license. See our [open access license policy](#) for more information.

Terms & Conditions applicable to all Open Access articles published with Elsevier:

Any reuse of the article must not represent the author as endorsing the adaptation of the article nor should the article be modified in such a way as to damage the author's honour or reputation. If any changes have been made, such changes must be clearly indicated.

The author(s) must be appropriately credited and we ask that you include the end user license and a DOI link to the formal publication on ScienceDirect.

If any part of the material to be used (for example, figures) has appeared in our publication with credit or acknowledgement to another source it is the responsibility of the user to ensure their reuse complies with the terms and conditions determined by the rights holder.

Additional Terms & Conditions applicable to each Creative Commons user license:

CC BY: The CC-BY license allows users to copy, to create extracts, abstracts and new works from the Article, to alter and revise the Article and to make commercial use of the Article (including reuse and/or resale of the Article by commercial entities), provided the user gives appropriate credit (with a link to the formal publication through the relevant DOI), provides a link to the license, indicates if changes were made and the licensor is not represented as endorsing the use made of the work. The full details of the license are available at <http://creativecommons.org/licenses/by/4.0>.

CC BY NC SA: The CC BY-NC-SA license allows users to copy, to create extracts, abstracts and new works from the Article, to alter and revise the Article, provided this is not

done for commercial purposes, and that the user gives appropriate credit (with a link to the formal publication through the relevant DOI), provides a link to the license, indicates if changes were made and the licensor is not represented as endorsing the use made of the work. Further, any new works must be made available on the same conditions. The full details of the license are available at <http://creativecommons.org/licenses/by-nc-sa/4.0>.

CC BY NC ND: The CC BY-NC-ND license allows users to copy and distribute the Article, provided this is not done for commercial purposes and further does not permit distribution of the Article if it is changed or edited in any way, and provided the user gives appropriate credit (with a link to the formal publication through the relevant DOI), provides a link to the license, and that the licensor is not represented as endorsing the use made of the work. The full details of the license are available at <http://creativecommons.org/licenses/by-nc-nd/4.0>.

Any commercial reuse of Open Access articles published with a CC BY NC SA or CC BY NC ND license requires permission from Elsevier and will be subject to a fee.

Commercial reuse includes:

- Associating advertising with the full text of the Article
- Charging fees for document delivery or access
- Article aggregation
- Systematic distribution via e-mail lists or share buttons

Posting or linking by commercial companies for use by customers of those companies.

20. Other Conditions:

v1.8

Questions? customercare@copyright.com or +1-855-239-3415 (toll free in the US) or +1-978-646-2777.

C.3. Comparison of friction and wear of articular cartilage on different length scales**ELSEVIER LICENSE
TERMS AND CONDITIONS**

Jan 13, 2016

This is a License Agreement between Kathrin Boettcher ("You") and Elsevier ("Elsevier") provided by Copyright Clearance Center ("CCC"). The license consists of your order details, the terms and conditions provided by Elsevier, and the payment terms and conditions.

All payments must be made in full to CCC. For payment instructions, please see information listed at the bottom of this form.

| | |
|--|--|
| Supplier | Elsevier Limited The Boulevard, Langford Lane Kidlington, Oxford, OX5 1GB, UK |
| Registered Company Number | 1982084 |
| Customer name | Kathrin Boettcher |
| Customer address | Boltzmannstraße 11 Garching, 85748 |
| License number | 3787060846737 |
| License date | Jan 13, 2016 |
| Licensed content publisher | Elsevier |
| Licensed content publication | Journal of Biomechanics |
| Licensed content title | Comparison of friction and wear of articular cartilage on different length scales |
| Licensed content author | Sandra Kienle, Kathrin Boettcher, Lorenz Wiegler, Joanna Urban, Rainer Burgkart, Oliver Lieleg, Thorsten Hugel |
| Licensed content date | 18 September 2015 |
| Licensed content volume number | 48 |
| Licensed content issue number | 12 |
| Number of pages | 7 |
| Start Page | 3052 |
| End Page | 3058 |
| Type of Use | reuse in a thesis/dissertation |
| Portion | full article |
| Format | both print and electronic |
| Are you the author of this Elsevier article? | Yes |
| Will you be translating? | No |
| Title of your thesis/dissertation | Biotribology and biomechanics of articular cartilage |
| Expected completion date | Jul 2016 |
| Estimated size (number of pages) | 100 |
| Customer Tax ID | DE811193231 |

| | |
|----------------------|---------------------|
| Elsevier VAT number | GB 494 6272 12 |
| Permissions price | 0.00 EUR |
| VAT/Local Sales Tax | 0.00 EUR / 0.00 GBP |
| Total | 0.00 EUR |
| Terms and Conditions | |

INTRODUCTION

1. The publisher for this copyrighted material is Elsevier. By clicking "accept" in connection with completing this licensing transaction, you agree that the following terms and conditions apply to this transaction (along with the Billing and Payment terms and conditions established by Copyright Clearance Center, Inc. ("CCC"), at the time that you opened your Rightslink account and that are available at any time at <http://myaccount.copyright.com>).

GENERAL TERMS

2. Elsevier hereby grants you permission to reproduce the aforementioned material subject to the terms and conditions indicated.

3. Acknowledgement: If any part of the material to be used (for example, figures) has appeared in our publication with credit or acknowledgement to another source, permission must also be sought from that source. If such permission is not obtained then that material may not be included in your publication/copies. Suitable acknowledgement to the source must be made, either as a footnote or in a reference list at the end of your publication, as follows:

"Reprinted from Publication title, Vol /edition number, Author(s), Title of article / title of chapter, Pages No., Copyright (Year), with permission from Elsevier [OR APPLICABLE SOCIETY COPYRIGHT OWNER]." Also Lancet special credit - "Reprinted from The Lancet, Vol. number, Author(s), Title of article, Pages No., Copyright (Year), with permission from Elsevier."

4. Reproduction of this material is confined to the purpose and/or media for which permission is hereby given.

5. Altering/Modifying Material: Not Permitted. However figures and illustrations may be altered/adapted minimally to serve your work. Any other abbreviations, additions, deletions and/or any other alterations shall be made only with prior written authorization of Elsevier Ltd. (Please contact Elsevier at permissions@elsevier.com)

6. If the permission fee for the requested use of our material is waived in this instance, please be advised that your future requests for Elsevier materials may attract a fee.

7. Reservation of Rights: Publisher reserves all rights not specifically granted in the combination of (i) the license details provided by you and accepted in the course of this licensing transaction, (ii) these terms and conditions and (iii) CCC's Billing and Payment terms and conditions.

8. License Contingent Upon Payment: While you may exercise the rights licensed immediately upon issuance of the license at the end of the licensing process for the transaction, provided that you have disclosed complete and accurate details of your proposed use, no license is finally effective unless and until full payment is received from you (either by publisher or by CCC) as provided in CCC's Billing and Payment terms and conditions. If full payment is not received on a timely basis, then any license preliminarily granted shall be deemed automatically revoked and shall be void as if never granted. Further, in the event that you breach any of these terms and conditions or any of CCC's Billing and Payment terms and conditions, the license is automatically revoked and shall be void as if never granted. Use of materials as described in a revoked license, as well as any use of the materials beyond the scope of an unrevoked license, may constitute copyright infringement

and publisher reserves the right to take any and all action to protect its copyright in the materials.

9. **Warranties:** Publisher makes no representations or warranties with respect to the licensed material.

10. **Indemnity:** You hereby indemnify and agree to hold harmless publisher and CCC, and their respective officers, directors, employees and agents, from and against any and all claims arising out of your use of the licensed material other than as specifically authorized pursuant to this license.

11. **No Transfer of License:** This license is personal to you and may not be sublicensed, assigned, or transferred by you to any other person without publisher's written permission.

12. **No Amendment Except in Writing:** This license may not be amended except in a writing signed by both parties (or, in the case of publisher, by CCC on publisher's behalf).

13. **Objection to Contrary Terms:** Publisher hereby objects to any terms contained in any purchase order, acknowledgment, check endorsement or other writing prepared by you, which terms are inconsistent with these terms and conditions or CCC's Billing and Payment terms and conditions. These terms and conditions, together with CCC's Billing and Payment terms and conditions (which are incorporated herein), comprise the entire agreement between you and publisher (and CCC) concerning this licensing transaction. In the event of any conflict between your obligations established by these terms and conditions and those established by CCC's Billing and Payment terms and conditions, these terms and conditions shall control.

14. **Revocation:** Elsevier or Copyright Clearance Center may deny the permissions described in this License at their sole discretion, for any reason or no reason, with a full refund payable to you. Notice of such denial will be made using the contact information provided by you. Failure to receive such notice will not alter or invalidate the denial. In no event will Elsevier or Copyright Clearance Center be responsible or liable for any costs, expenses or damage incurred by you as a result of a denial of your permission request, other than a refund of the amount(s) paid by you to Elsevier and/or Copyright Clearance Center for denied permissions.

LIMITED LICENSE

The following terms and conditions apply only to specific license types:

15. **Translation:** This permission is granted for non-exclusive world **English** rights only unless your license was granted for translation rights. If you licensed translation rights you may only translate this content into the languages you requested. A professional translator must perform all translations and reproduce the content word for word preserving the integrity of the article.

16. **Posting licensed content on any Website:** The following terms and conditions apply as follows: Licensing material from an Elsevier journal: All content posted to the web site must maintain the copyright information line on the bottom of each image; A hyper-text must be included to the Homepage of the journal from which you are licensing at <http://www.sciencedirect.com/science/journal/xxxxx> or the Elsevier homepage for books at <http://www.elsevier.com>; Central Storage: This license does not include permission for a scanned version of the material to be stored in a central repository such as that provided by Heron/XanEdu.

Licensing material from an Elsevier book: A hyper-text link must be included to the Elsevier homepage at <http://www.elsevier.com>. All content posted to the web site must maintain the copyright information line on the bottom of each image.

Posting licensed content on Electronic reserve: In addition to the above the following clauses are applicable: The web site must be password-protected and made available only to

bona fide students registered on a relevant course. This permission is granted for 1 year only. You may obtain a new license for future website posting.

17. **For journal authors:** the following clauses are applicable in addition to the above:

Preprints:

A preprint is an author's own write-up of research results and analysis, it has not been peer-reviewed, nor has it had any other value added to it by a publisher (such as formatting, copyright, technical enhancement etc.).

Authors can share their preprints anywhere at any time. Preprints should not be added to or enhanced in any way in order to appear more like, or to substitute for, the final versions of articles however authors can update their preprints on arXiv or RePEc with their Accepted Author Manuscript (see below).

If accepted for publication, we encourage authors to link from the preprint to their formal publication via its DOI. Millions of researchers have access to the formal publications on ScienceDirect, and so links will help users to find, access, cite and use the best available version. Please note that Cell Press, The Lancet and some society-owned have different preprint policies. Information on these policies is available on the journal homepage.

Accepted Author Manuscripts: An accepted author manuscript is the manuscript of an article that has been accepted for publication and which typically includes author-incorporated changes suggested during submission, peer review and editor-author communications.

Authors can share their accepted author manuscript:

- immediately
 - via their non-commercial person homepage or blog
 - by updating a preprint in arXiv or RePEc with the accepted manuscript
 - via their research institute or institutional repository for internal institutional uses or as part of an invitation-only research collaboration work-group
 - directly by providing copies to their students or to research collaborators for their personal use
 - for private scholarly sharing as part of an invitation-only work group on commercial sites with which Elsevier has an agreement
- after the embargo period
 - via non-commercial hosting platforms such as their institutional repository
 - via commercial sites with which Elsevier has an agreement

In all cases accepted manuscripts should:

- link to the formal publication via its DOI
- bear a CC-BY-NC-ND license - this is easy to do
- if aggregated with other manuscripts, for example in a repository or other site, be shared in alignment with our hosting policy not be added to or enhanced in any way to appear more like, or to substitute for, the published journal article.

Published journal article (JPA): A published journal article (PJA) is the definitive final record of published research that appears or will appear in the journal and embodies all value-adding publishing activities including peer review co-ordination, copy-editing, formatting, (if relevant) pagination and online enrichment.

Policies for sharing publishing journal articles differ for subscription and gold open access articles:

Subscription Articles: If you are an author, please share a link to your article rather than the full-text. Millions of researchers have access to the formal publications on ScienceDirect,

and so links will help your users to find, access, cite, and use the best available version. Theses and dissertations which contain embedded PJAs as part of the formal submission can be posted publicly by the awarding institution with DOI links back to the formal publications on ScienceDirect.

If you are affiliated with a library that subscribes to ScienceDirect you have additional private sharing rights for others' research accessed under that agreement. This includes use for classroom teaching and internal training at the institution (including use in course packs and courseware programs), and inclusion of the article for grant funding purposes.

Gold Open Access Articles: May be shared according to the author-selected end-user license and should contain a [CrossMark logo](#), the end user license, and a DOI link to the formal publication on ScienceDirect.

Please refer to Elsevier's [posting policy](#) for further information.

18. **For book authors** the following clauses are applicable in addition to the above:

Authors are permitted to place a brief summary of their work online only. You are not allowed to download and post the published electronic version of your chapter, nor may you scan the printed edition to create an electronic version. **Posting to a repository:** Authors are permitted to post a summary of their chapter only in their institution's repository.

19. **Thesis/Dissertation:** If your license is for use in a thesis/dissertation your thesis may be submitted to your institution in either print or electronic form. Should your thesis be published commercially, please reapply for permission. These requirements include permission for the Library and Archives of Canada to supply single copies, on demand, of the complete thesis and include permission for Proquest/UMI to supply single copies, on demand, of the complete thesis. Should your thesis be published commercially, please reapply for permission. Theses and dissertations which contain embedded PJAs as part of the formal submission can be posted publicly by the awarding institution with DOI links back to the formal publications on ScienceDirect.

Elsevier Open Access Terms and Conditions

You can publish open access with Elsevier in hundreds of open access journals or in nearly 2000 established subscription journals that support open access publishing. Permitted third party re-use of these open access articles is defined by the author's choice of Creative Commons user license. See our [open access license policy](#) for more information.

Terms & Conditions applicable to all Open Access articles published with Elsevier:

Any reuse of the article must not represent the author as endorsing the adaptation of the article nor should the article be modified in such a way as to damage the author's honour or reputation. If any changes have been made, such changes must be clearly indicated.

The author(s) must be appropriately credited and we ask that you include the end user license and a DOI link to the formal publication on ScienceDirect.

If any part of the material to be used (for example, figures) has appeared in our publication with credit or acknowledgement to another source it is the responsibility of the user to ensure their reuse complies with the terms and conditions determined by the rights holder.

Additional Terms & Conditions applicable to each Creative Commons user license:

CC BY: The CC-BY license allows users to copy, to create extracts, abstracts and new works from the Article, to alter and revise the Article and to make commercial use of the Article (including reuse and/or resale of the Article by commercial entities), provided the user gives appropriate credit (with a link to the formal publication through the relevant DOI), provides a link to the license, indicates if changes were made and the licensor is not represented as endorsing the use made of the work. The full details of the license are available at <http://creativecommons.org/licenses/by/4.0>.

CC BY NC SA: The CC BY-NC-SA license allows users to copy, to create extracts,

abstracts and new works from the Article, to alter and revise the Article, provided this is not done for commercial purposes, and that the user gives appropriate credit (with a link to the formal publication through the relevant DOI), provides a link to the license, indicates if changes were made and the licensor is not represented as endorsing the use made of the work. Further, any new works must be made available on the same conditions. The full details of the license are available at <http://creativecommons.org/licenses/by-nc-sa/4.0>.

CC BY NC ND: The CC BY-NC-ND license allows users to copy and distribute the Article, provided this is not done for commercial purposes and further does not permit distribution of the Article if it is changed or edited in any way, and provided the user gives appropriate credit (with a link to the formal publication through the relevant DOI), provides a link to the license, and that the licensor is not represented as endorsing the use made of the work. The full details of the license are available at <http://creativecommons.org/licenses/by-nc-nd/4.0>. Any commercial reuse of Open Access articles published with a CC BY NC SA or CC BY NC ND license requires permission from Elsevier and will be subject to a fee. Commercial reuse includes:

- Associating advertising with the full text of the Article
- Charging fees for document delivery or access
- Article aggregation
- Systematic distribution via e-mail lists or share buttons

Posting or linking by commercial companies for use by customers of those companies.

20. Other Conditions:

v1.8

Questions? customercare@copyright.com or +1-855-239-3415 (toll free in the US) or +1-978-646-2777.

C.4. Modulating mucin hydration and lubrication by deglycosylation and polyethylene glycol binding



RightsLink®

Home

Account Info

Help



WILEY

Title: Modulating Mucin Hydration and Lubrication by Deglycosylation and Polyethylene Glycol Binding

Author: Thomas Crouzier, Kathrin Boettcher, Anthony R. Geonnotti, Nicole L. Kavanaugh, Julie B. Hirsch, Katharina Ribbeck, Oliver Lieleg

Publication: Advanced Materials Interfaces

Publisher: John Wiley and Sons

Date: Sep 24, 2015

© 2015 The Authors. Published by WILEY-VCH Verlag GmbH & Co. KGaA, Weinheim

Logged in as:
Kathrin Boettcher
Account #:
3000979995

LOGOUT

Open Access Article

This article is available under the terms of the Creative Commons Attribution Non-Commercial License CC BY-NC (which may be updated from time to time) and permits non-commercial use, distribution and reproduction in any medium, provided the original work is properly cited.

For an understanding of what is meant by the terms of the Creative Commons License, please refer to [Wiley's Open Access Terms and Conditions](#).

Permission is not required for non-commercial reuse. For commercial reuse, please hit the "back" button and select the most appropriate commercial requestor type before completing your order.

BACK

CLOSE WINDOW

Copyright © 2016 [Copyright Clearance Center, Inc.](#) All Rights Reserved. [Privacy statement](#). [Terms and Conditions](#).
Comments? We would like to hear from you. E-mail us at customercare@copyright.com

D. Full list of publications

1. **Boettcher K**, Grumbein S, Winkler U, Nachtsheim J, Lieleg O. Adapting a commercial shear rheometer for applications in cartilage research. *Rev Sci Instrum* 2014; 85:093903.
2. Arends F, Nowald C, Pflieger K, **Boettcher K**, Zahler S, Lieleg O. The Biophysical Properties of Basal Lamina Gels Depend on the Biochemical Composition of the Gel. *PLoS ONE* 2015; 10:e0118090.
3. Kienle S, **Boettcher K**, Wiegleb L, Urban J, Burgkart R, Lieleg O., Hugel T. Comparison of friction and wear of articular cartilage on different length scales. *Journal of Biomechanics* 2015; 48:3052–8.
4. Crouzier T[#], **Boettcher K**[#], Geonnotti AR, Kavanaugh NL, Hirsch JB, Ribbeck K, Lieleg O. Modulating Mucin Hydration and Lubrication by Deglycosylation and Polyethylene Glycol Binding. *Adv. Mater. Interfaces* 2015; 2:1500308.
5. **Boettcher K**, Kienle S, Nachtsheim J, Burgkart R, Hugel T, Lieleg O. The structure and mechanical properties of articular cartilage are highly resilient towards transient dehydration. *Acta Biomaterialia* 2016; 29:180-187.
6. **Boettcher K**, Dorosz SG, Schmidt TA, Lieleg O. Porcine gastric mucins reduce friction and wear in cartilage boundary lubrication. *submitted*.
7. Grumbein S[#], Minev D[#], Tallawi M[#], **Boettcher K**, Prade F, Pfeiffer F, Grosse CU, Lieleg O. Hydrophobic Properties of Biofilm-Enriched Hybrid Mortar. *submitted*.

[#] These authors contributed equally

Bibliography

- [1] K. Kato, Wear in relation to friction — a review, *Wear*, vol. 241, no. 2, pp. 151–157, 2000.
- [2] K. Mylvaganam and L. C. Zhang, 4 - Micro/nano tribology, in *Tribology for Engineers*, J. P. Davim, Ed. Woodhead Publishing, 2011, pp. 121–160.
- [3] S. Affatato and F. Traina, 6 - Bio and medical tribology, in *Tribology for Engineers*, J. P. Davim, Ed. Woodhead Publishing, 2011, pp. 243–286.
- [4] D. Dowson and V. Wright, Bio-tribology, *Proceedings of the Conference on The Rheology of Lubrication*, pp. 81–88, 1973.
- [5] A. E. Jiménez and M. D. Bermúdez, 2 - Friction and wear, in *Tribology for Engineers*, J. P. Davim, Ed. Woodhead Publishing, 2011, pp. 33–63.
- [6] R. Gohar and H. Rahnejat, *Fundamentals of Tribology*, 2nd ed. London: Imperial College Press, 2012.
- [7] K. C. Ludema, *Friction, wear, lubrication: A textbook in tribology*. Boca Raton: CRC Press, 1996.
- [8] L. Burstein, 3 - Lubrication and roughness, in *Tribology for Engineers*, D. J. Paulo, Ed. Woodhead Publishing, 2011, pp. 65–120.
- [9] Y. Kondo, T. Koyama, and S. Sasaki, Tribological Properties of Ionic Liquids, in *Ionic Liquids - New Aspects for the Future*, J.-i. Kadokawa, Ed. InTech, 2013.
- [10] B. J. Hamrock, S. R. Schmid, and B. O. Jacobson, *Fundamentals of fluid film lubrication*. CRC Press, 2004.
- [11] Z. M. Jin, M. Stone, E. Ingham, and J. Fisher, (v) Biotribology, *Current Orthopaedics*, vol. 20, no. 1, pp. 32–40, 2006.
- [12] J. G. Wilkinson, Transport du colosse de Djéhouthitép, bas-relief de el-Bersheh, *[Public domain]*, via *Wikimedia Commons*, 1854. [Online]. Available: <https://commons.wikimedia.org/wiki/File%3AColosse-dj%C3%A9houtih%C3%A9tep2.jpg> [Accessed: 25.01.2016]
- [13] G. E. Yakubov, J. McColl, J. H. H. Bongaerts, and J. J. Ramsden, Viscous Boundary Lubrication of Hydrophobic Surfaces by Mucin, *Langmuir*, vol. 25, no. 4, pp. 2313–2321, 2009.
- [14] L. Ma, A. Gaisinskaya-Kipnis, N. Kampf, and J. Klein, Origins of hydration lubrication, *Nature communications*, vol. 6, p. 6060, 2015.
- [15] S. Jahn and J. Klein, Hydration Lubrication: The Macromolecular Domain, *Macromolecules*, vol. 48, no. 15, pp. 5059–5075, 2015.
- [16] G02 Committee, ASTM G40: Terminology Relating to Wear and Erosion, West Conshohocken, PA.
- [17] G02 Committee, ASTM G117: Guide for Calculating and Reporting Measures of Precision Using Data from Interlaboratory Wear or Erosion Tests, West Conshohocken, PA.
- [18] C. P. Neu, K. Komvopoulos, and A. H. Reddi, The Interface of Functional Biotribology and Regenerative Medicine in Synovial Joints, *Tissue Engineering Part B: Reviews*, vol. 14, no. 3, pp. 235–247, 2008.
- [19] ISO 14242:2014: Implants for surgery - Wear of total hip-joint prostheses. [Online]. Available: www.iso.org/iso/home/store/catalogue_ics/catalogue_detail_ics.htm?csnumber=63073 [Ac-

cessed: 25.01.2016]

- [20] K. T. Mäkelä, M. Matilainen, P. Pulkkinen, A. M. Fenstad, L. I. Havelin, L. Engesaeter, O. Furnes, S. Overgaard, A. B. Pedersen, J. Kärrholm, H. Malchau, G. Garellick, J. Ranstam, and A. Eskelinen, Countrywise results of total hip replacement. An analysis of 438,733 hips based on the Nordic Arthroplasty Register Association database, *Acta orthopaedica*, vol. 85, no. 2, pp. 107–116, 2014.
- [21] J. Park, Lakes, and R.S., *Biomaterials: An Introduction*, 3rd ed. New York, NY: Springer, 2007.
- [22] M. Nordin, *Basic Biomechanics of the Musculoskeletal System*, 4th ed. Philadelphia: Lippincott Williams and Wilkins, 2012.
- [23] A. Pham and M. Hull, Dehydration rates of meniscus and articular cartilage in vitro using a fast and accurate laser-based coordinate digitizing system, *Journal of Biomechanics*, vol. 40, no. 14, pp. 3223–3229, 2007.
- [24] K. A. Athanasiou, E. M. Darling, G. D. DuRaine, J. C. Hu, and A. H. Reddi, *Articular cartilage*, 1st ed. CRC Press, 2013.
- [25] J. A. Buckwalter, H. J. Mankin, and A. J. Grodzinsky, Articular cartilage and osteoarthritis, *Instructional course lectures*, vol. 54, pp. 465–480, 2005.
- [26] A. J. S. Fox, A. Bedi, and S. A. Rodeo, The basic science of articular cartilage: structure, composition, and function, *Sports health*, vol. 1, no. 6, pp. 461–468, 2009.
- [27] W. M. Lai, J. S. Hou, and V. C. Mow, A triphasic theory for the swelling and deformation behaviors of articular cartilage, *Journal of biomechanical engineering*, vol. 113, no. 3, pp. 245–258, 1991.
- [28] W. R. Walsh, M. Walton, W. Bruce, Y. Yu, R. M. Gillies, and M. Svehla, Cell Structure and Biology of Bone and Cartilage, in *Handbook of Histology Methods for Bone and Cartilage*, Y. H. An and K. L. Martin, Eds. Totowa, NJ: Humana Press, 2003, pp. 35–58.
- [29] S. Park, R. Krishnan, S. B. Nicoll, and G. A. Ateshian, Cartilage Interstitial Fluid Load Support in Unconfined Compression, *Journal of Biomechanics*, vol. 36, no. 12, pp. 1785–1796, 2003.
- [30] M. A. Soltz and G. A. Ateshian, Experimental verification and theoretical prediction of cartilage interstitial fluid pressurization at an impermeable contact interface in confined compression, *Journal of biomechanics*, vol. 31, no. 10, pp. 927–934, 1998.
- [31] C. J. Little, N. K. Bawolin, and X. Chen, Mechanical Properties of Natural Cartilage and Tissue-Engineered Constructs, *Tissue Engineering Part B: Reviews*, vol. 17, no. 4, pp. 213–227, 2011.
- [32] R. Korhonen, M. Laasanen, J. Töyräs, J. Rieppo, J. Hirvonen, H. Helminen, and J. Jurvelin, Comparison of the equilibrium response of articular cartilage in unconfined compression, confined compression and indentation, *Journal of Biomechanics*, vol. 35, no. 7, pp. 903–909, 2002.
- [33] M. Jin and A. J. Grodzinsky, Effect of Electrostatic Interactions between Glycosaminoglycans on the Shear Stiffness of Cartilage: A Molecular Model and Experiments, *Macromolecules*, vol. 34, no. 23, pp. 8330–8339, 2001.
- [34] M. A. MacConaill, The Function of Intra-Articular Fibrocartilages, with Special Reference to the Knee and Inferior Radio-Ulnar Joints, *Journal of Anatomy*, vol. 66, no. Pt 2, pp. 210–227, 1932.
- [35] J. S. Hou, V. C. Mow, W. M. Lai, and M. H. Holmes, An analysis of the squeeze-film lubrication mechanism for articular cartilage, *Journal of Biomechanics*, vol. 25, no. 3, pp. 247–259, 1992.
- [36] T. Murakami, K. Nakashima, S. Yarimitsu, Y. Sawae, and N. Sakai, Effectiveness of adsorbed film

- and gel layer in hydration lubrication as adaptive multimode lubrication mechanism for articular cartilage, *Proceedings of the Institution of Mechanical Engineers, Part J: Journal of Engineering Tribology*, vol. 225, no. 12, pp. 1174–1185, 2011.
- [37] C. W. McCutchen, Boundary lubrication by synovial fluid: demonstration and possible osmotic explanation, *Federation proceedings*, vol. 25, no. 3, pp. 1061–1068, 1966.
- [38] P. S. Walker, D. Dowson, M. D. Longfield, and V. Wright, "Boosted lubrication" in synovial joints by fluid entrapment and enrichment, *Annals of the Rheumatic Diseases*, vol. 27, no. 6, pp. 512–520, 1968.
- [39] R. I. Tanner, An Alternative Mechanism for the Lubrication of Synovial Joints, *Physics in Medicine and Biology*, vol. 11, no. 1, p. 119, 1966.
- [40] D. Dowson and G. R. Higginson, *Elastohydrodynamic lubrication*. Pergamon Press, 1977.
- [41] W. B. Hardy and L. Bircumshaw, Bakerian lecture – boundary lubrication – plane surfaces and the limitations of Amontón's law, *Proc. R. Soc. A*, vol. 108, pp. 1–27, 1925.
- [42] G. W. Greene, X. Banquy, D. W. Lee, D. D. Lowrey, J. Yu, and J. N. Israelachvili, Adaptive mechanically controlled lubrication mechanism found in articular joints, *Proceedings of the National Academy of Sciences*, vol. 108, no. 13, pp. 5255–5259, 2011.
- [43] S. E. Majd, R. Kuijer, A. Köwitsch, T. Groth, T. A. Schmidt, and P. K. Sharma, Both Hyaluronan and Collagen Type II Keep Proteoglycan 4 (Lubricin) at the Cartilage Surface in a Condition That Provides Low Friction during Boundary Lubrication, *Langmuir*, vol. 30, no. 48, pp. 14 566–14 572, 2014.
- [44] J. Seror, L. Zhu, R. Goldberg, A. J. Day, and J. Klein, Supramolecular synergy in the boundary lubrication of synovial joints, *Nat Commun*, vol. 6, p. 6497, 2015.
- [45] S. Abubacker, S. G. Dorosz, D. Ponjevic, G. D. Jay, J. R. Matyas, and T. A. Schmidt, Full-Length Recombinant Human Proteoglycan 4 Interacts with Hyaluronan to Provide Cartilage Boundary Lubrication, *Annals of Biomedical Engineering*, pp. 1–10, 2015.
- [46] R. C. Eguiluz, S. G. Cook, C. N. Brown, F. Wu, N. J. Pacifici, L. J. Bonassar, and D. Gourdon, Fibronectin mediates enhanced wear protection of lubricin during shear, *Biomacromolecules*, vol. 16, no. 9, pp. 2884–2894, 2015.
- [47] J. Seror, Y. Merkher, N. Kampf, L. Collinson, A. J. Day, A. Maroudas, and J. Klein, Articular Cartilage Proteoglycans As Boundary Lubricants: Structure and Frictional Interaction of Surface-Attached Hyaluronan and Hyaluronan–Aggrecan Complexes, *Biomacromolecules*, vol. 12, no. 10, pp. 3432–3443, 2011.
- [48] T. Murakami, S. Yarimitsu, K. Nakashima, Y. Sawae, and N. Sakai, Influence of synovia constituents on tribological behaviors of articular cartilage, *Friction*, vol. 1, no. 2, pp. 150–162, 2013.
- [49] R. Tadmor, N. Chen, and J. Israelachvili, Normal and Shear Forces between Mica and Model Membrane Surfaces with Adsorbed Hyaluronan, *Macromolecules*, vol. 36, no. 25, pp. 9519–9526, 2003.
- [50] S. Das, X. Banquy, B. Zappone, G. W. Greene, G. D. Jay, and J. N. Israelachvili, Synergistic Interactions between Grafted Hyaluronic Acid and Lubricin Provide Enhanced Wear Protection and Lubrication, *Biomacromolecules*, vol. 14, no. 5, pp. 1669–1677, 2013.
- [51] X. Banquy, D. W. Lee, S. Das, J. Hogan, and J. N. Israelachvili, Shear-Induced Aggregation of Mammalian Synovial Fluid Components under Boundary Lubrication Conditions, *Advanced Functional*

Materials, vol. 24, no. 21, pp. 3152–3161, 2014.

- [52] D. W. Lee, X. Banquy, and J. N. Israelachvili, PNAS Plus: Stick-slip friction and wear of articular joints, *Proceedings of the National Academy of Sciences*, vol. 110, no. 7, pp. E567–E574, 2013.
- [53] D. J. Gregory, B. P. Lane, and L. Sokoloff, Characterization of a bovine synovial fluid lubricating factor III. The interaction with hyaluronic acid, *Connective Tissue Research*, vol. 28, no. 4, pp. 245–255, 1992.
- [54] B. Zappone, M. Ruths, G. W. Greene, G. D. Jay, and J. N. Israelachvili, Adsorption, Lubrication, and Wear of Lubricin on Model Surfaces: Polymer Brush-Like Behavior of a Glycoprotein, *Biophysical Journal*, vol. 92, no. 5, pp. 1693–1708, 2006.
- [55] S. T. Chan, C. Neu, G. DuRaine, K. Komvopoulos, and A. Reddi, Tribological altruism: A sacrificial layer mechanism of synovial joint lubrication in articular cartilage, *Journal of Biomechanics*, vol. 45, no. 14, pp. 2426–2431, 2012.
- [56] J. Klein, Molecular mechanisms of synovial joint lubrication, *Proceedings of the Institution of Mechanical Engineers, Part J: Journal of Engineering Tribology*, vol. 220, no. 8, pp. 691–710, 2006.
- [57] I. M. Basalo, N. O. Chahine, M. Kaplun, F. H. Chen, C. T. Hung, and G. A. Ateshian, Chondroitin sulfate reduces the friction coefficient of articular cartilage, *Journal of Biomechanics*, vol. 40, no. 8, pp. 1847–1854, 2007.
- [58] E. D. Bonnevie, V. J. Baro, L. Wang, and D. L. Burris, In Situ Studies of Cartilage Microtribology: Roles of Speed and Contact Area, *Tribology letters*, vol. 41, no. 1, pp. 83–95, 2011.
- [59] M. Schwarz, B. Schneider-Wald, A. Krase, W. Richter, G. Reisig, M. Kreinest, S. Heute, P. Pott, J. Brade, and A. Schütte, Tribologische Messungen am Gelenkknorpel, *Der Orthopäde*, vol. 41, no. 10, pp. 827–836, 2012.
- [60] L. Shi, V. I. Sikavitsas, and A. Striolo, Experimental Friction Coefficients for Bovine Cartilage Measured with a Pin-on-Disk Tribometer: Testing Configuration and Lubricant Effects, *Annals of Biomedical Engineering*, vol. 39, no. 1, pp. 132–146, 2011.
- [61] S. M. Hsu and R. S. Gates, Boundary lubricating films: formation and lubrication mechanism, *Tribology International*, vol. 38, no. 3, pp. 305–312, 2005.
- [62] Z. Peng and M. Wang, Three dimensional surface characterization of human cartilages at a micron and nanometre scale, *Wear of Materials 2013*, vol. 301, no. 1–2, pp. 210–217, 2013.
- [63] M. Wang, Z. Peng, J. Wang, and X. Jiang, Wear characterisation of articular cartilage surfaces at a nano-scale using atomic force microscopy, *The International Conference on BioTribology 2011*, vol. 63, pp. 235–242, 2013.
- [64] S. R. Oungoulian, K. E. Hehir, K. Zhu, C. E. Willis, A. G. Marinescu, N. Merali, C. S. Ahmad, C. T. Hung, and G. A. Ateshian, Effect of glutaraldehyde fixation on the frictional response of immature bovine articular cartilage explants, *Journal of Biomechanics*, vol. 47, no. 3, pp. 694–701, 2014.
- [65] M. E. McGann, A. Vahdati, and D. R. Wagner, Methods to assess in vitro wear of articular cartilage, *Proceedings of the Institution of Mechanical Engineers, Part H: Journal of Engineering in Medicine*, vol. 226, no. 8, pp. 612–622, 2012.
- [66] D. W. Lee, X. Banquy, S. Das, N. Cadirov, G. Jay, and J. Israelachvili, Effects of molecular weight of grafted hyaluronic acid on wear initiation, *Acta Biomaterialia*, vol. 10, no. 5, pp. 1817–1823, 2014.
- [67] B. Zappone, K. J. Rosenberg, and J. Israelachvili, Role of nanometer roughness on the adhesion and

- friction of a rough polymer surface and a molecularly smooth mica surface, *Tribology letters*, vol. 26, no. 3, pp. 191–201, 2007.
- [68] C. Erggelet and B. Mandelbaum, *Principles of cartilage repair*. Heidelberg and Berlin: Steinkopff and Springer, 2008.
- [69] F. Eckstein and W. Wirth, Quantitative cartilage imaging in knee osteoarthritis, *Arthritis*, vol. 2011, p. 475684, 2011.
- [70] P.-T. Cheng, Pathologic Mineralization in Humans, in *Mechanisms and Phylogeny of Mineralization in Biological Systems: Biomineralization '90*, S. Suga and H. Nakahara, Eds. Tokyo: Springer Japan, 1991, pp. 241–245.
- [71] N. A. Cummings and G. L. Nordby, Measurement of synovial fluid pH in normal and arthritic knees, *Arthritis & Rheumatism*, vol. 9, no. 1, pp. 47–56, 1966.
- [72] T. Bennike, U. Ayturk, C. M. Haslauer, J. W. Froehlich, B. L. Proffen, O. Barnaby, S. Birkelund, M. M. Murray, M. L. Warman, A. Stensballe, and H. Steen, A Normative Study of the Synovial Fluid Proteome from Healthy Porcine Knee Joints, *J. Proteome Res.*, vol. 13, no. 10, pp. 4377–4387, 2014.
- [73] A. Y. Hui, W. J. McCarty, K. Masuda, G. S. Firestein, and R. L. Sah, A Systems Biology Approach to Synovial Joint Lubrication in Health, Injury, and Disease, *Wiley interdisciplinary reviews. Systems biology and medicine*, vol. 4, no. 1, pp. 15–37, 2011.
- [74] S. Ghosh, J. Bowen, K. Jiang, D. M. Espino, and Shepherd, Duncan E. T., Investigation of techniques for the measurement of articular cartilage surface roughness, *Micron*, vol. 44, pp. 179–184, 2013.
- [75] R. Stern, Hyaluronan catabolism: a new metabolic pathway, *European Journal of Cell Biology*, vol. 83, no. 7, pp. 317–325, 2004.
- [76] H. Saari, Y. T. Konttinen, C. Friman, and T. Sorsa, Differential effects of reactive oxygen species on native synovial fluid and purified human umbilical cord hyaluronate, *Inflammation*, vol. 17, no. 4, pp. 403–415, 1993.
- [77] A. G. Ogston and J. E. Stanier., The physiological function of hyaluronic acid in synovial fluid; viscous, elastic and lubricant properties, *The Journal of Physiology*, vol. 119, no. 2-3, pp. 244–252, 1953.
- [78] E. A. Balazs, D. Watson, I. F. Duff, and S. Roseman, Hyaluronic acid in synovial fluid. I. Molecular parameters of hyaluronic acid in normal and arthritic human fluids, *Arthritis & Rheumatism*, vol. 10, no. 4, pp. 357–376, 1967.
- [79] J. J. Kwiecinski, S. G. Dorosz, T. E. Ludwig, S. Abubacker, M. K. Cowman, and T. A. Schmidt, The effect of molecular weight on hyaluronan's cartilage boundary lubricating ability – alone and in combination with proteoglycan 4, *Osteoarthritis and Cartilage*, vol. 19, no. 11, pp. 1356–1362, 2011.
- [80] M. K. Cowman, T. A. Schmidt, P. Raghavan, and A. Stecco, Viscoelastic Properties of Hyaluronan in Physiological Conditions, *F1000Research*, vol. 4, p. 622, 2015.
- [81] J. Katta, T. Stapleton, E. Ingham, Z. M. Jin, and J. Fisher, The effect of glycosaminoglycan depletion on the friction and deformation of articular cartilage, *Proceedings of the Institution of Mechanical Engineers, Part H: Journal of Engineering in Medicine*, vol. 222, no. 1, pp. 1–11, 2008.
- [82] U.S. Food and Drug Administration. (1997) Hyalgan - P950027. [Online]. Available: http://www.accessdata.fda.gov/cdrh_docs/pdf/P950027a.pdf [Accessed: 2016-07-03]
- [83] N. Bellamy, J. Campbell, V. Robinson, T. Gee, R. Bourne, and G. Wells, Viscosupplementation for

- the treatment of osteoarthritis of the knee, *The Cochrane database of systematic reviews*, vol. 19, no. 2, p. CD005321, 2006.
- [84] D. Y. Wen, Intra-articular hyaluronic acid injections for knee osteoarthritis, *American family physician*, vol. 62, no. 3, pp. 565–70, 572, 2000.
- [85] T. E. Ludwig, M. M. Hunter, and T. A. Schmidt, Cartilage boundary lubrication synergism is mediated by hyaluronan concentration and PRG4 concentration and structure, *BMC musculoskeletal disorders*, vol. 16, no. 1, p. 386, 2015.
- [86] A. R. Jones, J. P. Gleghorn, C. E. Hughes, L. J. Fitz, R. Zollner, S. D. Wainwright, B. Caterson, E. A. Morris, L. J. Bonassar, and C. R. Flannery, Binding and localization of recombinant lubricin to articular cartilage surfaces, *Journal of Orthopaedic Research*, vol. 25, no. 3, pp. 283–292, 2007.
- [87] G. D. Jay and K. A. Waller, The biology of lubricin: near frictionless joint motion, *Matrix biology : journal of the International Society for Matrix Biology*, vol. 39, pp. 17–24, 2014.
- [88] G. D. Jay, J. R. Torres, D. K. Rhee, H. J. Helminen, M. M. Hytinen, C.-J. Cha, K. Elsaid, K.-S. Kim, Y. Cui, and M. L. Warman, Association between friction and wear in diarthrodial joints lacking lubricin, *Arthritis & Rheumatism*, vol. 56, no. 11, pp. 3662–3669, 2007.
- [89] T. A. Schmidt, D. A. Sullivan, E. Knop, and et al, Transcription, translation, and function of lubricin, a boundary lubricant, at the ocular surface, *JAMA Ophthalmology*, vol. 131, no. 6, pp. 766–776, 2013.
- [90] E. D. Bonnevie, D. Galesso, C. Secchieri, I. Cohen, and L. J. Bonassar, Elastoviscous Transitions of Articular Cartilage Reveal a Mechanism of Synergy between Lubricin and Hyaluronic Acid, *PLoS ONE*, vol. 10, no. 11, p. e0143415, 2015.
- [91] K. A. Elsaid, B. C. Fleming, H. L. Oksendahl, J. T. Machan, P. D. Fadale, M. J. Hulstyn, R. Shalvoy, and G. D. Jay, Decreased Lubricin Concentrations and Markers of Joint Inflammation in Synovial Fluids from Patients with Anterior Cruciate Ligament Injury, *Arthritis and rheumatism*, vol. 58, no. 6, pp. 1707–1715, 2008.
- [92] T. E. Ludwig, J. R. McAllister, V. Lun, J. P. Wiley, and T. A. Schmidt, Diminished cartilage-lubricating ability of human osteoarthritic synovial fluid deficient in proteoglycan 4: Restoration through proteoglycan 4 supplementation, *Arthritis & Rheumatism*, vol. 64, no. 12, pp. 3963–3971, 2012.
- [93] G. D. Jay, B. C. Fleming, B. A. Watkins, K. A. McHugh, S. C. Anderson, L. X. Zhang, E. Teeple, K. A. Waller, and K. A. Elsaid, Prevention of cartilage degeneration and restoration of chondroprotection by lubricin tribosupplementation in the rat following anterior cruciate ligament transection, *Arthritis and rheumatism*, vol. 62, no. 8, pp. 2382–2391, 2010.
- [94] U.S. National Institute of Health, Tolerability, Safety and Efficacy of Lubricin Eye Drops Versus Sodium Hyaluronate Eye Drops in Subjects With Moderate Dry Eye: NCT02510235, 2015. [Online]. Available: <https://www.clinicaltrials.gov/ct2/show/NCT02510235> [Accessed: 28.01.2016]
- [95] Lubris BioPharma. [Online]. Available: www.lubris.net/focus [Accessed: 28.01.2016]
- [96] O. Lieleg, I. Vladescu, and K. Ribbeck, Characterization of Particle Translocation through Mucin Hydrogels, *Biophysical Journal*, vol. 98, no. 9, pp. 1782–1789, 2010.
- [97] R. Bansil, J. Celli, J. Hardcastle, and B. Turner, The influence of mucus microstructure and rheology in H. pylori infection, *Frontiers in Immunology*, vol. 4, no. 310, 2013.
- [98] S. K. Linden, P. Sutton, N. G. Karlsson, V. Korolik, and M. A. McGuckin, Mucins in the mucosal

- barrier to infection, *Mucosal immunology*, vol. 1, no. 3, pp. 183–197, 2008.
- [99] R. Mejías-Luque, L. Cobler, and de Bolós C., MUC5AC (mucin 5AC, oligomeric mucus/gel-forming), *Atlas Genet Cytogenet Oncol*, vol. 14, no. 6, pp. 566–569, 2010.
- [100] A. Dédinaïté, Biomimetic lubrication, *Soft Matter*, vol. 8, no. 2, pp. 273–284, 2012.
- [101] G. D. Jay, Lubricin and surfacing of articular joints, *Current Opinion in Orthopaedics*, vol. 15, no. 5, pp. 355–359, 2004.
- [102] R. Bansil and B. S. Turner, Mucin structure, aggregation, physiological functions and biomedical applications, *Current Opinion in Colloid & Interface Science*, vol. 11, no. 2–3, pp. 164–170, 2006.
- [103] J. Celli, B. Gregor, B. Turner, N. H. Afdhal, R. Bansil, and S. Erramilli, Viscoelastic Properties and Dynamics of Porcine Gastric Mucin, *Biomacromolecules*, vol. 6, no. 3, pp. 1329–1333, 2005.
- [104] J. P. Celli, B. S. Turner, N. H. Afdhal, R. H. Ewoldt, G. H. McKinley, R. Bansil, and S. Erramilli, Rheology of gastric mucin exhibits a pH-dependent sol-gel transition, *Biomacromolecules*, vol. 8, no. 5, pp. 1580–1586, 2007.
- [105] O. Lieleg, C. Lieleg, J. Bloom, C. B. Buck, and K. Ribbeck, Mucin Biopolymers As Broad-Spectrum Antiviral Agents, *Biomacromolecules*, vol. 13, no. 6, pp. 1724–1732, 2012.
- [106] A. Scharfman, G. Lamblin, and P. Roussel, Interactions between human respiratory mucins and pathogens, *Biochemical Society Transactions*, vol. 23, pp. 836–839, 1995.
- [107] D. J. Thornton, From Mucins to Mucus, *Proceedings of the American Thoracic Society*, vol. 1, pp. 54–61, 2004.
- [108] H. Matsui, M. W. Verghese, M. Kesimer, U. E. Schwab, S. H. Randell, J. K. Sheehan, B. R. Grubb, and R. C. Boucher, Reduced Three-Dimensional Motility in Dehydrated Airway Mucus Prevents Neutrophil Capture and Killing Bacteria on Airway Epithelial Surfaces, *The Journal of Immunology*, vol. 175, pp. 1090–1099, 2005.
- [109] O. Lieleg and K. Ribbeck, Biological hydrogels as selective diffusion barriers, *Trends in Cell Biology*, vol. 21, no. 9, pp. 543–551, 2011.
- [110] R. A. Cone, Barrier properties of mucus, *Advanced Drug Delivery Reviews*, vol. 61, no. 2, pp. 75–85, 2009.
- [111] S. Lee, M. Müller, K. Rezwan, and N. D. Spencer, Porcine Gastric Mucin (PGM) at the Water/Poly(Dimethylsiloxane) (PDMS) Interface: Influence of pH and Ionic Strength on Its Conformation, Adsorption, and Aqueous Lubrication Properties, *Langmuir*, vol. 21, no. 18, pp. 8344–8353, 2005.
- [112] C. Atuma, V. Strugala, A. Allen, and L. Holm, The adherent gastrointestinal mucus gel layer: thickness and physical state in vivo, *American journal of physiology. Gastrointestinal and liver physiology*, vol. 280, no. 5, pp. G922–9, 2001.
- [113] J. L. Cook, C. T. Hung, K. Kuroki, A. M. Stoker, C. R. Cook, F. M. Pfeiffer, S. L. Sherman, and J. P. Stannard, Animal models of cartilage repair, *Bone & Joint Research*, vol. 3, no. 4, pp. 89–94, 2013.
- [114] H. Madry, M. Ochi, M. Cucchiaroni, D. Pape, and R. Seil, Large animal models in experimental knee sports surgery: focus on clinical translation, *Journal of Experimental Orthopaedics*, vol. 2, no. 1, p. 852, 2015.
- [115] T. A. Schmidt, N. S. Gastelum, Q. T. Nguyen, B. L. Schumacher, and R. L. Sah, Boundary lubrication

- of articular cartilage: Role of synovial fluid constituents, *Arthritis & Rheumatism*, vol. 56, no. 3, pp. 882–891, 2007.
- [116] A. Gigante and L. Callegari, The role of intra-articular hyaluronan (Sinovial) in the treatment of osteoarthritis, *Rheumatology International*, vol. 31, no. 4, pp. 427–444, 2011.
- [117] M. Caldara, R. S. Friedlander, N. L. Kavanaugh, J. Aizenberg, K. R. Foster, and K. Ribbeck, Mucin biopolymers prevent bacterial aggregation by retaining cells in the free-swimming state, *Current biology : CB*, vol. 22, no. 24, pp. 2325–2330, 2012.
- [118] K. Boettcher, S. Grumbein, U. Winkler, J. Nachtsheim, and O. Lieleg, Adapting a commercial shear rheometer for applications in cartilage research, *The Review of Scientific Instruments*, vol. 85, no. 9, p. 093903, 2014.
- [119] H. H. Huberti and W. C. Hayes, Patellofemoral contact pressures. The influence of q-angle and tend-ofemoral contact, *The Journal of Bone and Joint Surgery. American volume*, vol. 66, no. 5, pp. 715–724, 1984.
- [120] Biocolor Ltd, Blyscan Sulfated Glycosaminoglycan Assay. [Online]. Available: www.biocolor.co.uk/manuals/blyscan.pdf [Accessed: 17.11.2014]
- [121] Nano Focus AG, NanoFocus confocal technology. [Online]. Available: www.nanofocus.com/technology/measurement-principles/usurf-technology/confocal-technology-video [Accessed: 29.01.2016]
- [122] ISO 25178-2: 2012 Geometrical product specification (GPS) - Surface texture: Areal - Part 2: Terms, definitions and surface texture parameters. [Online]. Available: www.iso.org/iso/iso_catalogue/catalogue_tc/catalogue_detail.htm?csnumber=42785 [Accessed: 25.01.2016]
- [123] X. Jiang, P. Scott, D. Whitehouse, and L. Blunt, Paradigm shifts in surface metrology. Part II. The current shift, *Proceedings of the Royal Society of London A: Mathematical, Physical and Engineering Sciences*, vol. 463, no. 2085, pp. 2071–2099, 2007.
- [124] NanoFocus AG, *Reference Manual μ soft analysis extended: MountainsMap: Version 7.2.7344*. Digital Surf, 2015.
- [125] K. Boettcher, S. Kienle, J. Nachtsheim, R. Burgkart, T. Hugel, and O. Lieleg, The structure and mechanical properties of articular cartilage are highly resilient towards transient dehydration, *Acta Biomaterialia*, vol. 29, pp. 180–187, 2016.
- [126] S. Kienle, K. Boettcher, L. Wiegleb, J. Urban, R. Burgkart, O. Lieleg, and T. Hugel, Comparison of friction and wear of articular cartilage on different length scales, *Journal of Biomechanics*, vol. 48, no. 12, pp. 3052–3058, 2015.
- [127] T. Crouzier, K. Boettcher, A. R. Geonnotti, N. L. Kavanaugh, J. B. Hirsch, K. Ribbeck, and O. Lieleg, Modulating Mucin Hydration and Lubrication by Deglycosylation and Polyethylene Glycol Binding, *Advanced Materials Interfaces*, vol. 2, no. 18, p. 1500308, 2015.
- [128] M. Hall, D. Krawczak, N. Simha, and J. Lewis, Effect of dermatan sulfate on the indentation and tensile properties of articular cartilage, *Osteoarthritis and Cartilage*, vol. 17, pp. 655–661, 2009.
- [129] C. Canal Guterl, C. T. Hung, and G. A. Ateshian, Electrostatic and non-electrostatic contributions of proteoglycans to the compressive equilibrium modulus of bovine articular cartilage, *Journal of Biomechanics*, vol. 43, pp. 1343–1350, 2010.
- [130] J. P. Meyer, K. E. McAvoy, J. Jiang, and J. P. Brody, Rehydration Capacities and Rates for Various

- Porcine Tissues after Dehydration, *PLoS ONE*, vol. 8, p. e72573, 2013.
- [131] D. A. Zopf, C. L. Flanagan, H. B. Nasser, A. G. Mitsak, F. S. Huq, V. Rajendran, G. E. Green, and S. J. Hollister, Biomechanical evaluation of human and porcine auricular cartilage, *The Laryngoscope*, vol. 125, no. 8, pp. E262–8, 2015.
- [132] J. D. Abbott, Fibrocartilage, in *Rheumatology and Immunology Therapy*, L. W. Moreland, Ed. Springer Berlin Heidelberg, 2004, p. 328.
- [133] V. J. Baro, E. D. Bonnevie, X. Lai, C. Price, D. L. Burris, and L. Wang, Functional characterization of normal and degraded bovine meniscus: Rate-dependent indentation and friction studies, *Osteoarthritis*, vol. 51, pp. 232–240, 2012.
- [134] B. K. Zimmerman, E. D. Bonnevie, M. Park, Y. Zhou, L. Wang, D. L. Burris, and X. L. Lu, Role of interstitial fluid pressurization in TMJ lubrication, *Journal of dental research*, vol. 94, pp. 85–92, 2015.
- [135] G. Ateshian, M. Soltz, R. Mauck, I. Basalo, C. Hung, and W. Michael Lai, The Role of Osmotic Pressure and Tension-Compression Nonlinearity in the Frictional Response of Articular Cartilage, *Transport in Porous Media*, vol. 50, pp. 5–33, 2003.
- [136] H. T. Nia, I. S. Bozchalooi, Y. Li, L. Han, H.-H. Hung, E. Frank, K. Youcef-Toumi, C. Ortiz, and A. Grodzinsky, High-Bandwidth AFM-Based Rheology Reveals that Cartilage is Most Sensitive to High Loading Rates at Early Stages of Impairment, *Biophysical Journal*, vol. 104, no. 7, pp. 1529–1537, 2013.
- [137] Saleem Abubacker, Molecular Basis of Articular Cartilage Boundary Lubrication: Role of PRG4 Structure & Multimerisation, PhD thesis, University of Calgary, 2014. [Online]. Available: <http://hdl.handle.net/11023/2301> [Accessed: 07.03.2016]
- [138] D. P. Chang, N. I. Abu-Lail, J. M. Coles, F. Guilak, G. D. Jay, and S. Zauscher, Friction force microscopy of lubricin and hyaluronic acid between hydrophobic and hydrophilic surfaces, *Soft Matter*, vol. 5, p. 3438, 2009.
- [139] P. Hernigou, S. Quiennec, and I. Guissou, Hip hemiarthroplasty: from Venable and Bohlman to Moore and Thompson, *International Orthopaedics*, vol. 38, pp. 655–661, 2013.
- [140] R. Sonntag, J. Reinders, and J. P. Kretzer, Bio-Tribological Demands, in *Materials for Total Joint Arthroplasty*, R. Sonntag and J. P. Kretzer, Eds. Imperial College Press, 2015, pp. 1–13.
- [141] K. A. Athanasiou, D. J. Responde, W. E. Brown, and J. C. Hu, Harnessing Biomechanics to Develop Cartilage Regeneration Strategies, *Journal of biomechanical engineering*, vol. 137, p. 020901, 2015.
- [142] E. A. Makris, A. H. Gomoll, K. N. Malizos, J. C. Hu, and K. A. Athanasiou, Repair and tissue engineering techniques for articular cartilage, *Nature Reviews Rheumatology*, vol. 11, pp. 21–34, 2014.
- [143] K. Sun, H. Li, R. Li, Z. Nian, D. Li, and C. Xu, Silk fibroin/collagen and silk fibroin/chitosan blended three-dimensional scaffolds for tissue engineering, *European Journal of Orthopaedic Surgery & Traumatology*, vol. 25, pp. 243–249, 2015.
- [144] T. J. Klein, J. Malda, R. L. Sah, and D. W. Hutmacher, Tissue Engineering of Articular Cartilage with Biomimetic Zones, *Tissue Engineering Part B: Reviews*, vol. 15, pp. 143–157, 2009.
- [145] I.-C. Liao, F. T. Moutos, B. T. Estes, X. Zhao, and F. Guilak, Composite Three-Dimensional Woven Scaffolds with Interpenetrating Network Hydrogels to Create Functional Synthetic Articular Carti-

- lage, *Advanced Functional Materials*, vol. 23, no. 47, pp. 5833–5839, 2013.
- [146] M. Kyomoto and K. Ishihara, Hydrogels and Surface Modification, in *Materials for Total Joint Arthroplasty*, R. Sonntag and J. P. Kretzer, Eds. Imperial College Press, 2015, pp. 299–340.
- [147] K. L. Spiller, S. A. Maher, and A. M. Lowman, Hydrogels for the Repair of Articular Cartilage Defects, *Tissue Engineering Part B: Reviews*, vol. 17, pp. 281–299, 2011.
- [148] B. Sharma, S. Fermanian, M. Gibson, S. Unterman, D. A. Herzka, B. Cascio, J. Coburn, A. Y. Hui, N. Marcus, G. E. Gold, and J. H. Elisseeff, Human Cartilage Repair with a Photoreactive Adhesive-Hydrogel, *Science Translational Medicine*, vol. 5, p. 167ra6, 2013.
- [149] W. Schuurman, P. A. Levett, M. W. Pot, P. R. van Weeren, W. J. A. Dhert, D. W. Hutmacher, F. P. W. Melchels, T. J. Klein, and J. Malda, Gelatin-Methacrylamide Hydrogels as Potential Biomaterials for Fabrication of Tissue-Engineered Cartilage Constructs, *Macromolecular Bioscience*, vol. 13, pp. 551–561, 2013.
- [150] Y. Shi and D. Xiong, Microstructure and friction properties of PVA/PVP hydrogels for articular cartilage repair as function of polymerization degree and polymer concentration, *Wear*, vol. 305, pp. 280–285, 2013.
- [151] J. M. Harris and R. B. Chess, Effect of pegylation on pharmaceuticals, *Nature Reviews Drug Discovery*, vol. 2, pp. 214–221, 2003.
- [152] U.S. Food and Drug Administration. (2014) ReSure Sealant - P130004. [Online]. Available: http://www.accessdata.fda.gov/cdrh_docs/pdf13/P130004a.pdf [Accessed: 2016-07-03]
- [153] F. V. Sciarretta, 5 to 8 years follow-up of knee chondral defects treated by PVA-H hydrogel implants, *Eur Rev Med Pharmacol Sci*, vol. 17, no. 22, pp. 3031–3038, 2013.
- [154] J. Lange, N. Follak, T. Nowotny, and H. Merk, Results of SaluCartilage implantation for stage IV chondral defects in the knee joint area, *Der Unfallchirurg*, vol. 109, pp. 193–199, 2006.
- [155] K. Ushio, M. Oka, S.-H. Hyon, T. Hayami, S. Yura, K. Matsumura, J. Toguchida, and T. Nakamura, Attachment of artificial cartilage to underlying bone, *Journal of Biomedical Materials Research Part B: Applied Biomaterials*, vol. 68B, no. 1, pp. 59–68, 2004.
- [156] G. W. Greene, A. Olszewska, M. Osterberg, H. Zhu, and R. Horn, A cartilage-inspired lubrication system, *Soft Matter*, vol. 10, pp. 374–382, 2014.
- [157] Julia Nachtsheim, Friction-reducing effect of biopolymer solutions on articular cartilage surface, Semesterarbeit, Technische Universität München, 2013.
- [158] A. Singh, M. Corvelli, S. A. Unterman, K. A. Wepasnick, P. McDonnell, and J. H. Elisseeff, Enhanced lubrication on tissue and biomaterial surfaces through peptide-mediated binding of hyaluronic acid, *Nat Mater*, vol. 13, no. 10, pp. 988–995, 2014.
- [159] N. E. Larsen, H. D. Dursema, C. T. Pollak, and E. M. Skrabut, Clearance kinetics of a hylan-based viscosupplement after intra-articular and intravenous administration in animal models, *Journal of Biomedical Materials Research Part B: Applied Biomaterials*, vol. 100B, no. 2, pp. 457–462, 2012.
- [160] D. Jevsevar, P. Donnelly, G. A. Brown, and D. S. Cummins, Viscosupplementation for Osteoarthritis of the Knee, *The Journal of Bone & Joint Surgery*, vol. 97, pp. 2047–2060, 2015.
- [161] G. D. Jay, Tribonectins, U.S. Patent US8 680 057 B2, 2000.
- [162] M. Wimmer, M. Alini, and T. Kaup, Use of a mixture for the production of an agent for treating

- defective or degenerated cartilage in the production of natural cartilage replacement in vitro, U.S. Patent US2 007 275 032, 2007.
- [163] T. A. Schmidt, Control of rheological properties of mixed hyaluronate/lubricin solutions, U.S. Patent WO2 015 060 935, 2015.
- [164] M. Roba, E. G. Duncan, G. A. Hill, N. D. Spencer, and Tosatti, S. G. P., Friction Measurements on Contact Lenses in Their Operating Environment, *Tribology Letters*, vol. 44, no. 3, pp. 387–397, 2011.
- [165] L. Chai, R. Goldberg, N. Kampf, and J. Klein, Selective Adsorption of Poly(ethylene oxide) onto a Charged Surface Mediated by Alkali Metal Ions, *Langmuir*, vol. 24, pp. 1570–1576, 2008.
- [166] T. Drobek and N. D. Spencer, Nanotribology of Surface-Grafted PEG Layers in an Aqueous Environment, *Langmuir*, vol. 24, pp. 1484–1488, 2008.
- [167] M. Chen, W. H. Briscoe, S. P. Armes, and J. Klein, Lubrication at physiological pressures by polyzwitterionic brushes, *Science*, vol. 323, no. 5922, pp. 1698–1701, 2009.
- [168] M. Wathier, B. A. Lakin, P. N. Bansal, S. S. Stoddart, B. D. Snyder, and M. W. Grinstaff, A Large-Molecular-Weight Polyanion, Synthesized via Ring-Opening Metathesis Polymerization, as a Lubricant for Human Articular Cartilage, *J. Am. Chem. Soc.*, vol. 135, pp. 4930–4933, 2013.
- [169] K. Ishihara, Highly lubricated polymer interfaces for advanced artificial hip joints through biomimetic design, *Polym J*, vol. 47, pp. 585–597, 2015.
- [170] M. Kyomoto, T. Moro, K. Saiga, M. Hashimoto, H. Ito, H. Kawaguchi, Y. Takatori, and K. Ishihara, Biomimetic hydration lubrication with various polyelectrolyte layers on cross-linked polyethylene orthopedic bearing materials, *Biomaterials*, vol. 33, pp. 4451–4459, 2012.
- [171] M. Kyomoto, T. Moro, Y. Takatori, H. Kawaguchi, and K. Ishihara, Cartilage-mimicking, High-density Brush Structure Improves Wear Resistance of Crosslinked Polyethylene: A Pilot Study, *Clinical Orthopaedics and Related Research*, vol. 469, pp. 2327–2336, 2010.
- [172] S. Yarimitsu, T. Moro, M. Kyomoto, K. Watanabe, S. Tanaka, K. Ishihara, and T. Murakami, Influences of dehydration and rehydration on the lubrication properties of phospholipid polymer-grafted cross-linked polyethylene, *Proceedings of the Institution of Mechanical Engineers, Part H: Journal of Engineering in Medicine*, vol. 229, pp. 506–514, 2015.
- [173] U.S. Food and Drug Administration. (2005) Proclear: omafilcon A - K050717. [Online]. Available: http://www.accessdata.fda.gov/cdrh_docs/pdf5/k050717.pdf [Accessed: 2016-07-03]
- [174] Hiroko Tanioka, Multicenter follow-up study of a new artificial hip joint in which 2-methacryloyloxyethyl phosphorylcholine polymer is grafted onto the bearing surface of highly cross-linked ultrahigh molecular weight polyethylene liner, 2010. [Online]. Available: <https://upload.umin.ac.jp/cgi-open-bin/ctr/ctr.cgi?function=history&action=list&type=summary&recptno=R000004454&language=E> [Accessed: 2016-08-03]
- [175] S. M. Kurtz, *UHMWPE biomaterials handbook: Ultra high molecular weight polyethylene in total joint replacement and medical devices*, 3rd ed. Elsevier, 2015.
- [176] A.S Pharma, Saliva Orthana. [Online]. Available: <http://www.aspharma.co.uk/> [Accessed: 2016-11-03]
- [177] M. P. Sweeney, J. Bagg, W. P. Baxter, and T. C. Aitchison, Clinical trial of a mucin-containing oral spray for treatment of xerostomia in hospice patients, *Palliative medicine*, vol. 11, no. 3, pp. 225–232, 1997.

BIBLIOGRAPHY

- [178] P. Georgiades, Pudney, Paul D. A., D. J. Thornton, and T. A. Waigh, Particle tracking microrheology of purified gastrointestinal mucins, *Biopolymers*, vol. 101, no. 4, pp. 366–377, 2014.

